The role of the periaqueductal gray in respiratory control and breathlessness

Ms Olivia Faull BSc BPhEd

St Hilda's College

University of Oxford

A thesis submitted for the degree of

Doctor of Philosophy

Trinity 2015

For my family, who have always believed in me.

"What is more important for us, at an elemental level,
than the control, the owning and operation, of our own physical selves?
And yet it is so automatic, so familiar, we never give it a thought."

Oliver Sacks, 1998 *The Man Who Mistook His Wife for a Hat*

Acknowledgements

I would firstly like to say a huge thank you to my supervisor Kyle Pattinson, whose enthusiasm and careful science were the backbone of this DPhil. Despite warnings of madness when we first set out on this project, pushing the boundaries of what was possible with fMRI has made for an incredible learning experience, although probably also a few grey hairs. My labmates must also be thanked for their guidance and support throughout the last three years- you have all been an absolute pleasure to work with and a huge help in the making of this Thesis.

Over at FMRIB an enormous thank you must go to Mark Jenkinson, whose patience and tireless support helped me through the minefield that was the analysis of these studies. Also to Stuart Clare, who helped us optimise the scanner sequences, and to the technical team of Dave, Duncan, Matt and Chris. Special thanks to my Radiographers Mike and Jon, who never once bemoaned the masses of equipment and put every effort into making this lunacy possible.

I am very grateful for the financial support I received to complete this work- from the Commonwealth Scholarship Commission who funded my DPhil, and from the Medical Research Council and JABBS who funded the projects. To the volunteers who participated in these (sometimes uncomfortable) studies, this research was simply not possible without you and I am forever thankful.

To my family and friends in New Zealand and the UK, thank you so much for your unwavering belief. From the point at which this was simply an unfathomable dream through to writing these acknowledgements, you have all been amazing. Finally to Sam, who keeps me sane and alive, thank you for everything.

And from my time in England I have learned that if you are ever in doubt, the answer is always more tea.

Thesis abstract *DPhil Thesis, Trinity term 2015*

Olivia Faull, St Hilda's College

The role of the periaqueductal gray in respiratory control and breathlessness

Understanding respiratory control is crucial for improving the management of respiratory disease, and the accompanying breathlessness endured by its sufferers. A body of animal evidence supports the role of the midbrain periaqueductal gray (PAG) in modulating ascending and descending respiratory information, with the PAG subdivisions acting within a network that may contribute to the threatening perception of breathlessness.

In this Thesis we used ultra high field magnetic resonance imaging (MRI) at 7 Tesla to firstly identify activity within the columns of the PAG during the simple respiratory task of breath holding in humans, matching those previously reported in animals for slowed ventilatory responses. Extending this investigation to the perception of breathlessness, we then used a classical fear-conditioning paradigm to investigate anticipation and response to an aversive inspiratory resistive loading stimulus. We found activity in the lateral PAG (lPAG) during slowed breathing against an inspiratory resistance, and activity in the ventrolateral PAG (vlPAG) during anticipation of resistive loading. These results align with the proposed threat perception model in animals; with the vlPAG involved in passive responses to inescapable stress, while the lPAG is involved in active responses to threat.

Lastly, we investigated the role and connections of the PAG columns within the wider cortical breathlessness network, and any plastic changes evoked by exercise. Functional and connectivity results suggest the PAG column activities in breathlessness are influenced by top-down cortical networks, with the vlPAG involved in the affective emotional dimension of breathlessness, while the lPAG is involved in the sensory component. In a comparison between athlete and sedentary subjects, athletes displayed increased functional activity in the vlPAG and prefrontal cortex during anticipation of breathlessness, indicating possible affective changes in perception rather than a global 'de-sensitisation' to breathlessness.

Therefore, in this Thesis we have identified the columns of the PAG to be intricately involved with respiratory control and perception of breathlessness. It appears the PAG may be a critical point of distinction between aspects of breathlessness perception, with the vlPAG a possible area of adaptation of affective breathlessness in athletes, or conversely (mal)adaptation and a target for treatment in patients with chronic respiratory disease.

Olivia K Faull was supported by the Commonwealth Scholarship Commission

Publications

1. FAULL, O. K., JENKINSON, M., CLARE, S., AND PATTINSON, K. T. S. Functional subdivision of the human periaqueductal grey in respiratory control using 7 tesla fMRI. NeuroImage 113 (2015), 356364. *(Data from Chapter 2)*

2. EZRA, M., FAULL, O. K., JBABDI, S., AND PATTINSON, K. T. S. Connectivity-based segmentation of the periaqueductal gray matter in human with brainstem optimized diffusion MRI. Human brain mapping (2015).

3. BROOKES, J. C. W., FAULL, O. K., PATTINSON, K. T. S., AND JENKINSON, M. Physiological Noise in Brainstem fMRI. Frontiers in Human Neuroscience 7 (2013), 113.

4. FAULL, O. K., ROBERTSON, J., THOMAS, O., BRADWELL, A. R., ANTONIADES, C. A., AND PATTINSON, K. T. The Effect of Acetazolamide on Saccadic Latency at 3459 Meters. Wilderness & environmental medicine 26(1) (2015), 72-77.

5. FAULL, O. K., COTTER, J. D., AND LUCAS, S. J. E. Cerebrovascular responses during rowing: Do circadian rhythms explain morning and afternoon performance differences?. Scandinavian journal of medicine & science in sports (2014).

Contents

List of Figures

Chapter 1

Introduction

1.1 Abstract

In this Chapter we introduce the importance of investigating and understanding respiratory control and breathlessness, and our proposal for the intricate role of the midbrain periaqueductal gray (PAG). We will review the current evidence in animals and humans on the structure and respiratory functions of the PAG, and the interface with the wider cortical network of respiratory control. Furthermore, as the subdivisions of the PAG have been proposed to reside within a behavioural coordination system responding to threat, we propose how this could influence the threatening perception of breathlessness. We outline how the plasticity of the PAG may play a role in the reduction of heightened breathlessness anxiety using exercise therapy in patients with chronic lung disease. We introduce the technique of non-invasive magnetic resonance imaging (MRI) as a tool for this investigation, and outline how this Thesis aims to better understand the neural mechanisms of breathlessness for the development of more targeted treatments of this debilitating symptom in the future.

1.2 Introduction

Respiration is an essential facet of terrestrial life, with prolonged respiratory failure leading to death. Respiration is controlled to maintain homeostasis, adapting to activities and environments to sustain a sufficient oxygen supply to tissues (Kreuzer, 1982). Thus, respiration quickly adjusts to metabolic changes and challenges presented during acute demands such as those imposed by exercise, hypoxia (decreased oxygen) and hypercapnia (increased carbon dioxide), as well as exhibiting plasticity to cope with longer-term demands, such as pregnancy.

While extensive investigations into the functional neuroanatomy of respiratory control have been focused on the nuclei of respiratory rhythm generators in the medulla, the suprapontine control of respiration is less well understood. Importantly, the role of the midbrain periaqueductal gray matter (PAG) in respiratory control has been suggested since the 1930s, with an early study by Kabat (1935) in the cat identifying the PAG in the localised pathway for respiratory responses. More recently, investigations have identified that the PAG is subdivided into four separate columns, each with distinct respiratory functions. These respiratory functions point towards the PAG playing a key role as part of the integrated defence reaction, and thus it has been labelled as a behavioural modulator of breathing (Subramanian et al., 2008; Subramanian, 2012).

The PAG is not only a modulator of breathing; it has also been implicated in the coordination of patterns of cardiovascular, motor and pain responses (De Oca et al., 1998; Mobbs et al., 2007; Pereira et al., 2010; Tracey et al., 2002; Benarroch, 2012; Paterson, 2013). Encompassing all of these functions is the theory that the columns of the PAG are modulators to either internal, inescapable stressors (such as pain) and external, escapable stressors (such as a predator) (Bandler and Shipley, 1994; Bandler et al., 2000; Keay and Bandler, 2001). While animal models have allowed detailed investigation of functional neuroanatomy, they are limited by their invasive nature and in their behavioural interpretations, as subjective feedback is impossible. In contrast, human investigations are limited by the spatial resolution constraints of non-invasive neuroimaging, where voxel size can encompass the whole PAG and surrounding structures. Alternatively, small populations of very ill patients with chronic diseases undergo stereotaxic electrode placement in the PAG, although the location within the PAG is limited to dorsal or ventral placement (Green and Paterson, 2008; Hyam et al., 2012). Therefore, investigating the columns of the PAG in respiratory control and threat behaviours in humans remains a challenge.

The position, connectivity and respiratory functions of the PAG make it an ideal candidate for a centre of subcortical respiratory regulation in humans. The following literature

review aims to bring together the current animal and human findings on the role of the columns of the PAG in respiratory control, and how this aligns with the current model of the PAG within an integrated behavioural response to threat.

1.3 Literature review

1.3.1 Position and structure of the PAG

The PAG surrounds the cerebral aqueduct in the midbrain region of the brainstem, located at the junction of descending efferent commands and ascending sensory information. The human PAG is approximately 14 mm long and 4-5 mm wide, and does not completely encircle the aqueduct (Figure 1.1). Thus, the PAG is shaped like a celery stalk, with the ventral portion consisting of separate, well-differentiated nuclei that are not included in the PAG (Linnman et al., 2012). Although the grey matter of the PAG itself appears to be poorly differentiated, it is proposed to be subdivided into four columns: the dorsomedial (dmPAG), dorsolateral (dlPAG), lateral (lPAG) and ventrolateral (vlPAG) (Basnayake et al., 2011; Dampney et al., 2013; Linnman et al., 2012; Subramanian, 2012) (Figure 1.1). Strikingly, a recent study has used diffusion tensor imaging (DTI) data to segment the human PAG, using back-projections from the cortex (Ezra et al., 2015) to find a similar four-column structure to animals (Subramanian et al., 2008; Subramanian, 2012). Therefore, targeting these subdivisions is critical to improving our understanding of PAG function(s).

1.3.2 Respiratory functions of the PAG

Previously identified functions of the PAG include involvement in pain modulation, anxiety, vocalisation and cardiovascular control (Behbehani, 1995), and more recently as a behavioural modulator of breathing (Subramanian et al., 2008; Subramanian, 2012). The first suggestions of possible respiratory functions of the PAG came from direct electrical stimulation studies in animals. As previously mentioned, the earliest of these studies was by Kabat (1935) who found that stimulation of the PAG in the cat could evoke an increase in the rate of respiration, changes in the amplitude or depth of breathing, and also a spitting response (defensive vocal behaviour of the cat). More recently, excitatory respiratory responses were found by direct stimulation of the dorsal PAG in the rat (Hayward and Von Reitzenstein, 2002; Zhang et al., 2007). However, studies on anaesthetised animals can be problematic as anaesthesia can suppress brainstem areas involved with respiratory responses (Peters et al., 2008), and the use of electrical stimulation can simultaneously

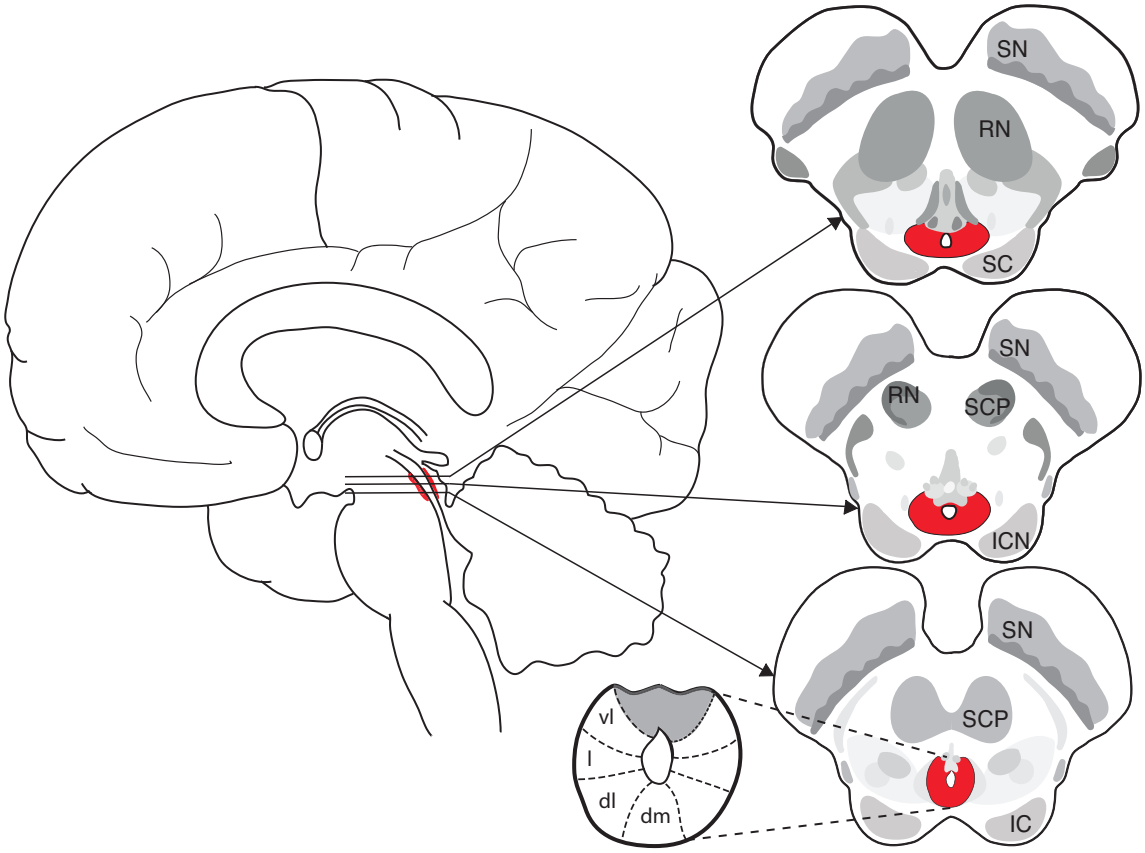

Figure 1.1: Representation of the location of the PAG within the brain, three axial slices and the subdivisions of the PAG. Shaded red areas represent the PAG surrounding the cerebral aqueduct. Abbreviations: IC= inferior colliculus; SCP= superior cerebellar peduncle; SN= substantia nigra; ICN= intercollicular nucleus; RN= red nucleus; SC= superior colliculus; vl, ventrolateral PAG, l, lateral PAG; dl, dorsolateral PAG; dm, dorsomedial PAG.

excite fibres of passage through a structure (Horn and Waldrop, 1998). Therefore, many questions pertaining to the respiratory function of the PAG remained unanswered.

Building on the results from electrical stimulation techniques, two of the latest studies into the respiratory functions of the PAG by Subramanian and colleagues (Subramanian et al., 2008; Subramanian, 2012) used excitatory amino acid stimulation to target cell bodies within the PAG subdivisions of rats and decerebrated cats. Consistently across these studies, stimulation of the dorsal PAG resulted in tachypnea (rapid breathing), lPAG caused prolonged inspiration, and the lateral portions of the lPAG and vlPAG induced either prolonged expiration (rats) or vocalisations such as mews or hisses (cats), with their associated expirations. Additionally, Subramanian et al. (2008) found that stimulation of the cat caudal vlPAG resulted in irregular breathing, while the dmPAG produced slow, deep breathing. Therefore, it appears that not only is the PAG a behavioural modulator of breathing, but specific areas within the PAG modulate different respiratory functions. Farmer et al. (2014) recently replicated many of these respiratory modulations using a decerebrate, perfused rat brainstem model. Interestingly, as no change in resting ventilation was observed with inhibition of the PAG columns, Farmer et al. (2014) concluded that the PAG is not involved in baseline respiratory motor pattern or rhythm. While the spatial resolution required to translate these animal findings to humans presents a challenge, it is vital that the columns of the PAG are targeted in future human research to fully understand the role of the PAG in respiration.

The possibility of investigating respiratory control in humans through direct excitation and recording of the subdivisions of the PAG is limited, due to the invasive nature of this type of research. However, stereotaxic electrodes are implanted in a range of human patients for treatment of movement disorder and chronic pain. Green and Paterson (2008) used these electrodes to record local field potentials of deep brain nuclei in the PAG, substantia nigra or gllobus pallidus interna while the patients underwent the task of imagining exercise. Imagining exercise evoked profound physiological responses, including increased respiratory rate, heart rate and blood pressure compared to rest. In conjunction with these cardiorespiratory changes, the greatest neural increases were seen in the PAG (43% activation increase compared to rest), which increased to 87% above rest when the patients completed physical exercise on a cycle ergometer. Additionally, Hyam et al. (2012) used deep brain stimulation (DBS) of the PAG and subthalamic nucleus to evoke increases in peak expiratory flow rate, while comparative stimulation of control nuclei (thalamus) did not evoke these respiratory changes. These results support an earlier animal study by Haxhiu et al. (2002), who found that stimulation of the vlPAG induced airway smooth muscle relaxation in ferrets and consequently postulated direct connections between the two.

Therefore, while DBS studies in humans are unable to make multiple comparisons between the subdivisions of the PAG, and are carried out on patients rather than healthy individuals, preliminary evidence supports the animal model for a tier of respiratory control residing within the PAG.

1.3.3 PAG within the respiratory network

The neurons responsible for the generation of autonomic respiration are proposed to reside inferior to the PAG in the ventrolateral medulla, in areas identified as the Pre-Bötzinger complex (PreBötC) and retrotrapezoid nucleus/parafacial respiratory group (RTN/pFRG) (Smith et al., 2009). Although the necessity of endogenous bursting properties in these neurons has been debated (Feldman et al., 2003), the network encompassing the PreBötC is thought by many to be critical to autonomic respiratory rhythm generation. There are direct inputs to this medullary network from the pontine respiratory group, and in particular the Kölliker-Fuse nucleus is proposed to play a role in both post-inspiratory activity and the processing of afferent sensory information of the respiratory network (Dutschmann et al., 2004). The resulting output of this ponto-medullary autonomic respiratory network is hypothesised as direct connections to ventilatory motor neurons, including the phrenic nerve for diaphragm control, abdominal motor nerves and the hypoglossal nerve for control of the tongue (Feldman et al., 2003; Smith et al., 2009).

An important mechanism that allows for subconscious control of ventilation is chemoreception. Chemoreception is the constant monitoring of blood gas concentrations, allowing for direct comparisons between respiratory rate and the requirements of the periphery (Ballantyne and Scheid, 2001). The role of the PAG in chemoreception is not yet fully understood, however recent research has revealed that PAG lesions dampen the respiratory response to hypercapnia (compared to lesions immediately outside the PAG), while resting ventilation, mean arterial blood pressure, heart rate and body temperature were unaffected by these lesions (Lopes et al., 2012, 2014; Schimitel et al., 2012). Although the PAG has not been identified as a chemoreceptive site itself, such as seen in the retro-trapezoid nucleus, medullary raphe, nucleus tractus solitarius and preBötC (Kuwaki et al., 2010), c-Fos labelling in all columns of the PAG was seen in association with activity in arterial chemoreceptors in anaesthetised rats (Hayward and Von Reitzenstein, 2002). Schimitel et al. (2012) has taken this information to suggest that a suffocation alarm system is encoded in the PAG. They found that PAG lesions in rats reduced the defensive behaviours evoked by selective anoxia in chemoreceptor cells (suffocation alarm), while additive CO_2 administration enhanced these behaviours. The authors concluded that this possible suffocation alarm in the

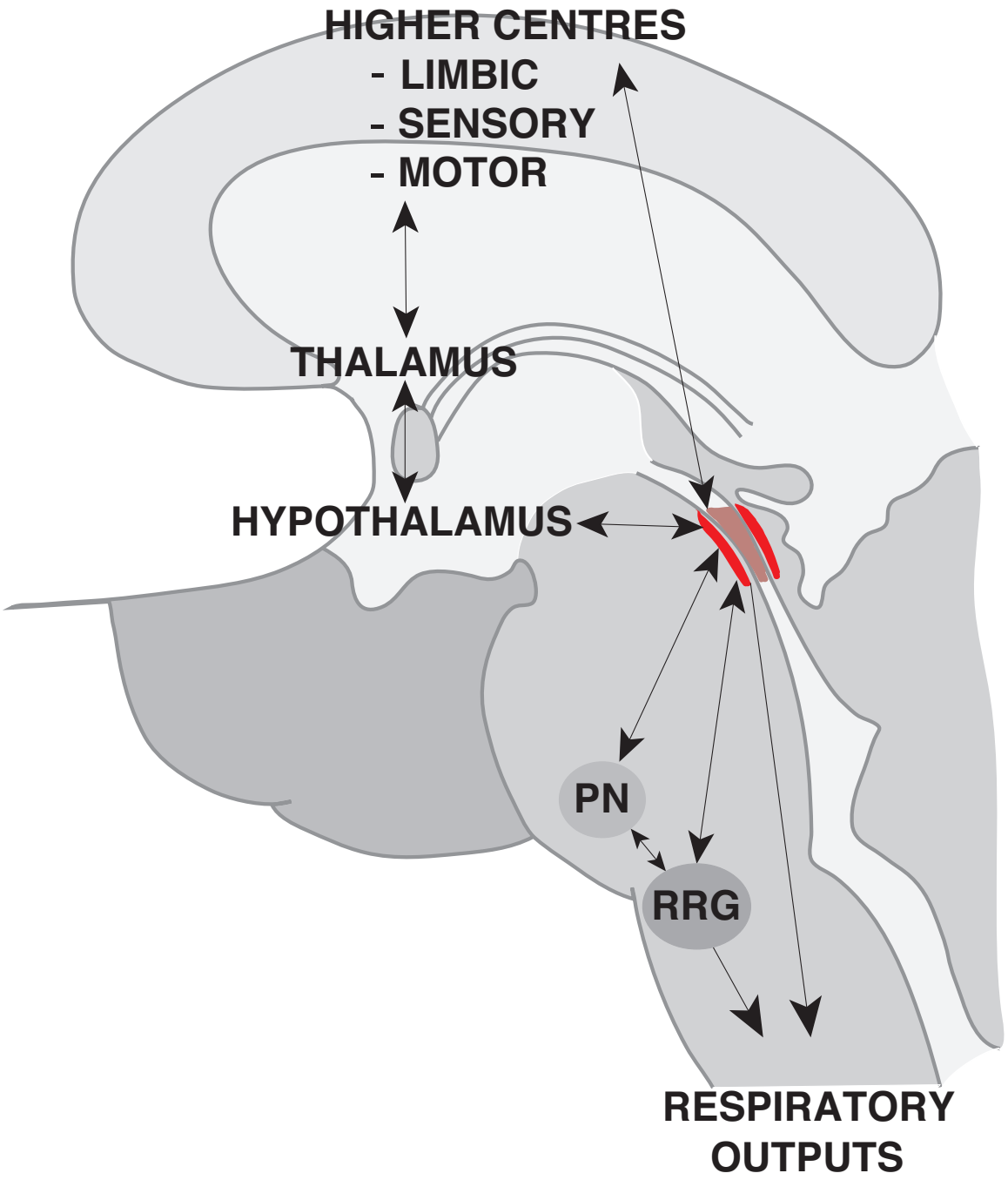

Figure 1.2: Schematic of where the PAG is hypothesised to fit within the wider respiratory circuit, receiving both descending and ascending respiratory information. Shaded red area indicates the position of the PAG. Abbreviations: PN= pontine nuclei; RRG= respiratory rhythm generators.

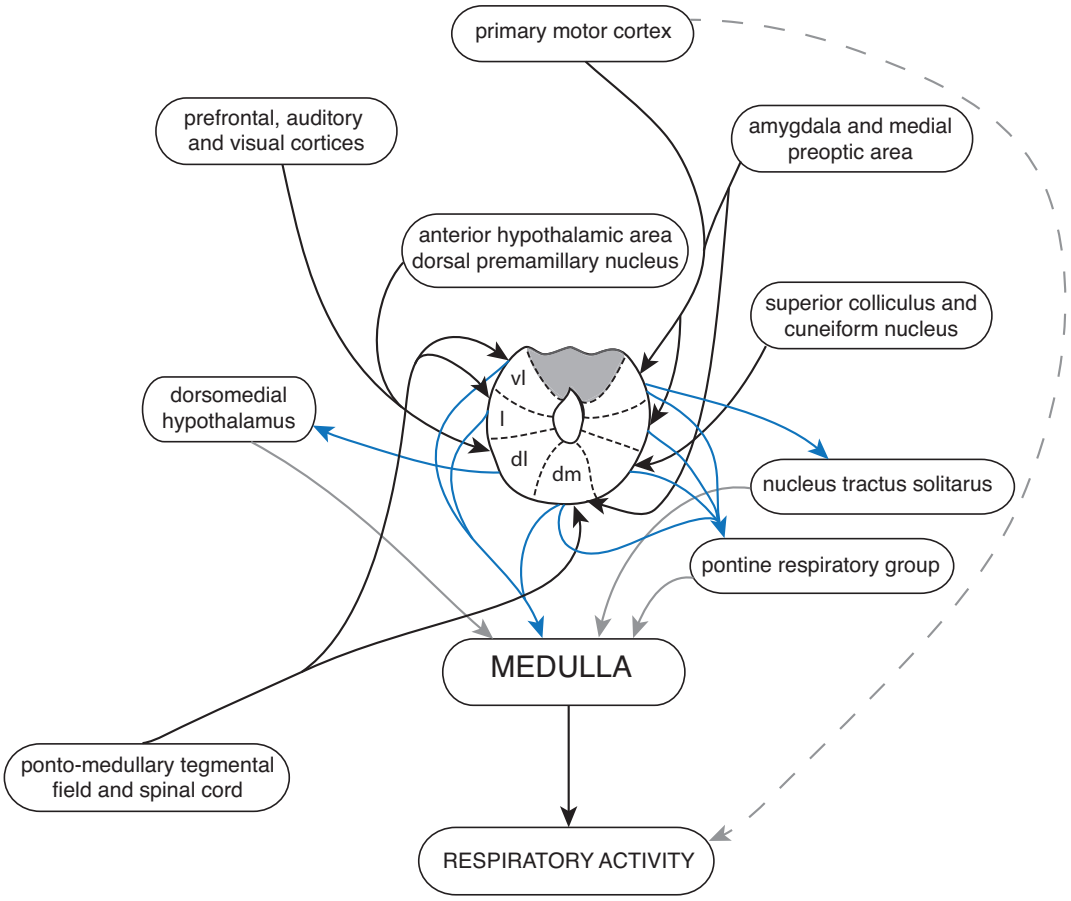

Figure 1.3: Anatomical connections of the subdivisions of the periaqueductal gray matter from research in animals, represented at the level of the inferior colliculus. Abbreviation: vl= ventro-lateral; l= lateral; dl= dorsolateral; dm= dorsomedial. Modified from Dampney et al. (2013). Solid black lines represent inputs to the PAG, blue lines represent outputs from the PAG, grey lines indicate circuitry that does not include the PAG, and the dashed line represents volitional motor efferents that do not involve the brainstem respiratory circuit.

PAG is activated by anoxia, resulting in defensive behaviours consistent with panic attacks, and additional hypersensitivity to hypercapnia. Therefore, while not a primary chemoreceptive site, the PAG may be involved in the integration of chemoreceptive information to allow for subconscious homeostatic monitoring of respiratory state.

Respiration extends beyond subconscious autonomic control, and ventilatory changes can be made during phonation, stress, or for voluntary breathing modifications. These changes indicate a higher respiratory control network, and both cortical and subcortical brain structures have been identified as modulators of respiration. Anatomical evidence exists for connections between the PAG and cortical areas identified in respiratory control, and a recent review by Dampney et al. (2013) comprehensively collated the inputs and outputs of the subdivisions of the PAG (summarised in Figure 1.2). Firstly, identified cortical areas for ventilatory commands that have been linked to the PAG include the motor and premotor cortices, and the supplementary motor area, which have been shown to alter phrenic and intercostal nerve firing rates for control of the diaphragm and thoracic respiratory muscles (Colebatch et al., 1991; Fink et al., 1996; Rikard-Bell et al., 1985). Meanwhile, the conscious sensations of respiration include both sensory thoracic proprioception and affective emotional evaluation (Davenport and Vovk, 2009). Interestingly, while the primary somatosensory cortex has been identified as the main sensory area for thoracic proprioception, there is no evidence of direct anatomical connections to the PAG. In contrast, inputs to the PAG have been identified from the cortical and subcortical limbic areas involved in emotional evaluation, such as the prefrontal cortex and amygdala (Beitz, 1982; Gabbott et al., 2005; Rizvi et al., 1991). Therefore, it is possible that the PAG is directly involved with both respiratory motor commands and the emotional evaluation of respiratory sensations.

Higher-level respiratory commands and sensations from the cortex are also integrated within subcortical gateways, which are pertinent for the regulation of respiratory information sent between the cortex and the autonomic respiratory centres in the brainstem. The thalamus is major subcortical gateway that has a well-documented involvement in sensory integration, including during functional respiratory tasks such as breath-holds (Pattinson et al., 2009b). However, the respiratory functions of the PAG indicate its potential involvement in a further sub-cortical system between the thalamus and brainstem, which can sub-consciously modulate respiration (Subramanian et al., 2008). Similarly, the PAG has previously been suggested as a site for the integration of autonomic cardiovascular information (Green et al., 2007), and with its respiratory functions it appears a likely candidate for similar respiratory control.

It is possible that the respiratory functions of the PAG act in conjunction with the hy-

pothalamus, as the caudal and dorsomedial hypothalamic nuclei (CH and DMH) have also been implicated in respiratory modulation (Horiuchi et al., 2009; Ryan and Waldrop, 1995). Direct connections have been identified between the PAG and both CH and DMH nuclei (Cameron et al., 1995; Horiuchi et al., 2009; Vertes and Crane, 1996), and it appears that the PAG may be influenced by the hypothalamus for integrated control of breathing (Dampney et al., 2008; Horn and Waldrop, 1998). For example, the respiratory outputs of the dlPAG can be virtually abolished by inhibition of the DMH, while inhibition of the PAG did not affect the respiratory responses that can be generated by disinhibition of the DMH (Horiuchi et al., 2009). The DMH also has a well-documented role in the pathway between the suprachiasmatic nucleus and the ventrolateral preoptic area for control of the transition between sleep and wakeful states (Chou et al., 2002), and the relationship between the DMH and PAG in respiration may support the observation that a subset of PAG cells correlate with respiratory patterns in a sleep state-dependent manner (Harper et al., 1991). Furthermore, connections between cortical motor areas and locomotor areas of the hypothalamus (Baev et al., 1985; Eldridge et al., 1981) may incorporate the PAG into the feedforward control of respiration associated with exercise, an idea that has been discussed elsewhere (Paterson, 2013). Therefore, it appears likely that the respiratory functions of the PAG act within a network that incorporates the CH and DMH, allowing respiratory control according to states of consciousness and activity.

Evidence also exists for ascending connections from the periphery to the PAG, and onwards to higher areas of sensation. Firstly, Eldridge et al. (1981) tested decerebrated, paralysed and ventilated cats, and found that afferent information from the vagus nerve inhibited the firing of midbrain respiratory neurons. Furthermore, Cameron et al. (1995) used an anterograde tracer to identify afferent ascending connections from the PAG to the hypothalamus, thalamus and other areas of the forebrain, which indicate possible feedback loops to the higher subcortical and cortical structures of the respiratory network. Onwards from the thalamic relay centres to the cortex in humans, Pattinson et al. (2009a) suggested different areas of the thalamus connect more strongly to different cortical regions based on diffusion tractography results, including connections between the thalamic ventral posterolateral (VPL) nuclei and the motor and sensory cortices, as well as connections between the thalamic anteroventral (AV) nuclei and the amygdala, prefrontal cortex and anterior cingulate cortex. Therefore, the PAG provides an optimal site for the integration of the passing motor, limbic and sensory respiratory information, with evidence to suggest resultant respiratory responses can be evoked directly from the firing of neurons within the PAG (Subramanian, 2012; Subramanian et al., 2008).

While the mechanisms of the respiratory actions generated by the PAG are not yet

thoroughly understood, it has been proposed that the PAG acts on respiratory neurons in both the medulla and nucleus tractus solitarius (Duffin and Hockman, 1972; Huang et al., 2000; Sessle et al., 1981), with mediation from the parabrachial nucleus of the pons (Hayward et al., 2004) (Figure 1.2). Most recently, Subramanian (2012) directly stimulated the sub-divisions of the PAG in rats, and examined the effect on both medullary respiratory neurons and the resultant respiratory behaviours. Dorsal PAG stimulation resulted in tachypnoea with excitation of both late inspiratory (late-I) and post-inspiratory (post-I) medullary neurons, which are believed to be involved with the conversion of inspiration to expiration (Morschel and Dutschmann, 2009; Rybak et al., 2004). Conversely, lPAG stimulation caused inspiratory prolongation (with activation of late-I with inhibition of post-I neurons), while vlPAG caused expiratory prolongation (activation of post-I neurons) (Subramanian, 2012). While these medullary outputs are yet to be confirmed in humans, this evidence supports the influence of the PAG on brainstem respiratory centres for control of breathing.

Care must be taken when attempting to translate these animal findings into human experiments. Non-invasive investigation of human respiratory control often employs a reverse model to animal experiments; where ventilatory tasks are conducted and brain activation is measured, as opposed to direct stimulation of neurons and measurement of respiratory responses. However, preliminary investigations in humans have suggested midbrain structures such as the PAG to be possibly involved in respiratory control (Horn and Waldrop, 1998). Midbrain activation has been identified during hypercapnic-stimulated breathing (Corfield et al., 2005), maximal inspirations (Topolovec et al., 2004) and resistive inspiratory loading (Gozal et al., 1995). However, the interpretation of the midbrain results of these studies is further limited by spatial resolution constraints, and thus an inability to localise activations within the subdivisions of the PAG. While there is enormous potential to contribute to our understanding of respiratory control with future PAG research, the challenge remains to accurately and non-invasively investigate the activation of the PAG and its sub-structures within the wider respiratory control network in humans.

1.3.4 PAG in response to threat

The columns of the PAG have been identified to function within a broad range of behaviours beyond respiration, including cardiovascular, motor and pain responses (De Oca et al., 1998; Mobbs et al., 2007; Pereira et al., 2010; Tracey et al., 2002; Benarroch, 2012; Paterson, 2013). Therefore, the PAG has been postulated to act as a behavioural modulator as part of the integrated defence system in animals Dampney et al. (2013); Keay and Bandler

(2001). A review by Dampney et al. (2013) highlighted the potential involvement of the dlPAG as a key structure within this defence system. Direct stimulation of the dlPAG results in tachypnea, a distinctly different respiratory behaviour to other areas of the PAG, and which Dampney et al. (2013) deemed consistent to the respiratory changes induced during a fight/flight defensive reaction. Furthermore, rat defensive behaviour upon exposure to a predator (cat) evoked increased c-Fos expression (marker of neuronal activation) in the rostral and intermediate dlPAG (Canteras and Goto, 1999), while purely physical stimuli such as radiant heat or muscle pain evoked c-Fos expression mainly in the lPAG or vlPAG (Keay and Bandler, 2001). This evidence was taken to suggest that the dlPAG may be a central command site within the defensive system in animals (Dampney et al., 2013).

Alternatively, rather than the dlPAG being the site of 'central command', the functional organisation of the columns of the PAG has been hypothesised to consist of active and passive coping strategies (Bandler and Shipley, 1994; Bandler et al., 2000). The lPAG and dlPAG are thought to employ active coping strategies for escapable stressors, which would be consistent with the tachypnea observed in animals (Subramanian et al., 2008), while the vlPAG employs passive coping strategies for inescapable stressors (vlPAG), such as that seen with physical stimuli (Keay and Bandler, 2001). Active coping strategies in the lPAG/dlPAG would require direct motor input from superior cortical structures, while passive strategies in the vlPAG would possibly require greater communication with the prefrontal and limbic areas to assess inescapable threat.

Importantly, recent work using diffusion tractography has revealed consistent columnar structure to animal models within the human PAG (Ezra et al., 2015), and differential connectivity patterns from the PAG columns to cortical structures (Figure 1.4). Ezra et al. (2015) found predominating frontal and limbic connections to the vlPAG, while sensory and motor areas connected to the dlPAG and lPAG. Therefore, both functional and connectivity differences suggest that the columns of the PAG have distinctive roles within the networks responsible for both respiratory control and threat perception, and may act as a gateway for incoming sensory information from the chest.

1.3.5 Literature review summary

In this review we have shown that converging evidence from animal models, DBS and preliminary imaging studies implicate the PAG in the intricate control of respiration. While animal models have shown that subdivisions of the PAG can produce distinct respiratory outputs, that same level of spatial resolution and localisation of signal has not yet been available in human imaging research. It has been suggested that the PAG modulates respi-

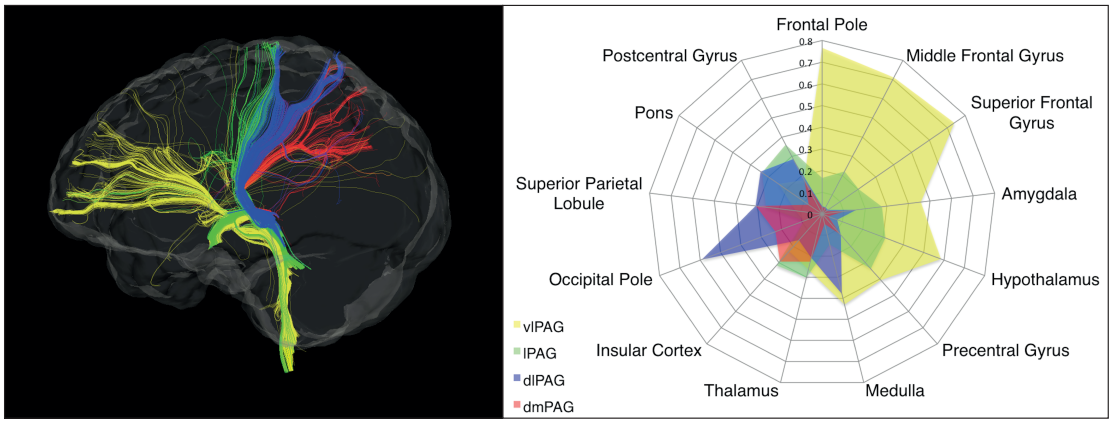

Figure 1.4: Schematic of the diffusion-based connectivity results in Ezra et al. (2015). Left: Three-dimensional fibre tracking of cortical and subcortical projections from the four division of the human PAG in a single subject. Tractography demonstrates differential connectivity patterns arising from the Dorsomedial (Red), Dorsolateral (Blue), Lateral (Green) and Ventrolateral (Yellow) aspects of the PAG (Image produced using DSI Studio). Right: Radial diagram of relative connectivity of the clusters to predefined targets averaged over 19 subjects. where the PAG is hypothesised to fit within the wider respiratory circuit, receiving both descending and ascending respiratory information. Shaded red area indicates the position of the PAG. Abbreviations: vlPAG, ventrolateral periaqueductal gray; lPAG, lateral periaqueductal gray; dlPAG, dorsolateral periaqueductal gray; dmPAG, dorsomedial periaqueductal gray.

ration in times of stress, where columns of the PAG are differentially involved according to whether a threat is perceived as escapable or inescapable. Lastly, recent diffusion imaging research has revealed connectivity patterns that support this columnar threat hypothesis in humans. Therefore, in an extension of the current literature, in this Thesis we will now explore the roles of the PAG columns in human respiratory control and in the threatening perception of breathlessness.

1.4 PAG in breathlessness

Breathlessness debilitates countless sufferers of chronic obstructive pulmonary disease (COPD), asthma, cardiovascular and neuromuscular diseases, cancer or panic disorder. Alternatively, self-imposed breathlessness can be experienced by people enduring extreme exercise, such as endurance athletes or high altitude climbers (Abraini et al., 1998). It is considered the main symptom of COPD, which leads to approximately 25 million certified sickness days, costs the NHS more than 4 billion, occupies more than 1 million inpatient UK bed days and generates approximately 40 million drug prescriptions each year (British Thoracic Society, 2006). Furthermore, breathlessness severity is a better predictor of mortality in patients with COPD than lung function (Celli et al., 2004).

Although the breathlessness in COPD is traditionally explained in terms of lung damage, discrepancies between breathlessness severity and objective measures of lung function are well known and remain unexplained (Herigstad et al., 2011; Lansing et al., 2009). Commonly, these discrepancies are rationalised in terms of abnormal muscle function and inaccurate lung function tests. An alternate explanation relates to abnormal brain processing of respiratory sensations. Breathlessness is a multi-dimensional sensation, including perception of 'work of breathing' from respiratory muscles in the torso, 'air hunger' from chemoreceptive signals in the blood, 'chest tightness' from and obstruction or restriction to the airways, to name a few (Lansing et al., 2009). To generalise across these dimensions, breathlessness can be roughly divided into sensory and affective components. If sensations of breathlessness are interpreted as threatening within the affective domain they can evoke a fearful response, which has been hypothesised to be caused by the mismatch of information between afferent respiratory signals and efferent ventilatory drive (Schwartzstein et al., 1989). With the differing respiratory functions and possible roles in threat perception, it is plausible that the columns of the PAG play distinctive roles within these components of breathlessness perception.

In human imaging research, the processing of breathlessness sensations in the brain has been identified non-invasively with functional magnetic resonance imaging (fMRI)

so far in the limbic insular cortex, anterior cingulate cortex and amygdala (outlined in Herigstad et al. (2011)). This limbic system involvement highlights affective components of breathlessness, where factors such as emotion and attention can also modulate the perception of breathlessness (De Peuter et al., 2004). Many emotive, cognitive, contextual and physiological factors can weigh in on the perception of breathlessness, in addition to the pathophysiology of a disease (for a full review see Hayen et al. (2013b)). However, a complete understanding of the mechanisms of breathlessness has not yet been deciphered (Nishino, 2011), including how structures such as the PAG can modulate ascending and descending respiratory information. Interestingly, a study by Brannan et al. (2001) used positron emission tomography (PET) imaging with a hypercapnia-induced hyperventilation stimulus in healthy individuals, and the activated response network included the pons, midbrain (including the PAG) and hypothalamus, in conjunction with limbic and paralimbic areas. While it must be noted that the large voxels associated with PET imaging limit the confidence of the localisation of activation to within the PAG, this study supports the notion that the midbrain is intricately involved in the integration of breathlessness sensations. Additionally, an fMRI study by Pattinson et al. (2009b) found a profoundly reduced urge to breathe score associated with voluntary breath holds following infusion of the drug remifentinal, and an associated decrease in activation of the PAG. These studies are the first implications that the PAG may be involved in the pathway of breathlessness perception, although these imaging techniques do not have the resolution to dissociate the columns of the PAG.

1.4.1 Conditioned breathlessness anxiety

Conditioning is a process of learning an association between two unrelated stimuli, such that a previously neutral stimulus may then evoke a fearful response (Pavlov and Anrep, 2003). For sufferers of breathlessness, the learned associations between environmental cues (such as climbing the stairs) and the fearful sensations of breathlessness can further perpetuate debilitating anxiety. This anxiety can lead to panic and ultimately activity avoidance (Hill et al., 2004; Lansing et al., 2009), meaning that the effects of breathlessness extend beyond just sensation management during the stimulus. Therefore, to fully understand breathlessness, we need to investigate the brain networks involved with both the management of breathlessness sensations, and the anticipatory network employed during a conditioned response to impending breathlessness. Understanding the relationships between these two conditions, as well as their contribution(s) to perception of breathlessness intensity and anxiety may help us to better target treatments and management of breathlessness

in patients with chronic respiratory disease.

Our understanding of fear conditioning has been substantially enhanced by modern neuroimaging techniques. Despite differences in conditioning paradigms, a consistent network of fear-related brain areas has been identified, including the amygdala, insula, and anterior cingulate cortex (Sehlmeyer et al., 2009). However, the ability to investigate the contribution of smaller nuclei, such as the columns of the PAG, to this fear-conditioning network is often limited in neuroimaging by resolution and statistical power. It is possible that the PAG columns may have fundamental roles within this network, and may be key contributors to misappropriated threat perception of breathlessness.

1.4.2 Breathlessness exposure and adaptations of the PAG

The ability of brain networks to adapt is imperative to maintain function throughout changing environments. The term 'plasticity' refers to the brain's ability to modify neuronal networks, often in conjunction with changes in behaviour. Brain plasticity is due to individual physical experiences and learning (Amunts et al., 1997), even beyond the major brain developments that occur throughout adolescence (Kolb and Whishaw, 1998). The neuronal modifications and adaptations can include changes in metabolic activity, increases in dendritic length, changes in spine density, synapse formation or increased glial cell activity (Kolb and Whishaw, 1998). Respiratory networks have been shown to exhibit plasticity as a result of stimuli such as intermittent hypoxia (Mitchell et al., 2001), hypercapnia (Baker et al., 2001), exercise (Turner et al., 1997), neural injury (Golder et al., 2001), and conditioning to a respiratory response (Gallego et al., 2001). These respiratory network adaptations serve to maintain the regulation of breathing in the face of development, changing environments or disease (Feldman et al., 2003).

Patients who suffer from repeated bouts of breathlessness may evoke plasticity within the pathways of respiratory sensation. In chronic pain patients, states of persistent hyperalgesia are thought to result from a 'central sensitisation' of the pain network; when cellular changes occur in the pain perception pathway. The PAG has been identified in descending pathways that facilitate pain transmission in hyperalgesia, and thus suggested to play a role in central sensitisation to pain (Gwilym et al., 2009; Lee et al., 2008; Zambreanu et al., 2005). It is possible that the PAG may play a similar role in sensitisation to breathlessness as that suggested within the pain network. Interestingly, a voxel-based morphometry MRI study found relative increases in midbrain grey matter of patients with panic disorder (Uchida et al., 2008), and while one fMRI imaging study compared breathlessness activations in the PAG between asthmatics and controls (von Leupoldt et al., 2009), any

differences in groups could not be interpreted due to inconsistencies in respiratory stimuli. Further research is needed to accurately investigate any differences in PAG activation during perception in those patients who are chronically exposed to threatening sensations of breathlessness. More specifically, if the proposed role of the PAG columns in the behavioural responses to threat perception applies in humans, it may be possible that breathlessness perception includes a heightened PAG response in these patients. Understanding the role of the PAG and its subdivisions in the modulation of breathlessness sensations may reveal a potential drug target for future treatments strategies in patients who experience debilitating sensations of breathlessness.

Currently, the most effective treatment for breathlessness in COPD is pulmonary rehabilitation, which is usually delivered as a 6 week course of exercise and education. Pulmonary rehabilitation does not affect lung function, but is thought to mediate its effects by desensitising and reducing the threat value of respiratory sensations (Brenes, 2003; Janssens et al., 2011b; Emery, 1994; Ries et al., 1995). With pulmonary rehabilitation, breathlessness related anxiety is reduced more than its physical intensity (Carrieri-Kohlman et al., 2001, 1996), and the magnitude of fear of breathlessness assessed prior to pulmonary rehabilitation predicts treatment success (Janssens et al., 2011b). It is thought that repeated exposure to "safe" breathlessness during pulmonary rehabilitation is what reduces its threat value, changing the underlying brain networks of breathlessness anxiety.

The act of exercise training in pulmonary rehabilitation may provide both positive breathlessness associations, and enhance this conditioning process. Gallego et al. (2001) suggested that learning processes underlie adaptations in respiratory control, and exercise is known to enhance general learning processes. This is supported by an increase in hippocampal neurogenesis following exercise training, associated with increased serum levels of brain derived neurotrophic factor (Erickson et al., 2011) and also possibly mediated by the exercise-induced increase in circulating insulin-like growth factor (Trejo et al., 2001). Therefore, exercise may be a key component within pulmonary rehabilitation to re-establish perception and anxiety of breathlessness, which may be determined by cortical adaptations occurring in both the cortex and columns of the PAG.

Performing repeated bouts of exercise involves repeated changes in respiration and respiratory stress. This training is known to evoke adaptations within the respiratory muscles themselves, and animal models have begun to provide specific evidence for correlating respiratory network plasticity. Notably, it has been found that chronic exercise training can induce structural remodelling in cardiorespiratory areas of the brain and brainstem, including the PAG (Ichiyama et al., 2002; Nelson et al., 2005). A decrease in dendritic connections of the PAG and other cardiorespiratory areas in the cortex and brainstem was found following

85 or 120 days of voluntary training in rats, and detraining reversed these adaptations (Nelson and Iwamoto, 2006). Furthermore, activation of the caudal hypothalamus, PAG and other cardiorespiratory centres in the rat diencephalon and brainstem were also reduced during a bout of submaximal exercise (as indicated by c-Fos labelling), following 80-100 days of exercise training (Ichiyama et al., 2002). These results imply plasticity of the PAG as a result of exercise training, although they cannot determine whether these changes are associated with altered perceptions of breathlessness.

1.5 Functional imaging of the PAG during breathlessness

A variety of imaging techniques exist to examine brain structure and function. The inventions of X-ray computerised axial tomography (CAT) and positron emission tomography (PET) in the in the 1970's were revolutionary in brain imaging, but both require the use of radioactive contrast material to determine the structure (CAT, PET) or function (PET) of the brain. However, a brain scanning technique that does not require radiation and instead utilises the magnetic properties of brain tissue (magnetic resonance imaging; MRI) was introduced in the 1980's, and quickly became the most widely-used imaging modality. However, despite the advantages of MRI for it's non-invasive nature, the population of people who can be scanned is restricted to those with no pacemakers or electrical implants, no (or non-ferrous) metallic implants and those who can lie still and flat on their back for the scan (usually 30 to 60 minutes).

1.5.1 Overview of MRI

MRI is a non-invasive method of brain scanning, manipulating magnetic properties within tissues to image the structure or function of the brain. The change in neuronal activity within areas of the brain can be approximated using functional MRI (fMRI). As neurons increase (or decrease) their firing rate, the subsequent change in the metabolic demand of the cells induces an change in blood flow and supply of metabolic oxygen to those neurons (Belliveau et al., 1991; Ogawa et al., 1992; Kwong et al., 1992). For increased neuronal firing, a local oversupply of blood results in an increased ratio of oxygenated to deoxygenated haemoglobin, and a change in the local magnetic properties within a tissue. This change in magnetism as a result of metabolic and blood flow changes gives us the blood oxygen level dependent (BOLD) contrast, and a non-invasive way of (indirectly) measuring changes in brain activity. When a subject performs a task inside the scanner, the correlating changes in BOLD from baseline can approximate changes in neuronal activity

in local areas of the brain associated with that task. The changes in signal are measured within 'voxels' (3 dimensional pixels) in the brain, and when larger static magnetic fields (B0) are used, more signal within the brain tissue allows for finer resolution and smaller voxels to better differentiate brain structures. Typically available scanning strengths are either 1.5 or 3 Tesla (B0 field strength), with voxel resolutions of 2-3 mm^3 or above. With the recent introduction of 7 Tesla MRI, functional resolutions can now be pushed to 1 mm^3, opening up the possibility of differentiating divisions of small nuclei such as the columns of the PAG.

1.5.2 Breathlessness within MRI

Breathlessness is a multidimensional sensation that is difficult to reproduce within the confines of an fMRI protocol. While it is possible to exercise in a supine position on a recumbent bicycle in an attempt to produce breathlessness, the movement induced by this task will mask all but the largest of BOLD activity within the brain. Alternatively, changes in hypercapnia can induce hyperventilation and subjective feelings of 'air hunger', which could be used to induce feelings of breathlessness. However, this is not possible with BOLD imaging as the cerebral vasodilatory effects of increased arterial pressure of carbon dioxide (PCO_2) will mask the local BOLD changes in functioning brain structures. Finally, an alternative stimulus that induces increased ventilatory effort and a simulation of breathlessness is the use of inspiratory resistive loading. Inspiring against an external resistor requires increased ventilatory work for adequate ventilation, and has been shown to induce a stable administration of respiratory discomfort for laboratory studies of breathlessness (Hayen et al., 2015). As discussed previously, a fundamental aspect of clinical breathlessness is the cued anticipation and threat perception of an impending aversive breathing stimulus. Therefore, as a model of breathlessness in the latter studies of this Thesis, we conditioned subjects to associate neutral stimuli to upcoming inspiratory loading, allowing us to investigate the PAG and wider cortex during both the anticipation and perception of the aversive respiratory stimulus.

1.6 Conclusion

The current literature has identified the columns of the PAG to be involved with respiratory control in animals, and it is hypothesised that these columns are differentially involved in the behavioural responses to different forms of threat. Therefore, the PAG is an ideal candidate in the perceptual and response pathways to the respiratory threat of breathless-

ness. Furthermore, due to the known plasticity of the PAG, the reduction in breathlessness anxiety found with exercise training in patients with chronic lung disease may be linked to underlying changes in the columns of the PAG within this breathlessness network.

1.7 Thesis outline, aims and hypotheses

The aim of this Thesis was to investigate the roles of the PAG columns in human respiratory control and perceptions of breathlessness. From the animal literature and preliminary findings in humans we hypothesise that the columns of the PAG will play important and distinctive roles within the sensation of ventilatory signals and the threat perception of breathlessness, with plastic changes evoked by exercise underlying alterations in breathlessness perception in health and disease. Therefore, in this Thesis we conducted a healthy volunteer investigation of the columns of the PAG in respiratory control and breathlessness, using the following series of studies:

1. Development of an fMRI protocol to identify activity in the columns of the human PAG during respiratory tasks using ultra high-field 7 T fMRI (Chapter 2).

2. Investigation of the roles of the PAG columns at high resolution in both conditioned anticipation and during breathlessness (Chapter 3)

3. Investigation of the place of the PAG columns within the wider cortical breathlessness network (Chapter 5), and any potential differences in subjective perception of breathlessness (Chapter 4) and associated changes in the function and connectivity of the PAG columns (Chapter 5) corresponding with exposure to exercise, using comparisons between of a group of endurance athletes and matched sedentary controls.

In the final Chapter of this Thesis (Chapter 6) we discuss the findings of these three studies, outlining their relevance and how they extend on the current animal and human literature of respiratory control and breathlessness.

Chapter 2

Functional subdivision of the human PAG in breath holding

2.1 Abstract

The periaqueductal grey (PAG) is a nucleus within the midbrain, and evidence from animal models has identified its role in many homeostatic systems including respiration. While the PAG has been extensively studied in animals, and has been identified previously in human imaging work (Corfield et al., 2005; Topolovec et al., 2004; Gozal et al., 1995; Pattinson et al., 2009b), attempting to localise respiratory-related activity to the columns of the human PAG has not yet to our knowledge been attempted. Animal models have also demonstrated a columnar structure that subdivides the PAG into four columns on each side, and these subdivisions have different functions with regard to respiration. In this Chapter we used ultra-high field functional MRI (7 T) to image the brainstem and superior cortical areas at high resolution (1 mm^3 voxels), aiming to identify activation within the columns of the PAG associated with respiratory control. Our results showed deactivation in the lateral and dorsomedial columns of the PAG corresponding with short ($<$10 s) breath holds, along with cortical activations consistent with previous respiratory imaging studies. These results demonstrate the involvement of the lateral and dorsomedial PAG in the network of conscious respiratory control for the first time in humans. This Chapter also reveals the opportunities of 7 T functional MRI for non-invasively investigating human brainstem nuclei at high-resolutions.

2.2 Introduction

The study of respiratory control is largely focused on the nuclei of the respiratory rhythm generators in the medulla, whilst suprapontine control of respiration is less well understood. The midbrain periaqueductal grey (PAG) is located at the junction of descending efferent commands and ascending sensory information, and has been suggested by animal models to participate within the localised pathway of respiratory response (Kabat, 1935; Subramanian et al., 2008; Subramanian, 2012). The PAG has been proposed to be subdivided into four columns on each side; ventrolateral (vlPAG), lateral (lPAG), dorsolateral (dlPAG) and dorsomedial (dmPAG) (Bandler and Shipley, 1994; Dampney et al., 2013; Subramanian et al., 2008; Subramanian, 2012). Direct excitation of these columns in animals has revealed distinct respiratory functions, such as irregular breathing with the vlPAG, prolonged inspirations, expirations and vocalisations from the lPAG, active breathing and tachypnea from the dlPAG, and slow, deep breathing from the dmPAG (Subramanian et al., 2008; Subramanian, 2012).

Whilst animal models allow detailed investigation of functional neuroanatomy, subsequent studies in humans are essential to understand the role of these PAG subdivisions. Human respiratory control networks cannot be assumed to match those derived from animals. Additionally, humans allow the study of conscious control of breathing with the addition of subjective feedback, which is not possible in animals. Understanding these respiratory networks is imperative for effective treatment of breathing disorders, such as breathlessness from chronic obstructive pulmonary disease and heart failure (Hayen et al., 2013b; Herigstad et al., 2011), sleep disordered breathing (Morrell et al., 2000), and the dangerous respiratory depression associated with opioid painkillers (Pattinson et al., 2009b).

Functional magnetic resonance imaging (fMRI) is a non-invasive technique that allows high-resolution functional imaging in humans (2–3 mm^3 voxels at 3 T). The recent introduction of ultra-high-field fMRI at 7 Tesla (7 T) vastly improves the signal-to-noise ratio of previous imaging, potentiating even higher resolution functional imaging ($<$2 mm^3) and the ability to specifically investigate small nuclei such as the subdivisions of the PAG, previously not possible at 3 T. However, 7 T imaging requires added methodological considerations during both scanning and analysis. Greater B0 inhomogeneities at 7 T cause increased distortion and drop-out during echo-planar imaging (EPI), and increases in resolution require longer acquisition times (TR) and decreases in temporal signal-to-noise. Additionally, high resolution functional scanning may reveal greater structural and functional differences between individuals, amplifying the importance of image registration for successful group statistical analysis.

Using MRI to investigate respiratory control presents further methodological challenges and requires additional considerations. Arterial pressure of carbon dioxide ($PaCO_2$) is a potent vasodilator of cerebral vessels, and thus changes in $PaCO_2$ often induced by respiratory challenges confound the blood oxygen level dependent (BOLD) signal (Pattinson et al., 2009a,b). Additionally, bulk susceptibility variations in the lungs during the respiratory cycle cause changes in the B0 magnetic field, producing physiological noise related to respiratory changes (McKay et al., 2008; Raj et al., 2001; Pattinson et al., 2009a). Finally, the location of the brainstem close to arteries and pulsating fluid-filled spaces (due to cardiac and respiratory cycles) (Cohen et al., 2002; Brookes et al., 2013) results in a particular susceptibility to physiological noise artifacts, yet it is of great importance as it houses many respiratory control centres.

2.2.1 Hypotheses

In this study we used 7 T scanning to investigate the role of the subdivisions of the PAG in short respiratory tasks, taking careful consideration of respiratory imaging confounds. Based on previous work in animals, we hypothesised that BOLD signal changes within the lPAG and dmPAG (associated with prolonged expirations and depressed breathing) would be associated with the inhibitory respiratory tasks of breath holds and vocalisations, but not associated with a simple sensory and motor task.

2.3 Methods

2.3.1 Subjects

The Oxfordshire Clinical Research Ethics Committee approved the study and subjects gave written, informed consent. Sixteen healthy, right-handed volunteers (10 males, 6 females; mean age $\pm$ SD, 28 $\pm$ 7 years) undertook one training session, followed immediately by one MRI scanning session. One subject was excluded from the analysis due to an inability to comply with experimental protocol. Prior to scanning, all subjects were screened for any contraindications to magnetic resonance imaging at 7 T.

2.3.2 Stimuli and tasks

During the BOLD scan, subjects performed 14 repeats of the following tasks: expiratory breath hold, vocalisation and the functional localiser finger and thumb opposition task (described to subjects as "finger tapping"; see explanation under **Functional localiser** below).

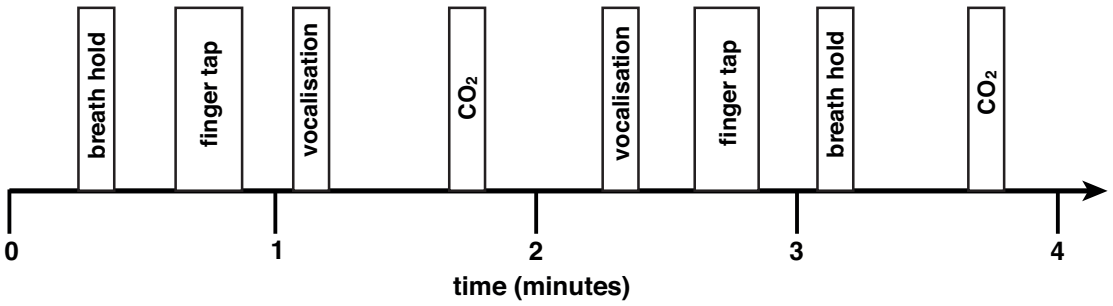

Figure 2.1: Example four minutes of the BOLD functional task, repeated throughout the acquisition. The order of the breath holds and vocalisations was semi-randomised between the finger opposition and CO_2 stimuli.

Carbon dioxide (CO_2) challenges were also interspersed between stimuli Changes in ventilation due to respiratory tasks can often cause increases in $PaCO_2$ (hypercapnia), which is a potent modulator of cerebral vessels and resultant cerebral blood flow (Cohen et al., 2002). Therefore, CO_2 challenges were administered to dissociate the changes in global BOLD signal due to changes in arterial pressure of CO_2 from the local BOLD signal changes correlating to activity associated with breath holds and vocalisations (Pattinson et al., 2009a,b). This paradigm was adapted from previous breath hold research (McKay et al., 2008; Pattinson et al., 2009a). Cues for these tasks were presented on the screen as the words 'HOLD', 'SING' and 'TAP' ('REST' was displayed for the remainder of the experiment, and CO_2 challenges were not indicated to subjects), in white letters on a black background. During the training session, the subjects had a chance to practice each of the tasks under observation. The instructions for the breath hold were to stop breathing at the end of the current breath, maintaining the hold until the 'HOLD' cue was exchanged for 'REST'. At the termination of the breath hold, the subject was asked to breathe out any remaining air in their lungs for an end-tidal CO_2 reading ($P_{ET}CO_2$; taken as an approximation for $PaCO_2$). The instructions for the vocalisation were to produce a closed-mouth single note from the top of the next breath, for the duration of the 'SING' cue. Both the 'HOLD' and 'SING' cues were presented for duration of 10 s; therefore the tasks were each less than 10 s. The finger opposition task consisted of an opposition movement conducted with the right hand, and the 'TAP' cue was presented for 15 s. Each of the three tasks was repeated 14 times within the BOLD scan of each subject.

Functional localiser Due to the size and location of the PAG, coupled with high resolution (1 mm^3 voxels) scanning, accurate registration in the cortex and brainstem was prioritised in all studies of this Thesis. A functional localiser task of finger opposition was included in each respiratory functional scan. It is well known that the cuneate nucleus of the medulla is a sensory nucleus in the fine touch and proprioception pathway, prior to decussation (Craven, 2011). Therefore, activation of the ipsilateral cuneate associated with the finger opposition task was used by Pattinson et al. (2009b), as a functional localiser to provide confidence in the precision of brainstem registrations. We repeated this task in the present study, to validate our methodology and assure the accuracy of the registration of the 1 mm^3 functional images.

2.3.3 Breathing system

A breathing system was used to allow the administration of small CO_2 challenges mixed with room air, via a venturi entrainment system (Figure 2.2). During scanning, medical air was administered through a loose fitting venturi mask (Ventimask, Intersurgical Ltd, Berkshire, UK) with a 1:1 entrainment ratio of compressed gas : room air. Gas was delivered to the mask a rate of 20 L/min, and the mask was designed to entrain an equivalent amount of room air. The resulting high gas flow rate delivered by this system (40 L/min) minimises rebreathing of expired gases. The ventimask is loose fitting and therefore considerably more comfortable than a tight fitting mask, but its predictable gas delivery characteristics allows control of end-tidal gases in the volunteer. For administration of short CO_2 challenges during the functional scan, medical air was substituted for a CO_2 mixture (10% CO_2, 21% O_2, balance nitrogen) at 20 L/min for periods of 10 seconds, the entrainment system meant that approximately 5% CO_2 was delivered to the face mask. The CO_2 challenges aimed to elevate $P_{ET}CO_2$ (taken as an indicator of $PaCO_2$) by approximately 0.8%, to match elevations caused by breath holds and vocalisations.

2.3.4 Physiological measurements

Physiological measures were recorded continuously during the training session and MRI scan. Chest movements were measured using respiratory bellows surrounding the chest at the approximate level of the 10th rib, and heart rate was measured using a pulse oximeter (9500 Multigas Monitor, MR Equipment Corp., NY, USA). $P_{ET}CO_2$ was sampled via nasal cannula, and subjects were asked to breathe through their nose (Salter Labs, California, USA). Expired gases were determined using a rapidly-responding gas analyser (CD-3A; AEI Technologies, Pittsburgh, USA). All physiological devices were connected to a data

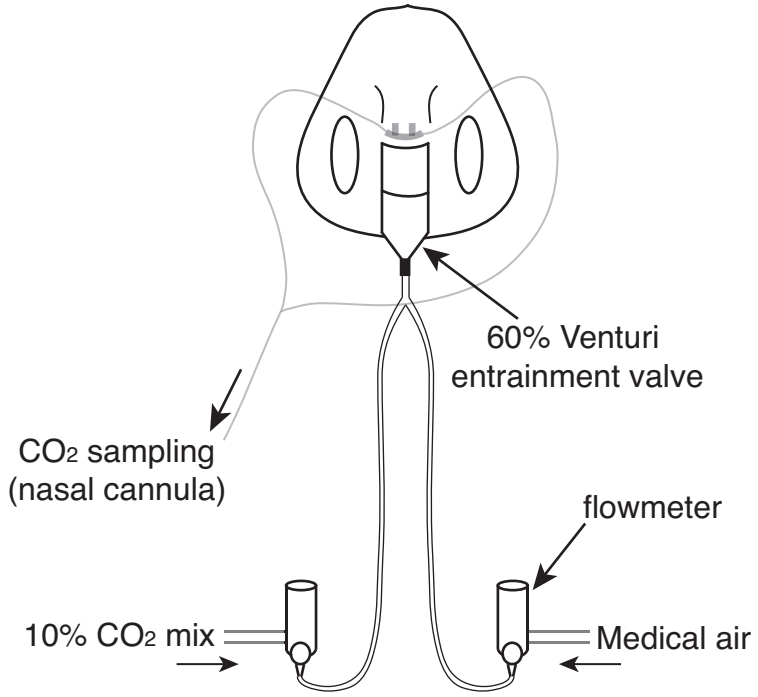

Figure 2.2: Schematic diagram of the venturi mask used in the breathing system.

acquisition device (MP150; Biopac Systems Inc., California, USA) coupled to a desktop computer with recording software (AcKnowledge 4.2; Biopac Systems Inc., California, USA).

2.3.5 MRI scanning sequences

MRI was performed with a 7 T Siemens Magnetom scanner, with 70 mT/m gradient strength and a 32 channel Rx, single channel birdcage Tx head coil (Nova Medical) for this and all following studies.

2.3.5.1 Brainstem BOLD scanning

A T2*-weighted, gradient echo EPI was used for functional scanning. To allow high resolution (1 mm^3) scanning, a reduced field of view (FOV) was used, with a coronal-oblique slice centred over the brainstem and superior cortical structures (Figure 2.3). The FOV comprised 54 coronal-oblique slices (sequence parameters: TE, 24 ms; TR, 5 s; flip angle, 90°; voxel size, 1 x 1 x 1 mm; field of view, 192 mm; GRAPPA factor, 3; echo spacing, 1 ms; slice acquisition order, descending), with 333 volumes acquired (scan duration, 28 mins 10 s).

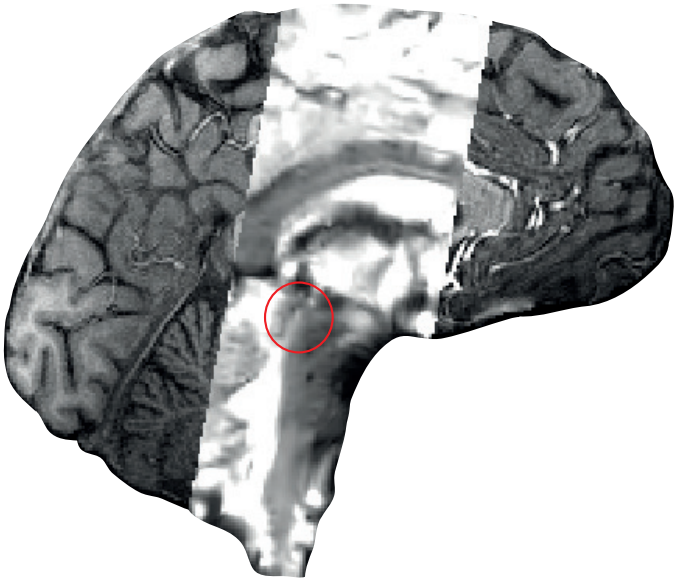

Figure 2.3: Functional scan resampled into structural space. The area of interest, the periaqueductal gray, is circled in red.

2.3.5.2 Structural scanning

A T1-weighted structural scan (MPRAGE, sequence parameters: TE, 2.96 ms; TR, 2200 ms; flip angle, 7°; voxel size, 0.7 x 0.7 x 0.7 mm; field of view, 224 mm; inversion time, 1050 ms; bandwidth; 240 Hz/Px) was acquired. This scan was used for registration of functional images.

2.3.5.3 Additional scanning

A single volume whole brain EPI was also acquired, with matched sequence parameters to the functional scan and extended slices (128 slices), to assist with registration. Fieldmap scans (sequence parameters: TE1, 4.08 ms; TE2, 5.1 ms; TR, 620 ms; flip angle, 39°; voxel size, 2 x 2 x 2 mm) of the B0 field were also acquired to assist distortion-correction.

2.3.6 Analysis

2.3.6.1 Preprocessing

Image preprocessing was performed using the Oxford Centre for Functional Magnetic Resonance Imaging of the Brain Software Library (FMRIB, Oxford, UK; FSL version 5.0.8; http://www.fmrib.ox.ac.uk/fsl/). The following processing methods were used prior to sta-

tistical analysis: motion correction and motion parameter recording (MCFLIRT (Jenkinson et al., 2002)), removal of the non-brain structures (skull and surrounding tissue) (BET (Smith, 2002)), spatial smoothing using a full-width half-maximum Gaussian kernel of 2 mm, and high-pass temporal filtering (Gaussian-weighted least-squares straight line fitting; 120 s). B0 field unwarping was conducted with a combination of FUGUE and BBR (Boundary-Based-Registration; part of FEAT: FMRI Expert Analysis Tool, version 6.0 (Greve and Fischl, 2009)).

2.3.6.2 Image registration

Careful attention was paid to image registration, as the finer resolution afforded by 7 T MRI requires greater registration accuracy for group statistics to be possible. After preprocessing, the functional scans were registered to the MNI152 (1 mm^3) standard space (average T1 brain image constructed from 152 normal subjects at the Montreal Neurological Institute (MNI), Montreal, QC, Canada) using a three-step process:

- Linear registration (FLIRT) with 6 DOF was used to align the partial FOV scan to the whole-brain EPI image (Jenkinson et al., 2002).
- Registration of subjects whole-brain EPI to T1 structural image was conducted using BBR (6 DOF) with (nonlinear) fieldmap distortion-correction (Greve and Fischl, 2009).
- Registration of the subjects T1 structural scan to 1 mm standard space was performed using an affine transformation followed by nonlinear registration (FNIRT) (Andersson et al., 2007).

2.3.6.3 Voxelwise analysis

fMRI data processing was performed using FEAT (FMRI Expert Analysis Tool), version 6.0, part of FSL (FMRIBs Software Library; www.fmrib.ox.ac.uk/fsl). Previous research has indicated that variations in the haemodynamic response function (HRF) are apparent throughout the brainstem and cortex (Woolrich et al., 2004a; Devonshire et al., 2012), and between subjects (Handwerker et al., 2004). To account for some of the noise as a result of possible delays in the HRF or slice-timing differences, we used an optimal basis set of three waveforms (FLOBS: FMRIBs Linear Optimal Basis Sets, default FLOBS supplied in FSL (Woolrich et al., 2004b)), instead of the standard gamma waveform. This models the changes induced by altered HRFs or slice-timing, but does induce some bias into the estimation of the main effect size. This bias takes the form of an underestimation of the

effect size, which is a conservative error that affects the statistical power, and therefore will not inflate the false positive rate. The second and third FLOBS waveforms, which model the temporal and dispersion derivatives, were orthogonalised to the first waveform, of which the parameter estimate was then passed up to the higher level to be used in group analysis. Time-series statistical analysis was performed using FILM, with local autocorrelation correction (Woolrich et al., 2001). The general linear model displayed in Figure 2.4 displays the explanatory variables (EVs) used to regress the components of the signal within the functional scan, including breath holding, vocalisations and finger opposition. $P_{ET}CO_2$ was included as an additional regressor, de-correlating the CO_2 induced BOLD changes from the respiratory stimuli throughout the functional scan. This trace was formed by linearly interpolating between the expired CO_2 peaks.

2.3.6.4 Retrospective image correction (RETROICOR)

One method for accounting for physiological noise is to retrospectively estimate and regress out noise from fMRI data using physiological recordings (Glover et al., 2000) (for a full review of physiological noise methods see (Brookes et al., 2013)). The cardiac and respiratory processes that were recorded along with scanner triggers, allowed determination of cardiac and respiratory phase with each acquired slice in the imaged volume. This assigned phase is then entered into a low-order Fourier expansion (Brooks et al., 2008; Glover et al., 2000; Harvey et al., 2008) to derive time course regressors that explain potential signal changes associated with cardiac and respiratory (or interacting) processes. We generated 3 cardiac, 4 respiratory and 1 interaction regressor, according to previous model optimisation research (Harvey et al., 2008). This process is automated using FEATs PNM (Physiological Noise Modelling) tool (Glover et al., 2000). These regressors were then entered into the statistical model as noise regressors of no interest.

2.3.6.5 Group analysis

The first EV for each of the three FLOBS regressors in the voxelwise statistical analysis using basis functions was extended to calculate mean activity at a group level for each of the breath hold, vocalisation, finger opposition and $P_{ET}CO_2$, in a mixed-effects analysis using FLAME (FMRIBs Local Analysis of Mixed Effects) (Woolrich et al., 2004a). Whole brain analysis was performed, where Z (Gaussianised T/F) statistic images were thresholded using clusters determined by $Z > 2.3$ and a (corrected) cluster significance threshold of $p < 0.05$. A small-volume-corrected analysis of the PAG (as our a-priori area of interest; mask = 698 voxels) was then conducted, with the PAG mask made based on anatomical

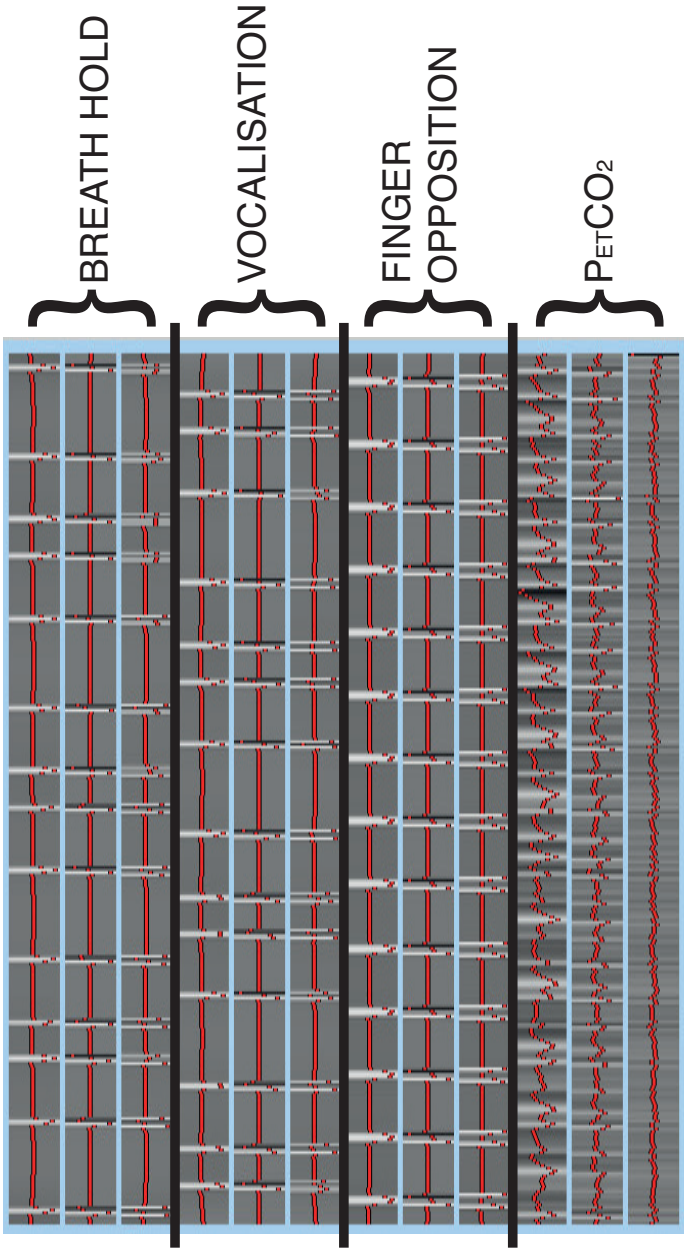

Figure 2.4: General linear model used in each single subject lower level analysis within FEAT. The EVs for each of the tasks (breath hold, vocalisation, finger opposition, and the $P_{ET}CO_2$ trace) are in sets of 3 for each of the FLOBS regressors used to model the task. The onset and duration of the breath holds and vocalisations were calculated from the recorded physiology traces, while the finger opposition onset and duration was taken from the logfile of the presented 'TAP' stimulus.

boundaries. Thresholding was conducted using both standard cluster-based thresholding and threshold-free cluster enhancement (TFCE) corrected for family-wise error. TFCE provides an alternative method to enhance cluster-like structures in an image, without a pre-determined initial cluster-forming threshold (Smith and Nichols, 2009). TFCE produces an output where voxel-wise values represent the amount of cluster-like local support, illustrating the significance of voxels within a cluster rather than the significance of the cluster as a whole, whilst maintaining strict false positive control by using permutation-based family-wise-error correction.

2.4 Results

2.4.1 Physiology

Group average heart rate (±SD) during the brainstem BOLD scanning was 65 (±11) beats per minute. An example respiratory trace is given in Figure 2.5. Baseline $P_{ET}CO_2$ (±SD) was 4.7% (0.7%), with breath holds increasing $P_{ET}CO_2$ by 0.8% (±0.2%) and 0.6% (±0.2%) with vocalisations. CO_2 challenges induced an average increase in $P_{ET}CO_2$ of 0.9% (±0.1%).

2.4.2 Periaqueductal gray analysis

The results from a small-volume family-wise-error corrected analysis of the PAG revealed significant ($p < 0.05$) deactivation in two areas correlating with the breath hold task (Figure 2.6). One of these deactivation clusters followed the lateral column on the right side of the PAG (12 voxels), and the second was located in the right caudal dorsolateral PAG (8 voxels). Uncorrected z scores within the PAG are also presented in Figure 2.6, demonstrating the deactivations extending to the inferior border of the PAG. Column locations were defined using tractography results from a recent diffusion tensor imaging study (Ezra et al., 2015). No significant activations or deactivations were found in the PAG for either vocalisation or the finger opposition task.

2.4.3 Cortex

We observed significant signal increases bilaterally in the motor cortex, supplementary motor cortex, middle cingulate and paracingulate cortices, primary sensory cortex, anterior insula and putamen (Figure 2.7). Breath holds also correlated with bilateral BOLD

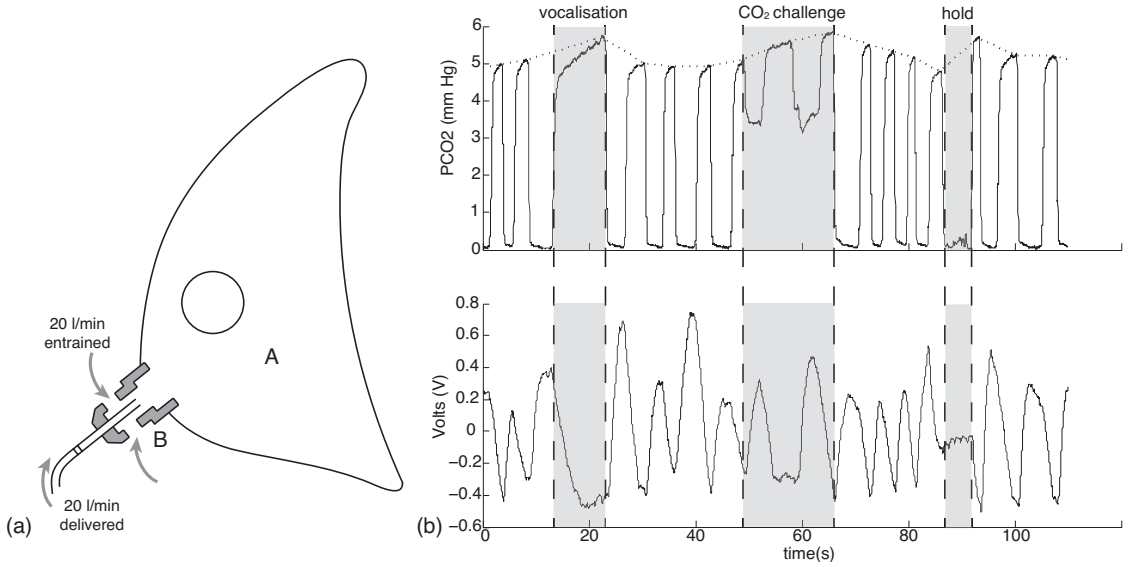

Figure 2.5: a) Schematic diagram of the venturi mask used in the breathing system. A: Loose plastic venturi mask B: Venturi entrainment device (1:1). b) A section of a respiratory trace from one subject demonstrating the tidal CO_2 trace (top) and the tidal volume trace from the bellows (bottom). The end-tidal CO_2 ($P_{ET}CO_2$) trace was formed by interpolating between the end expiration peaks (dotted line, top trace). The breath hold duration was calculated from the time between the end of expiration CO_2 trace and the beginning of the subsequent expiration trace, to minimise inclusion of head movement. The vocalisation duration was calculated from the duration between the beginning and end of a vocalisation expiration trace.

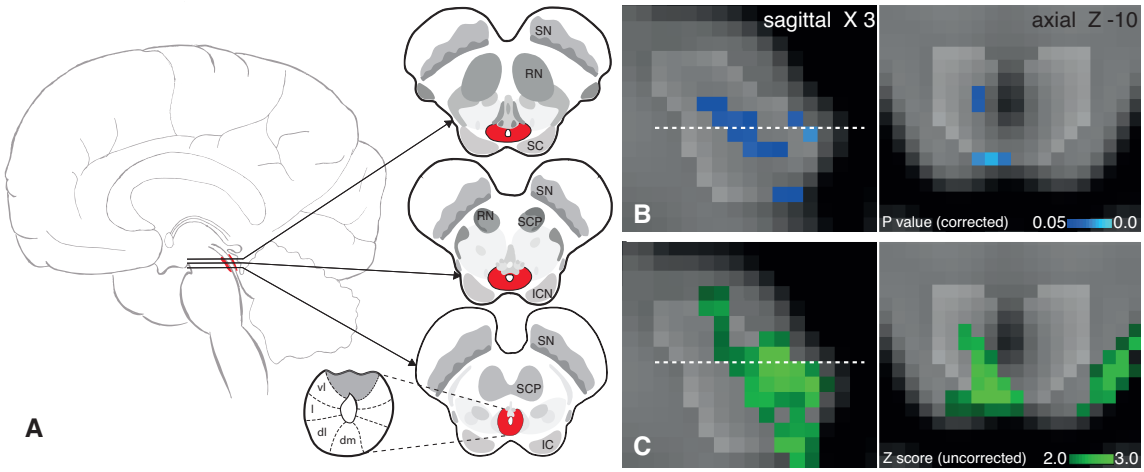

Figure 2.6: Periaqueductal gray (PAG) response to breath hold. A. Representation of the location of the PAG within the brain, three axial slices and the subdivisions of the PAG. B. Localisation of the functional decreases in BOLD signal within the PAG ($p < 0.05$; small-volume-corrected for multiple comparisons using overlaid PAG mask), where the images consist of a colour-rendered statistical map superimposed on a standard (MNI 1 mm^3) brain. Dashed line represents Z -10 location. C. Uncorrected Z score image of PAG deactivation from whole brain analysis, prior to masking. Abbreviations: SN, substantia nigra; RN, red nucleus; SC, superior colliculus; SCP, superior cerebellar peduncle; ICN, inter-colliculi nucleus; IC, inferior colliculus; vl, ventrolateral PAG, l, lateral PAG; dl, dorsolateral PAG; dm, dorsomedial PAG; sag, sagittal.

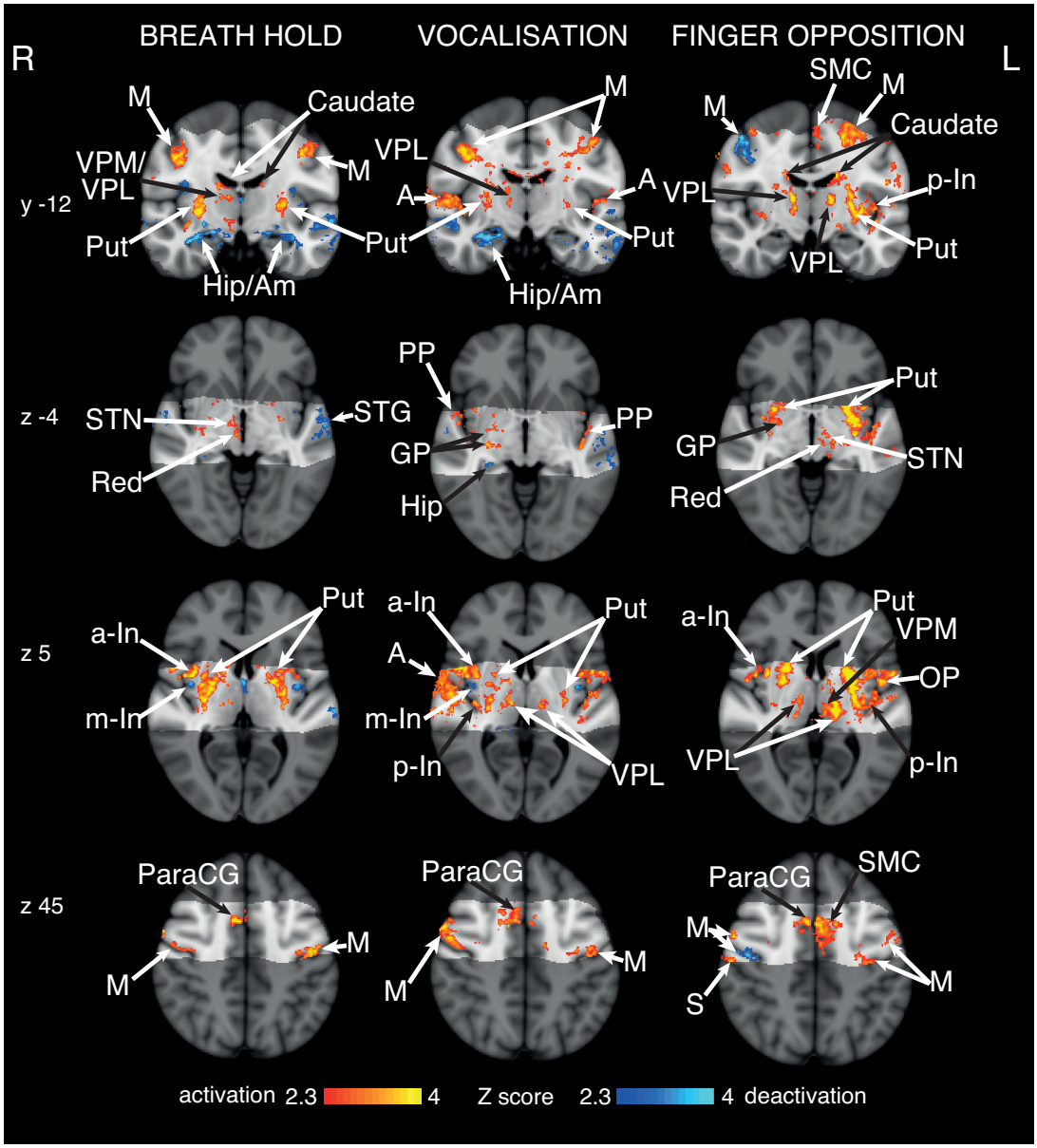

Figure 2.7: BOLD response to breath holds, vocalisations and finger opposition in 15 subjects, having accounted for CO_2-induced vasodilation. The images consist of a colour-rendered statistical map superimposed on a standard (MNI 1 mm^3) brain. The bright grey region represents the coverage of the coronal-oblique functional scan. Significant regions are displayed with a threshold $Z > 2.3$, with a cluster probability threshold of $p < 0.05$ (corrected for multiple comparisons). Abbreviations: M, motor cortex; Caudate, caudate nucleus; SMC, supplementary motor cortex; Put, putamen; A, auditory cortex; Hip hippocampus; Am, amygdala; thalamic nuclei: VPM ventral posteromedial nucleus; VPL, ventral posterolateral nucleus; MDN, medial dorsal nuclei; a-In, anterior insula; m-In, middle insula; p-In, posterior insula; PP, planum polare; STN, subthalamic nucleus; Red, Red nucleus; STG, superior temporal gyrus; GP, globus pallidus; OP, operculum; S, post central gyrus (sensory cortex); paraCG, paracingulate gyrus; activation, increase in BOLD signal; deactivation, decrease in BOLD signal. R (right) and L (left) indicate image orientation.

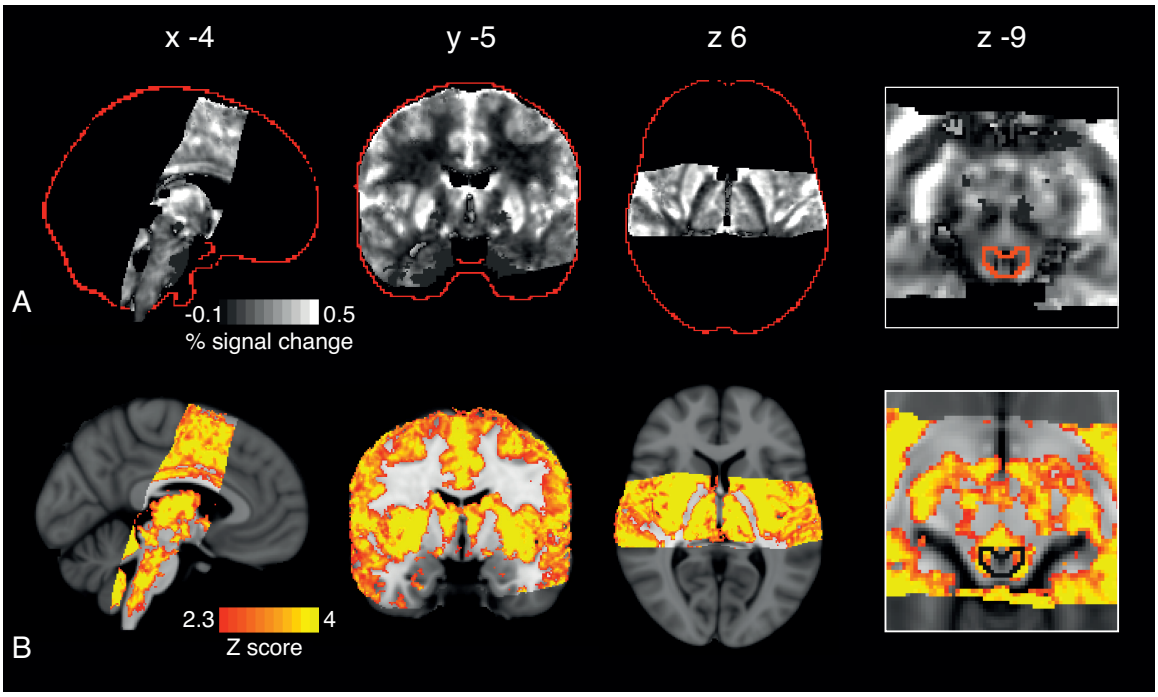

Figure 2.8: A. Global BOLD signal change correlating with changes in end tidal carbon dioxide ($P_{ET}CO_2$). The red lines indicate the edges of the the brain, derived from the MNI (1 mm^3) standard brain. Image on the right is a zoom to show signal changes within the PAG (outlined in red). B. Statistically significant generalised gray matter signal increases as a result of hypercapnia. PAG outlined in black on the far right. An end-tidal carbon dioxide ($P_{ET}CO_2$) trace was created by extrapolating between $P_{ET}CO_2$ peaks, and small hypercapnic challenges were administered during rest periods to dissociate hypercapnic effects from respiratory challenges. The images consist of a colour-rendered statistical map superimposed on a standard (MNI 1 mm^3) brain. Significant regions are displayed with a threshold $Z > 2.3$, with a cluster probability threshold of $p < 0.05$ (corrected for multiple comparisons).

signal increases in the supramarginal gyrus and caudate nucleus, whilst vocalisations correlated with right side supramarginal gyrus activation. Vocalisations were also associated with thalamic activation bilaterally in the VPL nucleus, Heschls gyrus (primary auditory cortex) and the planum polare. Conversely, breath holds were associated with right side BOLD signal increases in the thalamus (posterolateral and ventral posteromedial nuclei), subthalamic nucleus and red nucleus.

2.4.4 CO_2 challenges

The hypercapnia challenges and the resultant $P_{ET}CO_2$ regressor produced strong BOLD signal increases throughout the gray matter of the brain. Furthermore, increases in BOLD

signal correlating to the $P_{ET}CO_2$ regressor were observed within the PAG, localised to the grey matter and excluding the aqueduct (Figure 2.8).

2.4.5 Finger opposition task

Finger opposition resulted in significant signal increases bilaterally in the motor cortex (more extensive activation in the contralateral left motor cortex), supplementary motor cortex, middle cingulate and paracingulate cortices, primary sensory cortex, anterior insula cortex, operculum, caudate nucleus and putamen (Figure 2.9). Bilateral signal increases were seen in the thalamic VPL nuclei, as well as the left thalamic VPM nucleus. In addition, activations were observed in the left subthalamic and red nuclei, left pons, right (ipsilateral) cuneate nucleus of the medulla, and bilateral cerebellum (VI and VIIIa lobules).

2.5 Discussion

2.5.1 Main findings

Assuming that the human PAG has a columnar structure similar to that in animals, and corresponding with recent human neuroimaging findings (Ezra et al., 2015) (included in Appendix), we have identified respiratory-related activity that appears to be localised within the lateral and caudal dorsomedial columns of the PAG. Cortical activity associated with breath holding was consistent with previous results (Cowie and Holstege, 1992; McKay et al., 2008; Pattinson et al., 2009a), and highly localised within cortical regions. As expected, with the control sensory and motor task of finger opposition, BOLD activity was identified within the ipsilateral cuneate nucleus in the medulla, a sensory nucleus processing fine touch and proprioception, validating our methodology.

2.5.2 PAG and respiratory control

This study has demonstrated differential activity localised within the columns of the PAG (lPAG and dmPAG), correlating with the respiratory task of a breath hold. In comparison, no observable differences in any areas of the PAG were found with a respiratory vocalisation task, nor with a motor finger opposition task. This study is the first to functionally localise respiratory activity within the human PAG, with sufficient resolution (1 mm^3) to have confidence in the positions of activations in relation to the current theory of columnar subdivisions. Using a Gaussian kernel of 2 mm (FWHM) for spatial smoothing, blurring

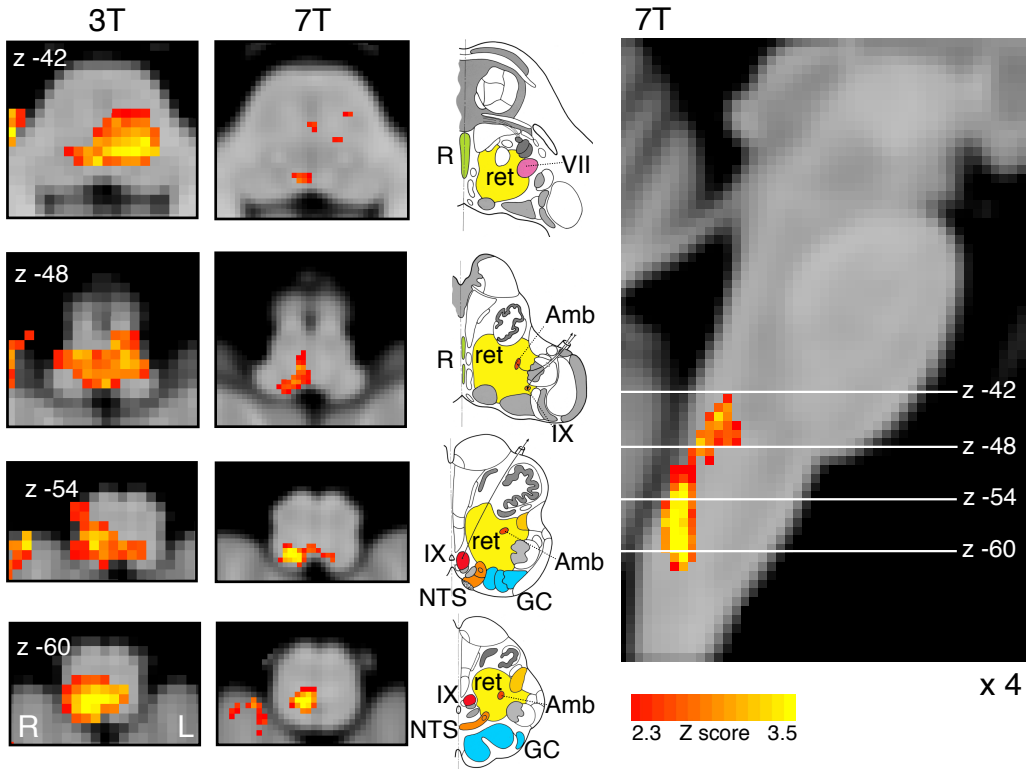

Figure 2.9: Demonstration of the use of finger opposition as a functional localiser in brainstem FMRI at 3T and at 7T, by imaging activation in the ipsilateral cuneate nucleus of the medulla (z -54). The 3T data is derived from previously-published results (Pattinson et al., 2009b). This technique provides confidence in the analysis model and registration accuracy of the current 7 T study. The images consist of a colour-rendered statistical map superimposed on a standard (MNI 1 mm^3) brain. Significant regions are displayed with a threshold $Z > 2.3$, with a cluster probability threshold of $p < 0.05$ (corrected for multiple comparisons). The sagittal image on the right displays the position of slices, for clarity only displayed from the 7T acquisition. Abbreviations: R, raphe nuclei; ret, nuclei reticularis; VII, facial nucleus; Amb, nucleus ambiguous; IX, glossopharyngeal nucleus; NTS, nucleus tractus solitaries; GC, gracile (medial) and cuneate (lateral) nuclei (in blue). R (right) and L (left) indicate image orientation. Original line drawings adapted from Duvernoy (Duvernoy, 1995)

of the BOLD signal changes within the PAG was minimised. The deactivation seen within the lPAG, in particular, follows a columnar structure that is consistent with previous work from animal models.

Whilst there have been previous neuroimaging studies reporting involvement of the PAG as a whole, the function(s) of the PAG have predominantly been linked to pain, anxiety, bladder and bowel control, and cardiovascular regulation (Linnman et al., 2012). There have been some implications of PAG involvement in respiratory control (Corfield et al., 2005; Pattinson et al., 2009b; Topolovec et al., 2004), however this research has been limited by functional resolution, extensive smoothing, or registration issues that have impeded group-level analysis, making accurate localisation to the PAG or its subdivisions impossible. In addition, significant results within the PAG have been found using statistics uncorrected for multiple comparisons (Mobbs et al., 2007), and a more recent 7 T study used a column segmentation of the PAG that is inconsistent with animal literature, and masking of the cerebral aqueduct to dissociate activity within PAG columns (Satpute et al., 2013). Therefore, the results of this study demonstrate the potential for 7 T MRI to be used to investigate the roles of the subdivisions of the PAG within respiratory control using robust statistical methodology, when careful attention is paid to registration and noise correction of functional data.

Deactivation within the PAG was localised to the lateral column and caudal section of the dorsomedial column. This activity during inhibition of ventilation is consistent with previous respiratory control experiments in animals, where these columns have been associated with ventilatory behaviours such as prolonged inspirations and expirations (lPAG), and slow, deep breathing (dmPAG). Conversely, the vlPAG and dlPAG have been associated with more active (dlPAG) and irregular (vlPAG) ventilation in animals (Subramanian et al., 2008; Subramanian, 2012). Whilst excitation of the vlPAG and lPAG in decerebrate cats has previously produced vocalisations of mews and hisses (Subramanian et al., 2008), we did not see activation in any of the PAG columns during vocalisations. It is possible that the vocalisation pathway within the cortex and brainstem is not consistent from animals to humans, or possibly that brainstem movement during vocalisations masked these activations in the current experiment.

Whilst one cannot determine from the BOLD signal whether the deactivations in the PAG represent either changes in motor drive or incoming sensory information, it has been established that the lateral PAG receives somatotopically organised spinal sensory afferents (Craven, 2011; Keay and Bandler, 2001) and could thus be involved in monitoring ventilatory feedback from the chest. Conversely, evidence exists for direct descending connections from the lateral and dorsomedial PAG to the midline medulla (Cowie and Holstege, 1992),

demonstrating the potential for involvement in descending motor commands to respiratory centres in the medulla. Ezra et al. (2015) revealed strong connectivity between the lateral column of the PAG and the primary motor and sensory cortices in humans, which supports our hypothesis of the potential role of the lPAG in either respiratory sensation or in the descending motor drive for changes in ventilation. Therefore, it is possible that the lPAG is involved with monitoring respiratory sensations from the chest as they ascend up to higher cortical areas of sensation or, together with the dmPAG, in the descending motor drive for changes in respiration.

The secondary findings of this study were that cortical activations associated with breath holding at 7 T largely agree with previous breath hold research at 3 T (Feinberg et al., 2010; McKay et al., 2008; Pattinson et al., 2009a), with a higher degree of localisation. It is possible that the cortical results were underestimated, due to slice-timing differences across the field of view with a 5 second TR. However, despite the possibly conservative nature of these results, the cortical consistency displayed with short 10 second breath holds, and additional deactivation of the lPAG and dmPAG, suggests that these PAG areas are part of the conscious breathing control network that is invoked during voluntary cessation of breathing.

2.5.3 Finger opposition task

As well as a control sensorimotor task, the finger tap analysis was used as a robust comparison between ultra-high field and lower field fMRI studies, for confidence in analysis techniques and subsequent interpretation of results. Importantly, we had a firm a priori hypothesis that localised BOLD signal increase would be seen in the ipsilateral cuneate nucleus of the medulla, which is a sensory nucleus in the fine touch and proprioception pathway (Craven, 2011). This activation was consistent with previous findings at 3 T (Figure 2.9), and demonstrates the registration accuracy within the brainstem to allow activations within small nuclei to survive group analysis. Therefore, this medullary activity was used to validate the registration and modelling in the current study. However, medullary and pontine activations previously seen with breath holds at 3 T (McKay et al., 2008; Pattinson et al., 2009b) were only apparent subthreshold in this study, and did not survive multiple comparison correction, possibly due to the reduction in signal experienced when voxel size is reduced to 1 mm^3.

2.5.4 Scanning and analysis techniques

While the use of ultra-high field MRI at 7 T permits improved spatial resolution in functional imaging, it is accompanied by a compounding of many of the challenges experienced with lower resolution imaging. The use of 7 T increases intrinsic voxel signal compared to 3 T, whilst decreasing the voxel size to 1 mm^3 reduces this signal, requiring longer scan acquisitions to amass adequate statistical power. Furthermore, acquiring 1 mm^3 voxels requires a longer repetition time (TR) compared to larger voxels for the same brain coverage. To limit the TR to 5 seconds we restricted our field of view to a coronal-oblique slice, to collect enough time points within the functional scan for adequate temporal SNR. Restricting the field of view compromises wider brain network analysis, and techniques such as parallel imaging (Arthurs and Boniface, 2002; Feinberg et al., 2010) may allow broader brain coverage in future high-resolution studies.

Previous research has shown a widespread decrease in BOLD signal with breath holds, proposed as a result of vascular effects (Thomason et al., 2005). However, as can be seen in Figure 2.7, this study found differential activation and deactivation, rather than a global decrease in BOLD signal correlating with breath holds. There are some key differences in techniques and analysis methods that may explain the possible discrepancies between the current study and previous fMRI investigations. Firstly, the breath hold used in the current study is an end-of-breath hold, which produces a different chest diameter in the scanner bore, and will result in differences in intrathoracic pressures and physiological noise in the B0 field. Further, Thomason et al. (2005) postulated that the decrease in BOLD signal resulted from a decrease in intrathoracic pressure and cerebral blood flow (CBF), while a recent paper by Hayen et al. (2013a) showed that a decrease in intrathoracic pressure (while maintaining stable end-tidal CO_2) actually resulted in a small increase in CBF. Additionally, Thomason et al. (2005) did not report any measurements of $P_{ET}CO_2$, and thus the effect of hypercapnia in this study cannot be fully explored. Therefore, while there are significant challenges in dissociating task-specific fMRI signal from residual vascular effects of breath holds, we feel the techniques used in the current study have minimised the influence of this task-related noise.

This novel study of the PAG columns in respiratory control is both encouraging in its respiratory results, and a useful methodological development for high-resolution imaging practice. To improve the quality of our data, in the following study (Chapter 3) we chose to increase our voxel size from 1 to 1.5 mm^3, as the intrinsic spatial SNR of 1 mm^3 voxels may not be great enough to detect more complicated functional changes such as those involved in the perception of breathlessness. Increasing the voxel size (whilst remaining centred over the PAG with a reduced FOV) also allows a shortened TR for increased temporal SNR, and

aids registration of functional scans with improved alignment of larger voxels. Lastly, we chose to continue to include the finger opposition task as a functional localiser, as this has proven extremely useful for confirming both accurate registration and task modelling.

2.6 Conclusions

Imaging the brainstem using 7 T MRI is known to be extremely challenging. However, with rigorous physiological noise modelling, consideration of different HRF within the brainstem, and careful attention to distortion minimisation, we have successfully imaged respiratory-related activity within columns of the PAG. In particular, reductions in the BOLD signal within the lPAG and dmPAG was associated with short breath holds, consistent with animal research. Therefore, these results indicate that the lateral and dorsomedial PAG columns are activated as part of the volitional respiratory control network, and are involved with either the motor inhibition or sensation of depressed ventilation, or both. This study demonstrates that 7 T MRI can successfully be used for functional investigations into brainstem respiratory nuclei, and that the columns of the PAG may have an important role within the respiratory control network in humans.

To extend these findings from respiratory control into investigations of breathlessness, in the following Chapter (Chapter 3) we used an aversive inspiratory resistance stimulus in place of simple respiratory manoeuvres. Both anticipation of resistance and resistance itself were of particular interest, as the anticipation of the impending threat of breathlessness may have differential involvement of the PAG compared to the response of the aversive respiratory stimulus itself.

Chapter 3

Conditioned respiratory threat in the subdivisions of the human PAG

3.1 Abstract

The sensation of life-threatening breathlessness is the most important disabling symptom of respiratory disease. The periaqueductal gray (PAG) has been suggested to be intricately involved in integrating the behavioural and respiratory response to threat in animals. Following our findings of the involvement of the columns of the PAG with simple respiratory control, here we aimed to investigate how the different columns of the PAG are involved with the perceived threat of breathlessness. In line with animal models, we tested the hypothesis that the ventrolateral PAG is involved in passive anticipation while the lateral PAG is involved in the active response during an aversive breathing stimulus. Such an understanding might reveal potential future targets for (mal)adaptation in respiratory disease. Eighteen healthy subjects were conditioned to associate three shapes with certain, uncertain or no impending inspiratory resistance in an aversive delay-conditioning paradigm, and scanned the following day using brainstem optimised functional MRI at 7 T. Our results showed decreased BOLD signal in the lPAG during resistive loaded breathing, and during anticipation BOLD signal scaled with resultant breathlessness intensity perception. Conversely, an increase in BOLD signal was seen in the vlPAG during the anticipation of resistive loaded breathing, which was reduced with a less well-conditioned anticipation cue. We propose that lPAG activity is involved with the sensorimotor active response to breathlessness, while the vlPAG lies within the threat perception network for impending breathlessness. Our results demonstrate, for the first time in humans, the differential roles of the subdivisions of the PAG in response to the respiratory threat of breathlessness.

3.2 Introduction

Continued respiratory function is crucial for sustaining life, and perceived threat to respiration can induce an integrated stress reaction and crippling anxiety to its sufferers. A potentially pivotal nucleus within the breathlessness perception pathway is the midbrain periaqueductal gray (PAG). The PAG is well situated to play a role in the threat identification and integrative response to breathlessness, as it has major cortical inputs from areas involved with emotional regulation such as medial prefrontal, insula, anterior cingulate cortices and amygdala (Beitz, 1982; Gabbott et al., 2005; Rizvi et al., 1991), and descending connections to the respiratory nuclei of the medulla (Huang et al., 2000; Sessle et al., 1981; Hayward et al., 2004). In Chapter 2 we showed that activity associated with respiratory control can be identified within columns of the human PAG, and these columns have been proposed to act within active coping strategies for escapable threat (lPAG and dlPAG), or passive coping strategies to inescapable threat (vlPAG) in animal models (Keay and Bandler, 2001; Bandler and Shipley, 1994; Bandler et al., 2000). However, the roles of the different columns in human respiratory threat perception are yet to be investigated.

Clinical populations such as those with chronic obstructive lung disease (COPD), asthma, heart failure, cancer and panic disorder suffer from debilitating breathlessness. Importantly, conditioned anticipation of environmental cues associated with breathlessness is integral to its threat detection and designated response. Misappropriated threat perception during anticipation can cause incapacitating anxiety in its own right, and may exacerbate the resultant symptoms (Porro et al., 2002; Price et al., 1999; Wager et al., 2004).

Anticipation of threatening sensations relies on cues from the environment. Conditioning is a process of learning an association between two unrelated stimuli, such that a previously neutral stimulus (conditioned stimulus, CS) may evoke anxiety due to learned associations with an aversive stimulus (unconditioned stimulus, US) (Pavlov and Anrep, 2003). Our understanding of anticipation of conditioned threat has been substantially enhanced by modern neuroimaging techniques, and despite differences in conditioning paradigms, a consistent network of brain areas has been identified, including the amygdala, insula, and anterior cingulate cortex (Sehlmeyer et al., 2009). However, despite the proposed integral role of the PAG in threat perception, the ability to investigate contributions of smaller nuclei is often limited in neuroimaging by resolution and statistical power, and thus key structures such as the PAG have not yet been investigated in humans.

The aim of this study was to investigate the roles of the PAG columns during both the perception of breathlessness and its anticipation. We used an aversive delay-conditioning paradigm to associate neutral shapes with upcoming resistive loaded breathing. To in-

vestigate if uncertainty of an aversive breathing stimulus altered the threat response, as previously reported in pain (Rhudy and Meagher, 2000; Ploghaus et al., 2003), we used three separate anticipation cues with a CS-US contingency pairing of 100%, 50% and 0%.

3.2.1 Hypotheses

In accordance with animal models, we hypothesised that the vlPAG would be active during anticipation of resistance, as threat is detected and passive coping strategies are employed to manage an upcoming inescapable stressor. Conversely, we hypothesised activity in the lPAG during inspiratory resistive loading with slowed, deep breathing, corresponding with results in animals (Subramanian et al., 2008; Subramanian, 2012) and our previous work in Chapter 2.

3.3 Methods

3.3.1 Subjects

Eighteen healthy, right-handed volunteers (12 males, 6 females; mean age $\pm$ SD, 28 $\pm$ 4 years) undertook one training session, followed by one MRI scanning session within 24 hours. Prior to scanning, all subjects were screened for any contraindications to magnetic resonance imaging at 7 T.

3.3.2 Stimuli and tasks

Subjects were trained using an aversive delay-conditioning paradigm to associate simple shapes with an aversive inspiratory resistive loading stimulus. Conditioned responses to cues that depict an upcoming respiratory stressor may motivate avoidance behaviours in patients who suffer from chronic airways disease (Ley, 1999), and may increase perception of respiratory stress if unavoidable (De Peuter et al., 2004). Therefore, conditioning a group of healthy subjects to associate neutral cues with an aversive respiratory stimulus allows us to create a platform of understanding of the underlying brain networks, from which we may better understand how patient groups with chronic airways disease deviate from these norms. Furthermore, this methodology allows us to investigate brain networks associated with both conditioned response to an upcoming aversive respiratory stimulus (resistive loading), as well as the response to the stimulus itself.

Conditioning of upcoming inspiratory resistance to neutral cues was conducted in a separate training session, between 12 and 24 hours prior to the MRI scan. The purpose

of the conditioning session was for subjects to learn to associate a different symbol (star, triangle or square; randomised order) to three breathing conditions, and the conditioned response to these symbols was then investigated by repeating the protocol with fMRI. The breathing conditions were as follows:

- Certain upcoming inspiratory resistance: symbol presentation always paired with inspiratory resistance (100% contingency pairing)
- Uncertain upcoming inspiratory resistance: symbol presentation paired with inspiratory resistance during 50% of the occasions (50% contingency pairing)
- No upcoming resistance: symbol presentation is never paired with inspiratory resistance (0% contingency pairing)

The certain or uncertain resistance symbol was presented on the screen for 30 s, which included a 5–15 s anticipation period before the resistance was applied (where applicable). The symbol depicting no upcoming resistance was presented for 20 s, and each condition was repeated 10 times in a semi-randomised order (Figure 3.1). A finger opposition task was also included in the protocol, where an opposition movement was conducted with the right hand, with the cue TAP presented for 15 s (10 repeats).

Rating scores of breathing difficulty were recorded after every symbol and at the beginning and end of the task, using a visual-analogue scale (VAS) with a sliding bar that the subjects moved between 'Not at all difficult' (0%) and 'Extremely difficult' (100%). Subjects were also asked to rate how anxious each of the symbols made them feel using a VAS between 'Not at all anxious' (0%) and 'Extremely anxious' (100%) immediately following the functional protocol. Subjects were asked to record how many hours of physical activity they typically completed per week, the intensity of the exercise (easy, moderate or intense) and what types of exercise they performed.

3.3.3 Breathing system

A breathing system was constructed to remotely administer periods of inspiratory resistance during scanning (Figure 3.2). During rest periods, compressed medical air was delivered to the breathing system and gas flow was maintained at a rate that was sufficient to allow free breathing, so that the reservoir bag never collapsed on inspiration. During inspiratory resistance, delivery of compressed air was stopped, and once the reservoir bag collapsed, inspiration was through the resistance arm of the circuit inhaling atmospheric air (see Figure 3.2 for details).

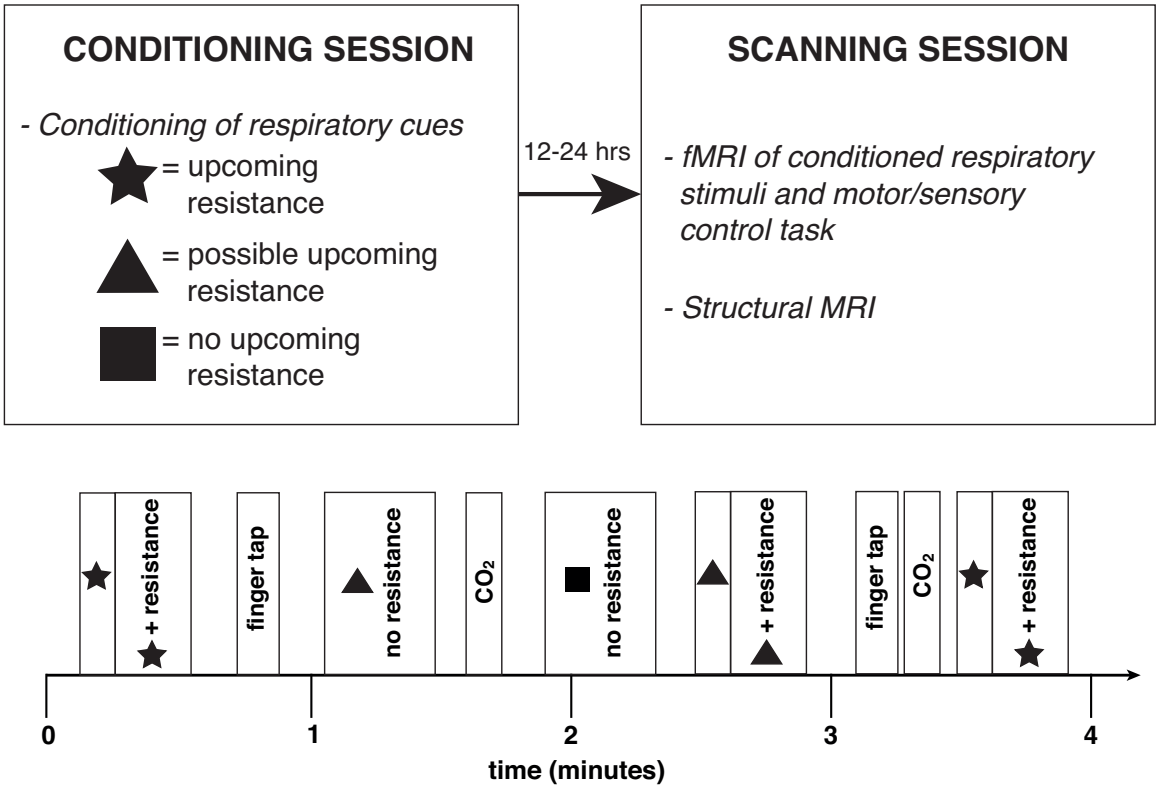

Figure 3.1: Top: Experimental overview. Bottom: Example four minutes of the BOLD sequence, repeated throughout the acquisition. The order of the cues was semi-randomised between the finger opposition and CO_2 stimuli, and the shapes were randomised acrossed subjects.

To minimise the effect of changing arterial oxygen and carbon dioxide levels upon the BOLD signal, the following steps were employed: 1) Additional medical oxygen was delivered, and the flow rate was manually adjusted to minimise fluctuations in pressure of end-tidal oxygen ($P_{ET}O_2$), aiming to keep $P_{ET}O_2$ at 18 kPa (very slightly above normal), and 2) At designated time points during rest periods of the functional scan, CO_2 challenges were administered by switching the flow of compressed air for a 10% CO_2 mixture (10% CO_2; 21% O_2; balance nitrogen) at 20 L/min for periods of 5–10 seconds, aiming to raise $P_{ET}CO_2$ an equivalent amount as observed during the resistive loading periods. The subjects nose was blocked using foam earplugs and they were asked to breathe through their mouth for the duration of the experiment.

3.3.4 Physiological measurements

Physiological measures were recorded continuously during the training session and MRI scan. Chest movements were measured using respiratory bellows surrounding the chest at the approximate level of the 10th rib, and heart rate was measured using a pulse oximeter (9500 Multigas Monitor, MR Equipment Corp., NY, USA). $P_{ET}CO_2$ and $P_{ET}O_2$ were sampled via a port beside the mouth piece of the breathing system. Expired gases were determined using a rapidly-responding gas analyser (Gas Analyser; ADInstruments Ltd, Oxford, United Kingdom), and pressure at the mouth was measured using a pressure transducer (MP 45, 50 cmH2O, Validyne Corp., Northridge, CA, USA) connected to an amplifier (Pressure transducer indicator, PK Morgan Ltd, Kent, UK). All physiological devices were connected to a data acquisition device (Powerlab; ADInstruments Ltd, Oxford, United Kingdom) coupled to a desktop computer with recording software (Labchart 7; ADInstruments Ltd, Oxford, United Kingdom).

3.3.5 MRI scanning sequences

MRI was performed with a 7 T Siemens Magnetom scanner, with 70 mT/m gradient strength and a 32 channel Rx, single channel birdcage Tx head coil (Nova Medical).

3.3.5.1 Brainstem BOLD scanning

A T2*-weighted, gradient echo EPI was used for functional scanning. To allow high resolution (≤ 2 mm^3) scanning, a reduced field of view (FOV) was used, with a coronal-oblique slice centred over the brainstem and superior cortical structures. The FOV comprised 36 slices (sequence parameters: TE, 24 ms; TR, 2.11 s; flip angle, 90 deg; voxel size, 1.5 x 1.5

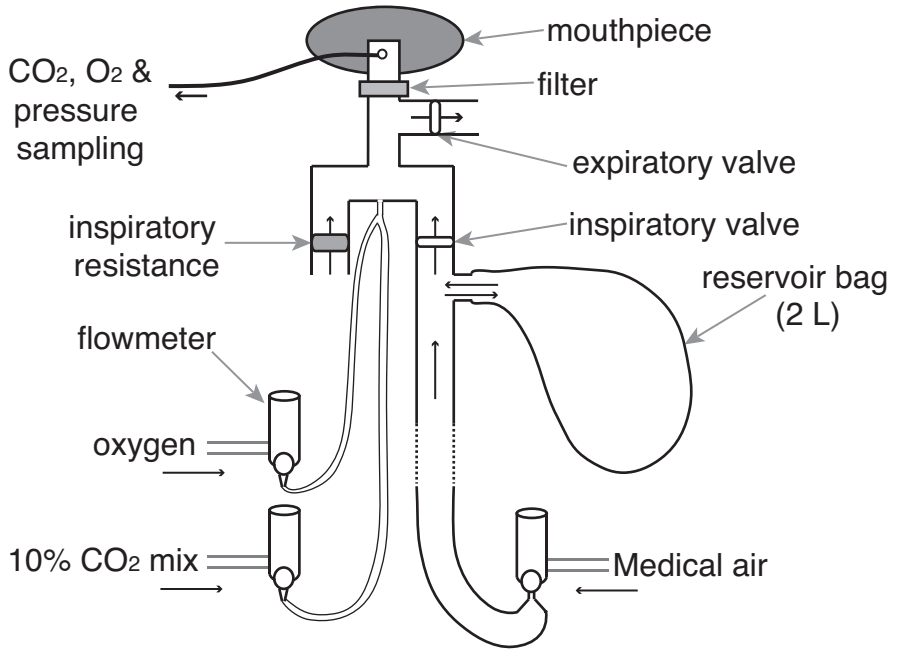

Figure 3.2: Schematic diagram of breathing system that allows remote administrations of inspiratory resistance. Medical air is supplied through a flow meter to the subject, with a reservoir of 2 L. Excess flow and expiration escapes through the one-way expiratory valve, close to the mouth to minimise re-breathing (inspiratory and expiratory valves: Hans Rudolf, Kansas City, MO, USA). Resistive loading is induced by stopping the delivery of medical air, and when the reservoir bag has deflated the subject draws air through the resistor (porous glass disc). Normal breathing is resumed by resupply of the medical air to the inspiratory arm and reservoir bag. A diving mouthpiece (Scubapro UK Ltd, Mitcham, UK) connects to a bacterial and viral filter (GVS, Lancashire, UK), and respiratory gases and respiratory pressure are sampled via polyethylene extension tubing (Vygon SA, Ecouen, France). One sampling line leads to a pressure transducer (MP 45, 50 cmH2O, Validyne Corp., Northridge, CA, USA) connected to an amplifier (Pressure transducer indicator, PK Morgan Ltd, Kent, UK), and a second sampling line to a gas analyser that samples oxygen and CO2 (Gas Analyser; ADInstruments Ltd, Oxford, United Kingdom). A hyperoxic state was achieved through a constant administration of oxygen at a rate of 0.5 L/min. Small carbon dioxide challenges (10% CO_2 at 20 L/min mixed with medical air at 20+ L/min; raising $P_{ET}CO_2$ to match inspiratory resistance $P_{ET}CO_2$ fluctuations) were administered periodically throughout scanning.

x 1.5 mm; field of view, 192 mm; GRAPPA factor, 3; echo spacing, 1 ms; slice acquisition order, ascending), with 835 volumes (scan duration, 29 mins 40 s).

3.3.5.2 Structural scanning

A T1-weighted structural scan (MPRAGE, sequence parameters: TE, 2.96 ms; TR, 2200 ms; flip angle, 7°; voxel size, 0.7 x 0.7 x 0.7 mm; field of view, 224 mm; inversion time, 1050 ms; bandwidth; 240 Hz/Px) was acquired. This scan was used for registration of functional images.

3.3.5.3 Additional scanning

A single volume whole brain EPI was also acquired, with matched sequence parameters to the functional scan and extended slices, to assist with registration. Fieldmap scans (sequence parameters: TE1, 4.08 ms; TE2, 5.1 ms; TR, 620 ms; flip angle, 39°; voxel size, 2 x 2 x 2 mm) of the B0 field were also acquired to assist distortion-correction.

3.3.6 Analysis

3.3.6.1 Preprocessing

Image preprocessing was performed using the Oxford Centre for Functional Magnetic Resonance Imaging of the Brain Software Library (FMRIB, Oxford, UK; FSL version 5.0.8; http://www.fmrib.ox.ac.uk/fsl/). The following processing methods were used prior to statistical analysis: motion correction and motion parameter recording (MCFLIRT (Jenkinson et al., 2002)), removal of the non-brain structures (skull and surrounding tissue) (BET (Smith, 2002)), spatial smoothing using a full-width half-maximum Gaussian kernel of 2 mm, and high-pass temporal filtering (Gaussian-weighted least-squares straight line fitting; 120 s). B0 field unwarping was conducted with a combination of FUGUE and BBR (Boundary-Based-Registration; part of FEAT: FMRI Expert Analysis Tool, version 6.0 (Greve and Fischl, 2009)).

Data demonising was conducted using a combinations of independent components analysis (ICA) and retrospective image correction (RETROICOR). ICA can be used to decompose fMRI data into different spatial and temporal components. Noise components can then be identified and removed from the 4D fMRI data. FSL's MELODIC (Multivariate Exploratory Linear Optimised Decomposition into Independent Components) was used to decompose data, prior to manual classification and removal of movement, cerebral spinal

fluid (CSF) and scanner artifact noise components. Classification of noise was based on spatial location of signal and signal frequency (Griffanti et al., 2014).

The cardiac and respiratory processes that were recorded (along with scanner triggers) allowed determination of cardiac and respiratory phase with each acquired slice in the imaged volume, and subsequent denoising using RETROICOR. This assigned phase is then entered into a low-order Fourier expansion (Brooks et al., 2008; Glover et al., 2000; Harvey et al., 2008) to derive time course regressors (3 cardiac, 4 respiratory and 1 interaction regressor) that explain potential signal changes associated with cardiac and respiratory (or interacting) processes. This process is automated using FEATs PNM (Physiological Noise Modelling) tool (Glover et al., 2000).

To ensure noise was not reintroduced through the combination of ICA denoising and RETROICOR, the following process was followed:

1. ICA DENOISING

- ICA decomposition of **raw fMRI** data using MELODIC
- Manual noise classification and removal of noise components (**ICA noise**) from **raw fMRI** (Salimi-Khorshidi et al., 2014; Griffanti et al., 2014) = **FIXed data**

2. PNM REGRESSION

- PNM time course regressors created from physiological recordings
- Calculation of signal associated with PNM noise:
  - PNM regression of **FIXed data** using FEAT
  - Residual 4D fMRI data following PNM regression = **PNM residuals**
  - Calculation of signal identified by PNM regressors: Subtraction of **PNM residuals** from **FIXed data** = **PNM signal**

3. COMBINING ICA DENOISING AND PNM REGRESSION

- Remove overlap between **FIX noise** and **PNM signal**: Run **PNM signal** through FIX cleanup (FIX (Salimi-Khorshidi et al., 2014; Griffanti et al., 2014)) using **FIX noise** = **FIXed PNM signals**
- Remove **FIXed PNM signals** from **FIXed data** = **clean fMRI data**

3.3.6.2 Image registration

Careful attention was paid to image registration accuracy for group statistics in small brainstem nuclei to be possible. After preprocessing, the functional scans were registered to the MNI152 (1 mm^3) standard space (average T1 brain image constructed from 152 normal subjects at the Montreal Neurological Institute (MNI), Montreal, QC, Canada) using a three-step process.

- Linear registration (FLIRT) with 6 DOF was used to align the partial FOV scan to the whole-brain EPI image (Jenkinson et al., 2002).
- Registration of subjects whole-brain EPI to T1 structural image was conducted using BBR (6 DOF) with (nonlinear) fieldmap distortion-correction (Greve and Fischl, 2009).
- Registration of the subjects T1 structural scan to 1 mm standard space was performed using an affine transformation followed by nonlinear registration (FNIRT) (Andersson et al., 2007).

3.3.6.3 Voxelwise and group analysis

Voxelwise analysis incorporated HRF modelling using three FLOBS regressors (as described in Chapter 2), and the first level model is demonstrated in Figure 3.3. The first of each of the three FLOBS regressors from the voxelwise statistical analysis was extended to a group level, in a mixed-effects analysis using FLAME (FMRIBs Local Analysis of Mixed Effects) (Woolrich et al., 2004a). $P_{ET}CO_2$ was included as an additional regressor, de-correlating the CO_2 induced BOLD changes from the respiratory stimuli throughout the functional scan. This trace was formed by linearly interpolating between the expired CO_2 peaks. We included packyears (cigarettes per day x number of years) as a confound regressor to account for any minimal subject history of smoking. Z statistic images were thresholded using clusters determined by $Z > 2.3$ and a (corrected) cluster significance threshold of $p < 0.05$. Univariate analysis of the group mean was performed, and anxiety ratings were used as a covariate of interest in a whole-brain linear regression. Small-volume masks of the vlPAG and lPAG (adapted from diffusion-based segmentation of the human PAG (Ezra et al., 2015)) and a mask of the whole PAG were used to investigate a-prior areas of interest, using standard cluster thresholding ($Z > 2.3$). A further higher level covariate analysis was performed, which included additional resistance and anxiety scores as demeaned regressors in the higher level analysis, where the average resistance score across

trials was calculated for each subject, and the anxiety score was taken as the anxiety of certain resistance (demonstrated in Figure 3.4).

3.3.6.4 Conditioned anticipation contrasts

It is common practice within the learning literature to contrast the conditioned cue that is paired with the stimulus (CS+) with a cue that is unpaired with the stimulus (CS-) (Büchel et al., 1998; Gottfried et al., 2002; Gottfried and Dolan, 2004; LaBar et al., 1998), which in the current study would be the certain (or uncertain) anticipation of resistance and the anticipation of no resistance, respectively. However, this contrast is not feasible beyond targeted PAG column analysis in the current study, as the length of the inspiratory resistance stimulus required to amass statistical power limits the number of possible repeats of each condition. Therefore, beyond the targeted analysis of the vlPAG during certain anticipation of resistance greater than anticipation of no resistance, the anticipation conditions have been analysed against baseline. However, the inclusion of three anticipatory cue conditions does allow greater decorrelation of the general cue response to each anticipation condition in the model.

3.4 Results

3.4.1 Behavioural scores

Mean anxiety and intensity scores for conditioned responses to the respiratory tasks are given in Table 3.1. Anxiety values were recorded immediately following the functional protocol in the scanning sessions, and intensity values recorded following each respiratory stimulus throughout the functional scan. Anxiety scores were significantly higher for the certain anticipation cue compared to the uncertain cue, and subsequent resistance was rated at a greater intensity following the certain cue.

*Table 3.1: Mean ($\pm$sd) anxiety and intensity ratings to the conditioned respiratory tasks. *Significantly ($p < 0.05$) different from no impending resistance condition; **Significantly ($p < 0.05$) different from no impending resistance and uncertain impending resistance*

	No resistance	Uncertain resistance	Certain resistance
Anxiety (%)	4.3 (5.1)	36.7 (22.3)*	48 (26.7)**
Intensity (%)	4.7 (3.1)	55.5 (20.9)*	62.9 (21.5)**

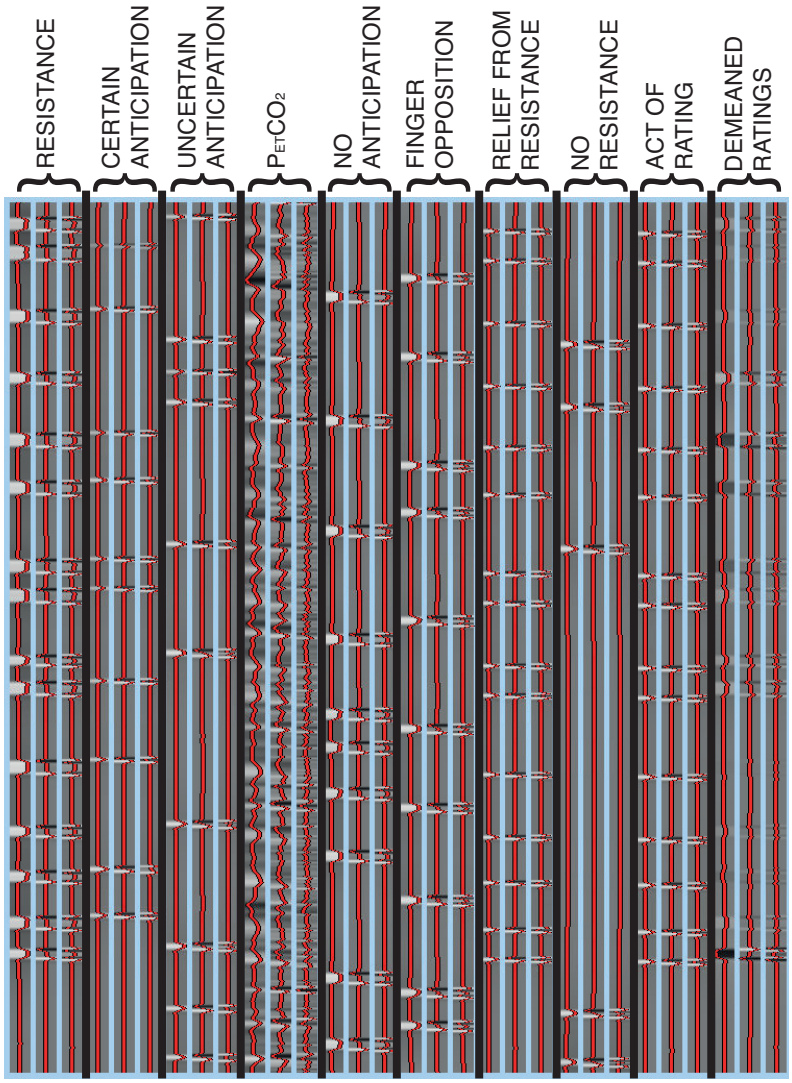

Figure 3.3: General linear model used in each single subject lower level analysis within FEAT. The FLOBS function creates three EVs for each regressor. The 'resistance' onset and duration were calculated from the recorded inspiratory pressure physiological traces, while the anticipation durations were calculated from the onset of the stimulus to the beginning of the resistance. For the 'uncertain anticipation' trials where the resistance was not applied, the anticipation duration was calculated from the onset of the stimulus to the maximum anticipation duration for each subject. The remainder of the presentation of the uncertain anticipation cue was modelled in a separate regressor ('no resistance'). The '$P_{ET}CO_2$' trace was included to de-correlate the CO_2 induced BOLD changes from the respiratory stimuli throughout the functional scan, and was formed by linearly interpolating between the expired CO_2 peaks. Anticipation of no resistance ('no anticipation') and 'finger opposition' onset and duration represented the presentation of the corresponding stimuli on the screen, and 'relief from resistance' was modelled as the rest periods immediately following each resistance application, prior to ratings (4 s duration). The 'act of rating' regressor was included to remove noise from the physical act of pressing the button box, and spanned each of the rating periods. Finally, 'demeaned ratings' matched the 'resistance' regressor for timings, and the intensity of the regressor was the demeaned intensity value assigned to each of the inspiratory resistance blocks. Contrasts consisted of mean values of the first EV of each set of three regressors.

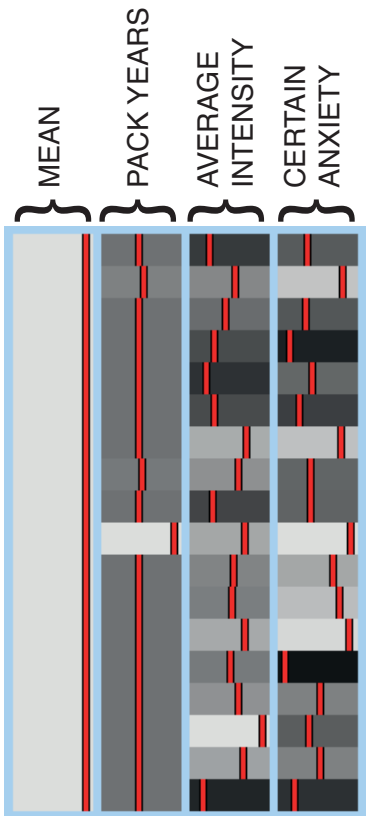

Figure 3.4: General linear model used in the group higher level analysis within FEAT. For each lower level contrast, positive and negative contrasts were calculated for the group mean ('mean'), plus covariates of the average intensity ('average intensity'; calculated from lower level intensity ratings for each subject) and anxiety of certain upcoming resistance ('certain anxiety'). A pack years covariate of no interest was also included to account for any small history of smoking in each of the subjects ('pack years'). An initial model of the first two regressors ('mean' and 'pack years') only was also conducted to maximise statistical power in the PAG.

*Table 3.2: Mean (±sd) physiological variables across conditioned respiratory tasks. *Significantly ($p < 0.05$) different from no impending resistance condition. Abbreviations: $P_{ET}CO_2$, pressure of end-tidal carbon dioxide; $P_{ET}O_2$, pressure of end-tidal oxygen; RVT, respiratory volume per unit time; bpm, breaths per minute. Pressure values are calculated as the average mouth pressure across all ventilatory cycles.*

	Anticipation			Resistance
	None	Uncertain	Certain	On
Average mouth pressure (cmH_2O)	-0.14 (0.11)	-0.17 (0.12)	-0.18 (0.24)	-5.80 (3.64)*
Peak mouth pressure (cmH_2O)	-	-	-	-14.7 (8.3)
$P_{ET}CO_2$ (%)	4.41 (0.71)	4.41 (0.67)	4.32 (0.68)*	4.46 (0.67)
$P_{ET}O_2$ (%)	18.1 (1.0)	18.1 (1.0)	18.3 (1.1)*	18.5 (1.0)*
Respiratory rate (bpm)	12.8 (3.7)	12.5 (3.8)	12.4 (3.6)	11.2 (4.6)
RVT (%)	-4.4 (7.4)	7.8 (19.6)*	11.0 (23.0)*	-16.1 (21.6)*

3.4.2 Physiology

Group average heart rate (±sd) during the brainstem BOLD scanning was 68 (±9) beats per minute. Ventilatory variables during each of the respiratory conditions are given in Table 3.2. While $P_{ET}O_2$ did rise marginally during inspiratory resistance and anticipation of resistance, the effect on global BOLD signal is approximately 70 times less than the effect of $P_{ET}O_2$ (Prisman et al., 2008), and would underestimate the effect size in a conservative manner that will not inflate the rate of false positives.

3.4.3 PAG analysis

The results of the targeted PAG subdivision analyses revealed significant increased BOLD activity in the vlPAG during the contrast of certain anticipation of resistance above anticipation of no resistance, and decreased BOLD in the lPAG during inspiratory resistance (Figure 3.5). A further exploratory analysis of the whole PAG showed that these activations were isolated to the vlPAG and lPAG in these conditions, although certain anticipation of resistance was now analysed against baseline for adequate statistical power (Figure 3.6). Furthermore, activity in the lPAG during certain anticipation of resistance was found to scale with intensity ratings across subjects (Figure 3.9). No areas of the PAG or cortex significantly scaled with intensity or anxiety ratings during inspiratory loading.

When comparing uncertain and certain anticipation of breathlessness, no significant difference was found in the PAG between the two conditions. However, during uncertain

anticipation of resistance, subthreshold PAG activity ($p = 0.11$) was identified in the same area of the right vlPAG as the significant cluster found with certain anticipation of resistance (Figure 3.7). Activity in neither the vlPAG, nor the lPAG scaled with anxiety across subjects.

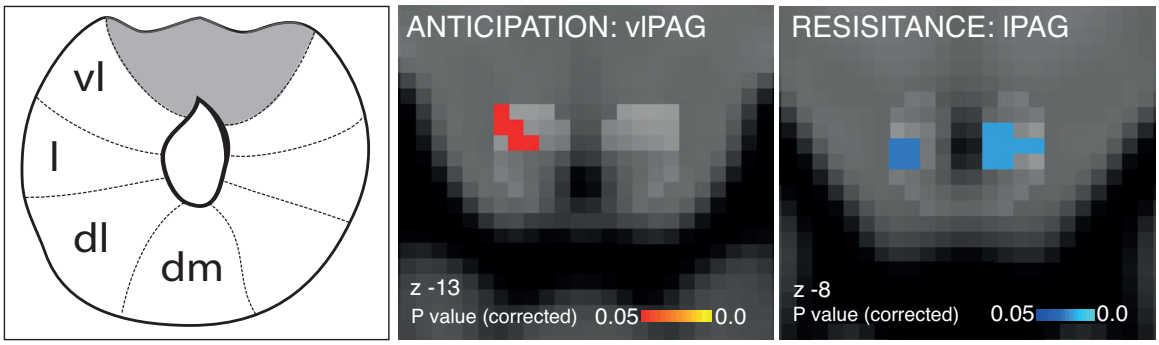

Figure 3.5: Left: Schematic representation of the columns of the midbrain periaqueductal gray (PAG), which almost surrounds the aqueduct. Middle: Ventrolateral PAG (vlPAG) activation during anticipation of resistance (certain anticipation > anticipation of no resistance; middle). Right: Lateral PAG (lPAG) deactivation during inspiratory resistance. Statistics are small-volume-corrected for multiple comparisons using highlighted PAG column masks, adapted from Ezra et al. (2015), and the images consist of a colour-rendered statistical map superimposed on a standard (MNI 1 mm^3) brain.

3.4.4 Cortical and subcortical respiratory results

We observed significant BOLD signal increases bilaterally in the motor cortex, supplementary motor cortex, primary sensory cortex, middle and posterior cingulate cortices, operculum, medulla and middle insular cortex, and decreased BOLD signal in the bilateral hippocampus and IX cerebellar lobe, for both certain and uncertain anticipation against baseline, and during inspiratory resistance (Figure 3.8). Inspiratory resistance also correlated with activations in the bilateral putamen, caudate, ventral posterior lateral nucleus of the thalamus (VPL) and subthalamic nucleus, and deactivations in the bilateral amygdala, lPAG and posterior nuclei of the thalamus. Additionally, both certain and uncertain anticipation correlated with deactivations in bilateral posterior insula. No significant cortical or subcortical differences were seen between certain and uncertain anticipation.

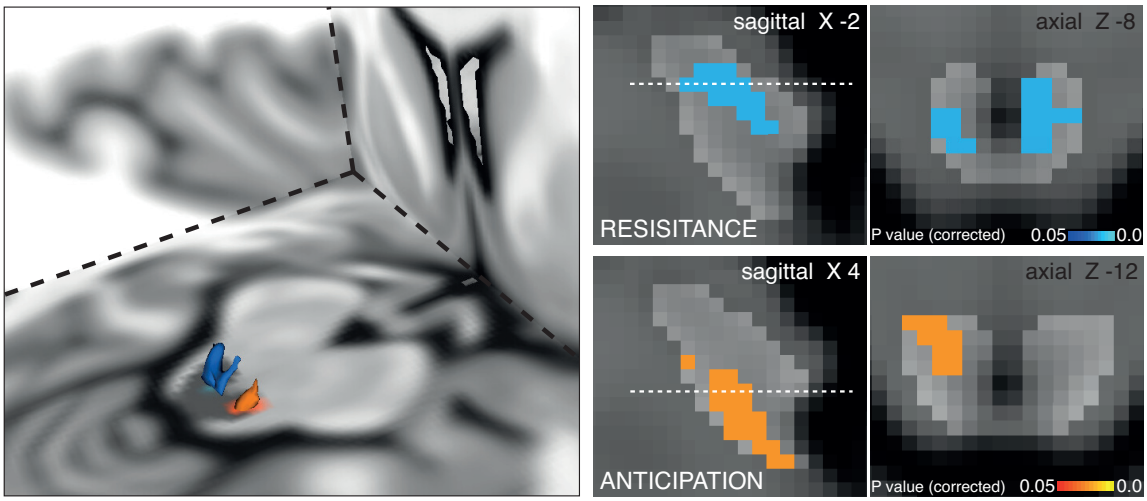

Figure 3.6: Periaqueductal gray (PAG) activation. Left: 3D representation of the PAG activations on the right. Right, top row: Deactivation during inspiratory resistance in bilateral lPAG ($p = 0.007$). Bottom row: Activation in the vlPAG during anticipation of certain resistance against baseline ($p = 0.021$). Statistics are small-volume-corrected for multiple comparisons using highlighted PAG mask, and the images consist of a colour-rendered statistical map superimposed on a standard (MNI 1 mm^3) brain. Dashed line represents Z location.

3.4.5 Finger opposition

Finger opposition resulted in consistent significant signal increases in both the brainstem and cortex with results from Chapter 2 and previous research (Pattinson et al., 2009b) (Figure 3.10), including bilateral activation in the motor cortex (more extensive activation in the contralateral left motor cortex), supplementary motor cortex, middle cingulate and paracingulate cortices, primary sensory cortex, anterior insula cortex, operculum, caudate nucleus and putamen (Figure 3.8). Bilateral signal increases were seen in the thalamic VPL nuclei, as well as the left thalamic ventral posterior medial (VPM) nucleus. In addition, activations were observed in the left subthalamic and red nuclei, right (ipsilateral) cuneate nucleus of the medulla, and bilateral cerebellum (VI and VIIIa lobules).

3.4.6 Breathlessness anxiety and exercise

While the effect of exercise was not investigated within brain networks of breathlessness in this study (due to limited statistical power and restricted field of view), a correlation was conducted between the anxiety scores for certain impending resistance and exercise exposure (number of hours of exercise per week x intensity; where 1 = easy, 2 = moderate, 3 = intense). A significantly negative correlation (R = -0.59; p = 0.009) was found between

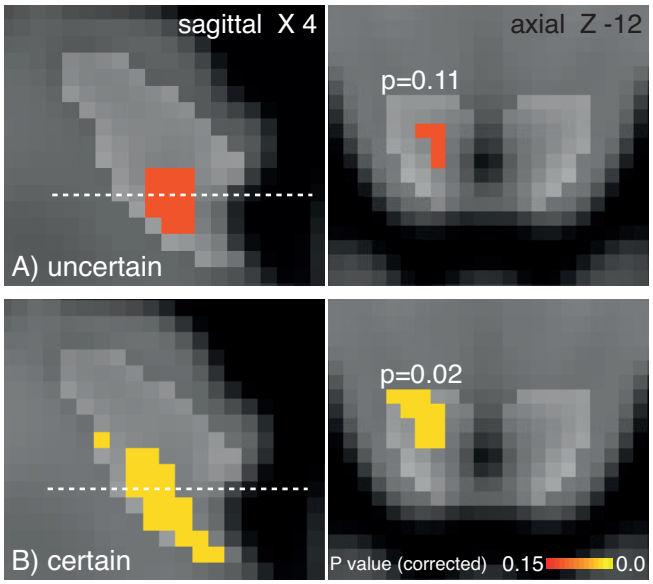

Figure 3.7: vlPAG activations during uncertain (A) and certain (B) anticipation of impending breathlessness. Uncertain anticipation produces subthreshold vlPAG activation in a consistent area to the certain condition. PAG mask displayed by light grey region. Images consist of a colour-rendered statistical map superimposed on a standard (MNI 1 mm^3) brain. Dashed line represents Z location.

these two variables (Figure 3.11).

3.5 Discussion

3.5.1 Main findings

In this Chapter we identified differential activity in the lateral and ventrolateral columns of the PAG during different respiratory tasks. We found decreased BOLD activity in the lPAG (bilateral) during an inspiratory resistance, and activity in this area during cued anticipation scaled with ratings of resistance intensity. Additionally, activity in the right vlPAG was identified during the cued anticipation of inspiratory resistance, with certain anticipation associated with significant increases in BOLD signal, while uncertain anticipation activity remained subthreshold. This reduced vlPAG activity during uncertain anticipation was paired with decreased anxiety ratings and intensity scores of the following stimulus, indicating a reduction in the conditioned threat response to a 50% (uncertain) predictive cue, compared to the 100% predictive cue (certain).

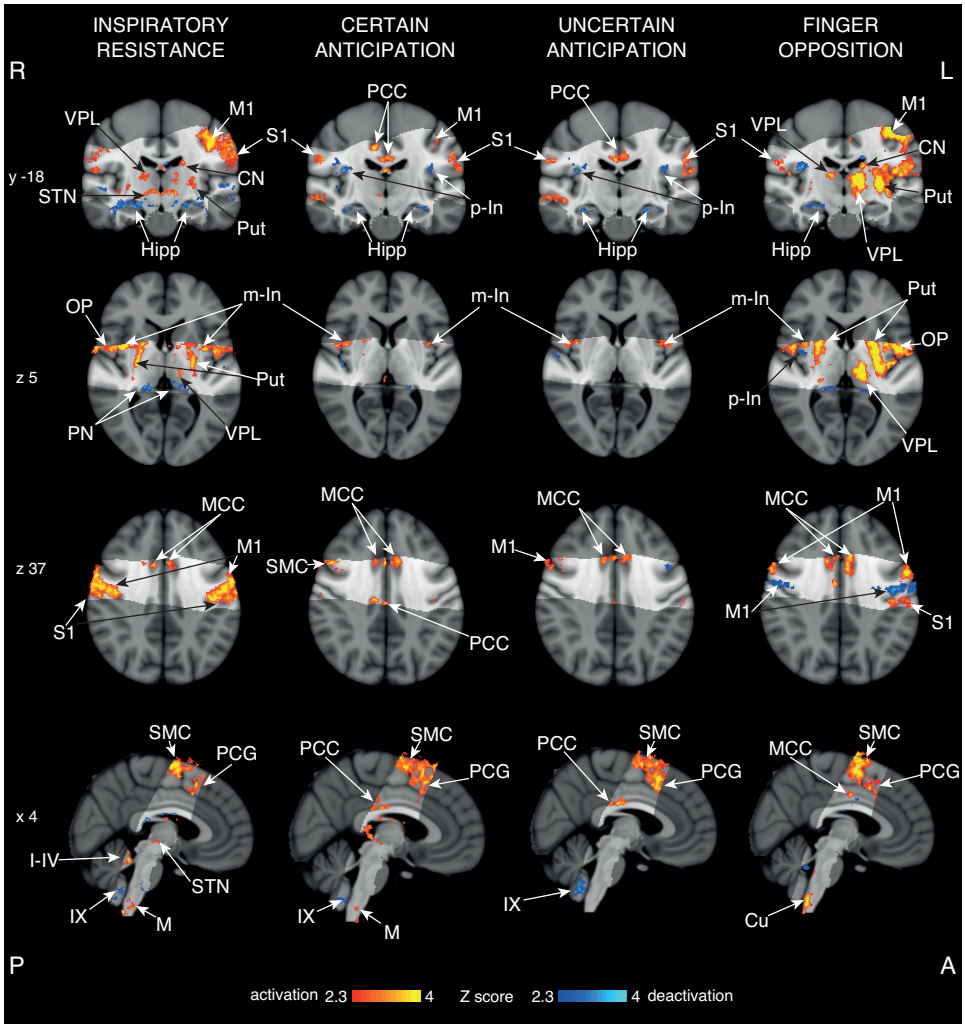

Figure 3.8: Mean cortical activations and deactivations identified during inspiratory resistance, certain anticipation, uncertain anticipation and finger opposition. The images consist of a colour-rendered statistical map superimposed on a standard (MNI 1 mm^3) brain. The bright grey region represents the coverage of the coronal-oblique functional scan. Significant regions are displayed with a threshold $Z > 2.3$, with a cluster probability threshold of $p < 0.05$ (corrected for multiple comparisons). Abbreviations: VPL, ventral posterior lateral nucleus (thalamus); M1, primary motor cortex; S1, primary sensory cortex; CN, caudate nucleus; Put, putamen; Hipp, hippocampus; STN, subthalamic nucleus; PCC, posterior cingulate cortex; MCC, middle cingulate cortex; p-In, posterior insular; m-In, middle insular; OP, operculum; SMC, supplementary motor cortex; PCG, paracingulate gyrus; PN, posterior nuclei of the thalamus; PAG, periaqueductal gray; M, solitary nucleus of the medulla; Cu, cuneate nucleus (medulla); I-IV, I-IV cerebellar lobe; IX, IX cerebellar lobe.

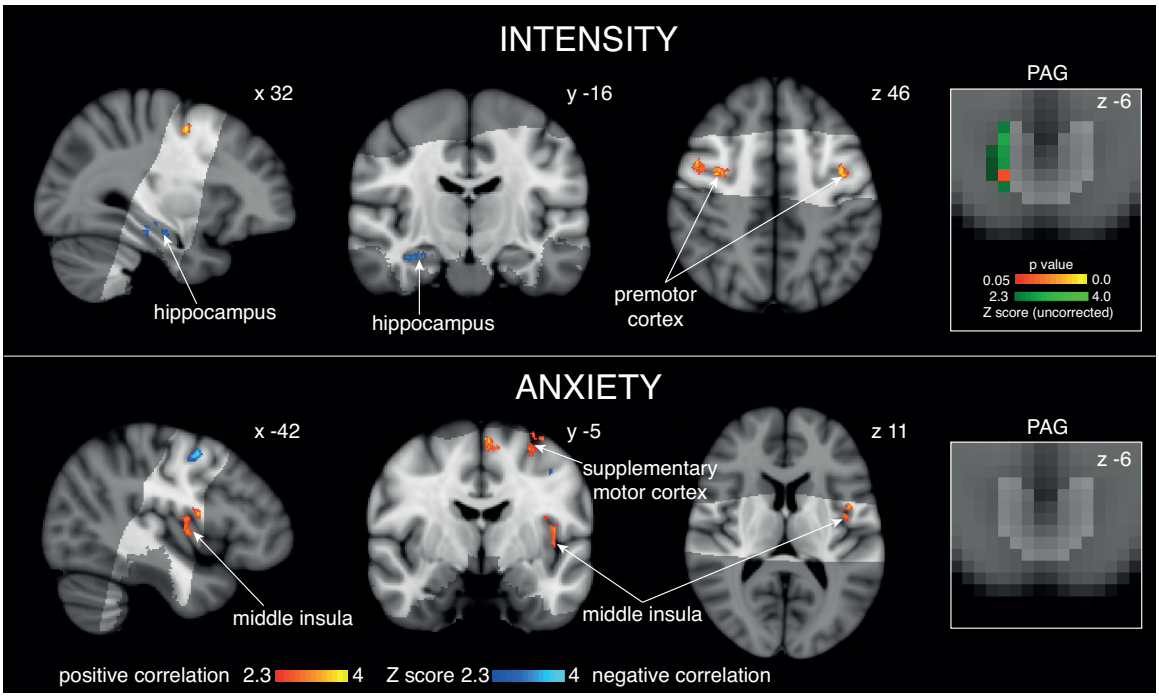

Figure 3.9: Correlations during certain anticipation with intensity and anxiety scores. Right: Positive correlation in the lPAG with intensity ratings (green uncorrected Z score, red/yellow TFCE-corrected for lPAG activity, PAG displayed in light grey). Left, top: Cortical correlations with average intensity score. Left, bottom: Cortical correlations with anxiety score for certain anticipation. Images consist of a colour-rendered statistical map superimposed on a standard (MNI 1 mm^3) brain.

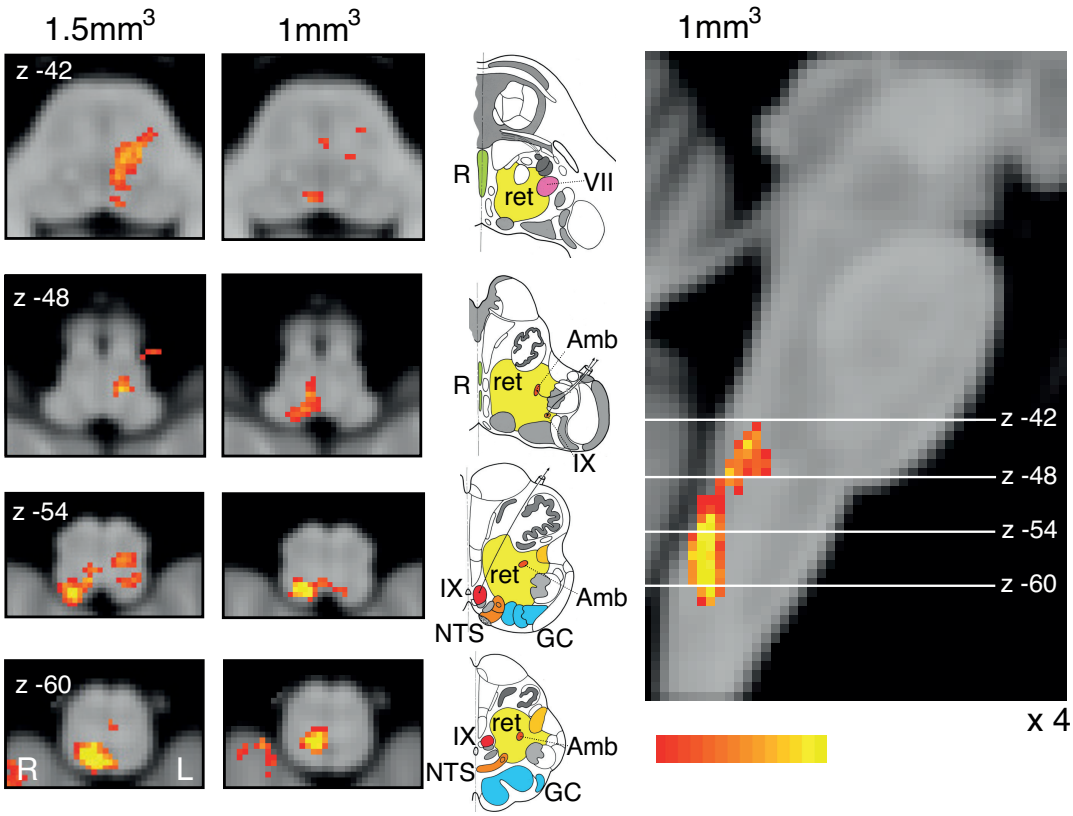

Figure 3.10: Demonstration of the use of finger opposition as a functional localiser in brainstem FMRI at 7 T, imaging activation in the ipsilateral cuneate nucleus of the medulla (z -54). The 7 T 1 mm^3 voxel data is derived from Chapter 2 (14 repeats of 15 sec finger opposition, 1 mm^3 voxels and TR = 5 sec) vs. the current 7 T study (10 repeats of 15 sec finger opposition, 1.5 mm^3 voxels and TR = 3.11 sec). This technique provides confidence in the analysis model and registration accuracy. The images consist of a colour-rendered statistical map superimposed on a standard (MNI 1 mm^3) brain. Significant regions are displayed with a threshold $Z > 2.3$, with a cluster probability threshold of $p < 0.05$ (corrected for multiple comparisons). The sagittal image on the right displays the position of slices, for clarity only displayed from the 7 T 1 mm^3 acquisition. Abbreviations: R, raphe nuclei; ret, nuclei reticularis; VII, facial nucleus; Amb, nucleus ambiguous; IX, glossopharyngeal nucleus; NTS, nucleus tractus solitaries; GC, gracile (medial) and cuneate (lateral) nuclei (in blue). R (right) and L (left) indicate image orientation. Original line drawings adapted from Duvernoy (Duvernoy, 1995).

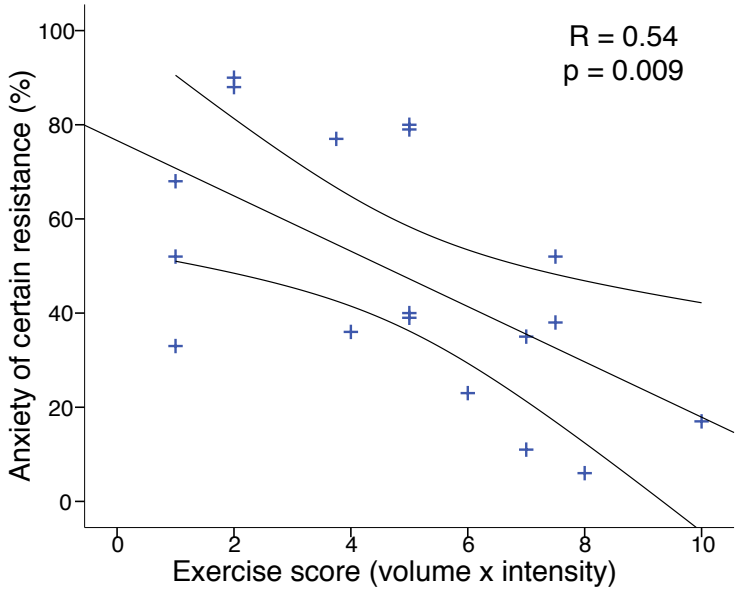

Figure 3.11: Plot of anxiety scores for certain impending resistance against exercise exposure score (number of hours of exercise per week x intensity; where 1 = easy, 2 = moderate, 3 = intense). Black lines represent regression line and 95% confidence intervals.

3.5.2 PAG and threat

Significantly, recent work using diffusion tractography has revealed consistent columnar structure to animal models within the human PAG (Ezra et al., 2015). During response to threat, functional organisation of these animal PAG columns has been hypothesised to consist of active and passive coping strategies (Keay and Bandler, 2001; Bandler and Shipley, 1994; Bandler et al., 2000). The lPAG and dlPAG are thought to employ active coping strategies for escapable stressors, consistent with the tachypnea observed in animals on stimulation of these columns (Subramanian et al., 2008), while the vlPAG employs passive coping strategies for inescapable stressors (vlPAG) such as that seen with a range of physical stimuli (Keay and Bandler, 2001). In the current investigation of the threat response to breathlessness, the aversive resisted breathing stimulus was an upcoming inescapable stressor, activating the vlPAG, while during the active stimulus response we observed lPAG activity. These results are the first in humans to adhere to the current models of distinctive threat perception of the animal PAG columns. While one recent study has also used 7 Tesla functional MRI to identify highly localised activity in areas of the PAG during exposure to aversive images in humans (Satpute et al., 2013), this study did not adhere to the columnar model of the PAG, nor consider the characteristic functions of these columns within

threat perception. We will now discuss each of the activated PAG columns and their potential role in the specific threat response to an aversive breathing stimulus as a model of breathlessness.

3.5.3 lPAG in conditioned breathlessness

The decrease in BOLD signal in the lPAG during an inspiratory resistance is consistent with our previous PAG findings. In Chapter 2 we identified decreased BOLD signal in the lPAG during the respiratory challenge of breath holds, and animal models have proposed the lPAG may play a role in respiratory behaviours such as prolonged inspirations and expirations (Subramanian et al., 2008). It is possible that the lPAG is an integral nucleus within the somatomotor pathways of respiratory control, and anatomical evidence exists to support this hypothesis. The lPAG has been reported to receive somatotopically organised spinal sensory afferents (Craven, 2011; Keay and Bandler, 2001), which could provide sensory information from the chest, and it propagates direct efferent connections to the midline medulla for possible descending respiratory motor commands. Additionally, human diffusion imaging has suggested preferential connectivity between somatomotor regions and the lPAG, compared to the vlPAG (Ezra et al., 2015). Our findings of activity in the lPAG whilst producing elevated inspiratory pressure supports the idea that this column of the PAG is involved in altered respiratory work, although whether this is in a motor or sensory capacity (or both) is currently unknown.

Interestingly, activity in the lPAG during anticipation was found to scale with perceived stimulus intensity across subjects. Anticipation of a stimulus allows system preparation and response selection, and activity in the lPAG that scales with the perceived intensity of the forthcoming stimulus indicates a possible top-down control during preparation for inspiratory resistance. The cortical structures that scaled alongside the lPAG with perceived intensity included the premotor cortex and hippocampus, which may indicate increased motor preparatory activity (Grafton et al., 1998; Rizzolatti et al., 2002) and greater working memory of the stimulus between the hippocampus and prefrontal cortex (Laroche et al., 2000). Conversely, lPAG activity during anticipation did not correlate with anxiety scores. This indicates that lPAG activity is less likely to be involved in the emotional component of resistance anticipation, whereas activity in structures such as the middle insula, which is known to be involved in self-awareness (Critchley et al., 2004; Gray et al., 2007), are coupled with anxiety ratings. Future work towards understanding whether the role of the lPAG is causative within this breathlessness intensity network may be integral to pinpointing perceptual disruptions in chronic sufferers of breathlessness.

3.5.4 vlPAG in conditioned breathlessness

The increase in BOLD signal identified in the vlPAG implies a role of the vlPAG in the conditioned response to the anticipation of breathlessness. Anticipation of resistance also activated a cortical network of motor, sensory and interoceptive areas, indicating the potential position of the vlPAG within a threat detection and preparatory network stimulated by a conditioned breathlessness cue. Additionally, although prefrontal cortical areas were not imaged in this study, human connectivity research suggests the vlPAG receives the predominant proportion of the input from the prefrontal cortex (Ezra et al., 2015), and animal models report direct connections between the posterior orbital frontal and anterior insula cortices to the vlPAG (An et al., 1998). Therefore, it is possible that communication between the vlPAG and areas of executive function, interoception and motor preparation are vital to the threat detection and response selection that occur during the cued anticipation of breathlessness. While this study has made inroads into functionally differentiating the columns of the PAG at high resolution, in Chapter 5 we explore how these columns function and communicate with the wider cortex to more fully understand their roles within the integrative breathlessness network.

Interestingly, there did not appear to be any significant differences (both within the vlPAG and superior cortical network) between uncertain and certain anticipation of resistance, but rather subthreshold vlPAG activity with uncertain anticipation. Furthermore, the reduction in vlPAG activity was paralleled by reduced anxiety and intensity scores in uncertain anticipation, indicating a smaller conditioned response was elicited by this cue. This supports the idea that the vlPAG is involved within the threat perception network for breathlessness, and the magnitude of this activity reflects greater conditioning and increased anticipatory preparation. Interestingly, it does not appear that uncertainty drives hypersensitivity and resultant increased anxiety or rating scores (Table 3.1), differing from previous research in pain (Ploghaus et al., 2003; Rhudy and Meagher, 2000). However, previous pain research has often used no anticipation cue to generate an uncertain stimulus response, which differs to our current approach of a less-predictive conditioned stimulus.

3.5.5 Breathlessness anxiety and exercise

Although not the primary focus of this study, anxiety scores for certain upcoming resistance were found to significantly negatively correlate with the subjects' regular exposure to exercise. This appears to align with the results from pulmonary rehabilitation studies, where treatment with exercise for those suffering COPD reduces breathlessness anxiety, possibly through desensitisation and/or reduction of the threat value of respiratory sensations

(Carrieri-Kohlman et al., 2001, 1996). The limited statistical power and restricted field of view in this study did not allow us to explore the brain mechanisms that may be modulating this change in anxiety, and the possible role of the PAG in these changes. Therefore, a primary aim of the final study of this Thesis is to investigate both the underlying physiological and psychological changes to ventilation and breathlessness with exercise, and the associated brain mechanisms (Chapters 4 and 5).

3.6 Conclusions

The results of this study suggest that the columns of the PAG may be differentially involved in the perception of breathlessness. This study corroborates with recent findings that the lPAG may be involved with the sensorimotor aspect of breathing control during the active response to breathlessness (Chapter 2), and top-down anticipatory activity may influence intensity perception of breathlessness. Conversely, the vlPAG appears to be only activated during anticipation of breathlessness, with decreased anticipatory cue conditioning resulting in reduced vlPAG activity. We propose that the vlPAG is involved with the learned anticipatory threat detection of a breathlessness stimulus, corroborating with the proposed model of the vlPAG in the passive threat response to an inescapable stressor.

Having thus far directed our investigation primarily at the columns of the PAG during respiratory control and breathlessness, from here we now need to investigate how this fits within the wider cortical network of breathlessness. This involves examining the co-activation of the PAG columns with the full cortex and sub-cortex, and the connectivity of the columns to these structures. Furthermore, previous research informs us that exercise treatment in COPD can decrease breathlessness perception. Therefore, we can begin to investigate the possible mechanisms of action of exercise within the PAG columns by examining any differences present in a group of individuals who regularly undergo exercise training (endurance athletes). These questions will be address in the final study of this Thesis, which is presented in Chapters 4 and 5.

Chapter 4

Exercise and the physiology and psychology of breathlessness

4.1 Abstract

Exercise can evoke sensations of breathlessness, either at prolonged high exercising intensities in healthy individuals, or at reduced exercise intensities when respiratory capacity is impeded in disease. Breathlessness is a frightening sensation that may impair exercise capacity, from healthy athletes through to sufferers of respiratory disease. While exercise training is used to evoke physiological system adaptations to improve health and performance, the effect of this training on our perceptions of physiological sensations is rarely considered. Therefore, in this Chapter we examined the effect of exercise training on the physiology and psychology of breathlessness, comparing a group of 20 endurance athletes and 20 age and sex-matched sedentary controls, before exploring any related differences in brain networks of breathlessness in Chapter 5. Subjects completed baseline spirometry and anxiety questionnaires, and both an incremental exercise test to exhaustion and a steady-state hypercapnic hyperventilatory challenge, with concurrent measures of breathlessness and breathing anxiety. While we found no evidence of de-sensitisation to respiratory sensations and breathlessness in athletes, we observed that athletes appear to have improved accuracy in the perception of their ventilation. Furthermore, athletes reported greater breathlessness anxiety at maximal exercise, possibly due to the increased homeostatic signalling caused by operating at high proportions of their maximal ventilatory capacity. Therefore, the results of this study can help us understand some of the contributing physiological factors to breathlessness perceptions, and how repeated exposure to breathlessness may improve ventilatory awareness in both athletes and patients with respiratory disease.

4.2 Introduction

In this Thesis we have thus far investigated the differential roles of the PAG columns in respiratory control and breathlessness. To further this investigation, we now need to explore how the PAG columns contribute within the wider cortical network of breathlessness, and how these brain networks might be altered to change perceptions of breathlessness. Our previous results in Chapter 3 indicated that exercise exposure is inversely proportional to breathlessness anxiety. Therefore, in this Chapter we first conduct a thorough investigation into the physiology and psychology of any exercise-induced changes in breathlessness perception, before we are able to understand corresponding changes in brain networks of breathlessness presented in Chapter 5.

Breathlessness is the sensation of not getting enough air, and can be induced when respiratory needs are perceived to outstrip current ventilation. Breathlessness can be induced in health or disease; in health either by increasing ventilatory needs through maximal exercise, or exercising in an environment with reduced atmospheric pressure (such as at high altitudes), or in disease when ability to ventilate is impaired. While ventilatory control during exercise is studied as a key component of exercise performance (Turner et al., 1997; Mahler et al., 1982; Martin et al., 1978; Schoene et al., 1984), the perception of ventilatory signals and breathlessness has received little attention. However, as exercise intensity can be consciously modulated based on perceived exertion and anxiety induced by sensations such as breathlessness, this may be a key component in the limitations of athletic performance. Furthermore, understanding how exercise induces adaptations in breathlessness perception may lead to more targeted training for improved performance, and enlighten us as to how exercise may be used to help the suffers of breathlessness associated with chronic respiratory disease.

Ventilation during exercise is tightly controlled. A balance of neurally-modulated initial increases in ventilation and peripheral feedback stimulate increased ventilation that corresponds with exercise intensity (Waldrop et al., 1996; Kaufman and Forster, 1996). The increased CO_2 production with increasing exercise effort is a subtle form of hypercapnia (elevated CO_2), which is intricately linked to the multidimensional sensation of breathlessness. Hypercapnia drives the sensation often labelled as 'air hunger' within breathlessness (Banzett et al., 1996), and together with the top-down neural drive to breathe results in a cascade of information up to emotional limbic and sensory areas of breathlessness perception in the brain (Liotti et al., 2001). The linear relationship between exercise intensity and arterial CO_2 continues until a point labelled the 'anaerobic threshold', where ventilation increases disproportionately to exercise intensity. Deviation from this linear trend is cur-

rently understood to be due to the additional involvement of anaerobic metabolism, with the added respiratory drive allowing buffering of the produced lactic acid by HCO_3^- ions, resulting in the expulsion of CO_2 (Stegmann et al., 1981). This capacity to 'over-ventilate' beyond our metabolic needs also maintains blood-oxygen saturation (for exercising at sea level) during even maximal exercise in the majority of individuals, and thus ventilation itself has typically not been considered a limiting factor to exercise performance (McArdle et al., 2006; Bassett and Howley, 2000). However, the modulating influence of the perception of breathlessness during this ventilatory response at sub-maximal and maximal exercise intensities has not yet been considered.

Breathlessness can be induced with even low intensities of exercise when respiratory capacity is impaired, such as in chronic obstructive pulmonary disease (COPD), asthma, cardiovascular and neuromuscular diseases, cancer or panic disorder. In COPD, breathlessness is considered the most debilitating symptom of the disease. Patients with COPD have increased work of breathing due to their obstruction, reduced maximal lung capacities and maximal ventilation, and as a result are repeatedly exposed to breathlessness with minimal exercising exertions as a result of their disease. Despite the root of this disease lying within the lungs, perception of breathlessness is not directly related to lung (dys)function and is actually a better predictor of disease mortality (Celli et al., 2004). The discrepancies between breathlessness severity and objective measures of lung function may be explained by abnormal brain processing of respiratory sensations.

Currently, the most effective treatment for breathlessness in COPD is pulmonary rehabilitation, involving 6 weeks of exercise training and education. Despite no changes in lung function, breathlessness and its associated anxiety are reduced as a result of this treatment (Carrieri-Kohlman et al., 2001, 1996), and the pre-treatment magnitude of symptom perception predicts treatment success (Janssens et al., 2011b). So how does exercise treatment change the misappropriated respiratory sensations? Does exercise reduce the intensity and 'de-sensitise' patients to respiratory sensations? Or does repeated exposure to 'safe' breathlessness during exercise in pulmonary rehabilitation reduce the threat value of breathlessness? While there is mixed opinion in the literature as to whether exercise can alter the ventilatory response to hypercapnia (Mucci et al., 1998; Byrne-Quinn et al., 1971; Godfrey et al., 1971; Scoggin et al., 1978; Mahler et al., 1982), there is almost no reported evidence on whether exercise (independent of disease) changes the perception of breathlessness. Understanding the mechanisms by which exercise reduces breathlessness anxiety will help us to better target treatment of this symptom in chronic respiratory disease.

Therefore, in this study we tested whether exercise 'de-sensitises' healthy volunteers to sensations of breathlessness. We investigated the differences in perception of breathless-

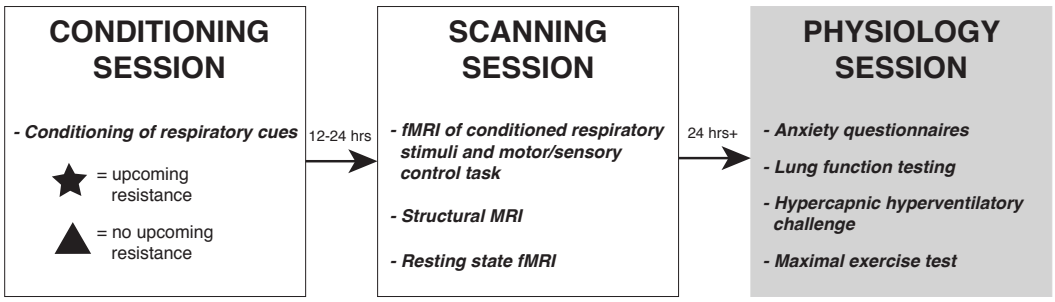

Figure 4.1: Experimental overview of Chapters 4 and 5. The testing session discussed in this Chapter is identified in grey.

ness in two groups of subjects who greatly differ in their exposure to exercise and breathlessness: endurance athletes and sedentary individuals. As well as physiological measures, we assessed subjective perceptions of breathlessness and anxiety of breathing during sub maximal and maximal exercise, and during isolated increases in ventilation (hyperventilation). Understanding the effect of exercise exposure on breathlessness perception is an important step in both the clinical understanding of the effects of exercise as a treatment option for breathlessness, and may also improve our understanding of the limits of athletic performance.

4.2.1 Hypotheses

In accordance with the inverse relationship found between exercise and breathlessness in Chapter 3 and pulmonary rehabilitation studies (Carrieri-Kohlman et al., 2001, 1996), we hypothesised that athletes would be 'de-sensitised' to breathlessness during exercise. This would manifest itself in decreased intensity and anxiety of breathlessness scores relative to ventilatory changes at both sub-maximal and maximal exercise. Correspondingly, we also expected to see decreased breathlessness scores during hyperventilation alone.

4.3 Methods

4.3.1 Experimental overview

This Chapter contains the protocols and findings of the physiology session of the final study of this Thesis (demonstrated in Figure 4.1).

4.3.2 Subjects

In this Chapter we compared 20 endurance athletes and 20 age- and sex-matched sedentary subjects (20 males, 20 females; mean age $\pm$ SD, 26 $\pm$ 7 years; age-matched $\pm$2 years) in a cross-sectional design, as a longitudinal study of the effects of exercise was not feasible within the scope of this Thesis. The athlete group consisted of subjects who participated in organised endurance exercise training 5 or more times per week, while the sedentary group comprised subjects who were not involved in any organised exercise, and minimal commuting exercise. One athlete subject did not complete the maximal exercise test due to injury.

4.3.3 Questionnaires

Due to the cross-sectional nature of this experiment, a thorough baseline comparison between the two groups was necessitated. Psychological questionnaires were included and chosen to allow a comprehensive scoring of each subject's general anxiety and depression, as well as anxiety of bodily sensations. The questionnaires consisted of:

- Spielberger State-Trait Anxiety Inventory (STAI (Spielberger, 2010))
- Anxiety Sensitivity Index (ASI (Reiss et al., 1986))
- The Centre for Epidemiologic Studies Depression Scale (CES-D (Radloff, 1977))

Subjects were asked to record how many hours of physical activity they typically completed per week, the intensity of the exercise (easy, moderate or intense) and what types of exercise they performed. They were also asked to recall and record their last week of exercising activity.

4.3.4 Spirometry

Spirometry was used to asses lung capacity and function. A full inspiration and expiration was used to measure forced vital capacity (FVC) of the lungs, and the best of three FVC measurements was recorded. The corresponding fraction of expired volume in the first second (FEV1/FVC) was recorded as an indicator of any airway obstruction (FEV1$<$70%). Maximal voluntary ventilation (MVV) was also tested to assess each subject's ability to ventilate of their own volition, where subjects were asked to maximally ventilate through the mouthpiece and turbine for 10 sec. The best of two MVV measurements were recorded. Spirometry measurements were recorded using a mouthpiece (Hans Rudolf, Kansas City,

MO, USA) and turbine connected to gas and flow analyser (Cortex Metalyser 3B, Cranlea Human Performance Ltd., Birmingham, UK), and subjects wore a nose clip for all spirometry tests. Metasoft studio software (Cortex, Versions 3.9.9 and 4.9.0, Cranlea Human Performance Ltd., Birmingham, UK) was used to calculate all spirometry measurements.

4.3.5 Steady-state hypercapnic ventilatory response test

One of the key components of breathlessness is an increase in ventilatory drive, and both the physiological and subjective responses to elevated ventilation may be an important component of breathlessness perception. Therefore, in this Chapter we also measured the physiological and subjective effects of an isolated increase in ventilation (hyperventilation), using a hypercapnic stimulus (increased partial pressure of arterial CO_2).

To administer the hypercapnic stimulus, a breathing system was designed to administer adjustable quantities of humidified medical air, CO_2 and O_2, and gas sampling was displayed on a computer (using Labchart 7; ADInstruments Ltd, Oxford, United Kingdom) to monitor expired gases at all times (Figure 4.2). Expired gases were determined using a rapidly-responding gas analyser (Gas Analyser; ADInstruments Ltd, Oxford, United Kingdom), and ventilatory flow and volume were determined using a spirometer (ADInstruments Ltd, Oxford, United Kingdom).

Hypercapnia protocol Subjects were positioned supine and attached to the breathing system. Eight minutes of resting breathing was initially recorded, with subjects rating their breathlessness and anxiety of breathing every four minutes using a visual analogue scale (VAS; 0-100%) presented on a screen and controlled via a button box. Resting values of $P_{ET}CO_2$ and $P_{ET}O_2$ were determined during this baseline period, before two levels of hypercapnia were administered. The hypercapnic periods involved a 3 min elevation in $P_{ET}CO_2$ of 0.8% (6.1 mm Hg) and 1.5% (11.2 mm Hg) (randomised order, separated by four minutes of breathing medical air) whilst $P_{ET}O_2$ was maintained at resting levels throughout the experiment (iso-oxia). A final four minutes of breathing medical air followed the second hypercapnic stimulus to finish the test. Subjects were asked to rate their breathlessness and anxiety at the end of each block of hypercapnia and medical air.

4.3.6 Maximal exercise test

To assess any possible changes in breathlessness perception as a result of exercise, subjects performed an incremental sub-maximal to maximal exercise test with concurrent ventilatory and breathlessness measures. A relative sub-maximal point of reference of the

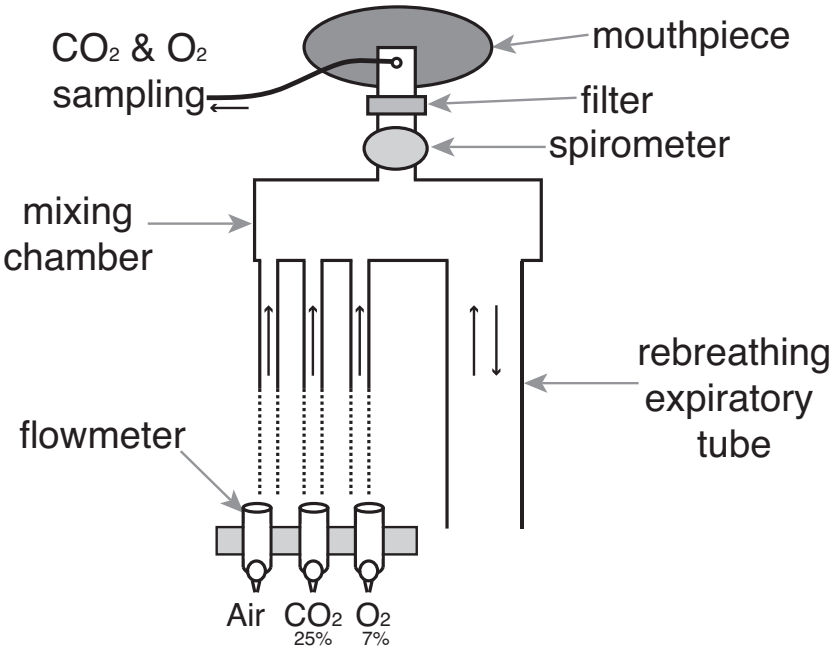

Figure 4.2: Breathing system used to administer hypercapnic challenges. At rest, humidified medical air is administered into the mixing chamber at a rate sufficient to avoid re-breathing of expired gases. A diving mouthpiece (Scubapro UK Ltd, Mitcham, UK) connects to a bacterial and viral filter (GVS, Lancashire, UK), and respiratory gases are sampled via polyethylene extension tubing (Vygon SA, Ecouen, France). A sampling line connects to a gas analyser that samples O_2 and CO_2 (Gas Analyser; ADInstruments Ltd, Oxford, United Kingdom), and end-tidal oxygen ($P_{ET}O_2$) and carbon dioxide ($P_{ET}CO_2$) were monitored at all times using physiological monitoring software (Labchart 7; ADInstruments Ltd, Oxford, United Kingdom) on a computer monitor. During hypercapnia, the medical airflow was reduced and a CO_2 mixture (25% CO_2; 21% O_2; balance N_2) was delivered into the mixing chamber to adjust expired $P_{ET}CO_2$ to either 0.8 % or 1.5 % (randomised) above rest, and a hypoxic mixture (7% O_2; balance N_2) was added to maintain $P_{ET}O_2$ at rest levels. A spirometer connected to a data acquisition device (Spirometer and Powerlab; ADInstruments Ltd, Oxford, United Kingdom) simultaneously recorded ventilatory flow and volume within Labchart.

'anaerobic threshold' was used for comparison between the two groups, as well as maximal exercise measures.

The incremental exercise test to exhaustion was completed on a stationary bike. A face mask (Hans Rudolf, Kansas City, MO, USA) and turbine were connected to a gas and flow analyser (Cortex Metalyser 3B, Cranlea Human Performance Ltd., Birmingham, UK) to measure expired gases and ventilatory flow on a breath-by-breath basis (Metasoft studio software, Cortex, Versions 3.9.9 and 4.9.0, Cranlea Human Performance Ltd., Birmingham, UK). Exercise began between 50-150 W (depending on predicted VO_{2peak}) at a self-selected cadence (target of 90 rpm), and 3 min stages of 50 W increments were completed until exhaustion. Breathlessness and anxiety of breathing were rated on a 0-100% VAS scale at the beginning of the exercise test, in the last 30 sec of each stage and at exhaustion. Anaerobic threshold was determined by visual inspection using the V-slope method (Stegmann et al., 1981).

4.4 Results

4.4.1 Baseline physiology and psychology

Differences in baseline physiological measures were observed between the two subject groups, while there were no differences in any baseline psychological measures. Athletes were significantly taller, with larger lung vital capacities, larger predicted value lung capacities and maximal voluntary ventilation (Table 4.1). All subjects had a FEV1/FVC fraction greater than 0.7, with no differences between the groups, indicating no airway obstruction (Swanney et al., 2008).

4.4.2 Incremental exercise test to exhaustion

A summary of the physiological and psychological variables measured during incremental exercise are presented in Table 4.3. As expected, work rate is greater in athletes at both anaerobic threshold and maximal exercise, and the anaerobic threshold of athletes is at a greater percentage of their maximum, indicating increased aerobic fitness (Bassett and Howley, 2000). At maximal exercise, the increase in ventilation from baseline is greater in athletes, and peak volume of oxygen consumption (VO_{2peak}) is larger in the athlete group. At maximal exercise, athletes ventilated at a much greater proportion of their MVV than their sedentary counterparts.

While no there was no difference in breathlessness intensity values at maximal exer-

*Table 4.1: Mean (±sd) baseline group physiology measures. Abbreviations: BMI, body mass index; FVC, forced vital capacity; FEV1/FVC, forced expiratory volume in 1 second as a fraction of forced vital capacity; MVV, maximal voluntary ventilation. Exercise exposure ('Exercise') was measured as the number of hours per week x intensity of exercise (1-3: easy, moderate, intense). *Significantly different (p<0.05) between groups*

	Athletes	Sedentary
Height (m)*	1.8 (0.9)	1.7 (0.1)
Weight (kg)	75.2 (10.1)	68.7 (13.6)
BMI (kg/m^2)	23.1 (2.8)	23.3 (3.5)
FVC (L)*	5.7 (0.9)	4.2 (1.2)
FVC (% predicted)*	109.5 (9.4)	91.0 (19.5)
FEV1/FVC (%)	78.2 (7.0)	81.3 (4.6)
MVV (L/min)*	150.9 (42.8)	113.0 (39.5)
Exercise (volume x intensity)*	20.3 (6.0)	1.8 (1.9)

*Table 4.2: Group questionnaire scores (mean (±sd)). *Significantly different (p<0.05) between groups*

	Athletes	Sedentary
Trait anxiety	29.6 (5.9)	30.8 (6.8)
Pre-exercise state anxiety	27.8 (6.5)	25.6 (5.4)
Anxiety sensitivity index	13.5 (6.1)	16.1 (7.7)
Depression	6.4 (4.2)	7.6 (4.7)

cise between the groups, athletes rated significantly higher in breathlessness anxiety than sedentary subjects. Further investigation revealed that breathlessness anxiety at maximal exercise positively correlated with measured VO_{2peak}, while breathlessness intensity did not (Figure 4.4).

4.4.3 Steady-state hypercapnic ventilatory response test

Mean group values for end-tidal gases, ventilation and subjective ratings of breathlessness during rest and the two steps of the hypercapnic hyperventilatory challenge are presented in Table 4.4. Ventilation is presented as both an absolute value and percentage change from baseline, to account for differences in lung physiology between the groups (Table 4.1). No differences were observed between groups for subjective ratings of either intensity and

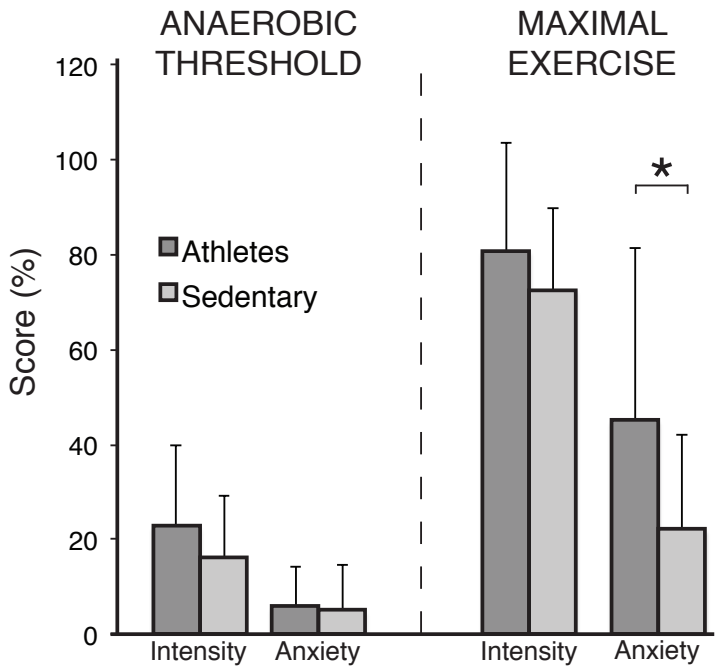

*Figure 4.3: Breathlessness intensity and anxiety scores (on a scale of 0-100%) at anaerobic threshold and maximal exercise for both athletes and sedentary subjects. Bars represent group mean, and error bars standard deviation. *Significantly different between the groups ($p < 0.05$).*

*Table 4.3: Physiological and psychological variables during an incremental exercise test to exhaustion on a cycle ergometer (mean (±sd)). Subjective scores are change from baseline. Abbreviations: VO_2, volume of oxygen consumed; V_E, ventilation; MVV, maximal voluntary ventilation. *Significantly different ($p<0.05$) between groups*

Anaerobic threshold	Athletes	Sedentary
Work rate (% of max)*	67.6 (7.7)	59.7 (12.8)
VO_2 (mL/kg/min)	19.5 (4.4)	20.3 (4.5)
V_E (% of max)	53.4 (10.0)	52.6 (13.3)
Breathlessness intensity (%)	22.9 (17.1)	16.1 (13.2)
Breathlessness anxiety (%)	5.9 (8.2)	5.2 (9.6)
Maximal exercise	**Athletes**	**Sedentary**
Work rate (W)*	325.0 (59.5)	173.8 (45.5)
VO_{2peak} (mL/kg/min)*	50.8 (7.3)	31.6 (7.4)
V_E (% above baseline)*	1051.7 (276.0)	665.7 (298.2)
V_E (% MVV)*	101.6 (27.2)	73.7 (30.1)
Breathlessness intensity (%)	80.7 (22.7)	72.5 (17.2)
Breathlessness anxiety (%)*	45.3 (36.3)	22.3 (20.0)

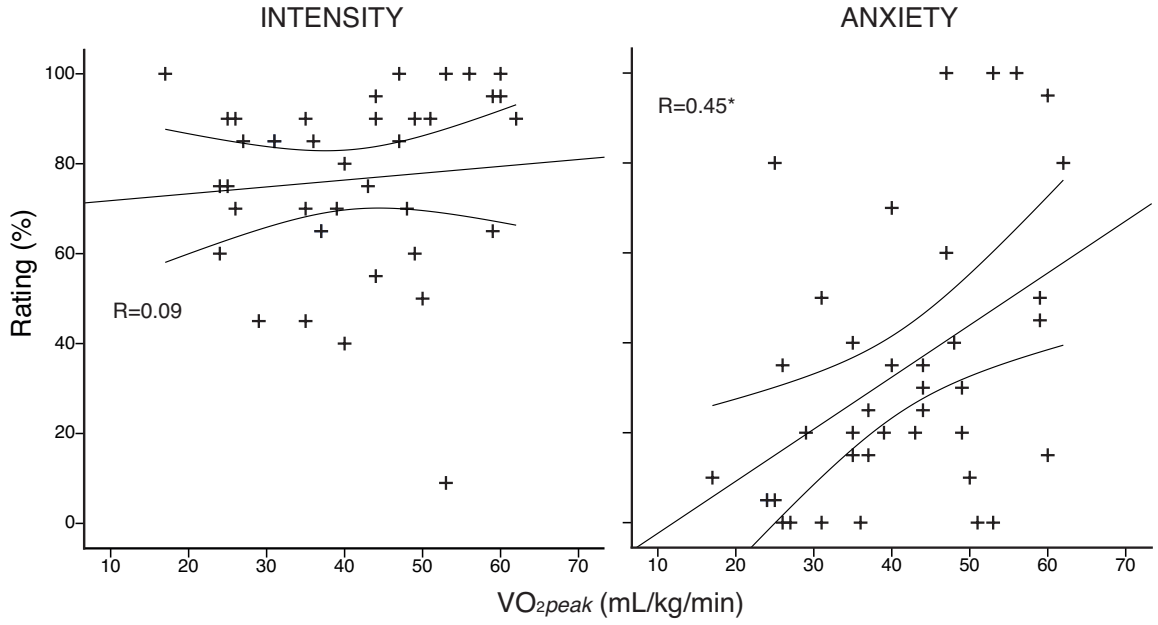

*Figure 4.4: Subject-specific anxiety and intensity scores plotted against peak volume of oxygen consumption (VO_{2peak}), measured during an incremental exercise test to exhaustion on a stationary bike. Intensity of breathlessness is plotted in the left column, and anxiety of breathlessness in the right column. *R correlation coefficient significant ($p < 0.05$).*

*Table 4.4: Physiological and psychological variables during rest and two levels of a hypercapnic hyperventilatory challenge (mild hypercapnia: aim of 0.8% (6.1 mm Hg); and moderate hypercapnia: aim of 1.5% (11.2 mm Hg) increase in $P_{ET}CO_2$). The order of hypercapnia levels was randomised between subjects, and results are presented as mean (±sd). Subjective ratings, $P_{ET}CO_2$ and $P_{ET}O_2$ during hypercapnia stages are presented as change from baseline. Abbreviations: $P_{ET}CO_2$, partial pressure of end-tidal carbon dioxide; V_E, ventilation. *Significantly different ($p<0.05$) between groups*

Rest	Athletes	Sedentary
$P_{ET}CO_2$ (%)	5.12 (0.67)	5.28 (0.46)
$P_{ET}O_2$ (%)	15.30 (1.01)	15.22 (0.85)
Ventilation (l/min)*	13.01 (3.63)	10.48 (2.54)
Intensity rating (%)	3.1 (4.5)	4.6 (3.8)
Anxiety rating (%)	3.1 (4.1)	5.1 (5.1)
Mild hypercapnia	Athletes	Sedentary
$P_{ET}CO_2$ increase (%)*	0.93 (0.10)	0.84 (0.12)
$P_{ET}O_2$ increase (%)	-0.2 (0.5)	0.0 (0.6)
Ventilation (l/min)	23.27 (10.23)	20.59 (4.80)
Change in ventilation (%)	87.2 (84.7)	104.3 (58.5)
Intensity rating (%)	23.0 (20.0)	17.3 (14.6)
Anxiety rating (%)	15.8 (16.3)	12.0 (12.8)
Moderate hypercapnia	Athletes	Sedentary
$P_{ET}CO_2$ increase (%)*	1.54 (0.12)	1.46 (0.11)
$P_{ET}O_2$ increase (%)	-0.0 (0.7)	0.3 (0.5)
Ventilation (l/min)	34.03 (14.59)	31.15 (11.45)
Change in ventilation (%)	174.4 (115.4)	205.6 (121.4)
Intensity rating (%)	38.9 (24.0)	43.2 (12.6)
Anxiety rating (%)	33.5 (25.4)	27.1 (15.0)

anxiety of breathlessness at both levels of hypercapnia, and $P_{ET}O_2$ remained stable across the entire experiment in both groups.

Hypercapnic ventilatory response (HCVR) was calculated using a linear regression between ventilation and $P_{ET}CO_2$, and no difference was found between the groups (mean (±sd): athletes 13.7 (9.6) vs sedentary 14.0 (7.4) (l/min / % change in CO_2)). For visual representation of individual subject HCVR see Figures D.1 and D.2.

As the hypercapnic ventilatory response did not differ between the two groups, we were then able to investigate the simple relationship between isolated changes in ventilation and the corresponding anxiety/intensity scores, to assess subjective awareness of changes in ventilation. During both mild and moderate hypercapnia, the athlete group showed a pos-

*Table 4.5: Regression (slope and regression coefficient) of changes in ventilation against subjective scores of intensity and anxiety of breathlessness, during mild and moderate hypercapnia (mild hypercapnia: aim of 0.8%; and moderate hypercapnia: aim of 1.5% increase in $P_{ET}CO_2$). *Significant regression coefficient; and ** significant regression coefficient that differs from sedentary group ($p<0.05$).*

Mild hypercapnia	Athletes	Sedentary
Intensity vs ventilation (slope (regression coefficient; R))	5.41 (0.79)*	1.75 (0.38)
Anxiety vs ventilation (slope (regression coefficient; R))	4.21 (0.70)**	-0.25 (0.06)
Moderate hypercapnia	**Athletes**	**Sedentary**
Intensity vs ventilation (slope (regression coefficient; R))	3.52 (0.64)**	2.00 (0.43)
Anxiety vs ventilation (slope (regression coefficient; R))	3.10 (0.59)**	-0.45 (0.11)

itive linear correlation for both intensity and anxiety with ventilation, while the sedentary group did not (Figures 4.5 and 4.6). This correlation was significantly greater in athletes than sedentary subjects for anxiety in both mild and moderate hypercapnia, and for intensity in moderate hypercapnia. Regression slopes and coefficients are presented in Table 4.5. Therefore, while mean differences in intensity and anxiety scores were not observed between the groups, it appears that an increase in ventilation closely corresponds with subjective ratings of breathlessness anxiety (and intensity) amongst the athlete group, while the sedentary group do not display any correspondence between ventilatory changes and breathlessness scores.

4.5 Discussion

4.5.1 Main findings

In this Chapter, we found that athletes do not appear to have reduced subjective perceptions of breathlessness intensity nor anxiety during exercise or hyperventilation alone. Therefore, it is unlikely that exercise 'de-sensitises' individuals to respiratory sensations, instead possibly inducing reappraisal of the threat of breathlessness when used as a treatment for patients with chronic respiratory disease.

We did find that athletes reported *increased* anxiety of breathlessness (but not intensity)

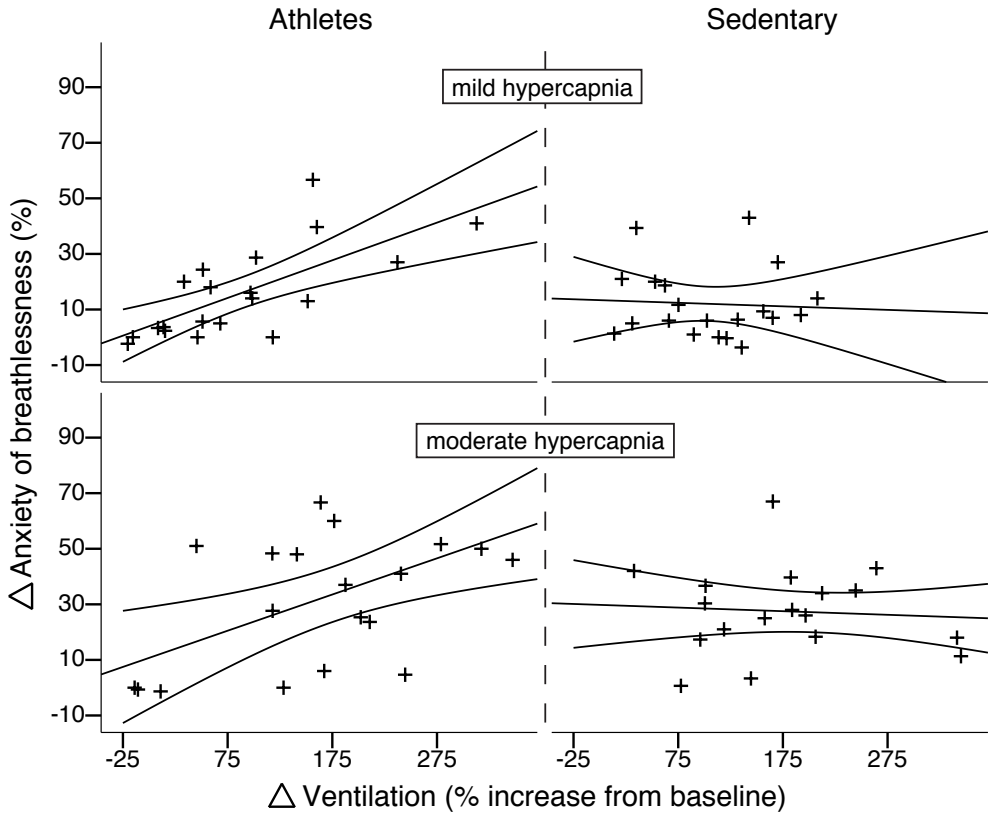

Figure 4.5: Subject-specific change in breathlessness anxiety scores plotted against percentage change in ventilation from baseline induced by both mild (top) and moderate (bottom) hypercapnia (mild hypercapnia: aim of 0.8%; and moderate hypercapnia: aim of 1.5% increase in $P_{ET}CO_2$). Athletes are plotted in the left column, and sedentary subjects in the right column. For both mild and moderate hypercapnia, athletes display a linear correlation between change in ventilation and change in anxiety score, that significantly differs from the null relationship seen in sedentary subjects.

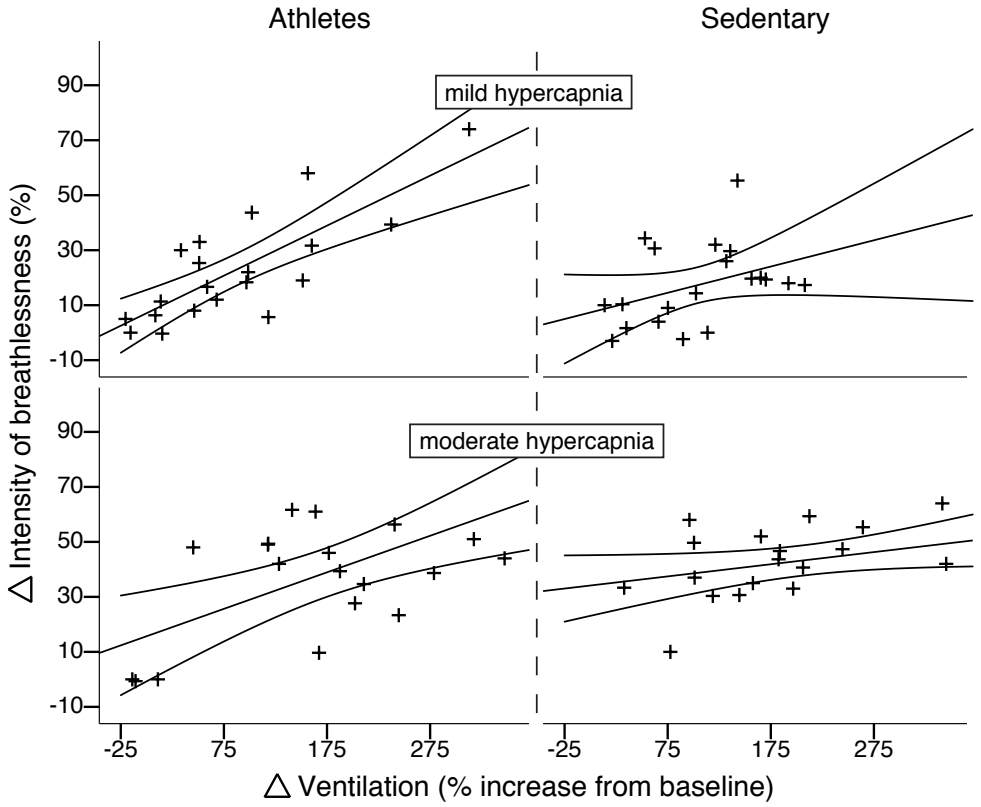

Figure 4.6: Subject-specific change in breathlessness intensity scores plotted against percentage change in ventilation from baseline induced by both mild (top) and moderate (bottom) hypercapnia (mild hypercapnia: aim of 0.8%; and moderate hypercapnia: aim of 1.5% increase in $P_{ET}CO_2$). Athletes are plotted in the left column, and sedentary subjects in the right column. For moderate (but not mild) hypercapnia, athletes display a linear correlation between change in ventilation and change in intensity score that significantly differs from the null relationship seen in sedentary subjects. 95% Confidence intervals are shown.

at maximal exercise, and were operating at a greater percentage of their maximal voluntary ventilation compared to sedentary subjects. As patients with chronic respiratory disease display reduced maximal ventilation, even low intensities of exercise can often induce ventilation at a high proportion of this MVV. Therefore, we can use these findings to better understand the breathlessness perception that occurs when operating at high proportions of maximal ventilatory capacities in both health and disease. Additionally, during isolated hyperventilation we found that athletes were more aware of changes in breathing compared to their sedentary counterparts. This may reflect adaptation resulting from increased exposure to breathlessness, which may also help us to understand some of the physiological and perceptual adaptations occurring with breathlessness in COPD.

4.5.2 Breathlessness and exercise

In contrast to our hypothesis, athletes were not desensitised to breathlessness during either sub-maximal or maximal exercise, and actually displayed increased breathlessness anxiety at their measured peak VO_2. This increase in breathing anxiety was not apparent at anaerobic threshold in athletes, indicating that this is not a general hypersensitivity to exercising breathlessness, but rather limited to maximal efforts. Interestingly, the ventilation reached during maximal exercise in athletes was a significantly greater proportion of measured maximal voluntary ventilation than sedentary subjects. This may be due to improved muscular metabolism and exercising capacity to place greater demands on the cardiorespiratory system, as this was also paired with a significantly greater increase in ventilation in the athlete group. Reaching a higher proportion of perceived maximal ventilation may result in conflicting feedback between a greater drive to breathe and the strain of ventilatory muscle work (Kaufman and Forster, 1996; Waldrop et al., 1996), contributing to an increase in breathing anxiety (Altose, 1985). Furthermore, the relationship between maximal exercising breathlessness anxiety and measures of peak VO_2 suggests that greater oxygen consumption by exercising muscles (measured using VO_2 (Stegmann et al., 1981)) may be involved in a feedback loop that drives increased ventilation and increases conscious sensory perceptions of breathing. Therefore, while exercise exposure does not appear to increase or decrease sensitivity to breathlessness, it may allow individuals to reach closer to their maximum ventilatory capacity and subsequently induce increased breathlessness anxiety.

4.5.2.1 Performance implications

Current opinion in the literature is that ventilation is not a limiting factor to exercise performance at sea level (McArdle et al., 2006; Bassett and Howley, 2000). However, this view of ventilation disregards the subjective perception of athletes who approach maximal ventilation, or the impact of ventilatory muscle fatigue (Romer and Polkey, 2008) which may regulate and limit performance in some individuals. Measures of VO_2 indicate the rate of metabolic consumption of oxygen by the working muscles (Stegmann et al., 1981), while above anaerobic threshold ventilation is driven beyond VO_2 demand by the accumulation of hydrogen ions from lactic acid produced by additional anaerobic metabolism (Wasserman et al., 1973). Endurance exercise training works by improving the efficiency and capacity of muscles to utilise oxygen and minimise anaerobic contribution to a sustainable power output, as well as improving the delivery of oxygen to tissues via the cardiorespiratory system (Hoffman, 2014; McArdle et al., 2006). However, the subjective effects of ventilatory drive as a result of the inevitable contribution of anaerobic metabolism at maximal exercise is not often considered. While debate thrives as to whether peripheral muscle factors or central cardiorespiratory factors limit exercise performance (Bassett and Howley, 2000), it may be that the athletes who are genetically endowed with a smaller lung volume, ventilatory capacity or respiratory muscle endurance, or a higher sensitivity to ventilatory signals are also at risk of breathlessness anxiety limiting their performance. In these athletes, additional targeted training of ventilatory muscle capacity and endurance through methods such as resisted breathing may improve their performance; a training method that has previously reported some positive results (Boutellier and Piwko, 1992; Volianitis et al., 2001; Sonetti et al., 2001). Therefore, while we are not suggesting that anxiety of breathlessness is the sole limiting factor to performance, it may be an indicator of nearing ventilatory capacity and a possible area for targeted improvement in susceptible athletes.

4.5.2.2 Clinical implications for patient groups

The exercise results of this study may contribute to our understanding of anxiety changes in clinical breathlessness. Patients with lung disease have reduced maximal voluntary ventilation (Aldrich et al., 1982), which may hasten the onset of exercising breathlessness anxiety by increasing the mismatch between ventilatory drive and feedback from the chest. Through repeated exposure to this increased exercising breathlessness, patients begin to fear and avoid activities that may induce this sensation, resulting in further deterioration of the ventilatory muscles in the chest and further reduction in maximal voluntary ventilation. This worsening cycle of breathlessness occurs as a result of conditioned responses

to breathless stimuli (Ley, 1999), although the exact physiological mechanisms inducing breathlessness anxiety as a result of disease are not yet known (Lansing et al., 2009). The treatment success of pulmonary rehabilitation has been linked to pre-treatment measures of anxiety (Janssens et al., 2011b), which may be associated with either higher sensitivity to this ventilatory mismatch, or a more significant drop in previous maximal ventilation caused by the disease. If so, pulmonary rehabilitation may act by increasing maximal ventilation through the work capacity of ventilatory muscles (independent of forced vital capacity), thus reducing anxiety and deconditioning patients to the association between exercise and anxiety to break the cycle. Future investigations in patients with COPD would need to test the changes in both sensitivity to ventilation and maximal voluntary ventilation relative to changes in breathlessness anxiety to further investigate this hypothesis.

4.5.3 Breathlessness and hyperventilation

In this Chapter we found no group differences between athletes and sedentary subjects in the physiological ventilatory response to hypercapnia, nor the subjective breathlessness ratings during hyperventilation. Therefore, it does not appear that the athletes tested in this Chapter are perceptively de-sensitised to either the physiology or subjective response to isolated hyperventilation, either by self-selection or as a result of training. However, further investigation revealed that athletes' breathlessness scores during hyperventilation positively correlate with the change in ventilation during the hypercapnic challenge, while the sedentary subjects did not. This relationship between the physiological change in ventilation and breathlessness implies a more finely-tuned perception of changes in breathing in athletes, possibly as a result of repeated exposure to elevated ventilation and breathlessness during endurance exercise training.

4.5.3.1 Performance implications

While a decrease in hyperventilatory response to hypercapnia in athletes has been debated in the literature (Mucci et al., 1998; Byrne-Quinn et al., 1971; Godfrey et al., 1971; Scoggin et al., 1978; Mahler et al., 1982), studies to date have used cross-sectional designs and therefore it is plausible that these discrepancies in reported results are due to underlying genetic differences of the samples studied. However, improved perception of ventilatory responses found in this study may allow better monitoring of exercise intensity and pacing during sporting performance. Fatigue of ventilatory muscles has been suggested as an important factor in endurance exercise, due to the competition for blood and metabolites with the working peripheral muscles (Harms et al., 2000; Johnson et al., 1996; Romer

and Polkey, 2008), and thus appropriate pacing may reduce this impact on performance. However, to fully understand the effect of exercise on the hypercapnic-hyperventilatory response, perceptions of breathlessness and any potential contributions to performance, dedicated longitudinal and placebo-controlled studies are required.

4.5.3.2 Clinical implications for patient groups

If repeated exposure to breathlessness can improve the accuracy of perception of changes in ventilation, chronic sufferers of lung disease may also have heightened perception of their breathing. However, due to the associations between breathlessness and disease amongst patients, improved ventilatory perception may contribute to increased anxiety in this group, enhancing the aversive conditioning to breathlessness cues (Ley, 1999). While the hyperventilatory response to hypercapnia has been previously found to be reduced in patients with COPD (Van de Ven et al., 2001), little research has been conducted into the subjective response to this hyperventilation. In an elegant review by Smoller et al. (1996), the intricacy of the relationship between physiological and subjective sensations of ventilation in panic anxiety, hyperventilation and breathlessness is outlined. The presence of chronic breathlessness can be considered a risk factor for anxiety and panic attacks, while panic disorder patients can also report debilitating sensations of breathlessness that exacerbate their anxiety (Smoller et al., 1996). It is possible that a tuned perception towards ventilation is a common contributing factor to these classes of disease, which may be enhanced by repeated breathlessness exposure. Therefore, one of the mechanisms for successful treatment with pulmonary rehabilitation might be the cognitive-behavioural effect of associating increases in ventilation with positive exercise training for health, rather than as a symptom solely of disease.

4.5.4 Study design

The use of an athlete model to understand exercise-induced adaptations to breathlessness is of course limited in its ability to understand disease. While this investigation can address possible de-sensitisations to intensity of respiratory sensations, it is limited in the ability to understand changes in anxiety of breathlessness. COPD patients have shown elevated anxiety of breathlessness to healthy controls (Janssens et al., 2011b), and thus there is scope to reduce anxiety, whereas the sedentary group studied in this experiment did not display elevated anxiety of breathlessness or other physiological sensations (ASI questionnaire).

Interestingly, the two groups also did not differ in their general anxiety questionnaire scores. While this does instill some confidence that any observed changes in breathless-

ness anxiety would not result from underlying differences in general anxiety, there is some evidence to suggest that exercise (and in particular aerobic endurance exercise) can have antidepressant and anxiolytic effects (Salmon, 2001). Therefore, while there is not a definitive stance in the literature that people who exercise are less anxious than those who are sedentary, it is possible that the demanding nature of this study was self-limiting to subjects who have generally low anxiety, and thus the sedentary group may not be a representation of their population. Therefore, as with all cross-sectional studies, care must be taken when interpreting findings and attributing any differences found in these results (or further imaging results) to be characteristic of all athletes or sedentary individuals.

Lastly, the nature of a cross-sectional study design itself limits the causal inference that can be placed on group comparisons, as measurements taken at a single time point do not encompass potential underlying subject differences in physiology and psychology. Therefore, considerations must be taken to account for fundamental differences between the groups when attempting to make comparisons. In one example of baseline group differences in this study, we observed that athletes had a greater predicted forced vital capacity of the lungs, maximal voluntary ventilation and resting ventilation. Therefore, particular care was taken in the analysis to normalise data within each subject for exercise and hyperventilation measures, such as calculating ventilation as a change from baseline or as a percentage of maximum, and using relative measures of exercise intensity (such as each subject's anaerobic threshold and maximum) at which to report subjective measures of breathlessness.

4.6 Conclusions

The results of this Chapter suggest that the athletes in this study are not desensitised to breathlessness during exercise or hyperventilation compared to sedentary controls, contrary to our hypotheses. Therefore, it is possible that previously-reported observed changes in breathlessness anxiety in patients with COPD undergoing exercise treatment is due to alteration of the threat perception of breathlessness. This study therefore provides the grounding to better understand future studies of breathlessness adaptations as a result of exercise in patient groups, and highlights the need for further mental skills training to improve threat perceptions of breathlessness.

In terms of the increased anxiety of breathlessness observed in athletes at maximal exercise, we postulate that this may be due to athletes reaching a greater proportion of their maximal ventilatory capacity. This may represent both a performance limitation and a clinically important homeostatic signalling system, which may be exacerbated in lung

disease patients with reduced maximal ventilation and a lower threshold for this signalling. Furthermore, while breathlessness perception during hyperventilation alone was not significantly different between the groups, athletes had a significantly different, linear relationship between changes in ventilation and subjective breathlessness scores compared to sedentary subjects. We hypothesise that this relationship may represent improved perception of changes in ventilation in athletes. Enhanced perception of ventilation may be an important adaptation in patients with chronic breathlessness and requires consideration in future studies, as this may lead to heightened anxiety of breathing and an increase in debilitation and morbidity of the disease.

We now take these results and incorporate them into our final study of the PAG within the wider breathlessness network, allowing us to also investigate the effect of exercise on these brain networks (Chapter 5). As the current results have shown no de-sensitisation in breathlessness anxiety during sub-maximal exercise or to hyperventilation in athletes, it is unlikely that there will be any significant differences in anxiety of inspiratory resistance in these subjects. However, if exercise does indeed evoke a reappraisal of the threat of breathlessness, it may be possible to observe subtle differences in the vlPAG and fronto-limbic activity of these athletes.

Chapter 5

The PAG within sensory and affective brain networks of breathlessness

5.1 Abstract

The multidimensional sensation of breathlessness is evoked when our ability to adequately ventilate is impaired, and comprises both sensory and affective components. Investigating the brain networks responsible for these components is integral in our understanding of misperceptions of ventilatory sensations, which may lead to excessive breathlessness anxiety in health or disease. We have previously shown that the columns of the PAG play important roles in human respiratory control and breathlessness (Chapters 2 and 3), and the PAG activity identified during anticipation of breathlessness suggests these columns are under top-down control from the higher cortex. Therefore, in this final Chapter we investigated the place of these PAG columns within the wider cortical breathlessness network, and the possible exercise-induced changes in the affective sub-network, as our results from Chapter 4 indicate that exercise does not produce global 'de-sensitisation' to breathlessness. 40 subjects (20 endurance athletes and 20 matched sedentary controls) were conditioned to associate cues with either certain upcoming resistive loading or no loading in a training session 12-24 hours prior to scanning, using an aversive delay-conditioning protocol. During scanning, subjects completed an anticipation and perception of resistive loading task protocol, and a resting state scan for functional connectivity analysis of the PAG columns. Our results showed that both vlPAG and lPAG activity were active within a broad cortical network during anticipation of breathlessness, with lPAG activity also scaling with the subjective intensity ratings of breathlessness during resistive loading. Functional connectivity analysis revealed preferential connectivity of the vlPAG to prefrontal and limbic structures within this network, while lPAG connected to sensorimotor structures. These findings indicate the the vlPAG is active within the affective cortical network of breathlessness, while the lPAG lies within the sensory component, making the PAG an important point of distinction within breathlessness perception. Finally, in the exercise comparison, athletes displayed increased activity in the vlPAG and medial prefrontal cortex during anticipation of aversive resistive loading, indicating possible adaptation within the affective perception of breathlessness. Together, these results suggest that the columns of the PAG have differing roles in breathing perception and distinct interactions with cortical areas, with the vlPAG and affective breathlessness network a legitimate target for future research towards understanding (mal)adaptations of breathlessness perception in health and disease.

5.2 Introduction

Breathlessness is a complex, multi-dimensional sensation that can cause crippling anxiety. The perception of breathlessness relies on an intricate network of sensory and affective components within the brain (Herigstad et al., 2011; Hayen et al., 2013b; Lansing et al., 2009), both perceiving ventilatory afferents and evaluating the threat of these respiratory sensations. While animal models have implicated the midbrain periaqueductal gray (PAG) as a key neural component in the behavioural modulation of breathing (Subramanian et al., 2008; Subramanian, 2012) and threat responses (Keay and Bandler, 2001; Bandler and Shipley, 1994; Bandler et al., 2000), our previous work has revealed that consistent activity can be localised to the columns of the human PAG during simple respiratory control (Chapter 2), and in the anticipation and response to breathlessness (vlPAG and lPAG: Chapter 3). However, while these results indicate that the columns of the PAG are potentially differentially involved in breathlessness perception, we do not yet know how this activity operates within the complex network of higher cortical structures.

The anticipation of impending breathlessness can evoke severe anxiety and contribute to the debilitating nature of breathlessness (as previously discussed in Chapter 3). These anticipatory responses come from learned cues from the environment (Pavlov and Anrep, 2003), and evoke top-down activity in brain networks to predict forthcoming sensory events (Engel et al., 2001) and influence symptom perception (Porro et al., 2002; Price et al., 1999; Wager et al., 2004). Therefore, the brain activity evoked from conditioned cues may reveal top-down processing of ventilatory sensations for breathlessness perception. While PAG activity has previously been reported to reside within top-down pathways of pain anticipation (Mobbs et al., 2007; Wager et al., 2004; Fairhurst et al., 2007) and perception (Tracey et al., 2002; Bingel et al., 2006; Fields, 2004; Zambreanu et al., 2005), the conflicting increases and decreases of PAG activity may be explained by the previous inability to localise this activity to the distinctly different PAG columns.

Furthermore, determining the connectivity between the PAG columns and remote areas of the brain can help us to identify whether these columns are modulated within sensory or affective sub-networks of breathlessness perception. 'Functional connectivity' within neuroimaging is a measure of the temporal synchronicity of activity within structures across the brain, and is dependent on the temporal coherence of neuronal spike trains in anatomically distinct regions (Gerstein and Perkel, 1969; Van Den Heuvel and Pol, 2010). Therefore, the co-activation of fMRI timeseries in the PAG columns and cortex at rest can be used as a measure of the functional connectivity between regions (Mandelbrot and Van Ness, 1968). In this Chapter we included both a breathlessness task of conditioned inspiratory resistive

loading and a resting-state functional scan, to investigate both the activity and connectivity of the columns of the PAG with the cortex and subcortex, and potentially revealing how this might delineate the functional contributions of the columns of the PAG to the perception of breathlessness.

Finally, identifying areas of change in brain structure and function (termed 'plasticity') within these top-down networks may help us to understand misperceptions of ventilatory symptoms and exacerbated breathlessness in health and disease. Exercise is known to induce changes in brain structure and function in both the cortex (Erickson et al., 2011; Turner et al., 1997) and PAG (Ichiyama et al., 2002; Nelson et al., 2005; Nelson and Iwamoto, 2006), and has also been used to successfully decrease breathlessness in patients with chronic obstructive pulmonary disease (COPD) (Carrieri-Kohlman et al., 2001, 1996). In Chapter 4 we observed that exercise does not appear to induce a global 'de-sensitisation' to breathlessness perception, and thus it is likely that any cortical adaptation as a result of exercise lies within the affective, emotional evaluation component of breathlessness, re-evaluating the threat of the imposed symptoms. Therefore, as well as attempting to decompose breathlessness perception into sensory and affective brain networks between the PAG and cortex, in this study we also begin to explore the mechanism of action of exercise on these networks, to better understand and develop treatment for misperceptions of breathlessness.

5.2.1 Hypotheses

In line with animal models and our previous PAG results (Chapters 2 and 3), in this Chapter we hypothesised that the vlPAG would be functionally active with, and display preferential connectivity to frontal and limbic structures as part of the top-down affective network of breathlessness perception. Conversely, the lPAG will be functionally active with (and connected to) sensorimotor cortical structures, as part of the sensory aspect of breathlessness. Lastly, we also hypothesised that exercise exposure would correspond with altered activity in the vlPAG and fronto-limbic areas during anticipatory threat-detection of inspiratory resistive loading, with a possible decrease in breathlessness anxiety rather than intensity.

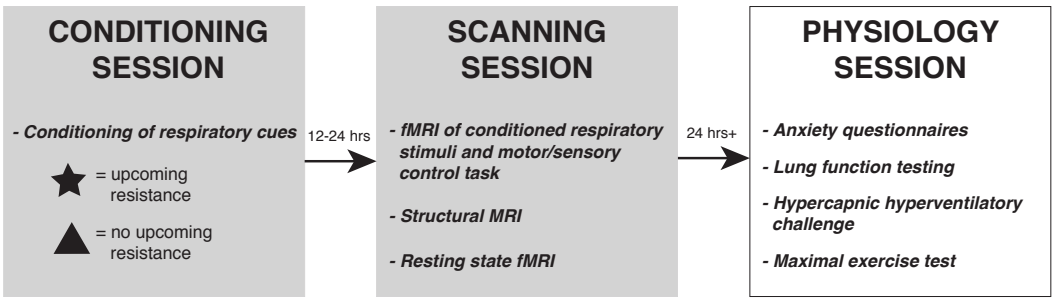

Figure 5.1: Experimental overview of Chapters 4 and 5. The testing sessions discussed in this Chapter are identified in grey.

5.3 Methods

5.3.1 Subjects

In this Chapter we studied 40 healthy, right-handed subjects, consisting of a group 20 endurance athletes and 20 age and sex-matched sedentary individuals (20 males, 20 females; mean age $\pm$ SD, 26 $\pm$ 7 years; age-matched $\pm$2 years). Athletes were amateur sportspeople who participated in organised endurance exercise training 5 or more times per week, while the sedentary subjects were not involved in any organised exercise, and minimal commuting exercise. These subjects also participated in the physiology testing session described in Chapter 4 (and outlined in Figure 5.1).

5.3.1.1 Experimental overview

Subjects completed one training session followed by one MRI scanning session, 12-24 hours later (highlighted in grey in Figure 5.1). Figure 5.1 demonstrates how the training and scanning sessions described in this Chapter were conducted with reference to the physiological testing session described in Chapter 4, which was conducted after the scanning sessions so as not to interfere with these results.

5.3.2 Stimuli and tasks

Subjects were trained using an aversive delay-conditioning paradigm to associate simple shapes with an upcoming inspiratory resistance stimulus. Two conditions were trained: 1) A shape that always predicted upcoming resistance (100% contingency pairing), and 2)

A shape that always predicted no upcoming resistance (0% contingency pairing) (Figure 5.2). This was altered from Chapter 3 to remove the uncertain anticipation condition (50% contingency pairing).

The 'certain upcoming resistance' symbol was presented on the screen for 30 s, which included a 5-15 s anticipation period before the resistance was applied. The 'no resistance' symbol was presented for 20 s, and each condition was repeated 14 times in a semi-randomised order. A finger opposition task was also included in the protocol, where an opposition movement was conducted between the right thumb and fingers, with the cue 'TAP' presented for 15 s (10 repeats). All subjects were checked following the training session and immediately prior to the MRI scan to verify that cues had been conditioned adequately.

Rating scores of breathing difficulty were recorded after every symbol and at the beginning and end of the task, using a visual-analogue scale (VAS) with a sliding bar that the subjects moved between 'Not at all difficult' (0%) and 'Extremely difficult' (100%). Subjects were also asked to rate how anxious each of the symbols made them feel using a VAS between 'Not at all anxious' (0%) and 'Extremely anxious' (100%) immediately following the functional protocol. Subjects were asked to record how many hours of physical activity they typically completed per week, the intensity of the exercise (easy, moderate or intense) and what types of exercise they performed.

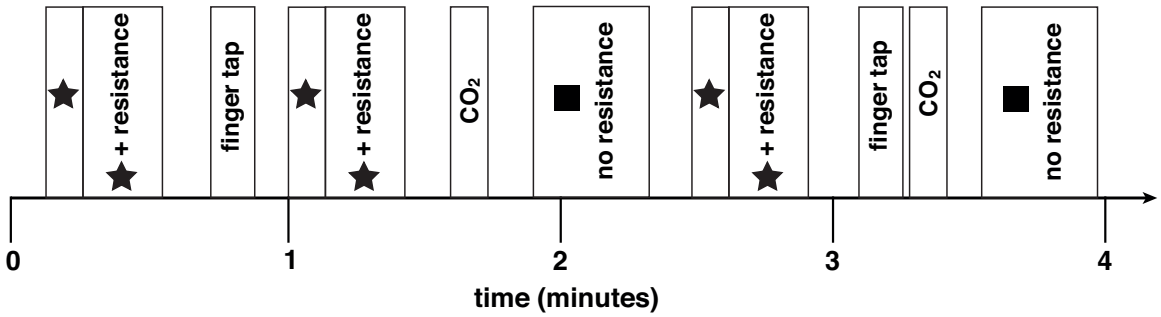

Figure 5.2: Example four minutes of the BOLD sequence, repeated throughout the acquisition.

5.3.3 Breathing system

A breathing system was used (previously described in Chapter 3; Figure 3.2) to remotely administer periods of inspiratory resistance as predicted by the conditioned cues. During rest periods, compressed medical air was delivered to the breathing system and gas flow was maintained at a rate that was sufficient to allow free breathing, so that the reservoir bag

never collapsed on inspiration. During inspiratory resistance, delivery of compressed air was stopped, and once the reservoir bag collapsed, inspiration was through the resistance arm of the circuit to inhale atmospheric air.

To minimise the effect of changing arterial oxygen and carbon dioxide levels upon the BOLD signal, the following steps were employed: 1) Additional medical oxygen was delivered, and the flow rate was manually adjusted to minimise fluctuations in pressure of end-tidal oxygen ($P_{ET}O_2$), aiming to keep $P_{ET}O_2$ at 18 kPa (very slightly above normal), and 2) At designated time points during rest periods of the functional scan, CO_2 challenges were administered by switching the flow of compressed air for a 10% CO_2 mixture (10% CO_2; 21% O_2; balance nitrogen) at 20 L/min for periods of 5-10 seconds, aiming to raise $P_{ET}CO_2$ an equivalent amount as observed during the resistive loading periods. The subjects nose was blocked using foam earplugs and they were asked to breathe through their mouth for the duration of the experiment.

5.3.4 Physiological measurements

Physiological measures were recorded continuously during the training session and MRI scan. Chest movements were measured using respiratory bellows surrounding the chest at the approximate level of the 10th rib, and heart rate was measured using a pulse oximeter (9500 Multigas Monitor, MR Equipment Corp., NY, USA). $P_{ET}CO_2$ and $P_{ET}O_2$ were sampled via a port beside the mouth piece of the breathing system. Expired gases were determined using a rapidly-responding gas analyser (Gas Analyser; ADInstruments Ltd, Oxford, United Kingdom), and pressure at the mouth was measured using a pressure transducer (MP 45, $\pm$50 cmH_2O, Validyne Corp., Northridge, CA, USA) connected to an amplifier (Pressure transducer indicator, PK Morgan Ltd, Kent, UK). All physiological devices were connected to a data acquisition device (Powerlab; ADInstruments Ltd, Oxford, United Kingdom) coupled to a desktop computer with recording software (Labchart 7; ADInstruments Ltd, Oxford, United Kingdom).

5.3.5 MRI scanning sequences

MRI was performed with a 7 T Siemens Magnetom scanner, with 70 mT/m gradient strength and a 32 channel Rx, single channel birdcage Tx head coil (Nova Medical).

5.3.5.1 Brainstem BOLD scanning

A T2*-weighted, gradient echo EPI was used for functional scanning. The FOV covered the whole brain and comprised 63 slices (sequence parameters: TE, 24 ms; TR, 3 s; flip angle, 90°; voxel size, 2 x 2 x 2 mm; field of view, 220 mm; GRAPPA factor, 3; echo spacing, 0.57 ms; slice acquisition order, descending), with 550 volumes (scan duration, 27 mins 30 s). A resting-state acquisition (eyes open) with a matching scan sequence was also performed, with 190 volumes (scan duration, 9 mins 30 s).

5.3.5.2 Structural scanning

A T1-weighted structural scan (MPRAGE, sequence parameters: TE, 2.96 ms; TR, 2200 ms; flip angle, 7°; voxel size, 0.7 x 0.7 x 0.7 mm; field of view, 224 mm; inversion time, 1050 ms; bandwidth; 240 Hz/Px) was acquired. This scan was used for registration of functional images.

5.3.5.3 Additional scanning

Fieldmap scans (sequence parameters: TE1, 4.08 ms; TE2, 5.1 ms; TR, 620 ms; flip angle, 39°; voxel size, 2 x 2 x 2 mm) of the B0 field were also acquired to assist distortion-correction.

5.3.6 Analysis

5.3.6.1 Preprocessing

Image preprocessing was performed using the Oxford Centre for Functional Magnetic Resonance Imaging of the Brain Software Library (FMRIB, Oxford, UK; FSL version 5.0.8; http://www.fmrib.ox.ac.uk/fsl/). The following processing methods were used prior to statistical analysis: motion correction and motion parameter recording (MCFLIRT (Jenkinson et al., 2002)), removal of the non-brain structures (skull and surrounding tissue) (BET (Smith, 2002)), spatial smoothing using a full-width half-maximum Gaussian kernel of 2 mm, and high-pass temporal filtering (Gaussian-weighted least-squares straight line fitting; 120 s). B0 field unwarping was conducted with a combination of FUGUE and BBR (Boundary-Based-Registration; part of FEAT: FMRI Expert Analysis Tool, version 6.0 (Greve and Fischl, 2009)).

Data denoising was conducted using a combination of independent components analysis (ICA) and retrospective image correction (RETROICOR), described in Chapter 3.

5.3.6.2 Image registration

After preprocessing, the functional scans were registered to the MNI152 (1 mm^3) standard space (average T1 brain image constructed from 152 normal subjects at the Montreal Neurological Institute (MNI), Montreal, QC, Canada) using a two-step process.

- Registration of subjects whole-brain EPI to T1 structural image was conducted using BBR (6 DOF) with (nonlinear) fieldmap distortion-correction (Greve and Fischl, 2009).
- Registration of the subjects T1 structural scan to 1 mm standard space was performed using an affine transformation followed by nonlinear registration (FNIRT) (Andersson et al., 2007).

5.3.6.3 Functional voxelwise and group analysis

Functional voxelwise analysis incorporated HRF modelling using three FLOBS regressors (as described in Chapter 2), and the first level model is demonstrated in Figure 5.3. The first of each of the three FLOBS regressors in the voxelwise statistical analysis was extended to a group level, in a mixed-effects analysis using FLAME (FMRIBs Local Analysis of Mixed Effects (Woolrich et al., 2004a)), with the group model demonstrated in Figure 5.4. In the higher level model, as well as mean BOLD activity, intensity and anxiety covariates were included to investigate BOLD activity in the PAG and cortex that scaled with these behavioural scores. Finally, an exercise group regressor was included in the model, to test whether exercise exposure induces differences in the function of the PAG columns and cortex during conditioned anticipation or resistive loading. Z statistic images were thresholded using clusters determined by $Z > 2.3$ and a (corrected) cluster significance threshold of $p < 0.05$. A small-volume mask of the whole PAG was used to investigate a-prior areas of interest, using standard cluster thresholding ($Z > 2.3$).

5.3.6.4 Resting functional connectivity analysis

Voxelwise single subject and group analyses were also performed on the acquired resting state scan. Masks of the PAG columns of interest that showed significant activation in the functional results (lPAG and vlPAG) were made within a whole-brain PAG mask, modelled on the diffusion-based segmentation of the PAG (Ezra et al., 2015), then transformed into subject space, and the mean timeseries within these seeds for each subject was used as a regressor in the design matrix at the lower level. A control seed of similar size to the PAG

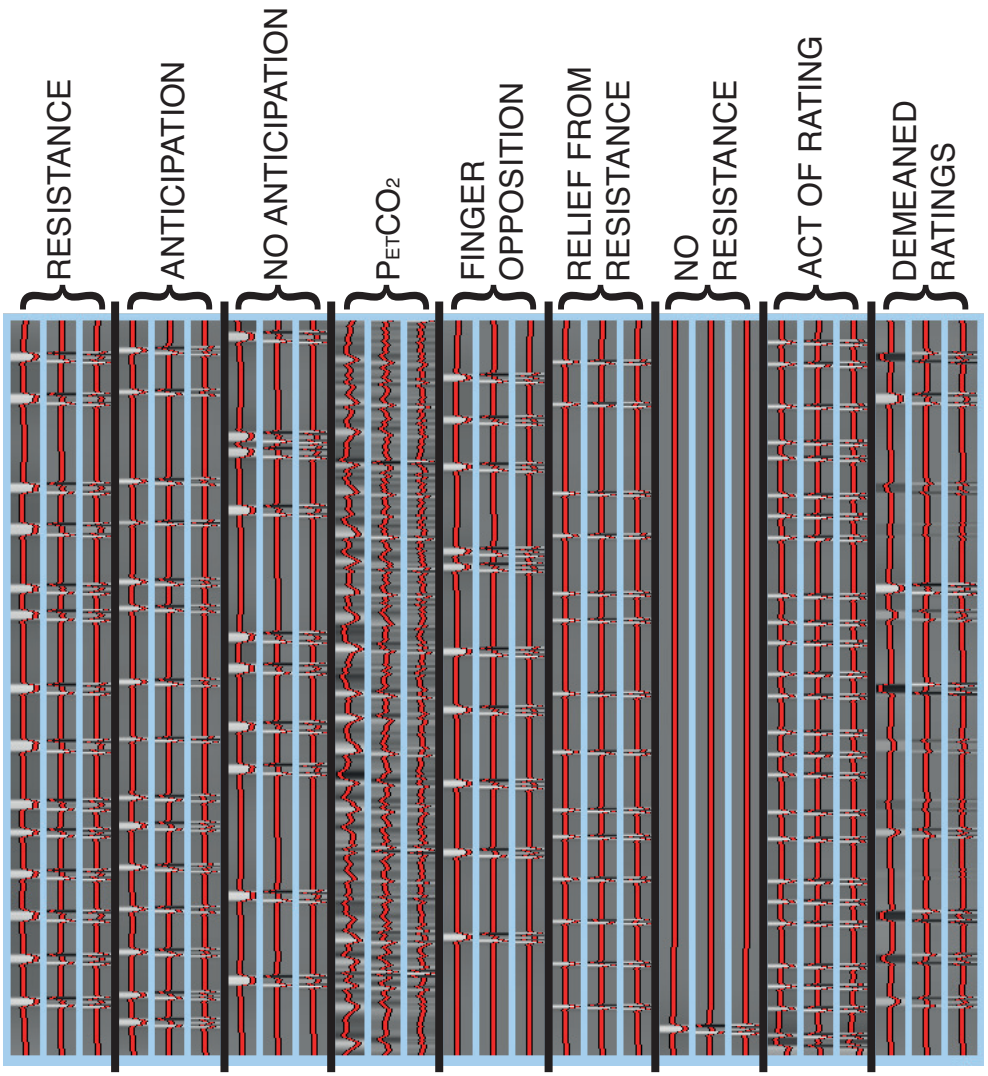

Figure 5.3: General linear model used in each single subject lower level analysis within FEAT. The FLOBS function creates three EVs for each regressor. The 'resistance' onset and duration were calculated from the recorded inspiratory pressure physiological traces, while the anticipation duration ('anticipation') was calculated from the onset of the stimulus to the beginning of the resistance. The '$P_{ET}CO_2$' trace was included to de-correlate the CO_2 induced BOLD changes from the respiratory stimuli throughout the functional scan, and was formed by linearly interpolating between the expired CO_2 peaks. Anticipation of no resistance ('no anticipation') and 'finger opposition' onset and duration represented the presentation of the corresponding stimuli on the screen, and 'relief from resistance' was modelled as the rest periods immediately following each resistance application, prior to ratings (4 s duration). The 'no resistance' regressor was a single trial where no resistance was applied following an anticipation period, allowing greater decorrelation between the anticipation and resistance regressors. The 'act of rating' regressor was included to remove noise from the physical act of pressing the button box, and spanned each of the rating periods. Finally, 'demeaned ratings' matched the 'resistance' regressor for timings, and the intensity of the regressor was the demeaned intensity value assigned to each of the inspiratory resistance blocks, to remove the trial-by-trial variability of subjective perceptions of resistive loading from the mean 'resistance' regressor. Contrasts consisted of mean values of the first EV of each set of three regressors.

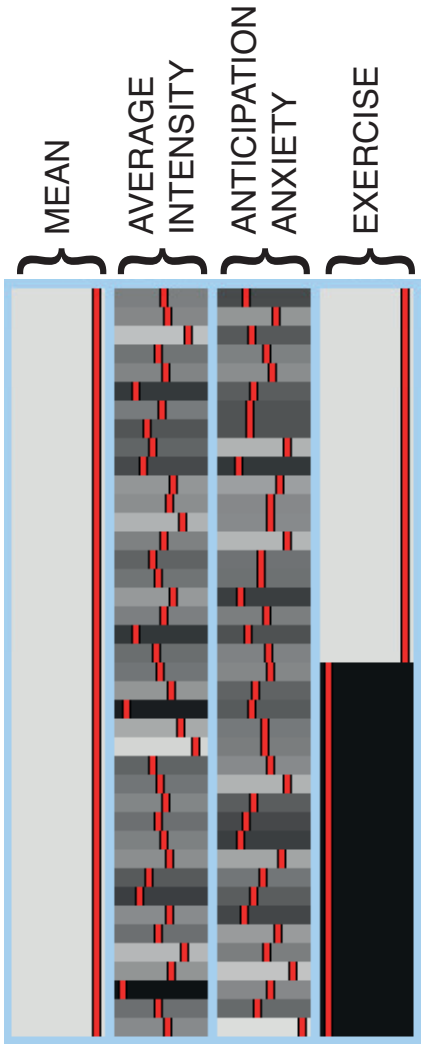

Figure 5.4: General linear model used in the group higher level analysis within FEAT. For each lower level contrast, positive and negative contrasts were calculated for the group mean ('mean'), plus covariates of the average resistive loading intensity ('average intensity'; calculated from lower level intensity ratings for each subject) and anxiety of upcoming resistance ('anticipation anxiety'). Lastly, an 'exercise' group comparison regressor was included to investigate differences between athletes and sedentary subjects.

seeds was made in the left primary auditory cortex in standard space, transformed into subject space and the mean timeseries calculated to act as a control connectivity analysis. The T1 structural image from each subject was segmented using hard segmentation in FAST (Zhang et al., 2001), transformed into functional EPI space and the mean timeseries from the cerebrospinal fluid and white matter were included as noise regressors of no interest. A convolution was not applied to any of the regressors, as the timeseries were taken from the preprocessed data rather than an external timing file. However, a temporal derivative was included for each regressor, to account for small delays in the connectivity between areas of the brain, producing a total of two EVs for each model regressor. This first level model is demonstrated in Figure 5.5. Each of the timeseries regressors were then extended to a mean at the group level.

5.4 Results

5.4.1 Functional breathlessness network results

5.4.1.1 Resistive loading physiology and psychology

All subjective measures included in the analysis are from the MRI scanning session. Mean anxiety and intensity scores for conditioned responses to the respiratory tasks in the whole group are given in Table 5.1, and display a conditioned anticipatory response to the certain upcoming resistance condition.

*Table 5.1: Mean ($\pm$sd) anxiety and intensity ratings to the conditioned respiratory tasks. *Significantly ($p < 0.05$) different from no impending resistance condition.*

	No resistance	Certain resistance
Anxiety (%)	2.5 (3.9)	34.0 (18.8)*
Intensity (%)	2.8 (3.5)	46.5 (16.0)*

5.4.1.2 Mean functional breathlessness network activity

The main contrasts of interest presented in these results are the activity during resistive loading (resistive loading $>$ baseline), and the aversive anticipation of resistive loading (anticipation of resistance $>$ anticipation of no resistance; CS+ $>$ CS-). The results of the

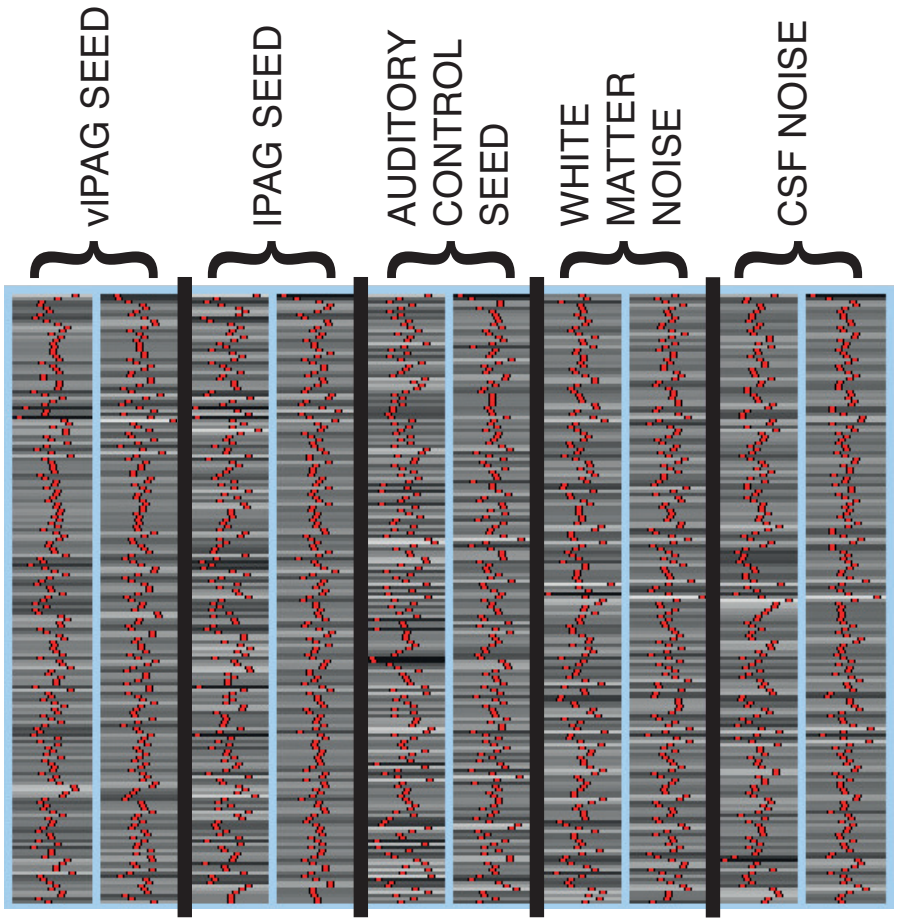

Figure 5.5: General linear model used in each single subject lower level PAG seed resting state analysis within FEAT. Each regressor also has a temporal derivative added, to account for small connectivity or noise delays across the brain. A mask of the vlPAG and lPAG columns were made from previous diffusion-based segmentation of the human PAG (Ezra et al., 2015), and transformed into subject space. The mean timeseries of these masks were calculated and entered into the model as the first two regressors of interest ('vlPAG seed' and 'lPAG seed'). A control seed in the primary auditory cortex (similar size to the PAG masks) was made in standard space, transformed into subject space and the mean timeseries calculated to act as a control ('auditory control seed'). Finally, two noise regressors were included in this model: White matter and cerebrospinal fluid (CSF) ('white matter noise' and 'CSF noise'). The mean timeseries for these regressors were calculated using subject-specific masks of the white matter and CSF. The contrast of interest consisted of group mean values of the first EV of each set of two regressors.

*Table 5.2: Mean (±sd) physiological variables across conditioned respiratory tasks. *Significantly ($p < 0.05$) different from no impending resistance anticipation condition. Abbreviations: $P_{ET}CO_2$, pressure of end-tidal carbon dioxide; $P_{ET}O_2$, pressure of end-tidal oxygen; RVT, respiratory volume per unit time; bpm, breaths per minute.*

	Anticipation of nothing	Anticipation of resistance	Resistance On
Average mouth pressure (cmH_2O)	-0.35 (0.77)	-0.46 (0.91)	-5.69 (2.99)*
Peak mouth pressure (cmH_2O)	-	-	-14.7 (8.3)
$P_{ET}CO_2$ (%)	4.67 (0.62)	4.62 (0.66)*	4.72 (0.72)
$P_{ET}O_2$ (%)	17.4 (1.6)	17.3 (1.4)	17.7 (1.7)*
Respiratory rate (bpm)	11.8 (3.4)	11.5 (3.8)	10.5 (4.5)*
RVT (%)	-2.3 (7.0)	3.0 (15.9)*	-16.6 (26.2)*

contrast of anticipation of resistance $>$ baseline are presented in the Appendix for Chapter 5, for comparisons with results in Chapter 3.

Anticipation Significantly increased BOLD activity was seen in both the vlPAG and lPAG, and cortically/subcortically in the dorsolateral prefrontal cortex, supplementary motor cortex, middle and posterior cingulate cingulate cortices, anterior and middle insula, subthalamic nucleus, operculum, cerebellar I-IV, primary visual cortex and primary sensory cortex. Decreased BOLD activity was observed in the anterior and posterior cingulate cortices, ventromedial prefrontal cortex, dorsomedial prefrontal cortex, posterior insula, inferior precuneus, hippocampus and amygdala, primary sensory cortex, pontine nuclei, ventral inferior nuclei of the thalamus and cerebellar IX (Figure 5.6).

Resistive loading During resistive loading, significantly increased BOLD activity was seen in the dorsolateral prefrontal cortex, ventral posterolateral nucleus of the thalamus, putamen, caudate nucleus, and primary sensory and motor cortices, supplementary motor cortex, middle cingulate cortex, anterior and middle insula, subthalamic nucleus, operculum, cerebellar I-IV, primary visual cortex and primary sensory cortex. Decreased BOLD activity was seen in the anterior and posterior cingulate cortices, ventromedial prefrontal cortex, inferior precuneus, hippocampus and amygdala, primary sensory cortex, and pontine nuclei (Figure 5.6).

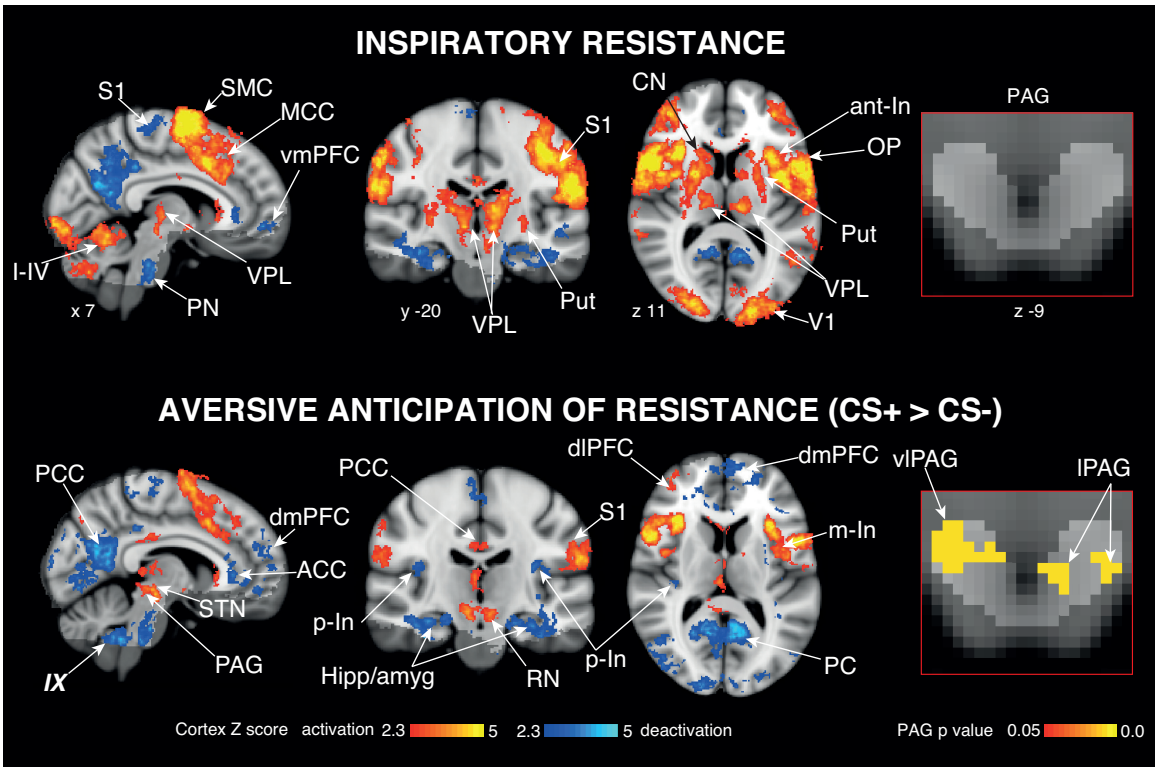

Figure 5.6: Mean BOLD response to inspiratory resistive loading and anticipation of aversive resistance (CS+ > CS-). The images consist of a colour-rendered statistical map superimposed on a standard (MNI 1 mm^3) brain, and significant regions are displayed with a threshold $Z > 2.3$, with a cluster probability threshold of $p < 0.05$ (corrected for multiple comparisons). Right: The bright grey region represents the periaqueductal gray, with significant clusters overlaid ($p < 0.05$; small-volume-corrected for multiple comparisons using represented PAG mask). Abbreviations: PAG, periaqueductal gray; vlPAG and lPAG, ventrolateral and lateral PAG; S1, primary sensory cortex; CN, caudate nucleus; SMC, supplementary motor cortex; Put, putamen; ACC, anterior cingulate cortex; MCC, middle cingulate cortex; PCC, posterior cingulate cortex; PC, precuneus; dlPFC, dorsolateral prefrontal cortex; dmPFC, dorsomedial prefrontal cortex; vmPFC, ventromedial prefrontal cortex; Hipp hippocampus; amyg, amygdala; a-In, anterior insula; m-In, middle insula; p-In, posterior insula; STN, subthalamic nucleus; RN, Red nucleus; OP, operculum; V1, primary visual cortex; IX and I-IV, cerebellar lobes; thalamic nuclei: VPL, ventral posterolateral nucleus; VIN, ventral inferior nuclei; activation, increase in BOLD signal; deactivation, decrease in BOLD signal.

5.4.1.3 Breathlessness network activity scaling with subjective ratings of intensity and anxiety

Anticipation BOLD activity that scaled with anxiety scores in the contrast of aversive anticipation of resistance was observed in the primary and supplementary motor cortices, superior parietal lobule, lateral occipital cortex and cuneus, while only activity in the bilateral ventral anterior nucleus of the thalamus scaled with intensity scores (Figure 5.7).

Resistive loading BOLD activity that scaled with subjective anxiety scores during resistive loading was observed in the lPAG, primary motor and sensory cortices, supplementary motor cortex, dorsolateral prefrontal cortex, middle insula, ventral posterolateral nucleus of the thalamus, and subthalamic nucleus. Only the middle insula correlated with intensity during resistive loading (Figure 5.7).

5.4.2 Functional connectivity of the lPAG and vlPAG

vlPAG The resting state connectivity analysis revealed significant functional connectivity between the vlPAG and the dorsomedial prefrontal cortex, dorsolateral prefrontal cortex, anterior insula, right middle insula, operculum, anterior cingulate, paracingulate gyrus, precuneus, visual cortex, hippocampus, subthalamic and red nuclei, parahippocampal gyrus, left supplementary motor cortex, caudate nucleus, and superior cerebellar lobes (Figure 5.8).

lPAG The resting state connectivity analysis of the lPAG revealed connectivity with the primary motor cortex, left primary sensory cortex, left superior parietal lobule, putamen, hippocampus and left amygdala, and right lateral occipital cortex (Figure 5.8).

Auditory control seed The resting state connectivity of the auditory control seed was predominantly to the auditory cortex, insula and primary sensory cortex (Figure 5.8).

5.4.3 The effect of exercise

5.4.3.1 Exercise and anxiety of inspiratory resistive loading

The negative correlation between exercise exposure and anxiety of inspiratory resistance was not found to be significant across the 40 subjects in this investigation ($R = -0.17$; $p = 0.29$; Figure 5.9), in contrast to the results presented in Chapter 3.

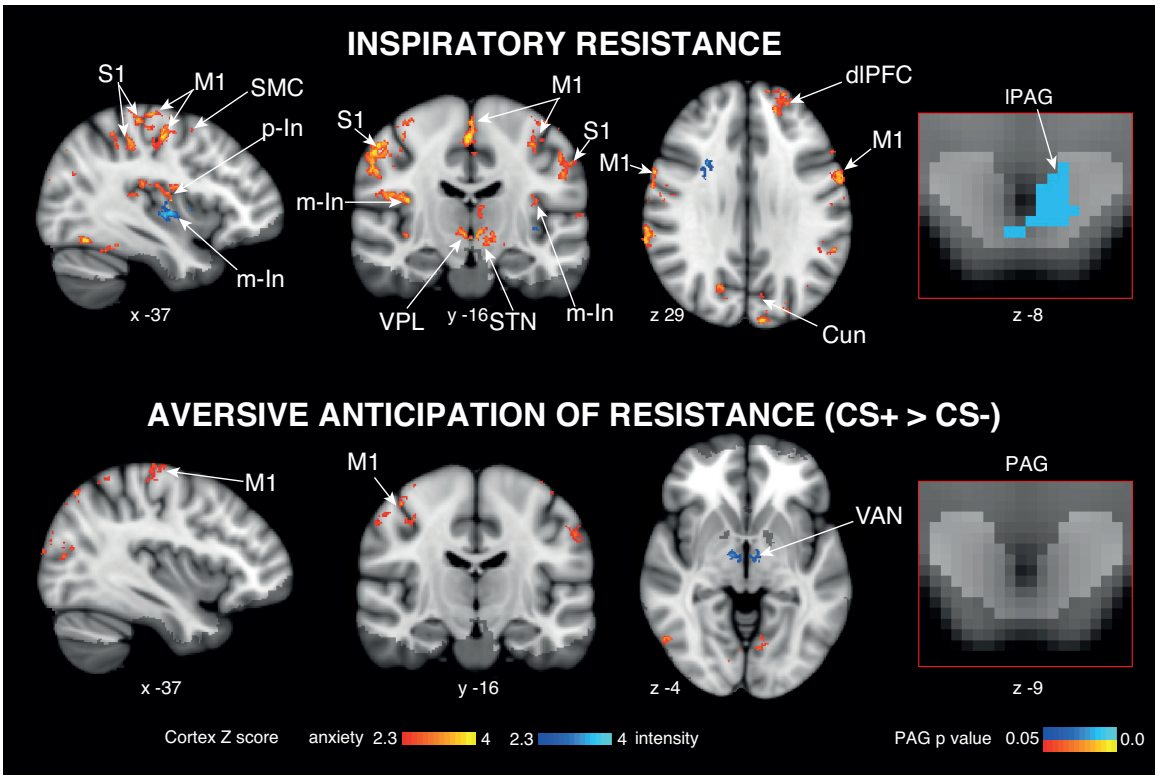

Figure 5.7: BOLD activity that scales with intensity (blue) and anxiety (yellow) ratings for inspiratory resistive loading and anticipation of aversive resistance (CS+ > CS-). The images consist of a colour-rendered statistical map superimposed on a standard (MNI 1 mm^3) brain, and significant regions are displayed with a threshold $Z > 2.3$, with a cluster probability threshold of $p < 0.05$ (corrected for multiple comparisons). Right: The bright grey region represents the periaqueductal gray, with significant clusters overlaid ($p < 0.05$; small-volume-corrected for multiple comparisons using represented PAG mask). Abbreviations: PAG, periaqueductal gray; lPAG, lateral PAG; S1, primary sensory cortex; M1, primary motor cortex; SMC, supplementary motor cortex; PCC, posterior cingulate cortex; Cun, cuneus; pC, precuneus; dlPFC, dorsolateral prefrontal cortex; m-In, middle insula; CN, caudate nucleus; STN, subthalamic nucleus; LOC, lateral occipital cortex; VPL, ventral posterolateral nucleus of the thalamus; VAN, ventral anterior nucleus of the thalamus.

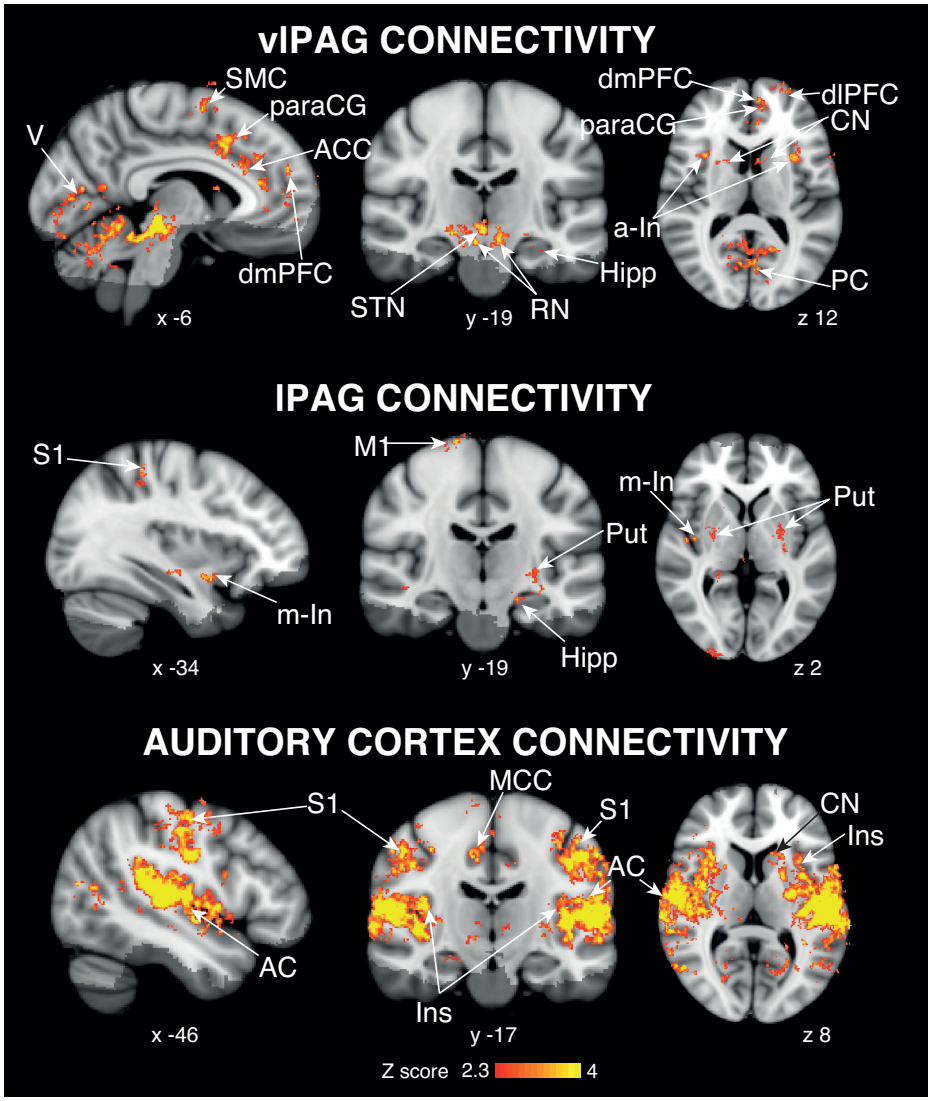

Figure 5.8: Mean resting state functional connectivity of the vlPAG and lPAG masks, and an auditory control seed. The images consist of a colour-rendered statistical map superimposed on a standard (MNI 1 mm^3) brain, and significant regions are displayed with a threshold $Z > 2.3$, with a cluster probability threshold of $p < 0.05$ (corrected for multiple comparisons). Abbreviations: S1, primary sensory cortex; M1, primary motor cortex; SMC, supplementary motor cortex; CN, caudate nucleus; Put, putamen; ACC, anterior cingulate cortex; MCC, middle cingulate cortex; paraCG, paracingulate gyrus; dlPFC, dorsolateral prefrontal cortex; dmPFC, dorsomedial prefrontal cortex; Hipp hippocampus; a-In, anterior insula; m-In, middle insula; Ins, insula; PC, precuneus; SMG, supramarginal gyrus; STN, subthalamic nucleus; RN, red nucleus; OP, operculum; AC, auditory cortex; V, visual cortex.

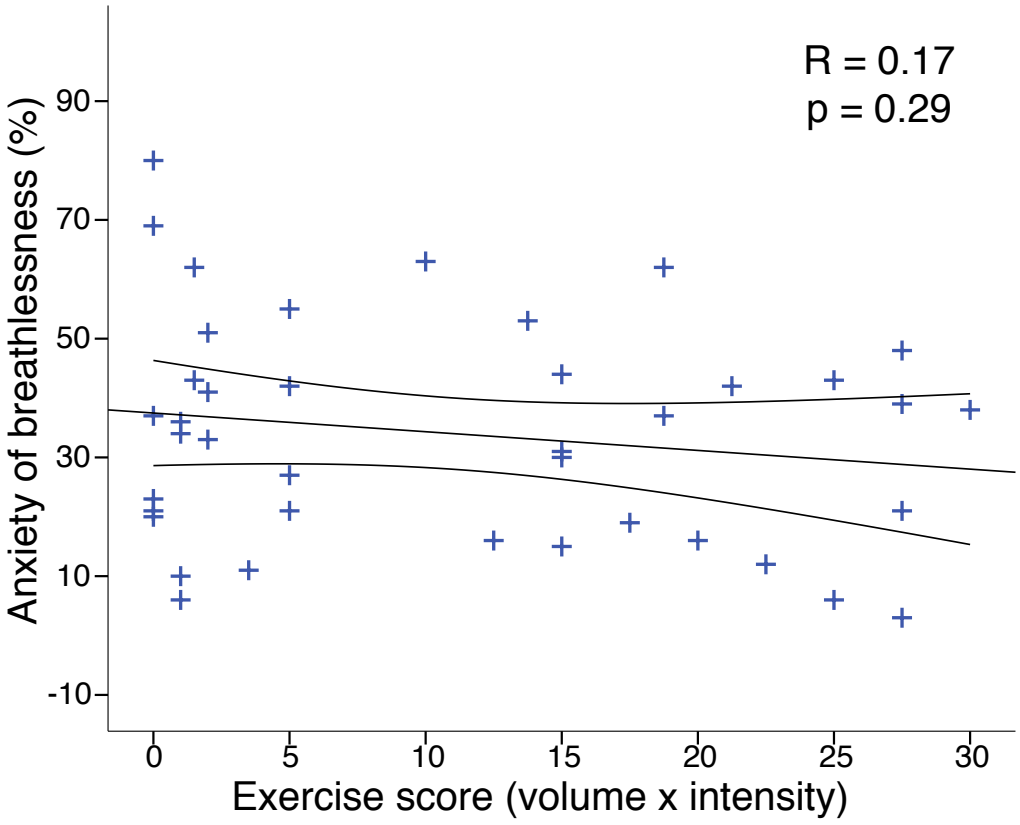

Figure 5.9: Plot of anxiety scores for certain impending resistance against exercise exposure score (number of hours of exercise per week x intensity; where 1 = easy, 2 = moderate, 3 = intense). Black lines represent regression line and 95% confidence intervals.

*Table 5.3: Physiological and psychological variables during inspiratory resistance protocol (mean (±sd)). *Significantly different ($p < 0.05$) between groups*

	Athletes	Sedentary
Peak inspiratory resistance (cmH_20)	-14.4 (8.5)	-12.0 (5.8)
Resistance intensity rating (%)	46.3 (14.1)	46.7 (18.1)
Resistance anxiety rating (%)	31.9 (17.8)	36.1 (20.0)
No resistance intensity rating (%)	2.3 (3.5)	3.4 (3.4)
No resistance anxiety rating (%)	2.8 (4.8)	2.2 (2.7)

5.4.3.2 Physiology and psychology of breathlessness

No differences between athletes and sedentary subjects were observed in any physiology measures reported in Table 5.2. Group results for subjective perceptions of resistive loading are presented in Table 5.3, and while no significant differences were apparent, a small (subthreshold; $p = 0.24$) decrease in anxiety was observed in the athlete group compared to sedentary subjects.

5.4.3.3 Functional activity differences between exercise groups

Anticipation The differences in brain activity between exercise groups did not survive thresholding in the aversive anticipation condition (anticipation of certain resistance > anticipation of no resistance; CS+ > CS-), and thus the results presented in this section are for the contrast of anticipation of certain resistance > baseline. During this anticipation of resistance (> baseline), athletes had greater BOLD activity in the vlPAG (using a specific vlPAG region of interest mask; $p = 0.05$), ventromedial prefrontal cortex, anterior and posterior cingulate cortices, paracingulate cortex and posterior insula (Figure 5.10).

Resistive loading BOLD activity was greater in sedentary subjects during inspiratory resistive loading in the middle insula, caudate nucleus, primary motor and sensory cortices, supramarginal gyrus, superior parietal lobule, operculum and cerebellum. In contrast, no BOLD activity was significantly greater in athletes than sedentary subjects during resistive loading.

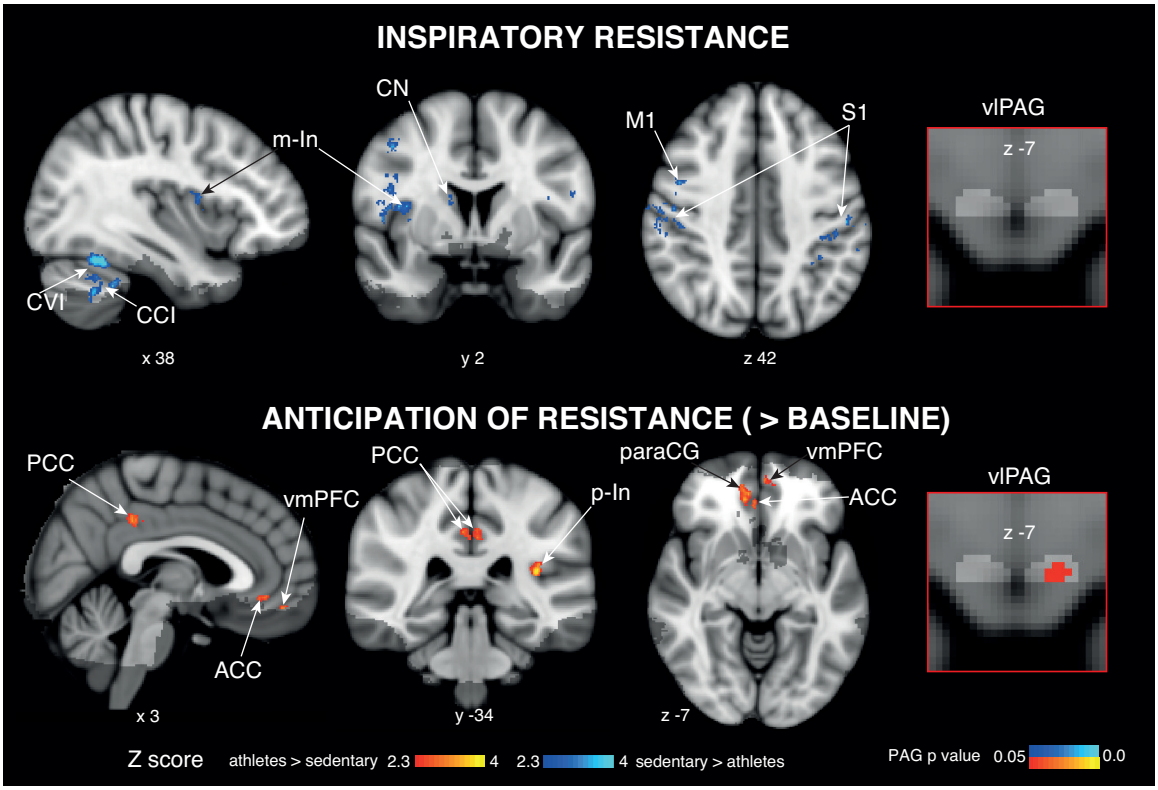

Figure 5.10: BOLD response that correlates with exercise group (athletes > sedentary in yellow; sedentary > athletes in blue) during inspiratory resistance and the anticipation of resistance. The images consist of a colour-rendered statistical map superimposed on a standard (MNI 1 mm^3) brain, and significant regions are displayed with a threshold $Z > 2.3$, with a cluster probability threshold of $p < 0.05$ (corrected for multiple comparisons). Abbreviations: ACC, anterior cingulate cortex; PCC, posterior cingulate cortex; paraCG, paracingulate gyrus; vmPFC, ventromedial prefrontal cortex; p-In, posterior insula; m-In, middle insula; CCI, cerebellar crus I; CVI, cerebellar VI.

5.5 Discussion

5.5.1 Main findings

In this Chapter we have shown that the columns of the PAG are potentially integrally and differentially involved in the top-down networks involved with the anticipation of breathlessness. Activity was identified in both the lPAG and vlPAG during conditioned anticipation of resistive loading within a network of complex cortical circuitry. To disentangle the influence of these cortical structures on the PAG columns, a resting state functional connectivity analysis revealed that these PAG columns have different connections within this breathlessness network, with vlPAG preferentially connecting to prefrontal areas and lPAG to motor and sensory areas. Therefore, we have revealed that the PAG may be imperative for separating top-down modulation of the sensory and affective components of breathlessness perception.

It is already known that exercise treatment reduces breathlessness perception in patients with COPD, independent of changes in lung function (Carrieri-Kohlman et al., 2001, 1996). Therefore, in this study we also compared athletes and sedentary individuals to assess whether exercise can induce adaptations in the PAG columns or wider cortex of the breathlessness network, in a preliminary investigation of exercise-induced plasticity independent of disease. While our previous results (Chapter 4) had shown that athletes did not appear to be 'de-sensitised' to perceptions of breathlessness, we speculated that any adaptations induced by exercise were thus likely due to reappraisal of the threat perception of breathlessness. In line with this hypothesis, in this study we found that athletes displayed altered vlPAG activity during anticipation of resistance compared to their sedentary counterparts. vlPAG activity was coupled with increased activity in prefrontal and sensory cortical areas, potentially reflecting different activity within the threat perception system of breathlessness, and possibly manifesting in the small (sub-threshold) decrease in anxiety of breathlessness observed in athletes. These findings provide a platform by which to investigate (mal)adaptation and altered breathlessness perception in diseases such as COPD and asthma, with the potential to understand and enhance treatment effects.

5.5.2 PAG columns within the anticipatory breathlessness network

Activity in both the vlPAG and lPAG was observed during aversive anticipation of resistive loading (CS+ $>$ CS-), indicating that both of these structures are involved in the top-down conditioned response to an impending breathlessness stimulus. As well as PAG activity, a widespread cortical network of breathlessness anticipation was also identified,

reflecting the complex processing of breathlessness as both a sensory and affective stimulus (Herigstad et al., 2011; Lansing et al., 2009; Hayen et al., 2013b). Activity was identified in limbic and evaluative structures such as the anterior and posterior cingulate cortices, anterior and middle insula (Vogt et al., 1992; Craig, 2009, 2002, 2003), and the dorsolateral prefrontal cortex, known to be involved in executive attention and working memory (Kane and Engle, 2002; MacDonald et al., 2000; Miller and Cohen, 2001). Additionally, activity in sensory awareness and preparatory motor structures was also identified, including primary sensory cortex (Calford, 2002), precuneus (Kjaer et al., 2001, 2002) and supplementary motor area (Roland et al., 1980; Fried et al., 1991; Nambu et al., 1996).

But how do we disentangle the roles of these PAG columns within the top-down sensorimotor and affective components of breathlessness? While both the lPAG and vlPAG were active during aversive anticipation of resistive loading, our functional connectivity results revealed that connectivity of the vlPAG appears to be extensive within limbic and frontal regions of the brain, consistent with previous diffusion imaging results (Ezra et al., 2015) (included in Appendix). Of particular note, vlPAG has high connectivity to many of the executive control and limbic structures active during anticipation of resistance, including the dorsolateral prefrontal cortex, and the anterior cingulate and paracingulate cortices. The vlPAG also preferentially communicates with the anterior insula and precuneus, known to play fundamental roles in the interoceptive sense of self (Cavanna and Trimble, 2006; Craig, 2009, 2002, 2003). Therefore, the extensive connectivity of the vlPAG to frontal and limbic structures supports the notion that it may play a key role in threat perception and affective evaluation of breathlessness within this complex cortical network.

Comparatively, resting state functional connectivity analysis of the lPAG revealed connections to sensorimotor areas of the brain, supporting the hypothesis that the lPAG is integrally involved in the sensorimotor aspect of breathlessness. Mean connectivity was shown to the primary sensory and motor cortices, middle insula and putamen, all areas identified within the sensorimotor circuitry of the brain (Purves et al., 2001; Simmons et al., 2013; Goble et al., 2012; Wymbs et al., 2012). To further support the role of the lPAG in the sensorimotor network of breathlessness, functional activity of the lPAG during the task of resistive loading was found to scale with ratings of breathlessness intensity, meaning greater lPAG activity was observed in subjects who perceived higher intensities of breathlessness during resistive loading. Therefore, it appears that the lPAG is a key component of the neural circuitry determining the subjective perception of breathlessness intensity, alongside other activated cortical structures such as the posterior insula. The posterior insula has been identified as part of the somatosensory system, with stroke lesions linked to somatosensory deficit (Cereda et al., 2002). Furthermore, the posterior insula has been pos-

tulated to contain a sensory representation prior to communication with the anterior insula in the pathway of interoception (Craig, 2002), and it is therefore possible that the lPAG and posterior insula are communicating to modulate the afferent sensation and efferent motor output of ventilation to regulate the perceived intensity of breathlessness.

While these results have shown that the complex, multi-dimensional anticipation of aversive breathlessness employs simultaneous activity in both the vlPAG and lPAG columns, both functional and connectivity results reveal that these are likely to be playing distinctly different roles within this perception. Animal models have previously hypothesised involvement in passive coping towards an inescapable threat from the vlPAG, and active response to threat in the lPAG (Keay and Bandler, 2001; Bandler and Shipley, 1994; Bandler et al., 2000), but are unable to link this to functional activity in the wider cortex or subjective perceptions due to decerebrate preparations (Subramanian et al., 2008; Subramanian, 2012). While our previous results (Chapter 3) revealed PAG activity that was consistent with animal models of threat, the current results demonstrate that these PAG columns are more than primitive threat reflexes; rather intricately and differentially linked to distinctive cortical networks. Therefore, it is now apparent that these active and passive responses to the threat of breathlessness result from a top-down modulation by a fronto-limbic (vlPAG) or sensorimotor sub-network (lPAG).

This decisive division in function and connections of the PAG columns within breathlessness perception may prove to be of great clinical importance. Conditions such as chronic lung disease or asthma are often characterised by misperception of respiratory symptoms, and we can now begin to provide a platform for investigating related adaptations of the PAG columns in disease. The most effective treatment currently for COPD is the use of exercise within pulmonary rehabilitation, resulting in a decrease in breathlessness anxiety (Carrieri-Kohlman et al., 2001, 1996). We have postulated this to be due to a reappraisal of the threat of breathlessness due to positive associations with exercise (Chapter 4), which may thus present itself in functional adaptations of the vlPAG and fronto-limbic cortical network. Therefore, we will now examine our group comparison between individuals who regularly partake in endurance exercise training and those who are sedentary, using a healthy volunteer model to understand how the PAG may be involved in this reappraisal of threatening breathlessness.

5.5.3 Effect of exercise on cortical networks of breathlessness

Indeed, a group comparison between athletes and sedentary subjects showed an increase in vlPAG and cortical activity during anticipation of resistance in athletes, but only in the con-

trast of anticipation > baseline, as results in anticipation of resistance > anticipation of no resistance did not survive thresholding (Figure 5.10). Additionally, an increase in cortical sensorimotor structures was observed in sedentary subjects during resistive loading (Figure 5.10). However, no significant difference in subjective ratings of breathlessness anxiety was apparent between the groups, nor a negative correlation between exercise exposure and and breathlessness anxiety (Figure 5.9), therefore these results are somewhat speculative.

Despite the consistency in breathlessness ratings between the groups, it is possible that altered function in the neuronal networks involved with cognitive evaluation and threat appraisal of breathlessness exist, driving the sub-threshold reduction in breathlessness anxiety observed in athletes (Table 5.3). This may explain the network of structures that showed altered functional BOLD activity in athletes during anticipation of resistance (> baseline), including the vlPAG, ventromedial prefrontal cortex, cingulate, and posterior insula. The posterior insula and posterior cingulate cortex have both been shown to have sensory functions (Vogt et al., 1992; Craig, 2009, 2002, 2003), and coupled with activity in the ventromedial prefrontal cortex and anterior cingulate, known for their roles in emotional processing (Roy et al., 2012; Bechara et al., 2000; Tranel et al., 2002; Urry et al., 2006; Büchel et al., 2002), may be involved in positive associations and reduced threat of breathlessness in athletes.

Remarkably, the activity observed in the ventromedial prefrontal cortex and anterior cingulate cortex are strikingly similar to that observed in patients with COPD, in a recent study examining brain responses to breathlessness-related-word-cues to model anticipatory breathlessness activity (Herigstad et al., 2015). These areas were found to scale with scores of depression and vigilance in patients, and it is therefore possible that they (and the vlPAG shown here) are integral to the modulation of threat perception in breathlessness. Therefore, these preliminary findings of exercise-induced changes in the brain circuitry of breathlessness indicate involvement of the vlPAG, providing a first step in the understanding of the mechanisms of exercise reducing heightened breathlessness anxiety in patients with chronic lung disease.

Lastly, while there was no difference in intensity perception between the groups, and no associated differences in lPAG activity, increased BOLD activity was found in cortical sensorimotor areas including the primary motor and sensory cortices, the caudate nucleus and middle insula (Purves et al., 2001; Simmons et al., 2013; Goble et al., 2012; Wymbs et al., 2012) during resistive loading in sedentary subjects. This difference between the groups may reflect a more efficient cortical processing of ventilatory sensation and drive in athletes, similar to that hypothesised in piano players during a finger tapping task (Jäncke et al., 2000). Plasticity of the cortex is known to occur with repeated motor and sensory

experiences (Stefan et al., 2000; Sanes and Donoghue, 2000; Calford, 2002; Trachtenberg et al., 2002), and while exercise may not have desensitised this group of athletes to the perception of breathlessness, neuronal circuitry may adapt to allow for more metabolically-efficient control of ventilation, or perhaps even the enhanced perceptions of ventilatory sensations observed in Chapter 4.

5.5.4 Methodological considerations

In the functional connectivity analysis of this study, care was taken to include a control seed region in the auditory cortex to compare with results from the columns of the PAG. This auditory control seed displayed high connectivity to the bilateral somatosensory and auditory cortical regions, consistent with the literature on the connections of the auditory cortex (Wild et al., 2012). Furthermore, white matter and cerebrospinal fluid timeseries were also included in this analysis, in addition to extensive denoising using ICA and RETROICOR during preprocessing, to dissociate the noise of global head movement and the pulsating aqueduct from the adjacent PAG columns.

In this study we were able to analyse the aversive anticipation of breathlessness contrast (CS+ $>$ CS-) when examining whole-group results, consistent with that typically used in conditioning and learning literature. The increase in statistical power required to analyse this contrast resulted from a simplified anticipation protocol from Chapter 3, with only certain anticipation of resistance and anticipation of no resistance, together with a greater number of subjects (n=40 vs n=18 in Chapter 3) and larger voxels (at the expense of a loss in resolution; voxel size 2 mm^3 vs 1.5 mm^3 in Chapter 3). Care must be taken as the increased voxel size in this study introduces potential blurring between the PAG and aqueduct. This may be problematic with interpretation of functional activity that scales with breathlessness intensity ratings, as this may be a simple reflection of increased noise generated by increased mouth pressure. However, the activity in the activated area of the lPAG did not correlate with mouth pressure (see Appendix for Chapter 5), and thus we are confident this is not due to increased noise from the aqueduct.

While the results from this study continue to support the hypothesis that the lPAG is involved in the active sensorimotor aspect of breathlessness, we did not find mean deactivation of the lPAG during inspiratory resistance that was observed in our previous results (Chapter 3). Instead, we found activity in the lPAG during resistive loading that scaled with intensity. This discrepancy may be explained by the reduction in perceptions of intensity by the subjects in this study compared to Chapter 3 (mean resistance rating ($\pm$sd) Chapter 5 vs Chapter 3: 46.5 (16.0) vs 62.9 (21.5); $p = 0.002$) despite similar inspiratory resistance

pressures (average peak mouth pressure ($\pm$sd) (cmH_2O) Chapter 5 vs Chapter 3: -14.7 (8.3) vs -13.2 (7.3); $p = 0.51$), or the increased voxel size contributing larger partial voluming effects and masking mean activity in the lPAG. Furthermore, in the aversive anticipation contrast, mean activity was also detected in the lPAG as well as the vlPAG activity reported in Chapter 3. It is possible that this activity represents preparatory activity in the lPAG of the somatomotor system for impending breathlessness, while this was unable to be detected in Chapter 3 due to the reduced statistical power.

5.6 Conclusions

In the final Chapter of this Thesis we have found that both the vlPAG and lPAG are active during conditioned anticipation of an aversive respiratory load, within a broad network of cortical structures that reflect the sensory and affective components of breathlessness. However, the connectivity of these PAG columns reveal distinctly different profiles to the higher cortical structures within this network, with the vlPAG preferentially connecting to fronto-limbic structures within the affective component of breathlessness perception, while the lPAG connects to sensorimotor structures within the sensory component. Furthermore, the lPAG is also involved with the active response to a resistive load, in a manner that scales with the perceived intensity of the stimulus. Therefore, it appears that the PAG may be a critical point of divergence within the perception of breathlessness, which is a key step forward in our understanding of this complex, frightening and often debilitating sensation.

To begin to understand the affect of exercise on brain networks of breathlessness, we also compared athletes to matched sedentary individuals in this study. In our previous Chapter (Chapter 4) we revealed that exercise does not appear to 'de-sensitise' athletes to the intensity of breathlessness, and we speculated that any induced changes would be due to reappraisal of the threat of breathlessness sensations. While no significant reduction in breathlessness intensity or anxiety was reported between the two groups in this Chapter, we found a difference in functional activity in the vlPAG and an affective cortical network involving the ventral prefrontal cortex in athletes during anticipation of resistance. Therefore, we have shown the vlPAG may be a key structure within a network of plasticity altered by exercise, and may be an important therapeutic target for misperceptions of breathlessness in diseases such as COPD.

Chapter 6

General discussion

6.1 Abstract

The aim of this Thesis was to investigate the roles of the PAG columns in respiratory control and breathlessness, and the potential changes in breathlessness induced by exercise. In Chapter 2 we presented a study that revealed the ability of 7 Tesla MRI to detect activity within columns of the PAG during simple respiratory tasks. In Chapter 3 we showed that the vlPAG and lPAG are differentially involved in breathlessness perception, in a manner fitting with animal models of the PAG in response to threat. In Chapter 5 we extended these results to reveal that beyond reflexive ventilatory coping strategies residing within the PAG, the connectivity of these columns to higher cortical structures suggests that they are under top-down cortical control, and represent a divergence of the sensory (lPAG) and affective (vlPAG) networks underlying the multidimensional nature of breathlessness. Lastly, in Chapters 4 and 5 we investigated the effect of exercise on perceptions of breathlessness and underlying brain networks. In Chapter 4 we found that exercise does not appear to globally 'de-sensitise' individuals to breathlessness, and we thus hypothesised that any changes associated with exercise may be affective in nature, with a re-evaluation of the threat of their respiratory sensations. Correspondingly, in Chapter 5 we found a difference in functional activity of the vlPAG and prefrontal cortex during anticipation of breathlessness, despite no significant differences in subjective ratings of breathlessness intensity or anxiety. These results reveal the possibility that the vlPAG is within a network of plasticity evoked by exercise training that may contribute to potential changes in affective breathlessness, and may be an important therapeutic target for future treatments of respiratory disease.

In this final Chapter we outline the main findings of this Thesis and discuss how these compare to the current animal and human PAG and breathlessness literature, revealing an integral place of the PAG within this perceptual network. We will briefly touch on how we might better understand the physiology of breathlessness by examining athletes operating at high proportions of their ventilatory capacity, and discuss how exercise might alter breathlessness perception and possible underlying adaptations of the PAG and cortex. We will address the methodological considerations of both imaging breathlessness and the use of 7 Tesla brainstem fMRI, before concluding by outlining the importance of this research in the understanding and treatment of breathlessness in the future.

6.2 Main Thesis findings

The primary aim of this Thesis was to investigate the role of the human PAG columns in respiratory control and perception of breathlessness. In accordance with animal models of PAG respiratory function and threat perception, we have found activity in the lPAG that occurs during voluntary changes in ventilation for both breath holds and breathing against an inspiratory resistance, while activity in the vlPAG occurs only during conditioned anticipation of an aversive breathing stimulus. Further connectivity analysis of these PAG columns revealed that the vlPAG preferentially communicates with prefrontal and limbic structures, and the lPAG to sensorimotor structures, leading us to believe that this may be a focal point of differentiation into the sensory and affective sub-networks of respiratory control and breathlessness.

To investigate the importance of the PAG columns within these breathlessness sub-networks, we tested the idea that the plasticity of the PAG may be involved in modulating previously-reported reductions in breathlessness using exercise treatment in patients with chronic obstructive pulmonary disease (COPD). Using an healthy volunteer athlete model, we found that exercise does not appear to globally 'de-sensitise' individuals to breathlessness, and instead any changes are possibly due to altered threat perceptions of breathlessness stimuli. Correspondingly, we found preliminary evidence for functional adaptations within a brain network encompassing the vlPAG and prefrontal cortex in athletes, exposing this as a legitimate target for potential (mal)adaptions in disease.

The physiological and psychological investigations into breathlessness perception in athletes during exercise can also provide some useful insights into breathlessness in disease. While our athlete model did not provide the expected significant reduction in breathlessness anxiety, possibly due to the comparative low anxiety of the sedentary subjects tested, we did find an increase in anxiety at maximal exercise and improved ventilatory perceptions in our athlete group. We have postulated that exercising anxiety may be due to increased homeostatic signalling from the chest when operating at high proportions of maximal ventilatory capacity, possible in both athletes and those with reduced lung function in respiratory disease, whereas typically ventilation has not been considered a limiting factor to exercise capacity. Lastly, more accurate ventilatory perception may be a result of repeated exposure to operating within a high proportion of ventilatory capacity, where this heightened awareness may serve to further facilitate anxiety in patients due to their associations between breathlessness and disease. Therefore, through the study of the effects of exercise on breathlessness independent of disease, we are able to deepen our understanding of both the effect on breathlessness perception and the underlying brain network adapta-

tions, and the physiology and psychology of operating at high proportions of ventilatory capacities.

6.3 Functional dissociation of the human PAG

6.3.1 lPAG functions and cortical connections

In all three respiratory imaging studies in this Thesis we have identified activity in the lPAG corresponding with volitional changes in ventilation. The ventilatory tasks employed were breath holding (Chapter 2) and breathing against an inspiratory resistive load (Chapters 3 and 5); which are both associated with a decrease in rate of breathing from resting values. These results align with animal models, where the lPAG has been associated with prolonged inspirations and expirations (summarised in Figure 6.1).

Beyond respiratory control, animal models have also hypothesised the lPAG to reside within a pathway of active response to an escapable threat. As the activity seen in the lPAG has corresponded with active, volitional responses to respiratory challenges, our results also align with this threat model of the PAG. Furthermore, activity in the lPAG was found to scale with perceived intensity of resistance during both cued anticipation and resistive loading (Chapters 3 and 5), with greater activity in those who perceive the stimulus as more intense. Therefore, it appears that the lPAG is not only acting in a reflexive, active response to a respiratory threat, but is under top-down modulation from a higher cortical network to anticipate and interpret the ventilatory sensations. Correspondingly, in Chapter 5 we observed preferential functional connectivity between the lPAG and sensorimotor areas of the cortex, consistent with recent work using using diffusion imaging (Ezra et al., 2015), and validating the lPAG within this sensorimotor network. Therefore, we propose that the lPAG has an integral place within the sensorimotor component of respiratory function and breathlessness.

6.3.2 vlPAG functions and cortical connections

In Chapters 3 and 5 of this Thesis, we found vlPAG activity during cued aversive anticipation of inspiratory resistance. The vlPAG has been hypothesised to contribute to the passive behavioural response to an identified inescapable threat, and our study design of applied inspiratory loading was an anticipated, inescapable respiratory threat. Furthermore, with a condition of 50% certainty of an upcoming inspiratory resistance in Chapter 3, we observed reduced activity in the vlPAG and a corresponding reduction in breathlessness anxiety and

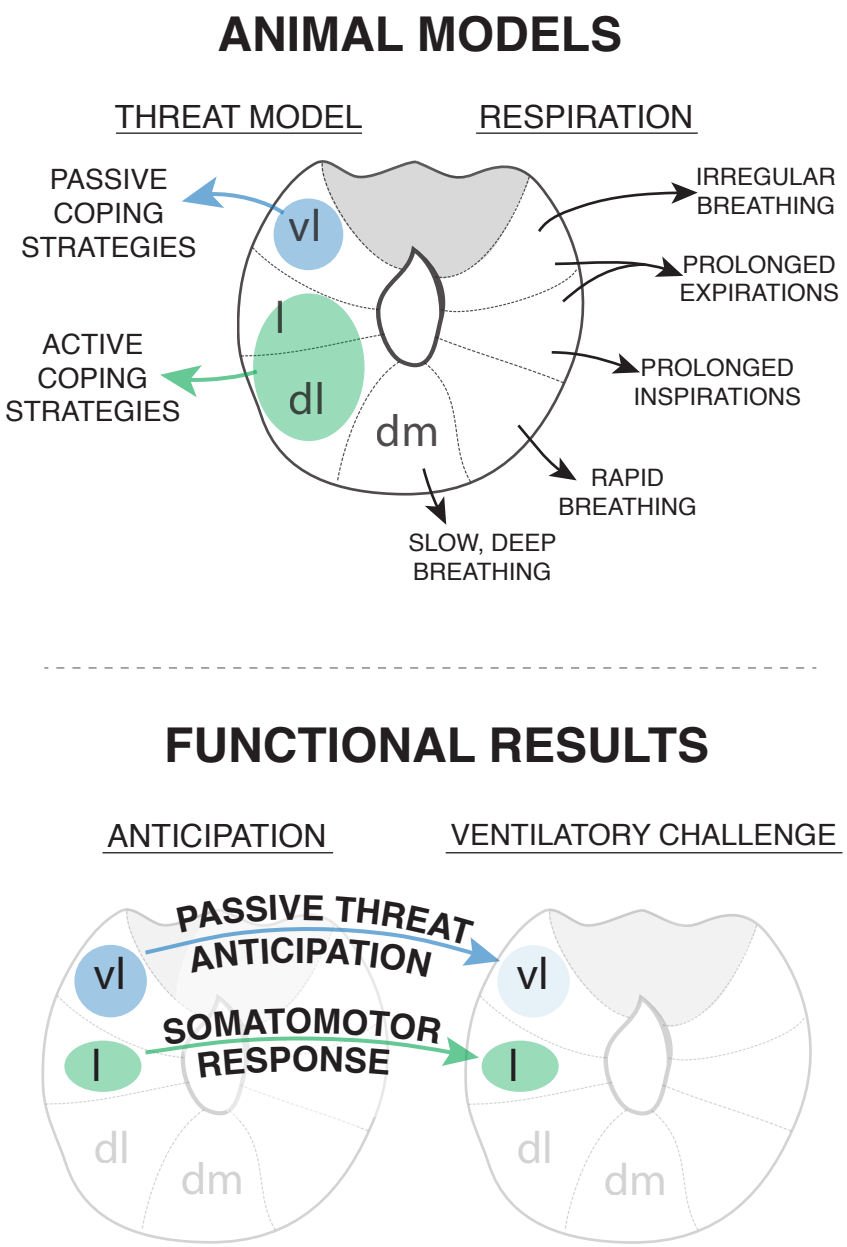

Figure 6.1: Top: Summary of the evidence from animals for PAG respiratory functions (right) and theorised role in threat perception/response (left). Bottom: Summary of the PAG results in this Thesis: vlPAG activity in the anticipatory threat detection of an aversive inescapable breathing response, and lPAG activity during anticipation and the volitional changes in ventilation (breath holds and breathing against an inspiratory resistance).

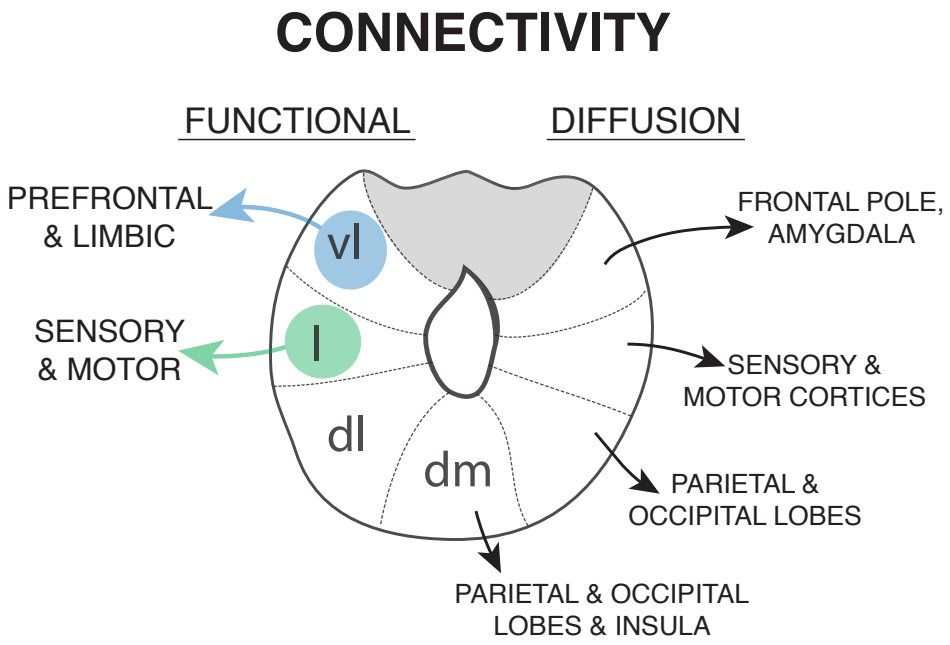

Figure 6.2: Summary of the cortical connections of the PAG in humans from previous diffusion research (right) and the functional connectivity results found in this Thesis (left).

intensity, indicating reduced vlPAG involvement when the conditioning of a predictive cue is weaker. However, the vlPAG is not acting in isolation during the anticipation of breathlessness, and the connectivity results in Chapter 5 extend the role of the vlPAG beyond primitive coping behaviours. We have shown that vlPAG preferentially communicates with prefrontal and limbic structures in a network that may represent the affective component of breathlessness, allowing for this cognitive assessment of respiratory threat. Therefore, the results of this Thesis support the model of the vlPAG involvement in passive response to an inescapable respiratory threat, and show that this is likely to occur within a top-down network of cognitive evaluation of breathlessness.

6.4 Cortical networks

Although the cortical networks of breathing control were not the primary interest of this Thesis, we found remarkably consistent activity during both volitional changes in breathing and anticipation of inspiratory loading across studies (Figure 6.3). Conscious changes in breathing involve both sensorimotor and affective processing, as adequate ventilation is integral to sustaining life and thus closely monitored by homeostatic mechanisms (Brannan et al., 2001; Dempsey et al., 1985; Klein, 1993). Within the limited field of view of Chapters 2 and 3, the cortical network associated with breath holding, vocalisations and breathing against an inspiratory load covers a network of primary motor and sensory structures, the subcortical basal ganglia and limbic areas such as the insula (Figure 6.3). These cortical areas align with previous breath hold research at 3 T (Feinberg et al., 2010; McKay et al., 2008; Pattinson et al., 2009a) and hypercapnia-stimulated hyperventilation using PET (Brannan et al., 2001), providing confidence in the legitimacy of the network of breathing control within which our PAG activations lie. Interestingly, improved statistical power in Chapter 5 revealed that much of this network more closely scales with scores of anxiety rather than perceived intensity of breathing. Therefore, it is possible that increased BOLD activity within this network is reflective of increased conscious awareness of breathing, and this awareness is tightly coupled with anxiety relating to the strong homeostatic drive towards sustainable ventilation (Brannan et al., 2001; Klein, 1993).

In Chapters 3 and 5 a consistent network was also found during the anticipation of inspiratory loading ($>$ baseline, Figure 6.3). Activity in primary motor and sensory structures was less extensive in anticipation compared with inspiratory loading, while activity was maintained in preparatory motor structures such as the supplementary motor cortex and basal ganglia (Groenewegen, 2003; Mink, 1996; Alexander et al., 1986). The full brain coverage in Chapter 5 revealed that this network extends to prefrontal cognitive evaluation

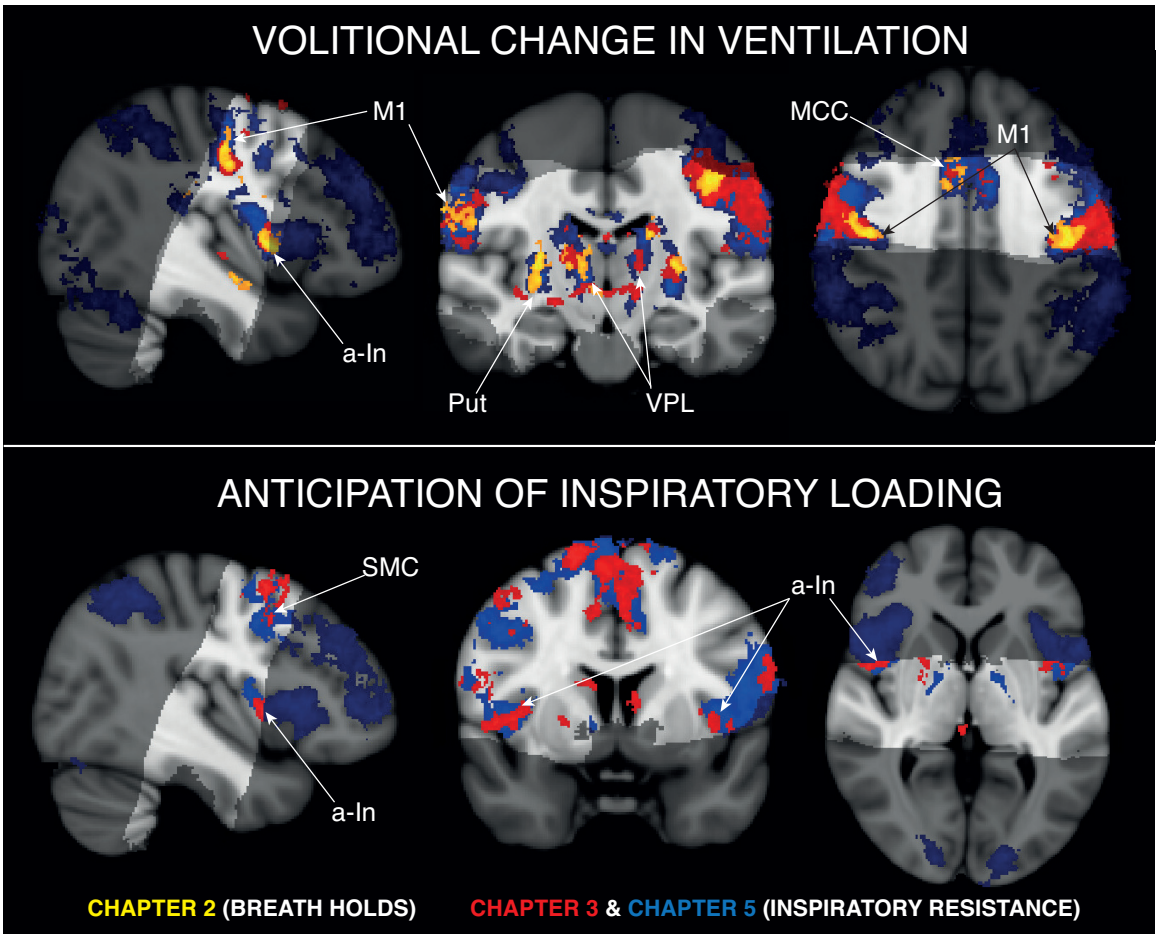

Figure 6.3: BOLD activity comparisons across studies: Chapter 2 (represented in yellow/orange; limited field of view), Chapter 3 (represented in red; limited field of view), and Chapter 5 (represented in blue; full brain coverage). Top: BOLD activity that corresponds with volitional changes in ventilation (Chapters 2, 3 and 5). Bottom: BOLD activity that corresponds with anticipation of inspiratory resistance (Chapters 3 and 5). The images consist of a colour-rendered statistical map superimposed on a standard (MNI 1 mm^3) brain, and significant regions are displayed with a threshold $Z > 2.3$, with a cluster probability threshold of $p < 0.05$ (corrected for multiple comparisons). Abbreviations: M1, primary motor cortex; a-In, anterior insula; SMC, supplementary motor cortex; MCC, middle cingulate cortex; Put, putamen; VPL, ventral posterolateral nucleus of the thalamus.

structures such as the dorsolateral prefrontal cortex (Kane and Engle, 2002; MacDonald et al., 2000; Miller and Cohen, 2001), and parietal structures for sensory awareness (Kjaer et al., 2001, 2002). Chapter 5 also revealed extensive deactivation of the resting 'default mode' during anticipation of resistance, which has been previously well-reported in task fMRI and reinforces the cognitively demanding nature of the anticipation of inspiratory loading (Raichle et al., 2001; Greicius and Menon, 2004; Fransson, 2005) (can be seen in Figure 5.6, Chapter 5). Therefore, the cortical networks associated with both volitional changes in ventilation and anticipation of an aversive breathing stimulus are consistent with previous literature, and instill confidence in the protocol and modelling in this Thesis to explore the role of the PAG columns within these breathing networks.

6.5 The effect of exercise on breathlessness

Due to previously reported findings of decreased breathlessness in patients with COPD following a course of pulmonary rehabilitation (Carrieri-Kohlman et al., 2001, 1996), we investigated the effect of exercise on the physiological, psychological and brain mechanisms of breathlessness within a healthy volunteer model. Despite no significant differences in perceptions of breathlessness during inspiratory loading, submaximal exercise or hypercapnic hyperventilation in a group of endurance athletes compared to matched sedentary controls, functional activity in the vlPAG was greater in athletes during anticipation of inspiratory resistance. Alongside the vlPAG, increased BOLD activity was observed in the ventral prefrontal cortex and anterior cingulate cortex, in a remarkably similar manner to activity recently shown in COPD patients prior to treatment (Herigstad et al., 2015) (Figure 6.4). Therefore, as opposed to our predicted 'de-sensitisation' to breathlessness anxiety with exercise, we found activity *more* similar to patients with COPD. However, activity in the same areas of the cortex does not equate to the same brain representations or cognitive processes (Poldrack, 2006), but rather may represent different adaptations in similar cortical structures. It may be that breathlessness holds greater associations in these two groups, with positive associations as a result of exercise exposure, and disease associations in patients with COPD. However, what this consistency in activity shows us is that this brain network (including the vlPAG) is likely an important contributor to the emotional evaluation of breathlessness, and potentially imperative in the treatment of heightened anxiety of breathlessness apparent in respiratory disease.

The strong associations formed between breathlessness and threat values may be due to repeated exposure to breathlessness in both athletes and patients with COPD. In Chapter 4 of this Thesis we found that athletes experience anxiety about their breathing during max-

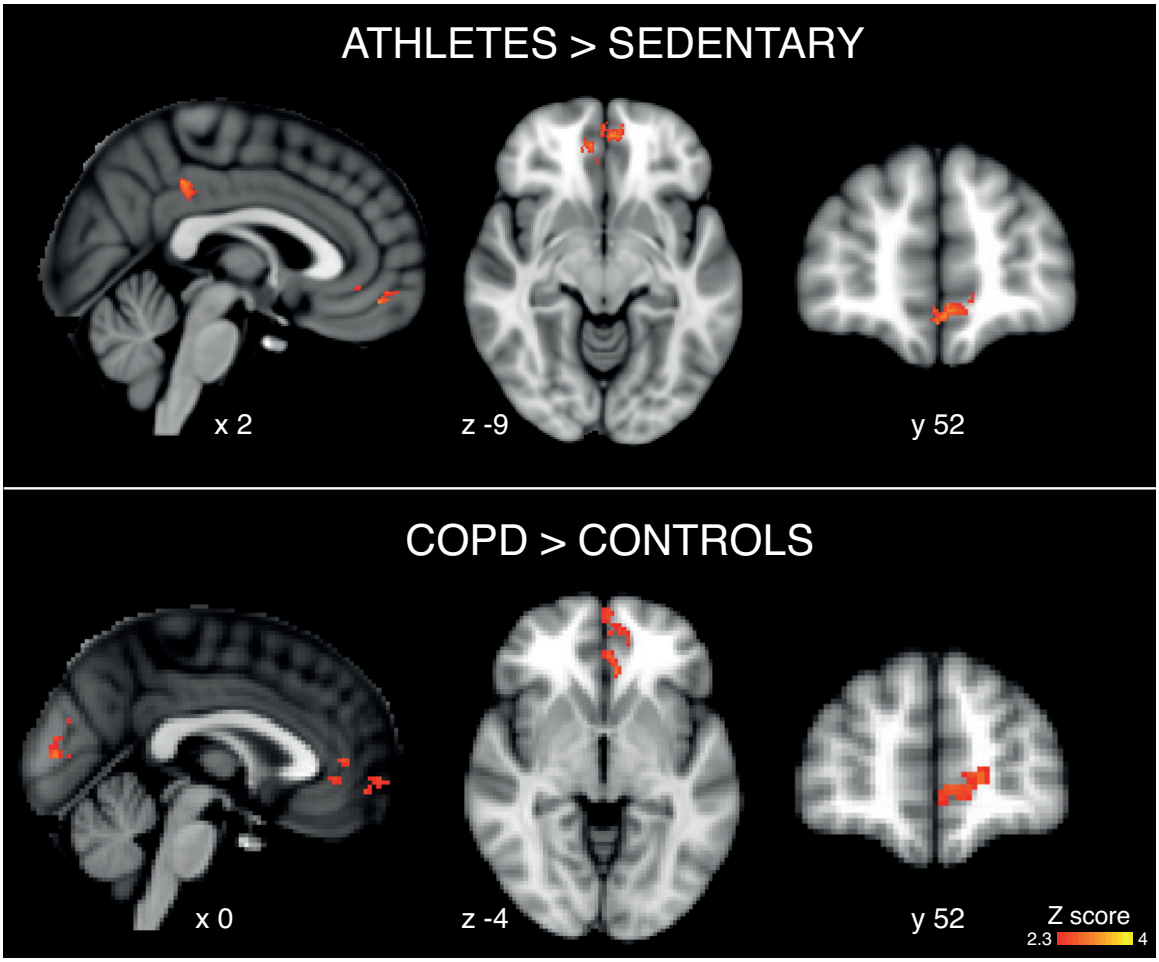

Figure 6.4: Top: Functional increase in prefrontal cortical activity during anticipation of breathlessness in athletes greater than matched sedentary controls (Data from Chapter 5). Bottom: Functional increase in prefrontal activity during presentation of breathlessness words in patients with COPD greater than matched controls (Data from Herigstad et al. (Herigstad et al., 2015)). The images consist of a colour-rendered statistical map superimposed on a standard (top, MNI 1 mm^3; bottom, MNI 2 mm^3) brain, and significant regions are displayed with a threshold $Z > 2.3$, with a cluster probability threshold of $p < 0.05$ (corrected for multiple comparisons).

imal exercise more than sedentary subjects, and were ventilating at a significantly greater proportion of their recorded maximal voluntary ventilation. Therefore, we have postulated that greater homeostatic signalling and threat detection may occur as a result of ventilation reaching close to maximal capacity, leading to increased anxiety. While athletes may associate their changes in ventilation and exercising breathlessness anxiety with positive performance outcomes, patients with COPD have reduced maximal voluntary ventilation (Aldrich et al., 1982) and will be exposed to threatening, anxiety-inducing breathlessness signalling with minimal physical effort associated with their disease. Furthermore, possibly as a result of exposure to this ventilatory exertion at high intensities of exercise, we found that subjective breathlessness scores in athletes more closely matched their changes in ventilation during hypercapnia, suggesting an improved ventilatory awareness. However, if a corresponding improvement in awareness of ventilation occurs in patients, this may serve to heighten breathlessness anxiety. Therefore, this cortical network (including the vlPAG) identified in athletes may be a site of adaptation during the positive or negative threat perception of breathlessness, which may exacerbate breathlessness anxiety in patients with COPD.

6.6 Methodological considerations

6.6.1 Imaging breathlessness

Breathlessness is a multifaceted sensation that is not yet fully understood (Herigstad et al., 2011; Hayen et al., 2013b; Janssens et al., 2011a). We know that perceptions of breathlessness can be exacerbated in respiratory disease (Bailey, 2004), and to understand the mechanisms of this exacerbation we first need to investigate breathlessness within a healthy population. Therefore, to examine the potential role of the PAG in breathlessness in this Thesis we chose to work within a healthy volunteer model. Furthermore, the resolution required to dissociate the PAG columns is possible only when using the 7 Tesla scanner, and current safety considerations exclude many patient groups from this machine. We also chose to use a simple anticipation-stimulus protocol in these initial studies of the PAG in breathlessness, without any element of subject control. In real life, a breathlessness cue (such as walking up the stairs) can often be avoided through the decisions made by an individual. Therefore, further studies that incorporate perceived subject control over upcoming stimuli, such as using a cognitive task to avoid a stimulus, may reveal different activity within PAG columns and the anticipatory network to those observed in these studies.

Even amongst healthy volunteers, imaging breathlessness is a difficult task. While

7 Tesla functional MRI can give us excellent resolution compared to other neuroimaging techniques such as PET, it is particularly susceptible to noise created by head and body movement, and any changes in $P_{ET}CO_2$. Therefore, we cannot apply a breathlessness stimulus evoked by exercise nor air huger from inhalation of carbon dioxide (Liotti et al., 2001), and imagination of breathlessness cannot be assumed to be the same as actual breathlessness. Instead, we chose to apply an adverse respiratory stimulus in the form of inspiratory resistance as an abstract form of breathlessness. While inspiratory resistive loading does not incorporate the multiple dimensions of real-world breathlessness, it does induce a threat to respiration that requires adequate preparation and a volitional change in ventilation. Although care must be taken when interpreting these results to breathlessness in the environment and to patients with respiratory disease, these results show that it is possible to identify changes in the columns of the human PAG, and it does appear to play a role when respiration is threatened. Lastly, while resistive loading has been shown to increase cerebral blood flow to a small degree (Hayen et al., 2013a), this global change would underestimate the effect size in a conservative manner rather than inflating false positives within the results.

6.6.2 Brainstem fMRI

A particular problem with brainstem fMRI is the inherently low signal to noise compared to cortical areas (Devonshire et al., 2012; Brookes et al., 2013; Harvey et al., 2008). The brainstem suffers from a larger influence of physiological noise, necessitating the use of either retrospective imaging techniques such as RETROICOR (RETROspective Image CORrection; (Glover et al., 2000; Harvey et al., 2008)), or data-driven approaches such as independent component analysis (ICA, reviewed in (Brookes et al., 2013)) to correct for cardiac and respiratory artifacts. RETROICOR was used in all studies, and ICA denoising was also added to preprocessing in Chapters 3 and 5 where shorter repetition time (TR) of functional scans allowed more reasonable separation of signal and noise within ICA decomposition.

Additionally, special care was taken during the registration of functional images in these studies. While greater details of brainstem structures in functional scans are able to be visualised with 1-2 mm^3 voxels, so too are the differences seen between individual brains, between hemispheres of a cerebrum or even between sides of a brainstem. Therefore, registration of functional scans through to the standard brain must be extremely accurate to allow reflective group statistics, particularly for smaller structures such as those within the brainstem. Registrations were performed outside of FEAT for Chapters 2 and 3, and rigorously checked in all studies, to ensure accurate alignment of the functional scans into

standard space. Furthermore, statistical results of respiratory tasks were not considered until the control motor/sensory task of finger opposition produced the expected activity in small brainstem nuclei, particularly the ipsilateral cuneate nucleus of the medulla, confirming accurate registrations and appropriate statistical modelling.

6.6.3 Subject selection

The cross-sectional nature of the comparisons made in Chapters 4 and 5 makes it difficult to isolate the effect of exercise across the two subject groups. Although the groups were matched for age, sex, handedness, and history of respiratory disease, many underlying genetic and environmental factors may influence their perception of breathlessness as well as exposure to exercise. Furthermore, the demanding and adverse nature of the study likely determined that only low-anxiety subjects volunteered to participate, and it is possible that these groups are not a representative sample of their respective populations. Further research using a longitudinal, placebo-controlled study design with an exercise intervention would be required to more accurately identify the effects of exercise on breathlessness perceptions and brain networks, as this was not within the scope of this Thesis.

6.7 Conclusion and implications

In this Thesis we have found that the columns of the human PAG are integrally and differentially involved in respiratory control and the perception of breathlessness. We have shown that the lPAG is involved within a sensorimotor network governing breath holds and breathing against an inspiratory load, with connectivity of the lPAG indicating it functions within the sensory aspect of breathlessness perception. Conversely, the vlPAG appears to be involved in the anticipation of an inescapable breathlessness stimulus, within a cortical network of cognitive and limbic structures for affective evaluation within the perception of breathlessness. Lastly, we revealed that exercise does not appear to de-sensitise individuals to breathlessness when using a model of endurance athletes compared to sedentary controls, although functional differences were apparent in a prefrontal and vlPAG network during anticipation of resistive loading. These differences adhere to the theory that exercise exposure may induce cognitive reappraisal of the threat of breathlessness, resulting in reduced breathlessness anxiety in patients with COPD. Therefore, as well as better understanding the role of the PAG in the complex, multi-dimensional sensation of breathlessness, we have revealed the PAG column as legitimate targets to understand and treat brain (mal)adaptations leading to debilitating anxiety in patients with chronic respiratory disease.

Appendix A

Published papers

NeuroImage 113 (2015) 356–364

Contents lists available at ScienceDirect

NeuroImage

journal homepage: www.elsevier.com/locate/ynimg

Functional subdivision of the human periaqueductal grey in respiratory control using 7 tesla fMRI

Olivia K. Faull [a,b,*], Mark Jenkinson [a], Stuart Clare [a], Kyle T.S. Pattinson [a,b]

[a] FMRIB Centre, Nuffield Department of Clinical Neurosciences, University of Oxford, Oxford, UK
[b] Nuffield Division of Anaesthetics, Nuffield Department of Clinical Neurosciences, University of Oxford, Oxford, UK

ARTICLE INFO

Article history:
Accepted 11 February 2015
Available online 19 February 2015

Keywords:
fMRI
Brainstem
Respiration
Periaqueductal grey

ABSTRACT

The periaqueductal grey (PAG) is a nucleus within the midbrain, and evidence from animal models has identified its role in many homeostatic systems including respiration. Animal models have also demonstrated a columnar structure that subdivides the PAG into four columns on each side, and these subdivisions have different functions with regard to respiration. In this study we used ultra-high field functional MRI (7 T) to image the brainstem and superior cortical areas at high resolution (1 mm^3 voxels), aiming to identify activation within the columns of the PAG associated with respiratory control. Our results showed deactivation in the lateral and dorsomedial columns of the PAG corresponding with short (~10 s) breath holds, along with cortical activations consistent with previous respiratory imaging studies. These results demonstrate the involvement of the lateral and dorsomedial PAG in the network of conscious respiratory control for the first time in humans. This study also reveals the opportunities of 7 T functional MRI for non-invasively investigating human brainstem nuclei at high-resolutions.

Introduction

The study of respiratory control is largely focused on the nuclei of the respiratory rhythm generators in the medulla, whilst suprapontine control of respiration is less well understood. The midbrain periaqueductal grey (PAG) is located at the junction of descending efferent commands and ascending sensory information, and has been suggested by animal models to participate within the localised pathway of respiratory response (Kabat et al., 1935; Subramanian, 2012; Subramanian et al., 2008). The human PAG is approximately 14 mm long and 4–5 mm wide (either side of the aqueduct), and almost completely encircles the aqueduct. The PAG has been proposed to be subdivided into four columns on each side; ventrolateral (vlPAG), lateral (lPAG), dorsolateral (dlPAG) and dorsomedial (dmPAG) (Bandler and Shipley, 1994; Dampney et al., 2013; Subramanian, 2012; Subramanian et al., 2008). Direct excitation of these columns in animals has revealed distinct respiratory functions, such as irregular breathing with the vlPAG, prolonged inspirations, expirations and vocalisations from the lPAG, active breathing and tachypnea from the dlPAG, and slow, deep breathing from the dmPAG (Subramanian, 2012; Subramanian et al., 2008).

Whilst animal models allow detailed investigation of functional neuroanatomy, subsequent studies in humans are essential to understand the role of these PAG subdivisions. Human respiratory control networks cannot be assumed to match those derived from animals. Additionally, humans allow the study of *conscious* control of breathing with the addition of subjective feedback, which is not possible in animals. Understanding these respiratory networks is imperative for effective treatment of breathing disorders, such as breathlessness from chronic obstructive pulmonary disease and heart failure (Hayen et al., 2013a; Herigstad et al., 2011), sleep disordered breathing (Morrell et al., 2000), and the dangerous respiratory depression associated with opioid painkillers (Pattinson, 2008).

Functional magnetic resonance imaging (fMRI) is a non-invasive technique that allows high-resolution functional imaging in humans (2–3 mm^3 voxels at 3 T). The recent introduction of ultra-high-field fMRI at 7 T vastly improves the signal-to-noise ratio of previous imaging, potentiating even higher resolution functional imaging (<2 mm^3) and the ability to specifically investigate small nuclei such as the subdivisions of the PAG, previously not possible at 3 T. However, 7 T imaging requires added methodological considerations during both scanning and analysis. Greater B_0 inhomogeneities at 7 T cause increased distortion and drop-out during echo-planar imaging (EPI), and increases in resolution require longer acquisition times (TR) and cause decreases in temporal signal-to-noise. Additionally, high resolution functional scanning may reveal greater structural and functional differences between individuals, amplifying the importance of image registration

* Corresponding author at: Nuffield Department of Clinical Neurosciences, University of Oxford, Oxford, UK. Fax: +44 1865 23079.
E-mail address: olivia.faull@ndcn.ox.ac.uk (O.K. Faull).

http://dx.doi.org/10.1016/j.neuroimage.2015.02.026

for successful group statistical analysis. Therefore, this study aimed to investigate and establish methods to image brainstem centres at 7 T.

Using MRI to investigate respiratory control presents further methodological challenges and requires additional considerations. Arterial pressure of carbon dioxide ($PaCO_2$) is a potent vasodilator of cerebral vessels, and thus changes in $PaCO_2$ often induced by respiratory challenges confound the blood oxygen level dependent (BOLD) signal (Pattinson et al., 2009a; Pattinson et al., 2009b). Additionally, bulk susceptibility variations in the lungs during the respiratory cycle cause changes in the B_0 magnetic field, producing physiological noise related to respiratory changes (Glover et al., 2000; Harvey et al., 2008; Raj et al., 2001). Finally, the location of the brainstem close to arteries and pulsating fluid-filled spaces (due to cardiac and respiratory cycles) (Brooks et al., 2013; Cohen et al., 2002) results in a particular susceptibility to physiological noise artefacts, yet it is of great importance as it houses many respiratory control centres.

In this study we used 7 T scanning to investigate the role of the subdivisions of the PAG in short respiratory tasks, taking careful consideration of respiratory imaging confounds. Based on previous work in animals, we hypothesised that BOLD signal changes within the lPAG and dmPAG (associated with prolonged expirations and depressed breathing) would be associated with the inhibitory respiratory tasks of breath holds and vocalisations, but not associated with a simple sensory and motor task.

Materials and methods

Subjects

The Oxfordshire Clinical Research Ethics Committee approved the study and volunteers gave written, informed consent. Sixteen healthy, right-handed volunteers (10 males, 6 females; mean age ± SD, 28 ± 7 years) undertook one training session, followed immediately by one MRI scanning session. One subject was excluded from the analysis due to an inability to comply with experimental protocol. Prior to scanning, all subjects were screened for any contraindications to magnetic resonance imaging at 7 T.

Breathing system

A breathing system was used to allow the administration of small CO_2 challenges mixed with room air, via a venturi entrainment system (Fig. 1a). The CO_2 challenges were administered to dissociate the changes in global BOLD signal due to changes in arterial PCO_2 from local BOLD signal changes correlating to activity associated with breath holds and vocalisations (Pattinson et al., 2009a). During scanning, medical air was administered through a loose fitting venturi mask (Ventimask, Intersurgical Ltd, Berkshire, UK) with a 1:1 entrainment ratio of compressed gas:room air. Gas was delivered to the mask at a rate of 20 L/min, and the mask was designed to entrain an equivalent amount of room air. The resulting high gas flow rate delivered by this system (40 L/min) minimises rebreathing of expired gases. The ventimask is loose fitting and therefore considerably more comfortable than a tight fitting mask, but its gas delivery characteristics allows control of end-tidal gases in the volunteer. For the CO_2 challenges during the functional scan, the medical air was substituted for a CO_2 mixture (10% CO_2, 21% O_2, balance nitrogen) at 20 L/min for periods of 10 s, the entrainment system meant that approximately 5% CO_2 was delivered to the face mask. The CO_2 challenges aimed to elevate end-tidal partial pressure of CO2 ($P_{ET}CO_2$) by approximately 0.8%, to match elevations caused by breath holds and vocalisations.

Physiological measurements

Physiological measures were recorded continuously during the training session and MRI scan. Chest movements were measured using respiratory bellows surrounding the chest at the approximate level of the 10th rib, and heart rate was measured using a pulse oximeter (9500 Multigas Monitor, MR Equipment Corp., NY, USA). The end-tidal partial pressure of CO_2 ($P_{ET}CO_2$) was sampled via nasal cannula (Salter Labs, California, USA) and determined using a rapidly-responding gas

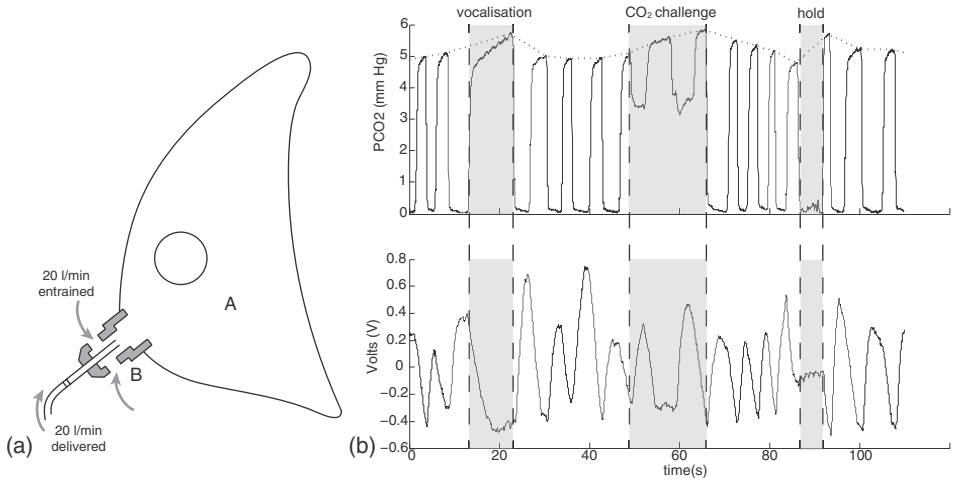

Fig. 1. a) Schematic diagram of the venturi mask used in the breathing system. A: Loose plastic venturi mask B: Venturi entrainment device (1:1). b) A section of a respiratory trace from one subject demonstrating the tidal CO_2 trace (top) and the tidal volume trace from the bellows (bottom). The end-tidal CO_2 ($P_{ET}CO_2$) trace was formed by interpolating between the end expiration peaks (dotted line, top trace). The breath hold duration was calculated from the time between the end of expiration CO_2 trace and the beginning of the subsequent expiration trace, to minimise inclusion of head movement. The vocalisation duration was calculated from the duration between the beginning and end of a vocalisation expiration trace.

analyser (CD-3A; AEI Technologies, Pittsburgh, USA). Subjects were asked to breathe through their nose for the entire experiment. All physiological devices were connected to a data acquisition device (MP150; Biopac Systems Inc., California, USA) coupled to a desktop computer with recording software (Acknowledge 4.2; Biopac Systems Inc., California, USA).

Magnetic resonance imaging

MRI was performed with a 7 T Siemens Magnetom scanner, with 70 mT/m gradient strength and a 32 channel Rx, single channel birdcage Tx head coil (Nova Medical). The fMRI experimental design is illustrated in Fig. 2.

Brainstem BOLD scanning

A T2*-weighted, gradient echo EPI functional scan consisted of 333 volumes, and lasted 28 mins and 10 s. The field of view (FOV) comprised 54 coronal–oblique slices of the brainstem and cortex (sequence parameters: TE, 24 ms; TR, 5 s; flip angle, 90°; voxel size, $1 \times 1 \times 1$ mm; GRAPPA factor, 3; echo spacing, 1 ms; slice acquisition order, descending).

Structural scanning

A T1-weighted structural scan (MPRAGE, sequence parameters: TE, 2.96 ms; TR, 2200 ms; flip angle, 7°; voxel size, $0.7 \times 0.7 \times 0.7$ mm; inversion time, 1050 ms; bandwidth; 240 Hz/Px) was acquired. This scan was used for registration of functional images, and anatomical overlay of brain activations.

Additional scanning

A single volume whole brain EPI was acquired with 128 slices in the same orientation as the functional scan (matched sequence parameters) for registration purposes. Fieldmap scans (sequence parameters: TE1, 4.08 ms; TE2, 5.1 ms; TR, 620 ms; flip angle, 39°; voxel size, $2 \times 2 \times 2$ mm) of the B_0 field were also acquired in the same orientation to assist distortion-correction of scans.

Stimuli and tasks

During the BOLD scan, subjects performed 14 repeats of the following tasks: expiratory breath hold, vocalisation and finger and thumb opposition task (described to subjects as "finger tapping"). This paradigm was (adapted from previous breath hold research (McKay et al., 2008; Pattinson et al., 2009a)). Cues for these tasks were presented on the screen as the words 'HOLD', 'SING' and 'TAP' ('REST' was displayed for the remainder of the experiment), in white letters on a black background. During the training session, the subjects had a chance to practice each of the tasks under observation. The instructions for the breath hold were to stop breathing at the end of the current breath, maintaining the hold until the 'HOLD' cue was exchanged for 'REST'. At the termination of the breath hold, the subject was asked to breathe out any remaining air in their lungs for an end-tidal CO_2 reading. The instructions for the vocalisation were to produce a closed-mouth single note from the top of the next breath, for the duration of the 'SING' cue. Both the 'HOLD' and 'SING' cues were presented for a duration of 10 s; therefore the tasks were each less than 10 s. The finger opposition task consisted of an opposition movement conducted with the right hand, and the 'TAP' cue was presented for 15 s. It is well known that the cuneate nucleus of the medulla is a sensory nucleus in the fine touch and proprioception pathway, prior to decussation (Craven, 2011). Therefore, activation of the ipsilateral cuneate associated with the finger opposition task was used by Pattinson et al. (2009a), as a functional localiser to provide confidence in the precision of brainstem registrations. We repeated this functional localiser task in the present study, to validate our methodology and assure the accuracy of the registration of the 1 mm^3 functional images. Each of the three tasks was repeated 14 times within the BOLD scan of each subject.

The respiratory stimuli of breath holding and vocalisations both cause an increase in arterial PCO_2 (hypercapnia), which leads to vasodilation of the cerebral vessels and an increase in blood flow (Cohen et al., 2002). Hypercapnia increases the grey matter BOLD signal in correlation with the local BOLD signal of interest from these stimuli. Therefore, to decorrelate the effects of hypercapnia from the localised BOLD responses correlating with breathing control, additional, repeated CO_2 challenges were interspersed during rest periods in the protocol. This means that the timecourse of the CO_2 is different to the time course of the breath holds. A CO_2 regressor was then created by extrapolating between end-tidal peaks, and this trace was entered into the general linear model as a physiological regressor of no interest (described in detail in Pattinson et al., 2009a).

Analysis

Preprocessing

Image preprocessing was performed using the Oxford Centre for Functional Magnetic Resonance Imaging of the Brain Software Library (FMRIB, Oxford, UK; FSL version 6.0; http://www.fmrib.ox.ac.uk/fsl/). The following processing methods were used prior to statistical analysis: motion correction (MCFLIRT; Jenkinson et al., 2002), removal of the nonbrain structures (skull and surrounding tissue) (BET; Smith, 2002; Woolrich et al., 2001), spatial smoothing using a full-width half-maximum (FWHM) Gaussian kernel of 2 mm, and high-pass temporal filtering (Gaussian-weighted least-squares straight line fitting; 120 s cutoff period). B_0 field unwarping was conducted with a combination of FUGUE and BBR (Boundary-Based-Registration; part of FEAT: FMRI Expert Analysis Tool, version 6.0) tools (Greve and Fischl, 2009; Jenkinson et al., 2002), and the functional scans were corrected for cardiac- and respiratory-related noise with RETROICOR (Brooks et al., 2008; Glover et al., 2000; Greve and Fischl, 2009; Harvey et al., 2008). Time-series statistical analysis was performed using FILM, with local autocorrelation correction (Andersson et al., 2007; Woolrich et al., 2001).

Image registration

Careful attention was paid to image registration, as the finer resolution afforded by 7 T MRI requires greater registration accuracy

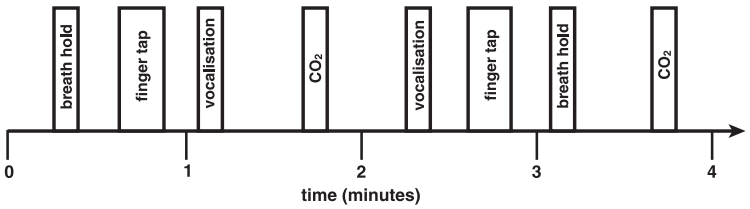

Fig. 2. Example four minutes of the BOLD sequence, repeated throughout the acquisition. The order of the breath holds and vocalisations was semi-randomised between the finger opposition and CO_2 stimuli.

for group statistics to be possible. After preprocessing, the functional scans were registered to the MNI152 (1 mm^3) standard space [average T1 brain image constructed from 152 normal subjects at the Montreal Neurological Institute (MNI), Montreal, QC, Canada] using a three-step process.

- Linear registration (FLIRT) with 6 degrees of freedom (DOF) was used to align the partial FOV scan to the whole-brain EPI image (Jenkinson et al., 2002; Worsley, 2001).
- Registration of subjects' whole-brain EPI to T1 structural image was conducted using BBR (6 DOF) with (nonlinear) fieldmap distortion-correction (Devonshire et al., 2012; Greve and Fischl, 2009).
- Registration of the subjects' T1 structural scan to 1 mm standard space was performed using an affine transformation followed by nonlinear registration (FNIRT) (Andersson et al., 2007; Handwerker et al., 2004).

Voxelwise analysis

fMRI data processing was performed using FEAT (FMRI Expert Analysis Tool), version 6.0, part of FSL (FMRIB's Software Library; www.fmrib.ox.ac.uk/fsl). The first-level analysis in FEAT incorporated a general linear model, where the finger opposition regressor was derived from the protocol timing values by convolution with an HRF basis set (see below). The two respiratory stimuli (breath holds and vocalisations) timings were modelled from the respiratory physiological traces (Fig. 1b). $P_{ET}CO_2$ was included as an additional regressor, decorrelating the CO_2-induced BOLD changes from the respiratory stimuli throughout the functional scan. This trace was formed by linearly interpolating between the expired CO_2 peaks. This technique assumed a linear rise in $P_{ET}CO_2$ throughout a breath hold, as values were only available for the breath immediately before and at the end of each hold. Previous research has indicated that variations in the haemodynamic response function (HRF) are apparent throughout the brainstem and cortex (Devonshire et al., 2012; Woolrich et al., 2004b), and between subjects (Handwerker et al., 2004; Smith and Nichols, 2009). To account for possible changes in the HRF, including slice-timing delays, we used an optimal basis set of three waveforms (FLOBS: FMRIB's Linear Optimal Basis Sets, default FLOBS supplied in FSL (Woolrich et al., 2004a)), instead of the standard gamma waveform. This models the changes induced by altered HRFs or slice-timing, but does induce some bias into the estimation of the main effect size. This bias takes the form of an underestimation of the effect size, which is a conservative error that affects the statistical power, and therefore will not inflate the false positive rate. The second and third FLOBS waveforms, which model the temporal and dispersion derivatives, were orthogonalised to the first waveform, of which the parameter estimate was then passed up to the higher level to be used in group analysis.

Voxelwise statistical analysis using basis functions was extended to a group level, in a mixed-effects analysis using FLAME (FMRIB's Local Analysis of Mixed Effects) (Woolrich et al., 2004b). *Z* statistic images were thresholded using clusters determined by $Z > 2.3$ and a (corrected) cluster significance threshold of $p < 0.05$. A small-volume-corrected analysis of the PAG (as our a-priori area of interest; mask = 698 voxels) was then conducted, using threshold-free cluster enhancement (TFCE) corrected for family-wise error. TFCE provides an alternative method to enhance cluster-like structures in an image, without a pre-determined initial cluster-forming threshold (Smith and Nichols, 2009). TFCE produces an output where voxel-wise values represent the amount of cluster-like local support, illustrating the significance of voxels within a cluster rather than the significance of the cluster as a whole whilst maintaining strict false positive control by using permutation-based family-wise-error correction (Smith and Nichols, 2009).

Results

Physiology

Group average heart rate (±SD) during the brainstem BOLD scanning was 65 (±11) beats per minute. An example respiratory trace is given in Fig. 1b. Baseline $P_{ET}CO_2$ (±SD) was 4.7% (±0.7%), with breath holds increasing $P_{ET}CO_2$ by 0.8% (±0.2%) and 0.6% (±0.2%) with vocalisations. CO_2 challenges induced an average increase in $P_{ET}CO_2$ of 0.9% (±0.1%).

Periaqueductal grey analysis

The results from a small-volume family-wise-error corrected analysis of the PAG revealed significant ($p < 0.05$) deactivation in two areas correlating with the breath hold task (Fig. 3). One of these deactivation clusters followed the lateral column on the right side of the PAG (12 voxels), and the second was located in the right caudal dorsolateral PAG (8 voxels). Uncorrected z scores within the PAG are also presented in Fig. 3, demonstrating the deactivations extending to the inferior border of the PAG. Column locations were defined using tractography results from a recent diffusion tensor imaging study (Ezra et al., ISMRM abstract, 2014). No significant activations or deactivations were found in the PAG for either vocalisation or the finger opposition task.

Cortex

We observed significant signal increases bilaterally in the motor cortex, supplementary motor cortex, anterior cingulate (ACC) and paracingulate cortices, primary sensory cortex, anterior insula and putamen (Fig. 4). Breath holds also correlated with bilateral BOLD signal increases in the supramarginal gyrus and caudate nucleus, whilst vocalisations correlated with right side supramarginal gyrus activation. Vocalisations were also associated with thalamic activation bilaterally in the VPL nucleus, Heschl's gyrus (primary auditory cortex) and the planum polare. Conversely, breath holds were associated with right side BOLD signal increases in the thalamus [ventral posterolateral (VPL) and ventral posteromedial (VPM) nuclei], subthalamic nucleus and red nucleus.

CO_2 challenges

The hypercapnia challenges and the resultant CO_2 regressor produced strong BOLD signal increases throughout the grey matter of the brain. Furthermore, increases in BOLD signal correlating to the CO_2 regressor were observed within the PAG, localised to the grey matter and excluding the aqueduct (supplementary Fig. 1).

Finger opposition task

Finger opposition resulted in significant signal increases bilaterally in the motor cortex (more extensive activation in the contralateral left motor cortex), supplementary motor cortex, anterior cingulate (ACC) and paracingulate cortices, primary sensory cortex, anterior insula cortex, operculum, caudate nucleus and putamen (supplementary Fig. 1). Bilateral signal increases were seen in the thalamic VPL nuclei, as well as the left thalamic VPM nucleus. In addition, activations were observed in the left subthalamic and red nuclei, left pons, right (ipsilateral) cuneate nucleus of the medulla (Fig. 5), and bilateral cerebellum (VI and VIIIa lobules).

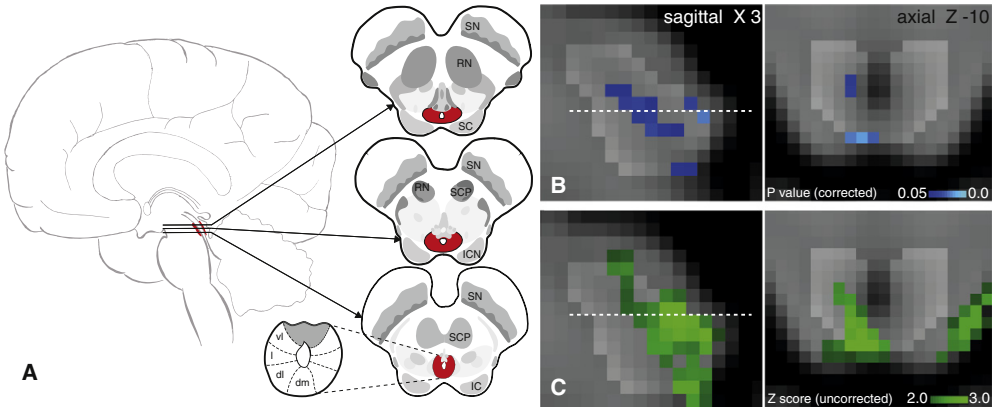

Fig. 3. Periaqueductal grey (PAG) response to breath hold. A. Representation of the location of the PAG within the brain, three sagittal slices and the current opinion of the subdivisions of the PAG. B. Localisation of the functional decreases in BOLD signal within the PAG ($p < 0.05$; small-volume-corrected for multiple comparisons using overlaid PAG mask), where the images consist of a colour-rendered statistical map superimposed on a standard (MNI 1 mm^3) brain. Dashed line represents Z-10 location. C. Uncorrected Z score image of PAG deactivation from whole brain analysis, prior to masking. Abbreviations: SN, substantia nigra; RN, red nucleus; SC, superior colliculus; SCP, superior cerebellar peduncle; ICN, inter-colliculi nucleus; IC, inferior colliculus; vl, ventrolateral PAG, l, lateral PAG; dl, dorsolateral PAG; dm, dorsomedial PAG.

Discussion

Main findings

Assuming that the human PAG has a columnar structure similar to that in animals, and corresponding with recent human neuroimaging findings (Ezra et al., 2014 ISMRM abstract; paper under review), we have identified respiratory-related activity that appears to be localised within the lateral and caudal dorsomedial columns of the PAG. Cortical activity associated with breath holding was consistent with previous results (Cowie and Holstege, 1992; Pattinson et al., 2009b; McKay et al., 2008), and highly localised within cortical regions. As expected, with the control sensory and motor task of finger opposition, BOLD activity was identified within the ipsilateral cuneate nucleus in the medulla, a sensory nucleus processing fine touch and proprioception, validating our methodology.

PAG and respiratory control

This study has demonstrated differential activity localised within the columns of the PAG (lPAG and dmPAG), correlating with the respiratory task of a breath hold. In comparison, no observable differences in any areas of the PAG were found with a respiratory vocalisation task, nor with a motor finger-tapping task. This study is the first to functionally localise respiratory activity within the human PAG, with sufficient resolution (1 mm^3) to have confidence in the positions of activations in relation to the current theory of columnar subdivisions. Using a Gaussian kernel of 2 mm (FWHM) for spatial smoothing, blurring of the BOLD signal changes within the PAG was minimised. The deactivation seen within the lPAG, in particular, follows a columnar structure that is consistent with previous work from animal models.

Whilst there have been many neuroimaging studies reporting involvement of the PAG (Linnman et al., 2012), the function(s) of the PAG have predominantly been linked to pain, anxiety, bladder and bowel control, and cardiovascular regulation (Linnman et al., 2012). Whilst there has been some implications of PAG involvement in respiratory control (Corfield et al., 1995; Pattinson et al., 2009a; Topolovec et al., 2004) this research has been limited by functional resolution, extensive smoothing, or registration issues that have impeded group-level analysis, making accurate localisation to the PAG or its subdivisions impossible. In addition, significant results within the PAG have been found using statistics uncorrected for multiple comparisons (Mobbs et al., 2007), and a more recent 7 T study used a column segmentation of the PAG that is inconsistent with animal literature, and masking of the cerebral aqueduct to dissociate activity within PAG columns (Satpute et al., 2013). Therefore, the results of this study demonstrate the potential for 7 T MRI to be used to investigate the roles of the subdivisions of the PAG within respiratory control using robust statistical methodology, when careful attention is paid to registration and noise correction of functional data.

Deactivation within the PAG was localised to the lateral column and caudal section of the dorsomedial column, (Ezra et al., ISMRM abstract, 2014). Activity in the lateral and dorsomedial columns of the PAG during inhibition of ventilation is consistent with previous respiratory control experiments in animals, where these columns have been associated with depressed ventilatory behaviours such as prolonged inspirations and expirations (lPAG), and slow, deep breathing (dmPAG). Conversely, the vlPAG and dlPAG have been associated with more active and irregular ventilation in animals (Subramanian, 2012; Subramanian et al., 2008). Whilst excitation of the vlPAG and lPAG in decerebrate cats has previously produced vocalisations of mews and hisses (Subramanian et al., 2008), we did not see activation in any of the PAG columns during vocalisations. It is possible that the vocalisation pathway within the cortex and brainstem is not consistent from animals to humans, or possibly that brainstem movement during vocalisations masked these activations in the current experiment.

Whilst one cannot determine from the BOLD signal whether the deactivations in the PAG represent either changes in motor drive or incoming sensory information, it has been established that the lateral PAG receives somatotopically organised spinal sensory afferents (Craven, 2011; Keay and Bandler, 2001) and could thus be involved in monitoring ventilatory feedback from the chest. Conversely, evidence exists for direct descending connections from the lateral and dorsomedial PAG to the midline medulla (Cowie and Holstege, 1992), demonstrating the potential for involvement in descending motor commands to respiratory centres in the medulla. Therefore, it is possible that the lPAG is involved with monitoring respiratory sensations from the chest as they ascend up to higher cortical areas of sensation or, together with the dmPAG, in the descending motor drive for changes in respiration.

A recent study used diffusion tensor imaging (DTI) to segment the human PAG (Ezra et al., 2014 ISMRM abstract; paper under review), and found a similar four-column structure with animal models of the

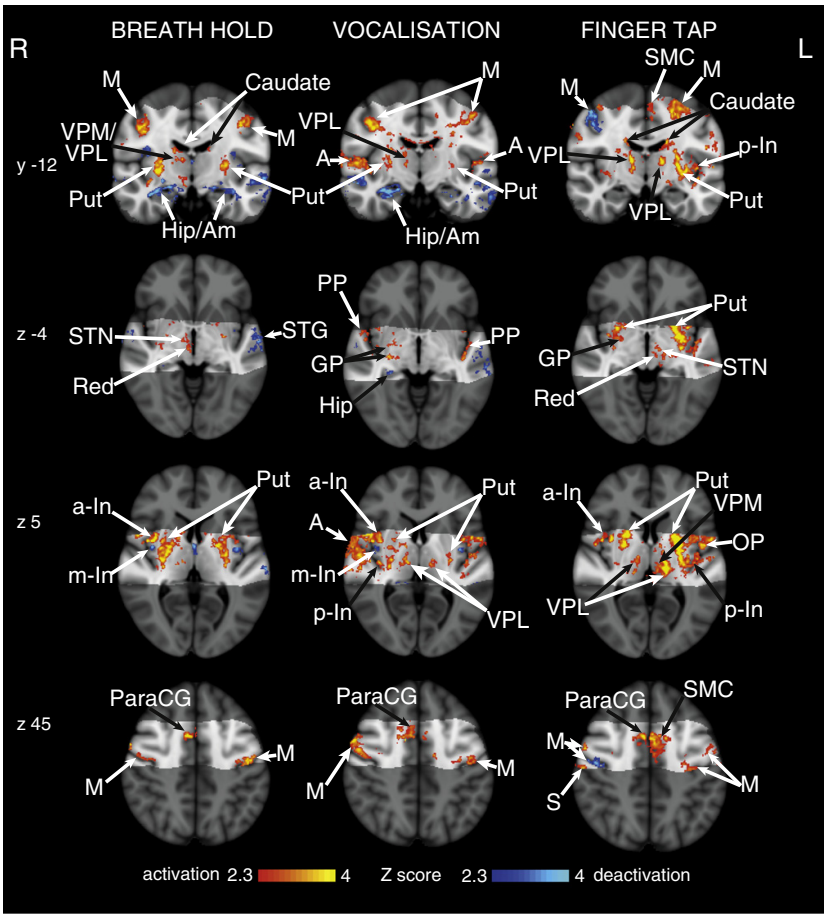

Fig. 4. BOLD response to breath holds, vocalisations and finger opposition in 15 subjects, having accounted for CO_2-induced vasodilation. The images consist of a colour-rendered statistical map superimposed on a standard (MNI 1 mm^3) brain. The bright grey region represents the coverage of the coronal-oblique functional scan. Significant regions are displayed with a threshold $Z > 2.3$, with a cluster probability threshold of $p < 0.05$ (corrected for multiple comparisons). Abbreviations: M, motor cortex; Caudate, caudate nucleus; SMC, supplementary motor cortex; Put, putamen; A, auditory cortex; Hip, hippocampus; Am, amygdala; thalamic nuclei: VPM, ventral posteromedial nucleus; VPL, ventral posterolateral nucleus; MDN, medial dorsal nuclei; a-In, anterior insula; m-In, middle insula; p-In, posterior insula; PP, planum polare; STN, subthalamic nucleus; Red, Red nucleus; STG, superior temporal gyrus; GP, globus pallidus; OP, operculum; S, post central gyrus (sensory cortex); paraCG, paracingulate gyrus; activation, increase in BOLD signal; deactivation, decrease in BOLD signal. R (right) and L (left) indicate image orientation.

PAG (Subramanian, 2012; Subramanian et al., 2008). Ezra et al. (2014) revealed strong connectivity between the lateral column of the PAG and the primary motor and sensory cortices in humans, which supports our hypothesis of the potential role of the lPAG in either respiratory sensation or in the descending motor drive for changes in ventilation. Further research combining functional and structural techniques (such as DTI) may help to advance our understanding of the role of the subdivisions of the PAG in human respiratory control.

The secondary findings of this study were that cortical activations associated with breath holding at 7 T largely agree with previous breath hold research at 3 T (Feinberg et al., 2010; Pattinson et al., 2009a; McKay et al., 2008), with a higher degree of localisation. It is possible that the cortical results were underestimated, due to slice-timing differences across the field of view with a 5 second TR. However, despite the possibly conservative nature of these results, the cortical consistency displayed with short 10 second breath holds, and additional deactivation of the lPAG and dmPAG, suggests that these PAG areas are part of the conscious breathing control network that is invoked during voluntary cessation of breathing.

Finger opposition task

As well as a control motor task, the finger opposition task was used as a robust comparison between ultra-high field and lower field fMRI studies, for confidence in analysis techniques and subsequent interpretation of results. Importantly, we had a firm a priori hypothesis that localised BOLD signal increase would be seen in the ipsilateral cuneate nucleus of the medulla, which is a sensory nucleus in the fine touch and proprioception pathway (Craven, 2011). This activation was consistent with previous findings at 3 T (Fig. 5), and demonstrates the registration accuracy within the brainstem to allow activations within small nuclei to survive group analysis. Therefore, medullary motor activity was used to validate the registration and modelling in the current study. However, medullary and pontine activations previously seen with breath holds at 3 T (Pattinson et al., 2009a; McKay et al., 2008) were apparent subthreshold, but did not survive multiple comparison correction, possibly due to the reduction in signal experienced when voxel size is reduced to 1 mm^3.

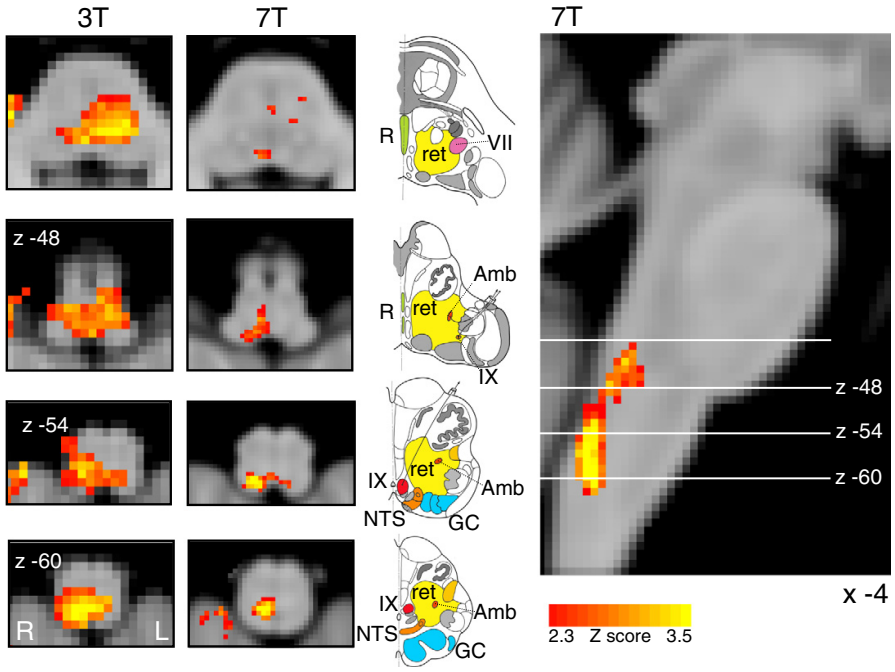

Fig. 5. Demonstration of the use of finger opposition as a functional localiser in brainstem fMRI at 3 T and at 7 T, by imaging activation in the ipsilateral cuneate nucleus of the medulla (z -54). The 3 T data is derived from previously-published results (Pattinson et al., 2009a). This technique provides confidence in the analysis model and registration accuracy of the current 7 T study. The images consist of a colour-rendered statistical map superimposed on a standard (MNI 1 mm^3) brain. Significant regions are displayed with a threshold $Z > 2.3$, with a cluster probability threshold of $p < 0.05$ (corrected for multiple comparisons). The sagittal image on the right displays the position of slices, for clarity only displayed from the 7 T acquisition. Abbreviations: R, raphe nuclei; ret, nuclei reticularis; VII, facial nucleus; Amb, nucleus ambiguous; IX, glossopharyngeal nucleus; NTS, nucleus tractus solitaries; GC, gracile (medial) and cuneate (lateral) nuclei (in blue). R (right) and L (left) indicate image orientation. Original line drawings adapted from Duvernoy (1995).

Scanning and analysis techniques

Whilst the use of ultra-high field MRI at 7 T permits improved spatial resolution in functional imaging, it is accompanied by a compounding of many of the challenges experienced with lower resolution imaging. The use of 7 T imaging increases intrinsic voxel signal compared to 3 T, whilst decreasing the voxel size to 1 mm^3 reduces this signal, requiring longer scan acquisitions to amass adequate statistical power. Furthermore, acquiring 1 mm^3 voxels requires a longer repetition time (TR) compared to larger voxels for the same brain coverage. To limit the TR to 5 s we restricted our field of view to a coronal–oblique slice, to collect enough time points within the functional scan for adequate temporal SNR. Restricting the field of view may compromise wider brain network analysis, and techniques such as parallel imaging (Arthurs and Boniface, 2002; Feinberg et al., 2010) may allow broader brain coverage in future high-resolution studies.

Brain imaging of respiratory tasks can be challenging due to stimulus-correlated noise, such as induced changes in blood gases and possible task-related head movement. To address these issues, the duration of the respiratory tasks in this study was limited to 10 s to minimise the changes in $PaCO_2$ and movement. The resulting unavoidable small changes in $PaCO_2$ were dissociated from the BOLD signal of the respiratory stimuli using short periods of additional CO_2 (10% CO_2 in air). However, the long TR (5 s) reduced statistical power by limiting the number of data points collected within each stimulus. This could be addressed in future studies by reducing the TR by either further decreasing the field of view, increasing the voxel size, or using parallel imaging techniques (Feinberg et al., 2010), which would allow more measured volumes within a short respiratory task.

Previous research has shown a widespread decrease in BOLD signal with breath holds, proposed as a result of vascular effects (Thomason et al., 2005). However, as can be seen in Fig. 4, this study found differential activation and deactivation, rather than a global decrease in BOLD signal correlating with breath holds. There are some key differences in techniques and analysis methods that may explain the possible discrepancies between the current study and previous fMRI investigations. Firstly, the breath hold used in the current study is an end-of-breath hold, which produces a different chest diameter in the scanner bore, and will result in differences in intrathoracic pressures and physiological noise in the B_0 field. Further, Thomason et al. (2005) postulated that the decrease in BOLD signal resulted from a decrease in intrathoracic pressure and cerebral blood flow (CBF), whilst a recent paper by Hayen et al. (2013b) showed that a decrease in intrathoracic pressure (whilst maintaining stable end-tidal CO_2) actually resulted in a small increase in CBF. Additionally, Thomason et al. (2005) did not report any measurements of end-tidal CO_2, and thus the effect of hypercapnia in this study cannot be fully explored. Therefore, whilst there are significant challenges in dissociating task-specific fMRI signal from residual vascular effects of breath holds, we feel the techniques used in the current study have minimised the influence of this task-related noise.

A particular problem with brainstem fMRI is the inherently low signal to noise compared to cortical areas (Brooks et al., 2013; Devonshire et al., 2012; Harvey et al., 2008). The brainstem suffers from a larger influence of physiological noise, necessitating the use of either retrospective imaging techniques such as RETROICOR (RETROspective Image CORrection; Glover et al., 2000; Harvey et al., 2008), or data-driven approaches such as independent component analysis (ICA, reviewed in Brooks et al., 2013) to correct for cardiac and respiratory artefacts. RETROICOR was used in the current study, but as no formal

comparison has been made between retrospective correction and ICA techniques, future work may benefit from ICA analysis or even a combination of both.

A current problem with brainstem imaging is at the existence of greater static B_0 field inhomogenieties compared to many areas of the cortex, due to proximity to bone and air-filled cavities. In this study significant signal loss was often seen in areas such as the anterior pons, although the degree of dropout varied between individuals. Whilst we did not explore the role of pontine nuclei in this study, future investigations may need to address this issue for further brainstem imaging.

Finally, special care was taken during the registration of functional images in this study. Whilst greater details of cerebral structures in functional scans are able to be visualised with 1 mm^3 voxels, so too are the differences seen between individual brains, between hemispheres of a cerebrum or even between sides of a brainstem. Therefore, registration of functional scans through to the standard brain must be extremely accurate to allow reflective group statistics, particularly for smaller structures such as those within the brainstem.

Whilst this study has shown that investigation of small brainstem nuclei is possible using ultra-high field fMRI, future research would greatly benefit from incorporating multiband echo planar imaging acquisition strategies (Moeller et al., 2010). This would reduce the TR, allowing more time points, greater brain coverage or even finer resolution scanning, for more detailed explorations into brainstem respiratory nuclei such as the PAG.

Conclusions

Imaging the brainstem using 7 T MRI is known to be extremely challenging. However, with rigorous physiological noise modelling, consideration of different HRF within the brainstem, and careful attention to distortion minimisation, we have successfully imaged respiratory-related activity in distinct columns of the PAG. In particular, reductions in the BOLD signal within the lPAG and dmPAG were associated with short breath holds, consistent with animal research. Therefore, these results indicate that the lateral and dorsomedial PAG columns are activated as part of the volitional respiratory control network, and are involved with either the motor inhibition, or sensation of depressed ventilation, or both. This study demonstrates that 7 T MRI can successfully be used for functional investigations into brainstem respiratory nuclei, and that the columns of the PAG may have an important role within the respiratory control network in humans.

Acknowledgements

This research was supported by an MRC (G0802826) Centenary Award as part of an MRC Clinician Scientist Fellowship awarded to Kyle T. S. Pattinson. This research was further supported by the National Institute for Health Research, Oxford Biomedical Research Centre based at Oxford University Hospitals NHS Trust and University of Oxford. Olivia K Faull was supported by the Commonwealth Scholarship Commission.

Appendix A. Supplementary data

Supplementary data to this article can be found online at http://dx.doi.org/10.1016/j.neuroimage.2015.02.026.

References

Andersson, J.L., Jenkinson, M., Smith, S., 2007. Non-linear Registration, aka SPATIAL Normalisation FMRIB Technical Report TR07JA2. FMRIB Analysis Group of the University of Oxford.

Arthurs, O.J., Boniface, S., 2002. How well do we understand the neural origins of the fMRI BOLD signal? Trends Neurosci. 25 (1), 27–31.

Bandler, R., Shipley, M.T., 1994. Columnar organisation in the midbrain periaqueductal gray: modules for emotional expression? Trends Neurosci. 17 (9), 379–389.

Brooks, J.C.W., Beckmann, C.F., Miller, K.L., Wise, R.G., Porro, C.A., Tracey, I., Jenkinson, M., 2008. Physiological noise modelling for spinal functional magnetic resonance imaging studies. Neuroimage 39 (2), 680–692.

Brooks, J.C.W., Faull, O.K., Pattinson, K.T.S., Jenkinson, M., 2013. Physiological noise in brainstem fMRI. Front. Hum. Neurosci. 7, 1–13.

Cohen, E.R., Ugurbil, K., Kim, S.-G., 2002. Effect of basal conditions on the magnitude and dynamics of the blood oxygenation level-dependent fMRI response. J. Cereb. Blood Flow Metab. 22 (9), 1042–1053.

Corfield, D.R., Fink, G.R., Ramsay, S.C., Murphy, K., Harty, H.R., Watson, J.D.G., Adams, L., Frackowiak, R.S.J., Guz, A., 1995. Evidence for limbic system activation during CO_2-stimulated breathing in man. J. Physiol. 488 (1), 77–84.

Cowie, R.J., Holstege, G., 1992. Dorsal mesencephalic projections to pons, medulla, and spinal cord in the cat: limbic and non-limbic components. J. Comp. Neurol. 319 (4), 536–559.

Craven, J., 2011. Major ascending and descending tracts in the spinal cord. Anaesth. Intensive Care Med. 12 (1), 26–27.

Dampney, R.A.L., Furlong, T.M., Horiuchi, J., Iigaya, K., 2013. Role of the dorsolateral periaqueductal grey in the coordinated regulation of cardiovascular and respiratory function. Auton. Neurosci. 175, 17–25.

Devonshire, I.M., Papadakis, N.G., Port, M., Berwick, J., Kennerley, A.J., Mayhew, J.E.W., Overton, P.G., 2012. Neurovascular coupling is brain region-dependent. Neuroimage 59 (3), 1997–2006.

Duvernoy, H., 1995. The human brainstem and cerebellum. Springer, New York.

Ezra, M., Faull, O.K., Jbabdi, S., Pattinson, K.T.S., 2014. Connectivity based segmentation of the periaqueductal grey matter in humans with diffusion tensor imaging. Proceedings of the 10th Annual Meeting of ISMRM. Milan, Italy (Abstract no. 2581).

Feinberg, D.A., Moeller, S., Smith, S.M., Auerbach, E., Ramanna, S., Glasser, M.F., et al., 2010. Multiplexed echo planar imaging for sub-second whole brain fMRI and fast diffusion imaging. PLoS One 5 (12), e15710.

Glover, G.H., Li, T., Ress, D., 2000. Image-based method for retrospective correction of physiological motion effects in fMRI: RETROICOR. Magn. Reson. Imaging Med. 44, 162–167.

Greve, D.N., Fischl, B., 2009. Accurate and robust brain image alignment using boundary-based registration. Neuroimage 48 (1), 63–72.

Handwerker, D.A., Ollinger, J.M., D'Esposito, M., 2004. Variation of BOLD hemodynamic responses across subjects and brain regions and their effects on statistical analyses. Neuroimage 21 (4), 1639–1651.

Harvey, A.K., Pattinson, K.T.S., Brooks, J.C.W., Mayhew, S.D., Jenkinson, M., Wise, R.G., 2008. Brainstem functional magnetic resonance imaging: disentangling signal from physiological noise. J. Magn. Reson. Imaging 28 (6), 1337–1344.

Hayen, A., Herigstad, M., Pattinson, K.T.S., 2013a. Understanding dyspnea as a complex individual experience. Clin. Psychol. Rev. 24 (5), 557–581.

Hayen, A., Herigstad, M., Kelly, M., Okell, T.W., Murphy, K., Wise, R.G., Pattinson, K.T., 2013b. The effects of altered intrathoracic pressure on resting cerebral blood flow and its response to visual stimulation. Neuroimage 66, 479–488.

Herigstad, M., Hayen, A., Wiech, K., Pattinson, K.T.S., 2011. Dyspnoea and the brain. Respir. Med. 105 (6), 809–817.

Jenkinson, M., Bannister, P., Brady, M., Smith, S., 2002. Improved optimization for the robust and accurate linear registration and motion correction of brain images. Neuroimage 17 (2), 825–841.

Kabat, H., Magoun, H.W., Ranson, S.W., 1935. Electrical stimulation of points in the forebrain and midbrain, the resultant alterations in blood pressure. Arch. Neurol. Psychiatry 34 (5), 931–955.

Keay, K.A., Bandler, R., 2001. Parallel circuits mediating distinct emotional coping reactions to different types of stress. Neurosci. Biobehav. Rev. 25 (669), 10.

Linnman, C., Moulton, E.A., Barmettler, G., Becerra, L., Borsook, D., 2012. Neuroimaging of the periaqueductal gray: state of the field. Neuroimage 60, 505–522.

McKay, L.C., Adams, L., Frackowiak, R.S.J., Corfield, D.R., 2008. A bilateral cortico-bulbar network associated with breath holding in humans, determined by functional magnetic resonance imaging. Neuroimage 40 (4), 1824–1832.

Mobbs, D., Petrovic, P., Marchant, J.L., Hassabis, D., Weiskopf, N., Seymour, B., Dolan, R.J., Frith, C.D., 2007. When fear is near: threat imminence elicits prefrontal-periaqueductal gray shifts in humans. Science 317 (5841), 1079–1083.

Moeller, S., Yacoub, E., Olman, C.A., Auerbach, E., Strupp, J., Harel, N., Ugurbil, K., 2010. Multiband multislice GE-EPI at 7 tesla, with 16-fold acceleration using partial parallel imaging with application to high spatial and temporal whole-brain fMRI. Magn. Reson. Med. 63 (5), 1144–1153.

Morrell, M.J., Finn, L., Kim, H., Peppard, P.E., Safwan Badr, M., Young, T., 2000. Sleep fragmentation, awake blood pressure, and sleep-disordered breathing in a population-based study. Am. J. Respir. Crit. Care Med. 162 (6), 2091–2096.

Pattinson, K.T.S., 2008. Opioids and the control of respiration. Br. J. Anaesth. 100 (6), 747–758.

Pattinson, K.T.S., Governo, R.J., MacIntosh, B.J., Russell, E.C., Corfield, D.R., Tracey, I., Wise, R.G., 2009a. Opioids depress cortical centers responsible for the volitional control of respiration. J. Neurosci. 29 (25), 8177–8186.

Pattinson, K., Mitsis, G.D., Harvey, A.K., Jbabdi, S., 2009b. Determination of the human brainstem respiratory control network and its cortical connections in vivo using functional and structural imaging. Neuroimage 44, 295–305.

Raj, D., Anderson, A.W., Gore, J.C., 2001. Respiratory effects in human functional magnetic resonance imaging due to bulk susceptibility changes. Phys. Med. Biol. 46 (12), 3331.

Satpute, A.B., Wager, T.D., Cohen-Adad, J., Bianciardi, M., Choi, J., Buhle, J.T., Wald, L.L., Feldman Barrett, L., 2013. Identification of discrete functional subregions of the human periaqueductal gray. Proc. Natl. Acad. Sci. 110 (42), 17101–17106.

Smith, S.M., 2002. Fast robust automated brain extraction. Hum. Brain Mapp. 17 (3), 143–155.

Smith, S.M., Nichols, T.E., 2009. Threshold-free cluster enhancement: addressing problems of smoothing, threshold dependence and localisation in cluster inference. Neuroimage 44 (1), 83–98.
Subramanian, H.H., 2012. Descending control of the respiratory neuronal network by the midbrain periaqueductal grey in the rat in vivo. J. Physiol. 591 (1), 109–122.
Subramanian, H.H., Balnave, R.J., Holstege, G., 2008. The midbrain periaqueductal gray control of respiration. J. Neurosci. 28 (47), 12274–12283.
Thomason, M.E., Burrows, B.E., Gabrieli, J.D.E., Glover, G.H., 2005. Breath holding reveals differences in fMRI BOLD signal in children and adults. Neuroimage 25, 824–837.
Topolovec, J.C., Gati, J.S., Menon, R.S., Shoemaker, J.K., Cechetto, D.F., 2004. Human cardiovascular and gustatory brainstem sites observed by functional magnetic resonance imaging. J. Comp. Neurol. 471, 446–461.
Woolrich, M.W., Ripley, B.D., Brady, M., Smith, S.M., 2001. Temporal autocorrelation in univariate linear modeling of fMRI data. Neuroimage 14 (6), 1370–1386.
Woolrich, M.W., Behrens, T.E.J., Smith, S.M., 2004a. Constrained linear basis sets for HRF modelling using Variational Bayes. Neuroimage 21 (4), 1748–1761.
Woolrich, M.W., Behrens, T.E.J., Beckmann, C.F., Jenkinson, M., Smith, S.M., 2004b. Multilevel linear modelling for FMRI group analysis using Bayesian inference. Neuroimage 21 (4), 1732–1747.
Worsley, K.J., 2001. Statistical analysis of activation images. Functional MRI: An Introduction to Methods 14, pp. 251–270.

◆ Human Brain Mapping 00:00–00 (2015) ◆

Connectivity-Based Segmentation of the Periaqueductal Gray Matter in Human With Brainstem Optimized Diffusion MRI

Martyn Ezra,* Olivia Kate Faull, Saad Jbabdi, and Kyle Thomas Shane Pattinson

Nuffield Department of Clinical Neurosciences, Oxford Centre for Functional Magnetic Resonance Imaging of the Brain, University of Oxford, Oxford, Oxfordshire, United Kingdom

Abstract: The periaqueductal gray matter (PAG) is a midbrain structure, involved in key homeostatic neurobiological functions, such as pain modulation and cardiorespiratory control. Animal research has identified four subdivisional columns that differ in both connectivity and function. Until now these findings have not been replicated in humans. This study used high-resolution brainstem optimized diffusion magnetic resonance imaging and probabilistic tractography to segment the human PAG into four subdivisions, based on voxel connectivity profiles. We identified four distinct subdivisions demonstrating high spatial concordance with the columns of the animal model. The resolution of these subdivisions for individual subjects permitted detailed examination of their structural connectivity without the requirement of an a priori starting location. Interestingly patterns of forebrain connectivity appear to be different to those found in nonhuman studies, whereas midbrain and hindbrain connectivity appears to be maintained. Although there are similarities in the columnar structure of the PAG subdivisions between humans and nonhuman animals, there appears to be different patterns of cortical connectivity. This suggests that the functional organization of the PAG may be different between species, and as a consequence, functional studies in nonhumans may not be directly translatable to humans. This highlights the need for focused functional studies in humans. *Hum Brain Mapp 00:000–000, 2015.*

Key words: diffusion; magnetic resonance imaging; periaqueductal gray; pain; cardiovascular; segmentation; brainstem; human; respiratory; fear

INTRODUCTION

The periaqueductal gray matter (PAG) is a poorly differentiated midbrain structure, known to be involved in a number of key homeostatic neurobiological functions, such as pain modulation and cardiorespiratory control [Linnman et al., 2012]. Situated at the confluence of ascending sensory and descending higher center pathways, the PAG plays an essential role in the integrations of these inputs [Benarroch, 2012].

Currently, most of our understanding of its structure and function comes from animal research. Despite its cytoarchitectonic homogeneity, animal models have shown significant heterogeneity with respect to anatomical

This research was supported by an MRC (G0802826) Centenary Award as part of an MRC Clinician Scientist Fellowship awarded to KTSP. KTSP and ME were further supported by the National Institute for Health Research, Oxford Biomedical Research Centre based at Oxford University Hospitals NHS Trust and University of Oxford.
*Correspondence to: Martyn Ezra, Nuffield Department of Clinical Neuroscience, University of Oxford, Oxford, Oxfordshire, OX3 9DU, United Kingdom. E-mail: martyn.ezra@conted.ox.ac.uk
Received for publication 31 October 2014; Revised 12 May 2015; Accepted 15 May 2015.
DOI: 10.1002/hbm.22855
Published online 00 Month 2015 in Wiley Online Library (wileyonlinelibrary.com).

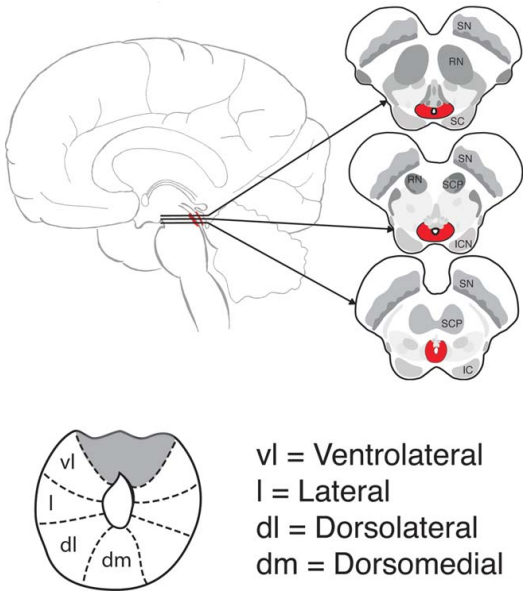

Figure 1.

a. Position of PAG within the midbrain surrounding the cerebral aqueduct. **b**. Divisions of the PAG derived from animal models. [Color figure can be viewed in the online issue, which is available at wileyonlinelibrary.com.]

connections, functional, and chemical properties between subdivisions of the PAG [Dampney et al., 2013]. These subdivisions are proposed as four longitudinal columns parallel to the aqueduct: the dorsomedial (dmPAG), dorsolateral (dlPAG), lateral (lPAG), and ventrolateral (vlPAG) (Fig. 1). The ventromedial aspect is not considered part of the PAG and is comprised of discrete nuclei.

The ability to differentiate these distinct subdivisions in vivo is critical to improving our understanding of the PAG and the efficacy of interventional therapies such as chronic pain modulation using deep brain stimulation (DBS). Thus, far attempts to segment the human PAG have yielded disappointing results in part due to its small size and location within the brainstem surrounding the cerebral aqueduct. Structural magnetic resonance imaging (MRI) studies have failed to differentiate subdivisions even in high-resolution ex vivo studies [Lambert et al., 2013]. Functional imaging techniques [positron emission tomography (PET), functional magnetic resonance imaging (fMRI)] do not yet possess the resolution required [Linnman et al., 2012], althought 7T fMRI is beginning to show promise [Faull et al., 2015].

Tracer studies performed in animals have demonstrated that subdivisions of the PAG have different anatomical connection patterns. This suggests the possibility of segmenting the human PAG based on anatomical connections to other areas of the brain. Diffusion-based tractography is a noninvasive MRI technique able to identify inter-regional white matter connectivity in vivo and has been successfully applied in several studies to segment other subcortical regions such as the thalamus [Johansen-Berg et al., 2005] and substantia nigra [Menke et al., 2010].

There have been a limited number of tractography studies of the human PAG, predominantly examining gross PAG cortical and subcortical connectivity [Linnman et al., 2012]. Only one study [Pereira et al., 2010] has investigated heterogeneity of anatomical connectivity within the PAG. However, this study was limited by only examining the ventral and dorsal aspects of the PAG and in the a priori selection of the seed locations. Interestingly they identified difference in connectivity, which did not completely match the nonhuman tracer studies.

It is the aim of this study to utilize high-resolution, brainstem optimized diffusion MRI to classify PAG voxels according to their connectivity profiles, and thus, segment the PAG into the four distinct connectivity defined regions predicted by the animal model of the PAG. These derived regions will be formed without a priori knowledge of their locations or structure and will enable detailed examination of the connectivity properties of the human PAG. We hypothesized that the connectivity defined regions, would correspond in spatial location to the animal model. However, these regions may demonstrate different connectivity profiles based on human variation observed in previous tractography studies.

MATERIALS AND METHODS

Subjects

Nineteen healthy subjects were included in this study (6 women and 13 men; mean ± SD age, 31.1 ± 5.2 years; range, 23–40 years; all right handed). All volunteers were screened for MR compatibility and scanned with ethical approval and informed consent in accordance with the Oxfordshire Clinical Research Ethics Committee. The research materials supporting this publication can be accessed by contacting martyn.ezra@conted.ox.ac.uk.

Image Acquisition

All images were acquired on a Siemens (Erlangen, Germany) Trio 3T scanner with a 12-channel head coil. Diffusion weighted images were acquired in the axial plane using an echo planar imaging sequence (3 acquisitions of 60 directions with 5 nondiffusion weighted images, *b*-value 1,000 s mm^{-2}, voxel size 1.5 × 1.5 × 1.5 mm, 100 slices). Field of view incorporated the whole brain including brainstem. Cardiac gating was performed to minimize

artifacts from pulsatile flow of the cerebrospinal fluid of which the brainstem is particularly sensitive [Brooks et al., 2013; Harvey et al., 2008]. Brainstem optimization has resulted in a unique high quality dataset that is not available on public databases. Each subject also had a T1 weighted high-resolution ($1 \times 1 \times 1$ mm voxels) structural image acquired to aid registration.

Diffusion MRI Data Preprocessing

Preprocessing was performed using FMRIB's diffusion toolbox (FDT) in the FSL software package (http://www.fmrib.ox.ac.uk/fsl/). This included extraction of non-brain tissue using brain extraction tool (BET) [Smith, 2002] and affine registration to a reference volume to correct for eddy currents and head motion using EDDYCORRECT [Jenkinson and Smith, 2001]. The data from the three acquisitions for each subject were averaged to improve the signal to noise ratio and voxelwise estimates of fiber orientation and uncertainty was carried out using BEDPOSTX [Behrens et al., 2003b, 2007].

Image Registration

After preprocessing, each subject's diffusion weighted scans were registered to the MNI152 1 mm standard space (average T1 brain image constructed from 152 normal subjects at the Montreal Neurological institute, Montreal, QC, Canada). Registration was performed as a three-step procedure via the high-resolution T1-weighted structural image with linear registration using FLIRT and nonlinear registration using FNIRT [Jenkinson and Smith, 2001; Jenkinson et al., 2002].

Definition of Seed and Target Masks

The PAG seed mask was drawn by hand using FSLview in FSL (http://www.fmrib.ox.ac.uk/fsl/). Each subject had a left and right PAG mask drawn in diffusion space using the B0 image as a template; this was made with reference to Duvernoy's atlas of the Human Brainstem and Cerebellum [Duvernoy, 2009]. The mask represents a conservative estimate of the PAG, to reduce contamination of our results by inclusion of adjoining areas.

The cortical and subcortical masks were defined from the Harvard Oxford cortical and subcortical structural atlases (part of FSLview), which are population-based probability atlas in MNI152 standard space. Masks were thresholded to include only voxels estimated at greater than 50% of probability of being in that structure. Masks of the medulla, pons and PAG were drawn in MNI152 standard space using FSLview with reference to Duvernoy's atlas of the Human Brainstem and Cerebellum [Duvernoy, 2009]. The hypothalamus mask was drawn in reference to an MRI atlas of the hypothalamus [Baroncini et al., 2012].

Probabilistic Tractography

Probabilistic tractography was carried out for each subject using previously described methods [Behrens et al., 2003b, 2007] with FDT (http://www.fmrib.ox.ac.uk/fsl/) with 10,000 samples per voxel. Estimates of the connections between each voxel in the PAG seed region and every voxel of the whole brain were then calculated. This generates a connectivity profile for each seed voxel and is derived from the number of samples that arrive at each target voxel. To reduce the false-positive connections, the path distribution estimates were thresholded to a connection probability of $P < 0.0003$. A high sample number and low threshold was chosen to improve identification of small cortical tracts. A cross-correlation matrix between the connectivity profiles of all voxels in the seed mask was then calculated [Johansen-Berg et al., 2004].

Tractography-Based Segmentation

The cross-correlation matrix was fed into a k means clustering algorithm [MacQueen, 1967]. K means treats each observation as having a location in space and uses an iterative algorithm to find partitions in which objects within each cluster are as close to each other, and as far from objects in other clusters as possible. The result is to cluster voxels together that share connectivity profiles.

K means clustering requires the number of clusters to be selected a priori, the animal model of the PAG has four distinct columns exist either side of the aqueduct. The left and right PAG were examined individually, with four clusters for each side being selected. Mapping the individual subject clusters on to a PAG mask drawn in MNI152 standard space and adding them together created group probability maps. This was performed by using linear transformation matrices generated by the registration of the individually drawn PAG masks in diffusion space to the PAG mask drawn in MNI152 standard space using FLIRT. This method was chosen opposed to using the whole brain registrations as it resulted in better spatial alignment of the results. The group probability maps for each cluster were thresholded to include >30% of the population.

Selection and Thresholding of the Clusters

The results of the clustering were examined to determine if it had been successful at an individual subject level. Successful clustering was defined as identification of a distinct cluster that had a spatial representation as predicted by the animal model of the PAG, that is, a cluster that was parallel to the aqueduct in the dorsomedial, dorsolateral, lateral, or ventrolateral aspect of the PAG. Previous tractography segmentation studies [Behrens et al., 2003a] have identified that results were reproducible in approximately 70% of subjects due to the performance of tractography. K means clustering is a hard clustering technique that will identify a predetermined number of

clusters. Therefore, arbitrary segmentation may take place in some subjects where tractography has been unable to identify any differences. To improve assessment of the connectivity profiles of the different columns, selection was performed to remove failed segmentation. This is based on the assumption that the human PAG is in concordance with the animal model. The clusters that were in concordance with the animal model of the PAG were selected for thresholding.

The human PAG is approximately 14 mm long and 4–5 mm wide either side of the aqueduct. Due to the spatial constraints of diffusion MRI (1.5 mm isotropic voxels) there is likely to be significant overlap between PAG columns within individual voxels. It is, therefore, necessary to threshold out the PAG voxels that poorly belong to any cluster. This was achieved by deriving the silhouette value for each voxel; this represents a measure of how similar that voxel is to other voxels in its own cluster, when compared to voxels in other clusters. Values below 0.25 were chosen to signify that the voxels were poorly differentiated [Kaufman and Rousseeuw, 1990]. The thresholded clusters were used for the generation of connectivity profiles and spatial maps.

Connectivity Profiles

To test if the connectivity profiles of the different columns of the human PAG resemble those derived from nonhuman tracer studies, we analyzed the probabilistic connections between each PAG column and predefined target regions (Table 1). The target regions examined have been shown to exhibit PAG connectivity in previous animal and human studies. Total PAG connectivity was first calculated for each subject to each target region, using probabilistic tractography (10,000 samples per voxel). To reduce the false-positive connections, target regions with average connection probability of $P < 0.0003$ were removed from the cluster connectivity profile analysis. Probabilistic tractography was then used to calculate the probability of connection between each column and the target region that survived thresholding for each subject. These results were then used to create anatomical connectivity profiles for each column, using the average relative connectivity between each column within the PAG to the individual target regions. Statistical analysis of connection probabilities was performed using SPSS 21.0 (SPSS). Repeated-measures MANOVA was performed to visualize the anatomical connection probabilities differences across the four columns.

Whole Brain Connectivity

To better assess the spatial patterns of whole brain connectivity to each PAG cluster we back-projected the results of the clustering onto the brain. This method has been described in detail previously [Menke et al., 2010], but in brief it involves identifying which column each voxel in the brain demonstrates the strongest connectivity to (thresholded at $P < 0.0003$). The result is a spatial map of the brain that demonstrates which locations are most likely to connect to each of the divisions of the PAG. Transforming the individual subject spatial maps into MNI152 space and adding them together created group probability maps. The group probability maps for each spatial map were thresholded to include > 30% of the population.

TABLE 1. Cortical and subcortical target regions known to demonstrate PAG connectivity in Humans and/or Animals

Cortical	Subcortical
Frontal Pole	Amygdala
Middle Frontal Gyrus	Hypothalamus
Superior Frontal Gyrus	Thalamus
Anterior Division of the Cingulate Gyrus	Pons
Paracingulate gyrus	Medulla
Precentral Gyrus	
Postcentral Gyrus	
Insular Cortex	
Superior Parietal Lobule	
Occipital Pole	

RESULTS

Clustering

Group probability maps of the clustering results for all subjects reproduced in MNI152 standard space demonstrated four distinct clusters either side of the cerebral aqueduct. These results demonstrate good spatial concordance with the columns derived from animal model of the PAG (Figs. 2 and 3). We suggest that cluster 1 (Red) is the dmPAG, cluster 2 (Blue) the dlPAG, cluster 3 (Green) the lPAG, and cluster 4 (Yellow) the vlPAG.

Performance of the tractography-based *k*-means segmentation at the subject level was assessed by visual inspection of the clusters in the subject's individual diffusion space. Successful clustering was defined as distinct clusters that have a spatial representation predicted by the animal model of the PAG. This was present in 100% of the left/right PAGs examined for cluster 4 (vlPAG). Clusters 1 (dmPAG), 2 (dlPAG), and 3 (lPAG) demonstrated successful clustering in 61%, 55%, and 84%, respectively (Fig. 4). The most common alternative spatial representation was a failure to segment cluster 1 (dmPAG) and cluster 2 (dlPAG) in parallel to the aqueduct but instead into rostral and cephalad clusters (26%).

Connectivity Profiles

The total PAG connectivity to the five subcortical (Fig. 5) and 10 cortical (Fig. 6) target regions demonstrates

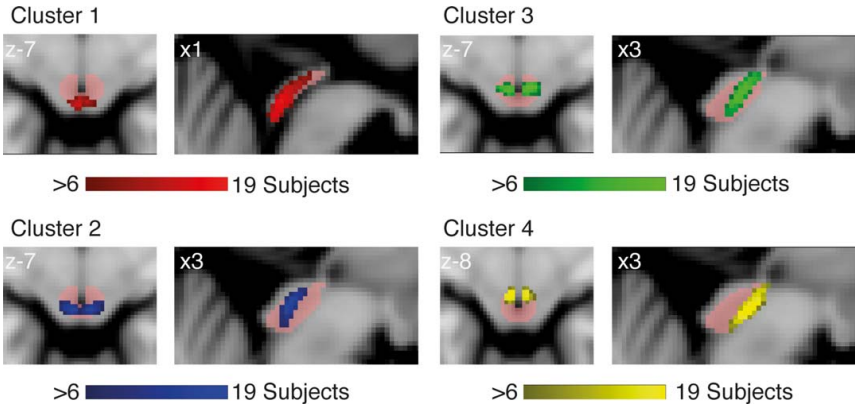

Figure 2.
Group probability maps of clustering results over PAG mask (Pink). Axial and right sided sagittal (left side omitted as equivalent to right) slices taken at the average the center of gravity of the cluster(s). Coordinates given in anatomical space. Results thresholded to include >35% of the population. [Color figure can be viewed in the online issue, which is available at wileyonlinelibrary.com.]

dominant connectivity of the PAG to the hypothalamus superiorly. The anterior division of the cingulate gyrus and paracingulate gyrus failed to reach the threshold of $P \geq 0.0003$ and were removed from subsequent analysis.

The relative connectivity of the columns to the target regions revealed different connectivity profiles for each cluster (Fig. 7). The vlPAG demonstrated dominant connectivity to the prefrontal cortical structures, hypothalamus, amygdala, precentral gyrus, and medulla. The lPAG had dominant postcentral gyrus and pontine connectivity, in addition to similar weaker connectivity to the prefrontal cortical areas, hypothalamus, and precentral gyrus. The dmPAG and dlPAG had similar patterns of cortical connectivity, but the dlPAG demonstrated distinct brainstem connectivity to the pons and medulla. The dlPAG also demonstrated stronger mean occipital pole connectivity; however, this was not statistically significant (Table 2), due to a large variance in occipital pole connectivity. Connectivity to the thalamus, and insular cortex was similar across all columns.

Repeated measures MANOVA tests were performed to assess the differences between the columns with respect to connectivity probability to all the target regions. Univariate tests were also performed to test the difference between columns for each target region (Table 2). The results showed there was no significant difference between the dmPAG and dlPAG ($P = 0.124$) and also the dlPAG and lPAG ($P = 0.08$) when comparing the probability of connection to the predefined target regions. There was a significant difference between the dmPAG and lPAG ($P = 0.031$), dmPAG and vlPAG ($P < 0.001$), dlPAG and vlPAG ($P = 0.01$), and lPAG and vlPAG ($P < 0.001$).

Back-Projections

Whole brain back-projections were used to assess the topographical distribution of the connectivity of each PAG column. Visualization of the cortical spatial maps revealed that the voxels most likely to connect to each PAG column had a similar distribution as identified by their connectivity profiles (Fig. 8).

Back-projections were also used to examine the spatial patterns of connectivity of the different PAG columns within specific subcortical structures, known to have differential patterns of PAG connectivity.

Hypothalamus

Within the hypothalamus vlPAG voxels were most likely to connect to voxels in the ventromedial hypothalamus, whereas lPAG voxels were most likely to connect to the dorsomedial hypothalamus (Fig. 9).

Midbrain

Within the midbrain, dlPAG voxels were most likely to connect to voxels of the nucleus cuneiformis (NCF), where as the vlPAG voxels were most likely to connect to voxels of the ventral tegmental area (VTA) and the dorsal raphe nucleus (DRN) (Fig. 10).

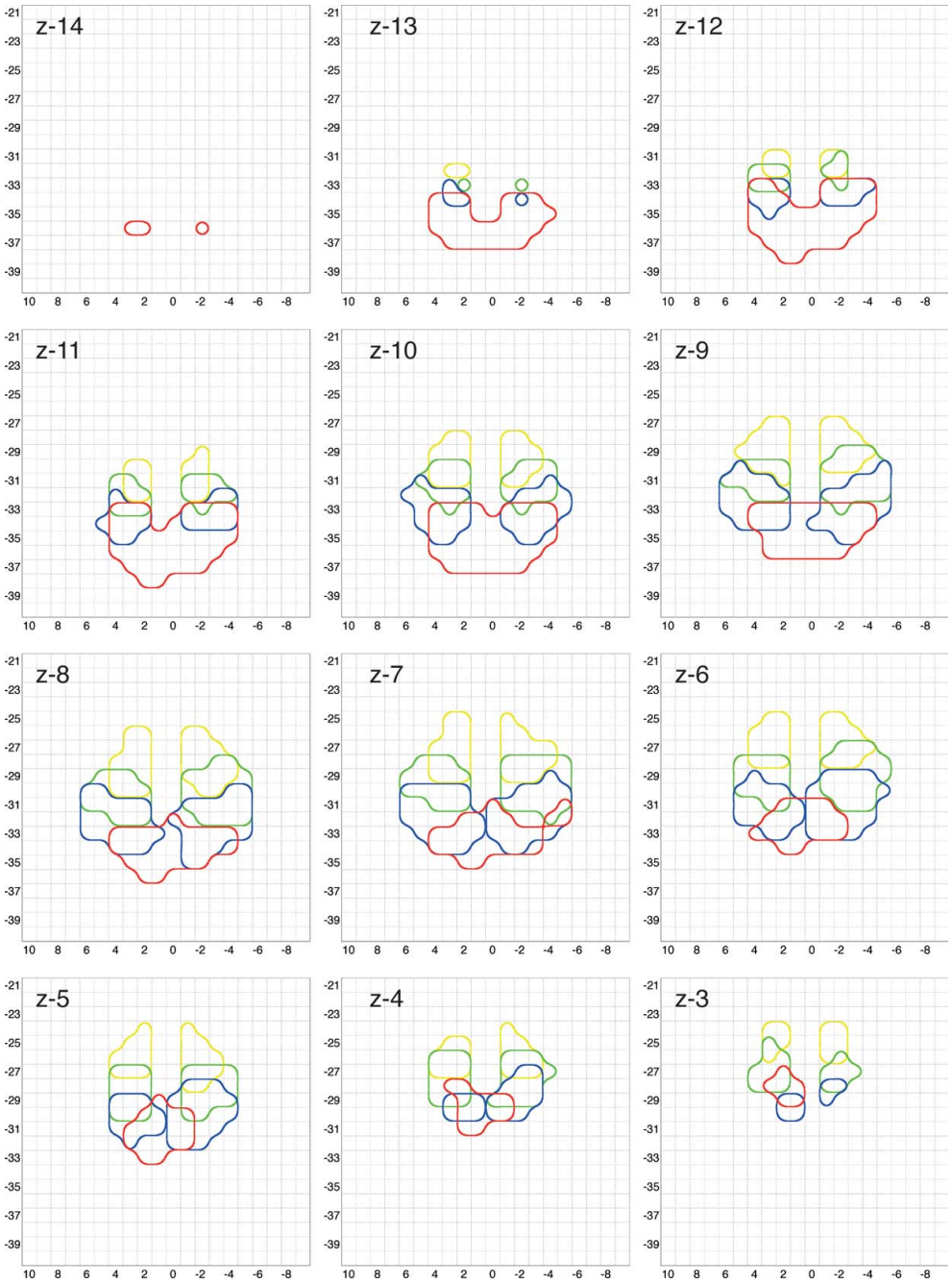

Figure 3.

PAG connectivity atlas. Axial slices through the whole PAG showing edges of thresholded (>35% of the population) group probability maps. *X*- and *Y*-axes give coordinates in anatomical space. *Z*-coordinate of each slice is indicated in the top left corner. [Color figure can be viewed in the online issue, which is available at wileyonlinelibrary.com.]

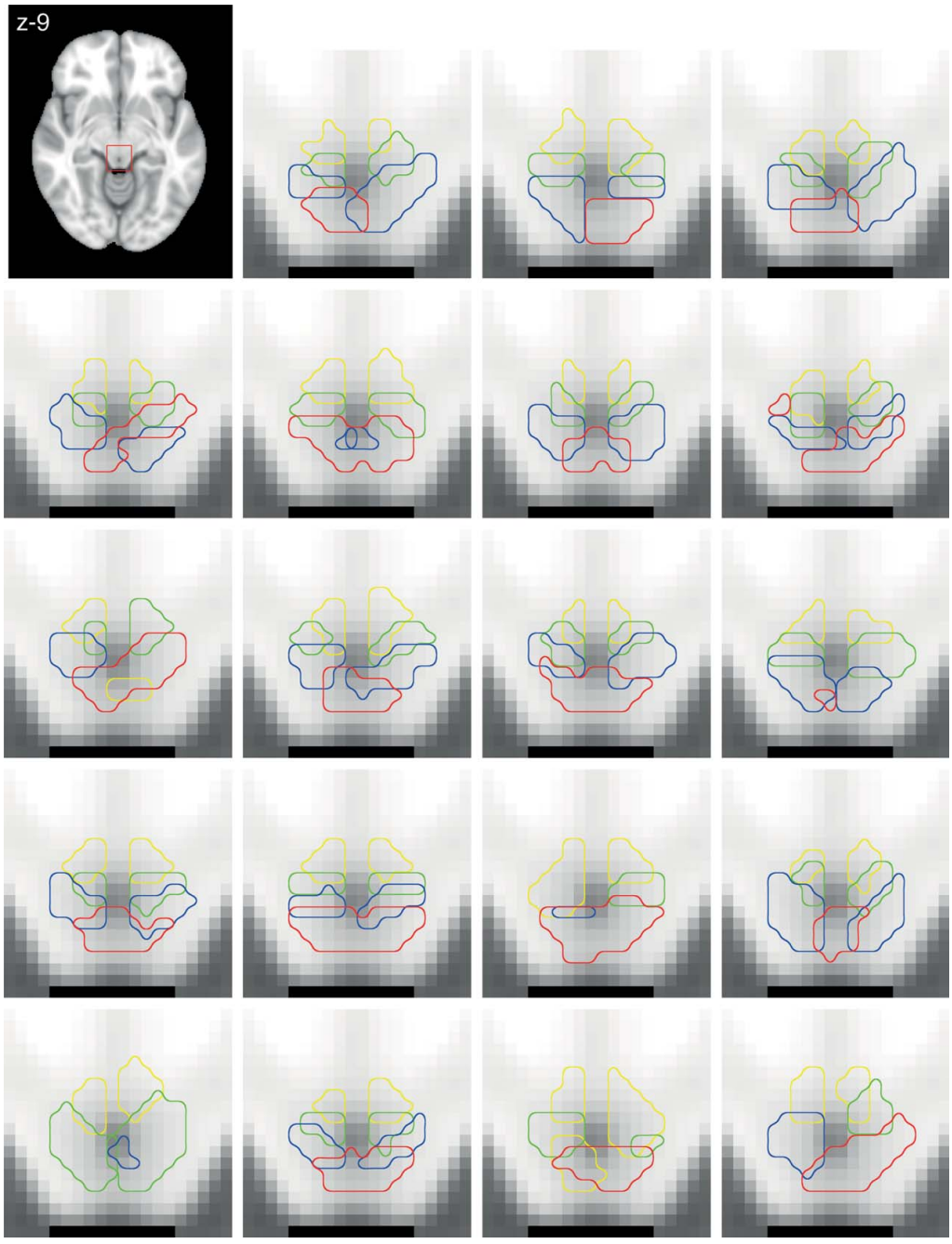

Figure 4.
Connectivity-based segmentation of the PAG in nineteen subjects. Top left panel indicates location of axial PAG slice with anatomical coordinate (taken at the midpoint of the PAG). Each subsequent panel represents data from an individual subject. [Color figure can be viewed in the online issue, which is available at wileyonlinelibrary.com.]

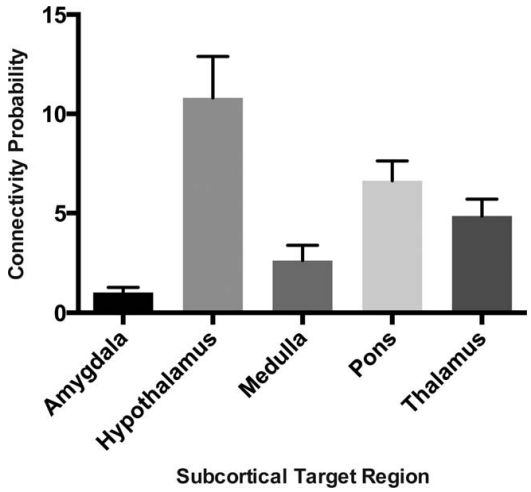

Figure 5.
This graph displays the mean connectivity probability between the whole PAG seed region and the subcortical targets. Error bars demonstrate the standard error of the mean.

Pons

In the dorsolateral pons, voxels were most likely to connect to the dlPAG. This region is consistent with locus ceruleus medially and parabrachial/Kölliker-Fuse complex laterally. In the dorsomedial pons, voxels were most likely to the vlPAG. This region is consistent with the pontine reticular formation (Fig. 10).

Medulla

Within the medulla, the dorsolateral voxels containing the nucleus tractus solitarius, gracile nucleus, and dorsoreticular nucleus were most likely to connect to the vlPAG. The ventrolateral medulla (VLM) voxels were most likely to connect to the dlPAG (Fig. 10).

DISCUSSION

High-resolution brainstem optimized diffusion MRI has enabled the segmentation of the human PAG into four distinct subdivisions parallel to the cerebral aqueduct, similar to that identified in nonhuman studies. This has permitted detailed examination of their structural connectivity without requiring an a priori starting location.

Clustering

At a group level, clustering was able to correctly identify four distinct clusters with a spatial representation predicted by the animal model of the PAG. At an individual subject level, clustering correctly identified these clusters in the majority of subjects. Although the clustering technique is unable to conclude how many columns the human PAG is derived from, while aiming to resolve four clusters, we identified a structure similar to that seen in the animal model.

Clustering was least successful in differentiating the dmPAG and dlPAG. The dmPAG and dlPAG possess similar patterns of cortical connectivity, but clear differences in brainstem connectivity. It is possible that the rostral-cephalic segmentation observed in some subjects may not result from arbitrary incorrect segmentation but from the organization of inputs into the individual PAG columns. Animal studies have identified a rostral-cephalic somatotrophic organization of inputs into the individual segments of the PAG, this may explain the pattern of segmentation observed. [Bandler et al., 2000; Keay and Bandler, 2001, 2002; Parry et al., 2008].

Connectivity Profiles

Total PAG connectivity to the cortical and subcortical target regions was consistent with other diffusion MRI studies [Hadjipavlou et al., 2006; Owen et al., 2007, 2008; Pereira et al., 2010; Sillery et al., 2005]. Connectivity to the anterior division of the cingulate gyrus and paracingulate gyrus failed to reach the threshold, despite strong connectivity being demonstrated in animal tracer studies [An et al., 1998]. This has been previously noted and is thought

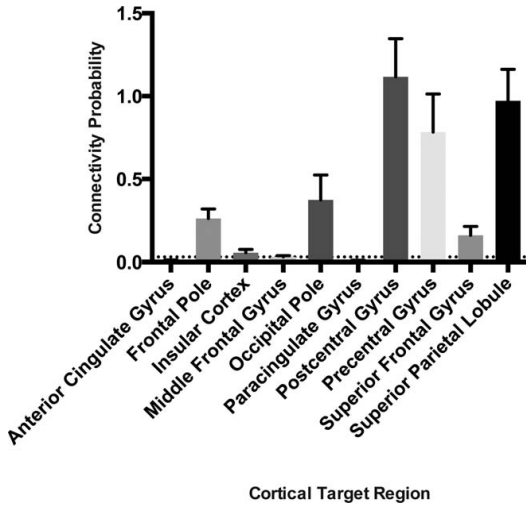

Figure 6.
This graph displays the mean connectivity probability between the whole PAG seed region and the cortical targets and threshold level (dotted line). Error bars demonstrate the standard error of the mean.

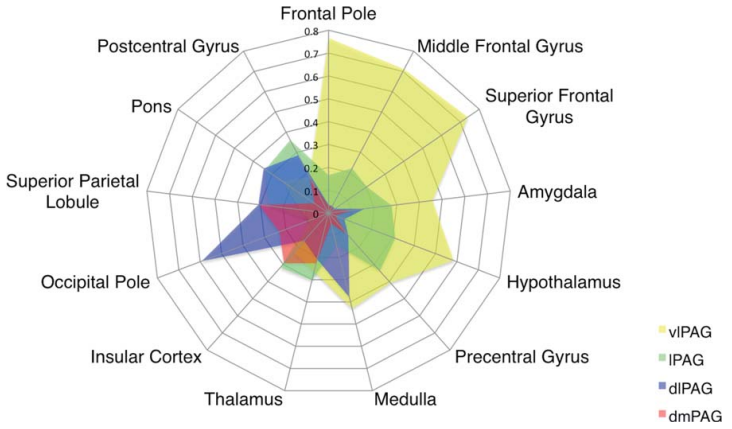

Figure 7.
Radial diagram of relative connectivity of the clusters to predefined targets. [Color figure can be viewed in the online issue, which is available at wileyonlinelibrary.com.]

to be due to the tracts perpendicular to, and passing through the corpus callosum bundle being blocked by large white matter tracts [Hadjipavlou et al., 2006].

Pereira et al. [2010], identified heterogeneity between dorsal and ventral PAG connectivity, which did not entirely correlate with animal studies. There are, however, limitations to their approach. Tractography was performed in healthy individuals, with seed locations derived from the mean electrode position of a different subject cohort receiving DBS. Differentiation of DBS electrode position used predefined anatomical relationships with other structures. This implies uniformity to the structure and position of the PAG, which cannot be assumed to be true. Therefore, the exact position of the seed location for tractography cannot be guaranteed. By segmenting the PAG using connectivity patterns and using these divisions to perform connectivity analysis we have overcome these limitations. We have been able to examine the connectivity of all four columns of the PAG without any prior assumptions of the location of different segments.

Patterns of cortical connectivity were generally consistent with the findings of animal tracer studies, with the exception of the prefrontal cortex (PFC). The precentral gyrus demonstrates dominant connectivity to the lPAG and vlPAG, and the occipital cortex strong connectivity to the dlPAG. This is in agreement with studies in rats; where primary motor areas project exclusively to the lPAG and vlPAG, while the secondary visual cortex preferentially

TABLE 2. Differences in anatomical connectivity probabilities for pairs of PAG columns, shown with *P* values (Bonferroni corrected)

	dmPAG vs. dlPAG	dmPAG vs. lPAG	dmPAG vs. vlPAG	dlPAG vs. lPAG	dlPAG vs. vlPAG	lPAG vs. vlPAG
Amygdala	0.63	0.291	0.001	0.017	<0.001	<0.001
Frontal Pole	0.685	0.002	0.001	0.002	0.001	<0.001
Hypothalamus	0.359	<0.001	<0.001	<0.001	<0.001	<0.001
Insular Cortex	0.247	0.418	0.54	0.45	0.801	0.318
Medulla	0.012	0.003	0.001	0.047	0.072	0.004
Middle Frontal	0.504	0.006	0.002	0.01	0.002	<0.001
Gyrus Occipital Pole	0.386	0.129	0.257	0.305	0.338	0.291
Pons	0.032	0.02	0.013	0.406	0.151	0.181
Postcentral Gyrus	0.139	0.18	0.547	0.974	0.003	<0.001
Precentral Gyrus	0.007	0.006	0.017	0.05	0.207	0.814
Superior Frontal Gyrus	0.426	0.01	0.023	0.009	0.028	0.009
Superior Parietal Lobule	0.783	0.582	0.066	0.069	0.001	0.005
Thalamus	0.589	0.362	0.622	0.079	0.417	0.447
Multivariate	0.124	0.031	<0.001	0.08	0.01	<0.001

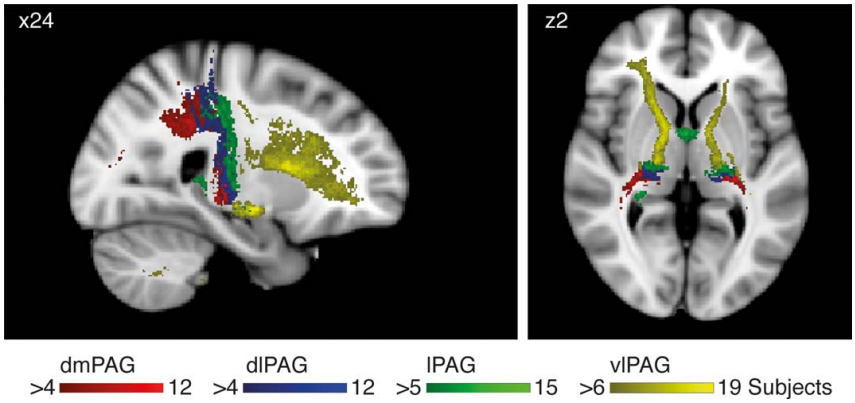

Figure 8.
Axial and sagittal cortical slices in MNI152 standard space of group probability maps of back projections from all four PAG columns. Coordinates given in anatomical space. Results thresholded to include >35% of the population. [Color figure can be viewed in the online issue, which is available at wileyonlinelibrary.com.]

innervate the dlPAG [Newman et al., 1989]. Furthermore, sensory cortex connectivity arose predominantly from the dlPAG and lPAG. This agrees with animal studies where dlPAG and lPAG receive somatotopically organized inputs from superficial nociceptors [Bandler et al., 2000; Keay and Bandler, 2001, 2002; Lumb, 2004; Parry et al., 2008].

Interestingly, we found significant differences in PFC connectivity. Tracer studies in macaques have shown distinct patterns of columnar PAG connectivity with different PFC structures. In animals, the dlPAG receives the dominant PFC input, primarily arising from the medial PFC. In contrast, the vlPAG receives input from orbital and anterior insular areas and the lPAG from the dorsomedial PFC [An et al., 1998]. Our results do not demonstrate the same columnar pattern of PFC connectivity, which arises predominantly from the vlPAG and partially from the lPAG, with minimal connectivity to the dlPAG.

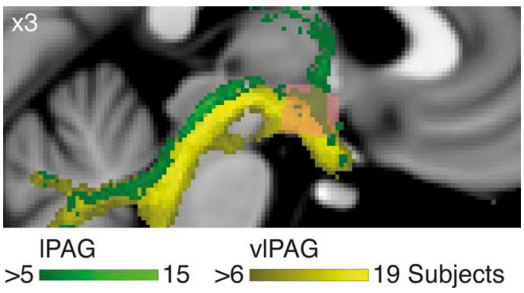

Figure 9.
Sagittal slice of the hypothalamus in MNI152 standard space of group probability maps of back projections. lPAG (Green) passing through the dorsomedial hypothalamus and vlPAG (Yellow) passing through the ventromedial hypothalamus. Hypothalamus mask superimposed (Pink). Coordinates given in anatomical space. Results thresholded to include >35% of the population. [Color figure can be viewed in the online issue, which is available at wileyonlinelibrary.com.]

Patterns dlPAG subcortical connectivity also differed to nonhuman studies. Hypothalamic and amygdala connectivity was modest when compared to the lPAG and vlPAG. This is in contrast to nonhuman studies in which some of the primary connections of the dlPAG arise from ventromedial hypothalamus via the amygdala [Motta et al., 2009]. Moreover, the spatial maps derived from the back-projections, identified dominant vlPAG connectivity to the ventromedial hypothalamus, rather than the dlPAG [An et al., 1998]. Our findings identified dlPAG connectivity to the brainstem, previously not demonstrated in animals. However, this may result from connectivity via the NCF as diffusion MRI cannot determine if a tract is direct or indirect. Connectivity between the NCF and dlPAG, and between the NCF and brainstem has been demonstrated in animals [Bernard et al., 1989; Redgrave et al., 1988, 1990].

Back-Projections

The PAG is proposed to function by orchestrating different coping strategies when exposed to external stressors. Differential PAG column connectivity to nuclei within the brainstem and subcortical structures is thought to play a critical role in orchestrating these differing responses.

Human DBS and animal studies have identified that dlPAG activation triggers active coping strategies,

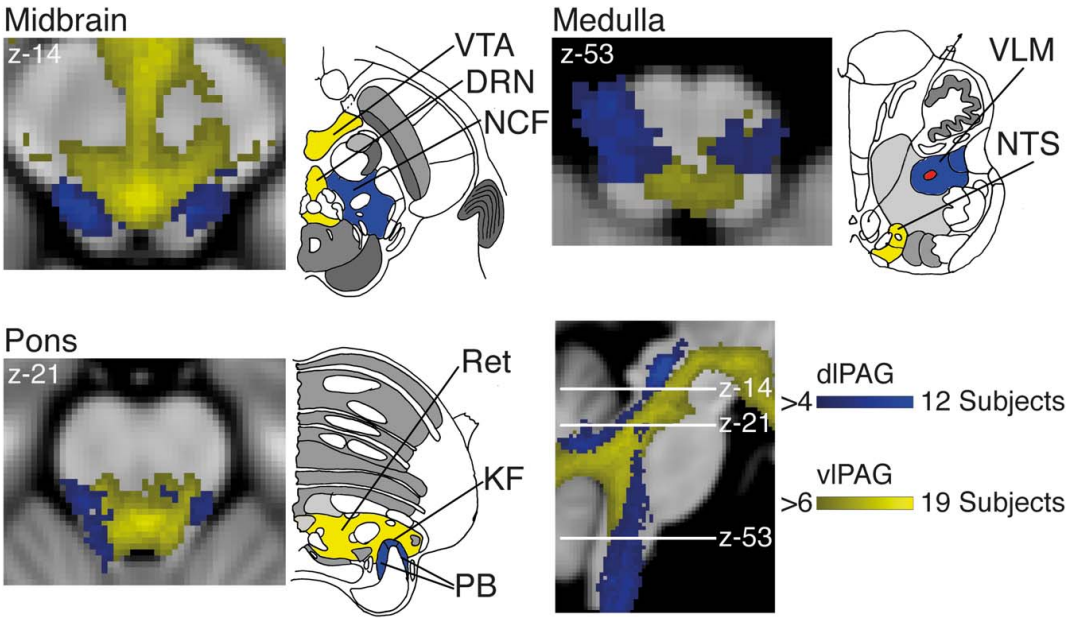

Figure 10.

Axial slices in MNI152 standard space of group probability maps of back projections from dlPAG (Blue) and vlPAG (Yellow) columns. Results thresholded to include >35% of the population. Coordinates given in anatomical space. VTA, ventral tegmental area; DRN, dorsal nucleus raphe; NCF, nucleus cuneformis; Ret pontine reticular formation; KF, Kölliker-Fuse; PB, parabrachial; VLM, ventrolateral medulla; NTS, nucleus tractus solitarius. Line drawing adapted from Duvernoy [Duvernoy, 2009]. [Color figure can be viewed in the online issue, which is available at wileyonlinelibrary.com.]

involving sympathoexcitation, hyperventilation and short-duration, non-opioid-mediated analgesia [Bandler et al., 2000; Green et al., 2005; Keay and Bandler, 2001; Pereira et al., 2010]. Our results are consistent with these observations. Within the midbrain dlPAG demonstrates connectivity with the NCF. This structure has nocifensive functions [Haws et al., 1989] and as previously discussed connectivity to the dlPAG. Furthermore, the dlPAG demonstrates connectivity to brainstem regions integral to cardiorespiratory control (either directly or indirectly). The dorsolateral pontine connectivity is likely to represent the locus ceruleus and parabrachial/Kölliker-Fuse complex, nuclei responsible for sensory processing of respiratory signals [Smith et al., 2009]. Connectivity in the VLM is like represent the ventral respiratory group, which includes the rhythm generating structures nucleus ambiguus, pre-Bötzinger complex, and retrotrapezoid nucleus [Smith et al., 2009]. In addition the rostral VLM also contains the C1 group of adrenaline-synthesizing neurons, which acts as a key blood pressure regulatory center [Guyenet, 2006].

In contrast, vlPAG activation elicits passive strategies, involving long duration, opioid-dependent analgesia associated with cardiovascular and respiratory depression [Bandler et al., 2000; Keay and Bandler, 2001; Lumb, 2004]. Again our findings support these functional observations. Within the midbrain the vlPAG demonstrates connectivity to the VTA and DRN. The VTA represents part of the mesolimbic reward circuitry [Oades and Halliday, 1987] and has a role in pain and aversive processing in humans [Dunckley et al., 2005]. Moreover, the serotonergic systems within the DRN are involved in the modulation of ongoing anxiety-related behavior and in behavioral sensitization [Abrams et al., 2004]. Connectivity in the dorsomedial medulla is likely to represent the nucleus tractus solitarius, a major relay of homeostatic information from the respiratory, cardiovascular and gastrointestinal systems [Bailey et al., 2007]. These structures have also been shown in non-humans tracer studies to possess connections to the vlPAG [Herbert and Saper, 1992; Kirouac et al., 2004].

Interpretation of Connectivity Patterns

Although our results demonstrate consistency in the organization of hindbrain and midbrain connections with nonhuman tracer studies, there are significant differences

in the connectivity patterns to the forebrain. Connectivity between the PAG and the hypothalamus, amygdala, and PFC are derived predominantly from the vlPAG rather than the dlPAG. These structures are key to processing fear, stress and anxiety [Shin and Liberzon, 2010], which influence the homeostatic neurobiological roles of the PAG. This suggests that the vlPAG maybe involved in these processes and would certainly tie in with the hindbrain connectivity seen, relating to anxiety and aversion processing. Interestingly, these findings correlate with human fMRI studies of visceral and somatic pain processing [Dunckley et al., 2005], where correlation between PAG activation and anxiety was observed during visceral pain (vlPAG processed) but not during somatic pain (dlPAG processes).

While significant correlation between humans and nonhuman primates' white matter anatomy has been observed using diffusion MRI [Jbabdi et al., 2013], there are some major differences, particularly within the PFC [Thiebaut de Schotten et al., 2012]. This is perhaps unsurprising given the degree of evolutionary expansion in this region [Semendeferi et al., 2001] and supports our findings of interspecies differences. It is important to remember that tractography does not inform us about precise nature of the synaptic connections made between two areas or their functional significance. These findings are important as a complement to the interpretation of functional imaging studies, particularly as high field strength fMRI becomes able to resolve activation within individual columns [Faull et al., 2015].

Limitations

As we have alluded to in the discussion, our study does not aim to identify the number of columns in the human PAG. We have sought to identify the structure and connectivity patterns of the PAG with the prior assumption that there are four columns either side of the cerebral aqueduct [Dampney et al., 2013]. We have chosen this approach for a number of reasons. First, there is convincing evidence from cross species nonhuman experiments that the PAG is comprised of four columns and importantly these divisions are not solely based on connectivity patterns but also functional and biochemical differences [Dampney et al., 2013]. Second, we believe that inferential statistics performed to identify the optimum number of clusters, would be of limited use. This would reflect only the mathematical distinctions within the connectivity data and would not take into account the unmeasured functional and biochemical difference. Division based on identifying the most distinct clusters would likely produce two clusters of the ventral and dorsal aspects of the PAG, where connectivity differences are greatest. We believe that the resolution of a structure similar to that of the animal model of PAG when aiming to resolve four columns, demonstrates that our data fits this model of the PAG. We accept the limitations of this design but feel that the assumptions we have made are not without strong scientific merit.

Conclusion

We have demonstrated, for the first time, subdivisions of the human PAG, as predicted by animal models. This has enabled resolution of individual column connectivity and the comparisons with animal tracer studies. Patterns of forebrain connectivity appear to be different to those found in nonhuman studies, whereas midbrain and hindbrain connectivity appears to be maintained. This suggests altered fear and anxiety processing in humans compared to animals. This study will aid the interpretation of future research into the PAG as well as translating clinically into improved planning of stereotactic interventions such as DBS.

ACKNOWLEDGMENTS

We thank David Paterson for his helpful comments on the paper and Dr Johannes Klein for his help with the diffusion imaging protocol. The authors declare no competing financial interests.

REFERENCES

Abrams JK, Johnson PL, Hollis JH, Lowry CA (2004): Anatomic and functional topography of the dorsal raphe nucleus. Ann N Y Acad Sci 1018:46–57.

An X, Bandler R, Ongur D, Price JL (1998): Prefrontal cortical projections to longitudinal columns in the midbrain periaqueductal gray in macaque monkeys. J Comp Neurol 401:455–479.

Bailey TW, Hermes SM, Whittier KL, Aicher SA, Andresen MC (2007): A-type potassium channels differentially tune afferent pathways from rat solitary tract nucleus to caudal ventrolateral medulla or paraventricular hypothalamus. J Physiol 582(Pt 2):613–628.

Bandler R, Keay KA, Floyd N, Price J (2000): Central circuits mediating patterned autonomic activity during active vs. Passive emotional coping. Brain Res Bull 53:95–104.

Baroncini M, Jissendi P, Balland E, Besson P, Pruvo JP, Francke JP, Dewailly D, Blond S, Prevot V (2012): MRI atlas of the human hypothalamus. Neuroimage 59:168–180.

Behrens TE, Johansen-Berg H, Woolrich MW, Smith SM, Wheeler-Kingshott CA, Boulby PA, Barker GJ, Sillery EL, Sheehan K Ciccarelli O, Thompson AJ, Brady JM, Matthews PM. (2003a): Non-invasive mapping of connections between human thalamus and cortex using diffusion imaging. Nat Neurosci 6:750–757.

Behrens TE, Woolrich MW, Jenkinson M, Johansen-Berg H, Nunes RG, Clare S, Matthews PM, Brady JM, Smith SM (2003b): Characterization and propagation of uncertainty in diffusion-weighted MR imaging. Magn Reson Med 50:1077–1088.

Behrens TE, Berg HJ, Jbabdi S, Rushworth MF, Woolrich MW (2007): Probabilistic diffusion tractography with multiple fibre orientations: What can we gain? Neuroimage 34:144–155.

Benarroch EE (2012): Periaqueductal gray: An interface for behavioral control. Neurology 78:210–217.

Bernard JF, Peschanski M, Besson JM (1989): Afferents and efferents of the rat cuneiformis nucleus: An anatomical study with reference to pain transmission. Brain Res 490:181–185.

Brooks JC, Faull OK, Pattinson KT, Jenkinson M (2013): Physiological noise in brainstem FMRI. Front Hum Neurosci 7:623

Dampney RA, Furlong TM, Horiuchi J, Iigaya K (2013): Role of dorsolateral periaqueductal grey in the coordinated regulation

of cardiovascular and respiratory function. Auton Neurosci 175:17–25.
Dunckley P, Wise RG, Fairhurst M, Hobden P, Aziz Q, Chang L, Tracey I (2005): A comparison of visceral and somatic pain processing in the human brainstem using functional magnetic resonance imaging. J Neurosci 25:7333–7341.
Duvernoy H. 2009. Internal Architecture of the Brain Stem with Key Axial Section. Duvernoy's Atlas of the Human Brain Stem and Cerebellum. Springer Vienna. pp. 53–93.
Faull OK, Jenkinson M, Clare S, Pattinson KT. (2015): Functional subdivision of the human periaqueductal grey in respiratory control using 7 tesla fMRI. NeuroImage 113:356–364.
Green AL, Wang S, Owen SL, Xie K, Liu X, Paterson DJ, Stein JF, Bain PG, Aziz TZ (2005): Deep brain stimulation can regulate arterial blood pressure in awake humans. Neuroreport 16:1741–1745.
Guyenet PG (2006): The sympathetic control of blood pressure. Nat Rev Neurosci 7:335–346.
Hadjipavlou G, Dunckley P, Behrens TE, Tracey I (2006): Determining anatomical connectivities between cortical and brainstem pain processing regions in humans: A diffusion tensor imaging study in healthy controls. Pain 123:169–178.
Harvey AK, Pattinson KT, Brooks JC, Mayhew SD, Jenkinson M, Wise RG (2008): Brainstem functional magnetic resonance imaging: Disentangling signal from physiological noise. J Magn Reson Imaging 28:1337–1344.
Haws CM, Williamson AM, Fields HL (1989): Putative nociceptive modulatory neurons in the dorsolateral pontomesencephalic reticular formation. Brain Res 483:272–282.
Herbert H, Saper CB (1992): Organization of medullary adrenergic and noradrenergic projections to the periaqueductal gray matter in the rat. J Comp Neurol 315:34–52.
Jbabdi S, Lehman JF, Haber SN, Behrens TE (2013): Human and monkey ventral prefrontal fibers use the same organizational principles to reach their targets: Tracing versus tractography. J Neurosci 33:3190–3201.
Jenkinson M, Smith S (2001): A global optimisation method for robust affine registration of brain images. Med Image Anal 5: 143–156.
Jenkinson M, Bannister P, Brady M, Smith S (2002): Improved optimization for the robust and accurate linear registration and motion correction of brain images. Neuroimage 17:825–841.
Johansen-Berg H, Behrens TE, Robson MD, Drobnjak I, Rushworth MF, Brady JM, Smith SM, Higham DJ, Matthews PM (2004): Changes in connectivity profiles define functionally distinct regions in human medial frontal cortex. Proc Natl Acad Sci USA 101:13335–13340.
Johansen-Berg H, Behrens TE, Sillery E, Ciccarelli O, Thompson AJ, Smith SM, Matthews PM (2005): Functional-anatomical validation and individual variation of diffusion tractography-based segmentation of the human thalamus. Cereb Cortex 15:31–39.
Kaufman L, Rousseeuw PJ (1990): Introduction, in Finding Groups in Data: An Introduction to Cluster Analysis. Hoboken, NJ: John Wiley & Sons, Inc.
Keay KA, Bandler R (2001): Parallel circuits mediating distinct emotional coping reactions to different types of stress. Neurosci Biobehav Rev 25:669–678.
Keay KA, Bandler R (2002): Distinct central representations of inescapable and escapable pain: Observations and speculation. Exp Physiol 87:275–279.
Kirouac GJ, Li S, Mabrouk G (2004): GABAergic projection from the ventral tegmental area and substantia nigra to the periaqueductal gray region and the dorsal raphe nucleus. J Comp Neurol 469:170–184.
Lambert C, Lutti A, Helms G, Frackowiak R, Ashburner J (2013): Multiparametric brainstem segmentation using a modified multivariate mixture of gaussians. Neuroimage Clin 2:684–694.
Linnman C, Moulton EA, Barmettler G, Becerra L, Borsook D (2012): Neuroimaging of the periaqueductal gray: State of the field. Neuroimage 60:505–522.
Lumb BM (2004): Hypothalamic and midbrain circuitry that distinguishes between escapable and inescapable pain. News Physiol Sci 19:22–26.
MacQueen J (1967): Some methods for classification and analysis of multivariate observations. Proceedings of the Fifth Berkeley Symposium on Mathematical Statistics and Probability, Volume 1: Statistics, 281–297, University of California Press, Berkeley, Calif.
Menke RA, Jbabdi S, Miller KL, Matthews PM, Zarei M (2010): Connectivity-based segmentation of the substantia nigra in human and its implications in parkinson's disease. Neuroimage 52:1175–1180.
Motta SC, Goto M, Gouveia FV, Baldo MV, Canteras NS, Swanson LW (2009): Dissecting the brain's fear system reveals the hypothalamus is critical for responding in subordinate conspecific intruders. Proc Natl Acad Sci USA 106:4870–4875.
Newman DB, Hilleary SK, Ginsberg CY (1989): Nuclear terminations of corticoreticular fiber systems in rats. Brain Behav Evol 34:223–264.
Oades RD, Halliday GM (1987): Ventral tegmental (a10) system: Neurobiology. 1. Anatomy and connectivity. Brain Res 434:117–165.
Owen SL, Heath J, Kringelbach ML, Stein JF, Aziz TZ (2007): Preoperative DTI and probabilistic tractography in an amputee with deep brain stimulation for lower limb stump pain. Br J Neurosurg 21:485–490.
Owen SL, Heath J, Kringelbach M, Green AL, Pereira EA, Jenkinson N, Jegan T, Stein JF, Aziz TZ (2008): Pre-operative DTI and probabilisitic tractography in four patients with deep brain stimulation for chronic pain. J Clin Neurosci 15:801–805.
Parry DM, Macmillan FM, Koutsikou S, McMullan S, Lumb BM (2008): Separation of a-versus C-nociceptive inputs into spinal-brainstem circuits. Neuroscience 152:1076–1085.
Pereira EA, Lu G, Wang S, Schweder PM, Hyam JA, Stein JF, Paterson DJ, Aziz TZ, Green AL (2010): Ventral periaqueductal grey stimulation alters heart rate variability in humans with chronic pain. Exp Neurol 223:574–581.
Redgrave P, Dean P, Mitchell IJ, Odekunle A, Clark A (1988): The projection from superior colliculus to cuneiform area in the rat. I. Anatomical studies. Exp Brain Res 72:611–625.
Redgrave P, Dean P, Westby GW (1990): Organization of the crossed tecto-reticulo-spinal projection in rat–I. Anatomical evidence for separate output channels to the periabducens area and caudal medulla. Neuroscience 37:571–584.
Semendeferi K, Armstrong E, Schleicher A, Zilles K, Van Hoesen GW (2001): Prefrontal cortex in humans and apes: A comparative study of area 10. Am J Phys Anthropol 114:224–241.
Shin LM, Liberzon I (2010): The neurocircuitry of fear, stress, and anxiety disorders. Neuropsychopharmacology 35:169–191.
Sillery E, Bittar RG, Robson MD, Behrens TE, Stein J, Aziz TZ, Johansen-Berg H (2005): Connectivity of the human periventricular-periaqueductal gray region. J Neurosurg 103:1030–1034.
Smith JC, Abdala AP, Rybak IA, Paton JF (2009): Structural and functional architecture of respiratory networks in the mammalian brainstem. Philos Trans R Soc Lond B Biol Sci 364:2577–2587.
Smith SM (2002): Fast robust automated brain extraction. Hum Brain Mapp 17:143–155.
Thiebaut de Schotten M, Dell'Acqua F, Valabregue R, Catani M (2012): Monkey to human comparative anatomy of the frontal lobe association tracts. Cortex 48:82–96.

Appendix B

Chapter 2 additional material

B.1 Peak voxel locations

Table B.1: Locations of signal maxima in response to the group mean breath hold regressor. Values derived from cluster-based analysis. The most significant maximum is listed for each anatomical location. Co-ordinates are in mm in standard space of MNI (1 mm^3): x, distance right (+) or left (-) of the mid saggital line; y, distance anterior (+) or posterior (-) from a vertical plane through the anterior commissure; z, distance above (+) or below (-) the intercommisurial plane.

	Left				Right			
	x	y	z	Z score	x	y	z	Z score
Activations								
Motor cortex	-59	4	20	4.64	51	9	22	5.34
Motor cortex	-43	-15	43	4.28	44	-13	40	4.2
Putamen	-20	-2	5	4.79	29	-14	2	4.83
Anterior Insula	-40	5	1	3.27	40	6	2	4.57
Cingulate cortex	-1	14	30	3	3	13	29	3.38
Paracingulate cortex	-4	8	48	3.03	7	8	45	5.02
Supramarginal gyrus	-59	-24	26	3.54	63	-22	26	4.89
Sensory cortex	-42	-17	43	4.55	43	-11	36	4.27
Supplementary MC	-5	6	54	3.82	3	7	64	4.3
Caudate nucleus	-17	-16	20	3.92	15	-9	20	3.77
Thalamus					11	-16	4	3.82
Thalamus					9	-14	11	4.11
Subthalamic nucleus					8	-11	-7	3.45
Red nucleus					6	-19	-4	3.26
Deactivations								
Middle Insula	-39	-6	13	3.97	39	-3	5	3.9
Hippocampus	-32	-20	-15	3.7	30	-13	-15	4.14
Parahippocampal gyrus	-26	-35	-15	3.43	27	-32	-16	3.87
Amygdala	22	-7	-11	4.25	-26	-6	-20	3.72
Pons	-5	-26	-27	3.8				
Pons	-4	-37	-36	3.35				
Cerebellum					2	-51	-46	4.31

Appendix C

Chapter 3 additional material

C.1 Peak voxel locations

Table C.1: Co-ordinates of local maxima of significant increases (activations) and decreases (deactivations) in the group BOLD response to inspiratory loading. Values derived from cluster-based analysis. The most significant maximum is listed for each anatomical location. Co-ordinates are in mm in standard space of MNI (1 mm^3): x, distance right (+) or left (-) of the mid saggital line; y, distance anterior (+) or posterior (-) from a vertical plane through the anterior commissure; z, distance above (+) or below (-) the intercommisurial plane. Abbreviations: VPL, ventroposterolateral nucleus of the thalamus.

	Left				Right			
	x	y	z	Z score	x	y	z	Z score
Activations								
Motor cortex	-58	4	70	6.73	59	2	40	6.55
Supplementary motor cortex	-3	-1	60	6.73	1	-4	70	4.82
Putamen	-25	-10	3	6.44	27	-2	-2	4.09
Sensory cortex	-59	-17	34	5.88	62	-13	28	5.41
Cingulate cortex	-6	13	35	3.59	9	13	37	4.32
Paracingulate cortex	-7	7	44	3.33	3	18	49	5.46
Operculum	-49	0	3	5.06	59	-1	10	4.79
Medulla	-2	-47	-64	3.5	7	-45	-64	3.58
Middle insula	-37	2	5	5.21	39	2	6	4.96
Caudate nucleus	-13	-3	22	3.69	15	0	18	4.00
VPL (thalamus)	-12	-24	2	4.64	14	-20	-4	4.43
Subthalamic nucleus	-2	-20	-3	5.11	13	-19	-4	3.55
Deactivations								
Hippocampus	-28	-14	-16	4.56	21	-20	-15	4.32
Amygdala	-21	-6	-12	5.21	20	-2	-19	4.17
Cerebellum	-7	-48	-48	3.76	8	-49	-45	3.77

Table C.2: Co-ordinates of local maxima of significant increases (activations) and decreases (deactivations) in the group BOLD response during certain anticipation of inspiratory loading (> baseline). Values derived from cluster-based analysis. The most significant maximum is listed for each anatomical location. Co-ordinates are in mm in standard space of MNI (1 mm^3): x, distance right (+) or left (-) of the mid saggital line; y, distance anterior (+) or posterior (-) from a vertical plane through the anterior commissure; z, distance above (+) or below(-) the intercommisurial plane.

	Left				Right			
	x	y	z	Z score	x	y	z	Z score
Activations								
Motor cortex	-48	-6	47	3.42	49	2	50	4.43
Supplementary motor cortex	-1	-1	72	4.98	6	6	66	3.97
Sensory cortex	-58	-18	34	3.44	3	-19	27	4.43
Cingulate cortex	-1	-23	30	3.95	3	-19	27	4.43
Paracingulate cortex	-1	14	43	4.6	1	14	42	3.93
Operculum	-45	4	0	2.94	49	2	4	4.6
Medulla					5	-40	-60	3.25
Middle insula	-38	2	1	3.51	42	5	3	3.81
Deactivations								
Hippocampus	-34	-23	-16	4.07	26	-11	-16	3.93
Amygdala	-19	-6	-13	4.24	16	-2	-1	4.07
Posterior insula	-36	-16	18	2.98	36	-18	19	3.3
Cerebellum					7	-52	-51	3.64

Table C.3: Co-ordinates of local maxima of significant increases (activations) and decreases (deactivations) in the group BOLD response during uncertain anticipation of inspiratory loading (> baseline). Values derived from cluster-based analysis. The most significant maximum is listed for each anatomical location. Co-ordinates are in mm in standard space of MNI (1 mm^3). x, distance right (+) or left (-) of the mid saggital line; y, distance anterior (+) or posterior (-) from a vertical plane through the anterior commissure; z, distance above (+) or below(-) the intercommisurial plane.

	Left				Right			
	x	y	z	Z score	x	y	z	Z score
Activations								
Motor cortex	-47	-6	47	3.91	55	9	41	3.62
Supplementary motor cortex	-1	-2	71	4.53	6	0	71	4.23
Sensory cortex	-55	-18	27	3.64	50	-15	25	3.93
Anterior cingulate cortex	-7	15	39	3.73	9	15	40	4.01
Posterior cingulate cortex	-1	-21	32	3.61	4	-19	27	3.81
Operculum	-43	-4	13	3.28	46	4	3	3.39
Middle insula	-39	3	3	3.53	42	5	2	3.52
Deactivations								
Hippocampus	-33	-23	-12	3.36	22	-15	-14	3.31
Amygdala	-20	-7	-12	3.63	21	-12	-12	2.9
Posterior insula	-35	-22	20	3.44	37	-18	18	3.36
Cerebellum					5	-56	-46	3.77

Table C.4: Co-ordinates of local maxima of significant increases (activations) and decreases (deactivations) in the group BOLD response to a finger opposition task. Values derived from cluster-based analysis. The most significant maximum is listed for each anatomical location. Co-ordinates are in mm in standard space of MNI (1 mm^3): x, distance right (+) or left (-) of the mid saggital line; y, distance anterior (+) or posterior (-) from a vertical plane through the anterior commissure; z, distance above (+) or below (-) the intercommisurial plane. Abbreviations: VPL, ventroposterolateral nucleus of the thalamus.

	Left				Right			
	x	y	z	Z score	x	y	z	Z score
Activations								
Motor cortex	-44	-16	52	6.07	52	-3	47	3.6
Supplementary motor cortex	-1	-5	57	5.21	5	0	58	4.72
Putamen	-31	-10	-1	6.63	24	7	2	4.83
Sensory cortex	-57	-23	23	4.11	58	-17	25	3.46
Cingulate cortex	-5	11	35	4.29	5	-7	37	3.88
Paracingulate cortex	-4	12	42	4.86	12	8	41	3.96
Operculum	-43	0	11	6.89	49	1	7	6.21
Medulla	-1	-47	-61	3.3	5	-49	-60	4.6
Caudate nucleus	-10	0	16	3.52	10	4	12	3.4
VPL (thalamus)	-15	-24	5	6.54	12	-18	12	4
Deactivations								
Hippocampus					27	-20	-13	3.66
Motor cortex	-45	-11	37	4.48	58	-4	35	4.04
Posterior insula					36	-5	15	4.34

C.2 Respiratory activity in the medulla

Mean BOLD activity was observed in the medulla, consistent with the location of respiratory nuclei during both inspiratory resistance and certain anticipation of resistance. This is displayed in Figure C.1.

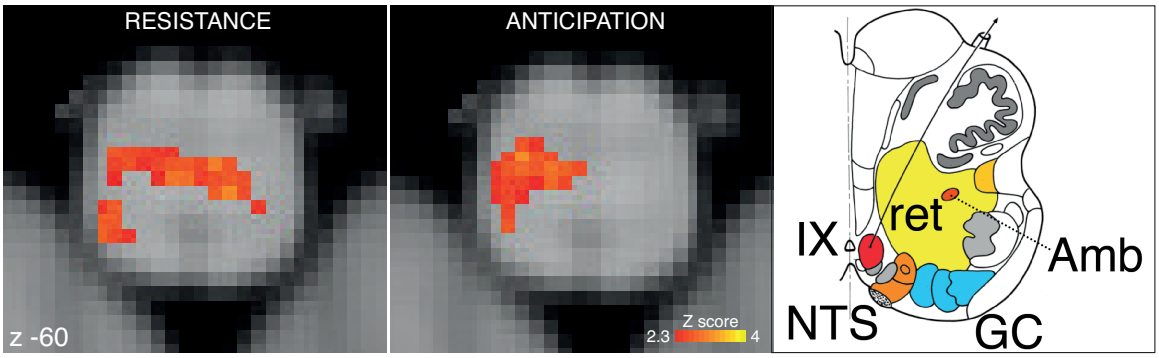

Figure C.1: Demonstration of the BOLD activity in the medulla during certain anticipation of resistance and throughout inspiratory resistance. The images consist of a colour-rendered statistical map superimposed on a standard (MNI 1mm^3) brain. Significant regions are displayed with a threshold $Z > 2.3$, with a cluster probability threshold of $p < 0.05$ (corrected for multiple comparisons). Abbreviations: ret, nuclei reticularis; Amb, nucleus ambiguous; IX, glossopharyngeal nucleus; NTS, nucleus tractus solitaries; GC, gracile (medial). Original line drawings adapted from (Duvernoy, 1995).

C.3 End-tidal pressure of carbon dioxide

The group BOLD activity relating to the $P_{ET}CO_2$ trace in Chapter 3 is displayed in Figure C.2 below. BOLD activity is localised to the grey matter in the cortex and brainstem, including the PAG.

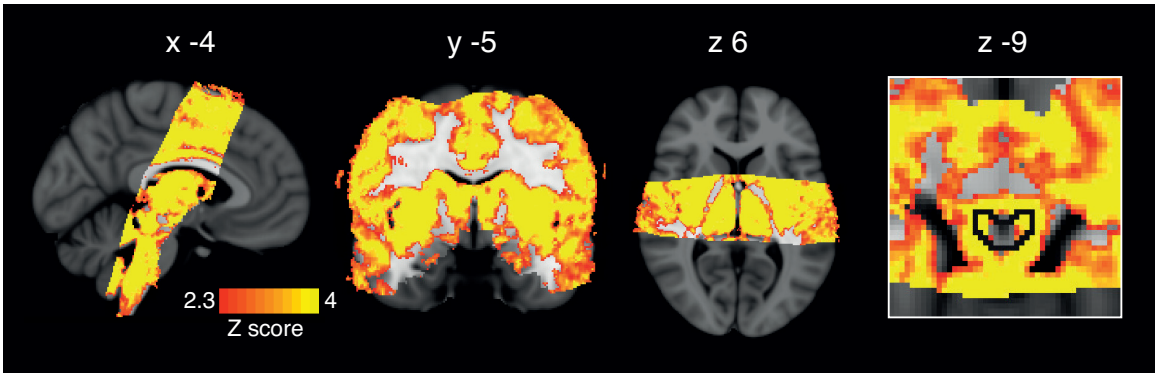

Figure C.2: Global BOLD signal change correlating with changes in end tidal carbon dioxide ($P_{ET}CO_2$). The red lines indicate the edges of the the brain, derived from the MNI ($1mm^3$) standard brain. Image on the right is a zoom to show signal changes within the PAG (outlined in red). A $P_{ET}CO_2$ trace was created by extrapolating between end-tidal CO_2 peaks, and small hypercapnic challenges were administered during rest periods to dissociate hypercapnic effects from respiratory challenges. The images consist of a colour-rendered statistical map superimposed on a standard (MNI $1mm^3$) brain. Significant regions are displayed with a threshold $Z > 2.3$, with a cluster probability threshold of $p < 0.05$ (corrected for multiple comparisons).

Appendix D

Chapter 4 additional material

D.1 Hypercapnic ventilatory response

The hypercapnic ventilatory response (HCVR) was calculated from the steady state hypercapnic ventilatory response test in Chapter 5, using a linear regression between ventilation and $P_{ET}CO_2$. Single subject regressions can be seen in the following figures for athletes (Figure D.1) and sedentary subjects (Figure D.2).

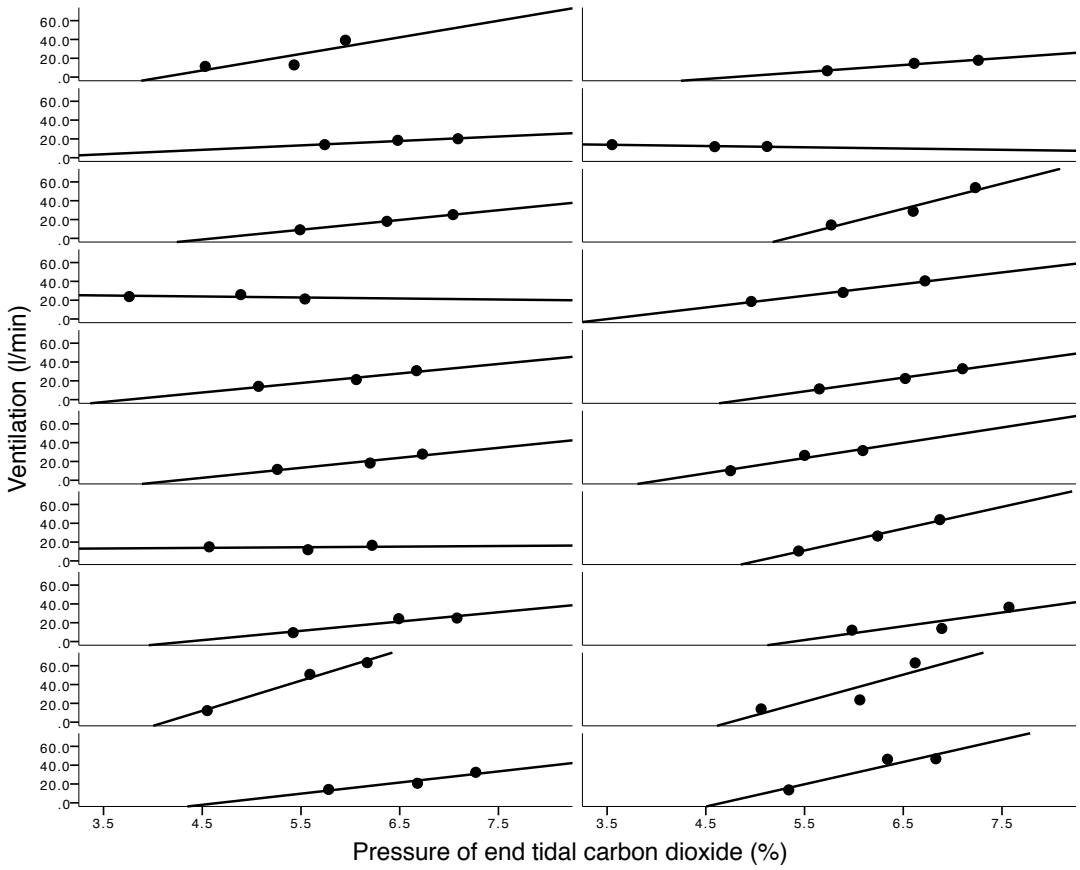

Figure D.1: Demonstration of the regression slopes between ventilation and $P_{ET}CO_2$ in each of 20 amateur endurance athletes.

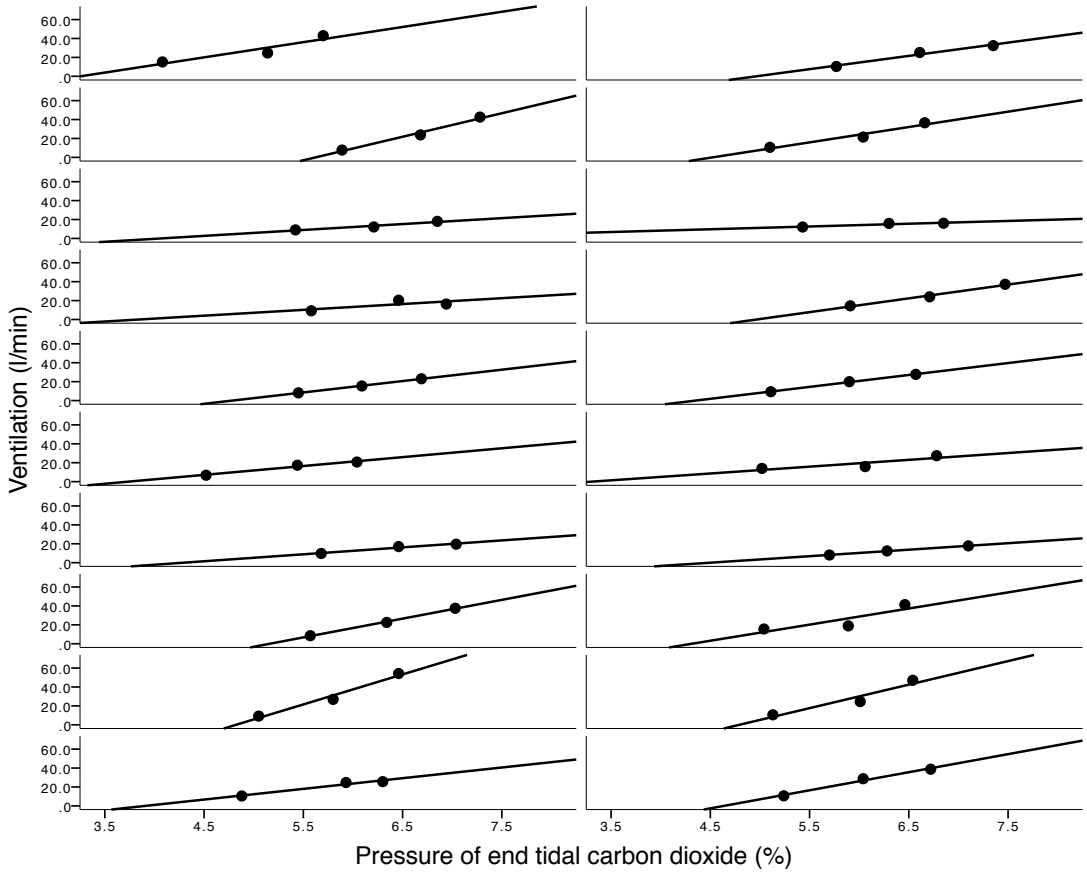

Figure D.2: Demonstration of the regression slopes between ventilation and $P_{ET}CO_2$ in each of 20 healthy sedentary subjects.

Appendix E

Chapter 5 additional material

E.1 Peak voxel locations

Table E.1: Co-ordinates of local maxima of significant increases (activations) and decreases (deactivations) in the group BOLD response to inspiratory loading. Values derived from cluster-based analysis. The most significant maximum is listed for each anatomical location. Co-ordinates are in mm in standard space of MNI (1 mm^3): x, distance right (+) or left (-) of the mid saggital line; y, distance anterior (+) or posterior (-) from a vertical plane through the anterior commissure; z, distance above (+) or below (-) the intercommisurial plane. Abbreviations: VPL, ventroposterolateral nucleus of the thalamus.

	Left				Right			
	x	y	z	Z score	x	y	z	Z score
Activations								
dorsolateral prefrontal cortex	-34	52	24	5.88	36	46	27	6.72
primary motor cortex	-48	-10	46	6.81	54	-3	36	6.27
supplementary motor cortex	-7	4	48	6.82	6	-6	63	6.49
primary sensory cortex	-56	-22	23	6.4	50	-9	36	6.21
middle cingulate cortex	-9	13	39	5.77	7	14	38	6.38
operculum	-45	-1	7	6.15	36	17	11	6.38
middle insula cortex	-39	1	6	5.81	45	4	4	6.02
anterior insula cortex	-35	6	6	5.5	39	19	7	5.79
putamen	-23	1	6	4.53	23	0	8	5.87
caudate nucleus	-16	-15	22	4.25	19	17	4	4.94
VPL	-9	-20	-1	4.74	10	-18	1	4.28
subthalamic nucleus	-4	-21	-6	3.38	8	-21	-7	2.77
Deactivations								
anterior cingulate cortex	-8	47	-3	3.95	1	35	4	3.82
posterior cingulate cortex	-5	-37	36	5.15	6	-38	36	4.3
hippocampus	-27	-31	-8	4.2	25	-9	-21	4.71
amygdala	-33	-1	-16	4.92	22	-9	-12	5.52
ventromedial prefrontal cortex	-6	49	-5	3.91	7	53	-5	4.04
inferior precuneus	-3	-65	24	4.91	4	-64	25	5.23
primary sensory cortex	-2	-36	61	4.27	3	-33	58	3.14
pontine nuclei	-6	-32	-35	4.36	6	-25	-36	4.16
primary motor cortex	-3	-33	61	3.74	5	-22	71	4.24

Table E.2: Co-ordinates of local maxima of significant increases (activations) and decreases (deactivations) in the BOLD response during the contrast of certain anticipation of inspiratory loading (> anticipation of no resistance). Values derived from cluster-based analysis. The most significant maximum is listed for each anatomical location. Co-ordinates are in mm in standard space of MNI (1 mm^3): x, distance right (+) or left (-) of the mid saggital line; y, distance anterior (+) or posterior (-) from a vertical plane through the anterior commissure; z, distance above (+) or below(-) the intercommisurial plane.

	Left				Right			
	x	y	z	Z score	x	y	z	Z score
Activations								
dorsolateral prefrontal cortex					42	47	8	4.06
supplementary motor cortex	-2	-1	61	4.88	4	2	64	5.03
posterior cingulate cortex	-2	-20	31	2.95	4	-25	30	3.76
anterior cingulate cortex	8	16	40	4.63				
operculum	-36	20	4	5.24	48	11	3	5.34
middle insula cortex	-39	1	6	5.06	39	21	1	6.47
Deactivations								
anterior cingulate cortex	-9	49	2	4.18	7	-34	36	3.9
posterior cingulate cortex	-4	-38	36	5.35	2	-55	22	4.92
dorsomedial prefrontal cortex	-5	59	8	4.62	4	52	24	3.79
hippocampus	-25	-12	-22	6.32	33	-28	-15	5.02
amygdala	-25	-5	-25	4.82	22	-10	-13	4.82
ventromedial prefrontal cortex	-1	53	-4	4.71	10	53	-1	3.51
inferior precuneus	-2	-63	15	5.6	13	-55	16	5.49
primary sensory cortex	-12	-41	67	3.36	3	-23	63	3.61
pontine nuclei	-3	-23	-39	4.72	7	-25	-34	4.28
posterior insula	-34	-25	17	3.83	39	-18	18	3.71
cerebellar IX					6	-46	-42	4.34

Table E.3: Co-ordinates of local maxima of voxels where BOLD activity positively correlates with subjective scores of breathlessness intensity and anxiety across subjects, during both inspiratory resistive loading and anticipation of resistance (> anticipation of no resistance). Values derived from cluster-based analysis. The most significant maximum is listed for each anatomical location. Co-ordinates are in mm in standard space of MNI (1 mm^3): x, distance right (+) or left (-) of the mid saggital line; y, distance anterior (+) or posterior (-) from a vertical plane through the anterior commissure; z, distance above (+) or below(-) the intercommisurial plane. Abbreviations: VPL, ventroposterolateral nucleus of the thalamus; VAN, ventral anterior nucleus of the thalamus.

	Left				Right			
	x	y	z	Z score	x	y	z	Z score
Resistive loading intensity								
middle insula	-36	-8	1	3.91				
Resistive loading anxiety								
dorsolateral prefrontal cortex	-23	56	30	4.15				
primary motor cortex	-60	4	28	4.28	58	-3	43	4.06
primary sensory cortex	-61	-10	37	3.72	52	-21	51	4.31
supplementary motor cortex	-2	-7	44	4.01	3	-15	54	4.56
middle insula	-34	-22	19	4.67	37	-16	17	4.1
VPL	-7	-14	0	3.44	8	-13	-2	3.85
subthalamic nucleus	-13	-17	-5	3.85	9	-14	-3	3.91
Anticipation intensity								
VAN	-8	-8	-2	3.62	10	-9	-4	3.46
Anticipation anxiety								
primary motor cortex	-34	-21	66	3.82	48	-10	51	3.76
superior parietal lobule	-28	-52	51	3.73	34	-42	56	3.77
lateral occipital cortex	-27	-88	25	3.98				
cuneus	-11	-73	24	3.89	18	-67	21	3.86

Table E.4: Co-ordinates of local maxima of voxels with the highest functional connectivity to their seed masks. Seed masks are the bilateral ventrolateral periaqueductal gray (vlPAG), lateral periaqueductal gray (lPAG) and left primary auditory cortex. Values derived from cluster-based analysis. The most significant maximum is listed for each anatomical location. Co-ordinates are in mm in standard space of MNI (1 mm^3): x, distance right (+) or left (-) of the mid saggital line; y, distance anterior (+) or posterior (-) from a vertical plane through the anterior commissure; z, distance above (+) or below(-) the intercommisurial plane.

	Left				Right			
	x	y	z	Z score	x	y	z	Z score
vlPAG connectivity								
dorsomedial prefrontal cortex	-8	48	12	5.13	27	40	31	4.03
anterior insula	-27	19	-10	4.05	29	26	-3	3.48
middle insula					37	-10	-3	4.36
operculum	-34	11	12	3.84	35	11	15	4.56
anterior cingulate cortex	-2	27	21	5.03	3	21	29	4.3
paracingulate gyrus					8	19	39	4.3
precuneus	-23	-56	6	5.19	9	-55	14	3.26
hippocampus	-26	-25	-13	4.63	29	-31	-9	3.94
parahippocampal gyrus	-30	-35	-14	4.27	30	-30	-21	4.62
supplementary motor cortex	-2	-2	60	4.77				
caudate nucleus	-12	6	18	4.08	14	6	15	4.5
visual cortex	-14	-71	4	4.39	14	-70	8	4.59
superior cerebellum	-5	-53	-9	5.83	6	-44	-15	5.43
lPAG connectivity								
primary motor cortex					15	-19	76	4.07
primary sensory cortex	-36	-39	44	4.16				
middle insula	-34	4	-14	4.26	41	-10	3	3.86
superior parietal lobule	-29	-42	43	4.03				
putamen	-25	2	-9	5.63				
hippocampus	-21	-16	-16	3.87	27	-38	-1	3.48
amygdala	-23	-12	-12	4.57				
lateral occipital cortex					15	-60	63	4.28
Auditory cortex connectivity								
auditory cortex	-41	-19	8	6.38	36	-23	10	5.62
primary sensory cortex	-54	-18	37	5.35	49	-12	34	5.35
anterior insula cortex	-33	16	11	4.07	30	16	8	5.5
middle insula cortex	-35	-22	7	5.68	39	-1	3	5.89
posterior insula cortex	-37	-25	8	6.19	37	-22	7	5.89

Table E.5: Co-ordinates of local maxima of significantly greater voxels in athletes greater than sedentary subjects during inspiratory resistive loading and anticipation of loading (> baseline). Values derived from cluster-based analysis, with negative z-scores indicating greater activity in sedentary subjects compared to athletes. The most significant maximum is listed for each anatomical location. Co-ordinates are in mm in standard space of MNI (1 mm^3): x, distance right (+) or left (-) of the mid saggital line; y, distance anterior (+) or posterior (-) from a vertical plane through the anterior commissure; z, distance above (+) or below(-) the intercommisurial plane.

	Left				Right			
	x	y	z	Z score	x	y	z	Z score
Resistive loading								
middle insula					37	2	13	-3.7
caudate nucleus					14	-6	21	-3.31
primary sensory cortex	-54	-23	47	-4.23	58	-12	40	-3.75
supramarginal gyrus	-62	-30	30	-3.85	58	-21	27	-3.74
superior parietal lobule	-36	-47	51	-4.68				
primary motor cortex					45	1	45	-3.61
operculum	-40	20	7	-4.63	49	-2	11	-4.07
cerebellar crus I					38	-45	-36	-4.04
cerebellar VI					38	-53	-23	-4.63
Anticipation (> baseline)								
ventromedial prefrontal cortex	-3	51	-10	3.4	6	46	-10	3.38
paracingulate gyrus	-11	49	-2	3.59	7	44	-7	3.43
anterior cingulate cortex					3	39	-7	3.04
posterior cingulate cortex	-4	-33	39	3.09	5	-38	39	3.68
posterior insula	-36	-33	16	4.18				

E.2 Comparisons with Chapter 3

E.2.1 Anticipation of resistance > baseline

In this final study we reproduced the activity in the vlPAG and cortex in the contrast of anticipation of resistance > baseline seen in Chapter 3 (Figure E.1). In addition, significantly increased BOLD activity was also observed in the lPAG during anticipation > baseline in Chapter 5, and cortically/subcortically in the dorsolateral prefrontal cortex, supplementary motor cortex, middle and posterior cingulate cingulate cortices, anterior and middle insula, subthalamic nucleus, operculum, cerebellar I-IV, primary visual cortex and primary sensory cortex, and decreased BOLD activity in the anterior and posterior cingulate cortices, ventromedial prefrontal cortex, dorsomedial prefrontal cortex, posterior insula, inferior precuneus, hippocampus and amygdala, primary sensory cortex, pontine nuclei, ventral inferior nuclei of the thalamus and cerebellar IX.

E.2.2 Anticipation of resistance > baseline scaled with breathlessness ratings

Consistent with Chapter 3 results, in this study we found lPAG activity that scaled with intensity of resistance during the anticipation period (anticipation > baseline: Figure E.2). Additional BOLD activity that scaled with anxiety scores during anticipation (> baseline) in Chapter 5 was identified in the dorsolateral prefrontal cortex, primary motor and sensory cortices, supplementary motor cortex, superior parietal lobule, lateral occipital cortex, cuneus and posterior cingulate cortex, and scalings with intensity scores included the middle insula, putamen, posterior cingulate cortex, inferior frontal gyrus and the middle temporal gyrus.

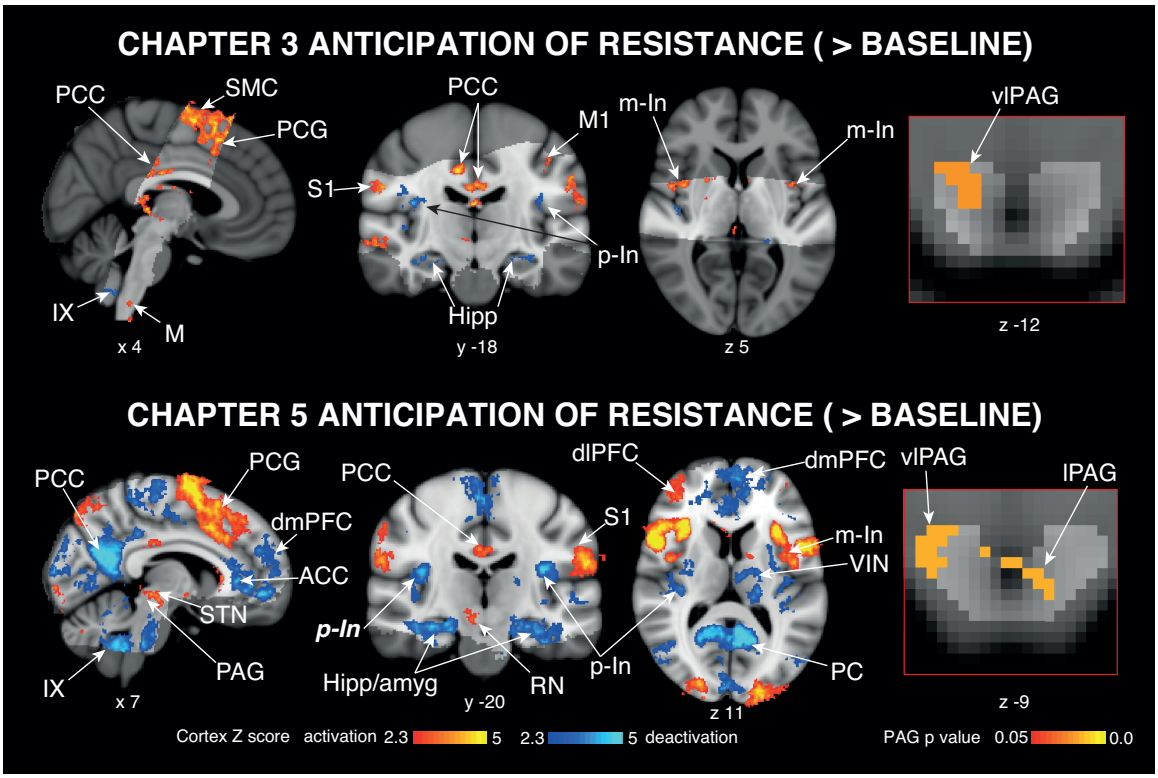

Figure E.1: Contrast of anticipation of resistive loading > baseline for Chapter 3 and Chapter 5. The images consist of a colour-rendered statistical map superimposed on a standard (MNI 1mm^3) brain, and significant regions are displayed with a threshold $Z > 2.3$, with a cluster probability threshold of $p < 0.05$ (corrected for multiple comparisons). Right: The bright grey region represents the periaqueductal gray (larger mask used in Chapter 5 to accommodate larger functional voxels), with significant clusters overlaid ($p < 0.05$; small-volume-corrected for multiple comparisons using represented PAG mask). Abbreviations: PAG, periaqueductal gray; vlPAG and lPAG, ventrolateral and lateral PAG; S1, primary sensory cortex; CN, caudate nucleus; SMC, supplementary motor cortex; Put, putamen; ACC, anterior cingulate cortex; MCC, middle cingulate cortex; PCC, posterior cingulate cortex; PC, precuneus; PCG, paracingulate gyrus; dlPFC, dorsolateral prefrontal cortex; dmPFC, dorsomedial prefrontal cortex; vmPFC, ventromedial prefrontal cortex; Hipp hippocampus; amyg, amygdala; a-In, anterior insula; m-In, middle insula; p-In, posterior insula; STN, subthalamic nucleus; RN, Red nucleus; OP, operculum; V1, primary visual cortex; IX and I-IV, cerebellar lobes; thalamic nuclei: VPL, ventral posterolateral nucleus; VIN, ventral inferior nuclei; activation, increase in BOLD signal; deactivation, decrease in BOLD signal.

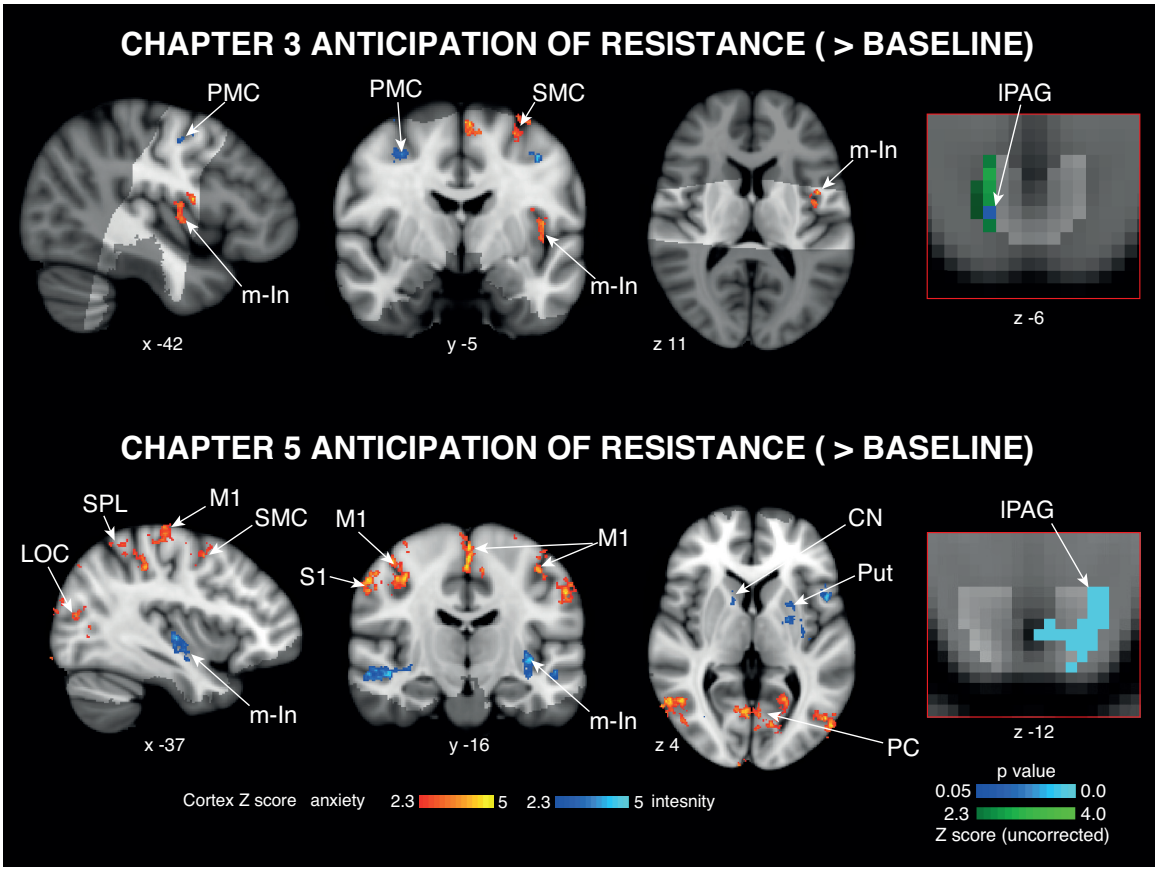

Figure E.2: BOLD response that scales with intensity (blue) and anxiety (yellow) ratings for anticipation > baseline in Chapter 3 and Chapter 5. The images consist of a colour-rendered statistical map superimposed on a standard (MNI 1mm^3) brain, and significant regions are displayed with a threshold $Z > 2.3$, with a cluster probability threshold of $p < 0.05$ (corrected for multiple comparisons). Right: The bright grey region represents the periaqueductal gray (larger mask used in Chapter 5 to accommodate larger functional voxels), with significant clusters overlaid ($p < 0.05$; small-volume-corrected for multiple comparisons using represented PAG mask). Abbreviations: PAG, periaqueductal gray; lPAG, lateral PAG; S1, primary sensory cortex; M1, primary motor cortex; SMC, supplementary motor cortex; PCC, posterior cingulate cortex; Cun, cuneus; pC, precuneus; dlPFC, dorsolateral prefrontal cortex; m-In, middle insula; CN, caudate nucleus; STN, subthalamic nucleus; LOC, lateral occipital cortex; VPL, ventral posterolateral nucleus of the thalamus; VAN, ventral anterior nucleus of the thalamus.

E.3 Inspiratory resistance trial-by-trial variability

The ratings of intensity of breathing following each inspiratory resistance challenge were included as demeaned regressors in both Chapters' 3 and 5 single subject GLMs. Including this rating regressor removes trial-by-trial variability from the inspiratory resistance mean regressor, modelling brain activity that varies depending on the change in subjective intensity ratings of each resistance stimulus. The results from the trial-by-trial rating regressor from Chapter 5 are presented here in Figure E.3.

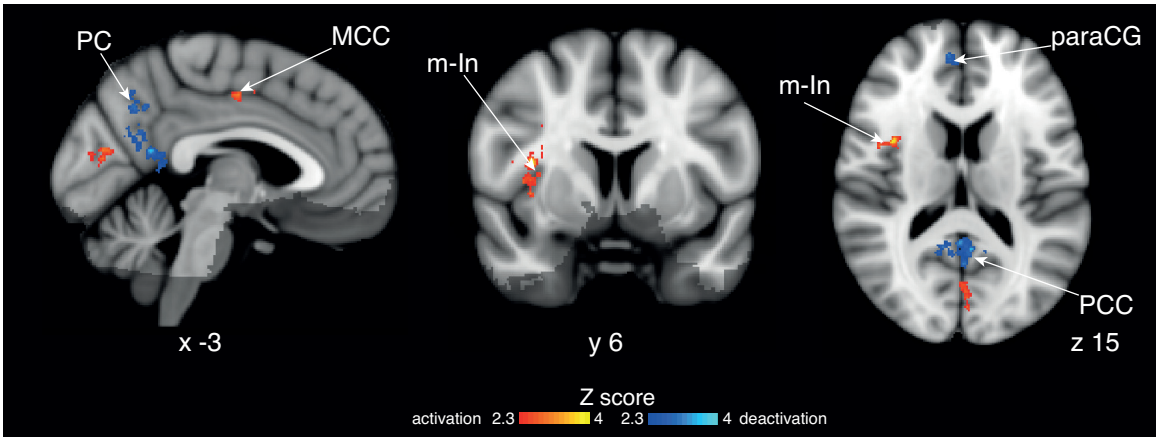

Figure E.3: Mean BOLD activity of the subject ratings of inspiratory resistance breathing intensity on a trial-by-trial basis. The images consist of a colour-rendered statistical map superimposed on a standard (MNI 1mm^3) brain. Significant regions are displayed with a threshold $Z > 2.3$, with a cluster probability threshold of $p < 0.05$ (corrected for multiple comparisons). Abbreviations: PC, precuneus; MCC, middle cingulate cortex; PCC, posterior cingulate cortex; m-In, middle insula; paraCG, paracingulate gyrus.

E.4 Validation of lPAG activity scaling with intensity scores

The loss of resolution in Chapter 5 with voxels of 2 x 2 x 2 mm reduces definition and the ability to dissociate between the PAG and the cerebral aqueduct. Therefore, we wanted to ensure that the activity seen in the lPAG during inspiratory resistance (scaled with intensity scores) was not simply a reflection of increased signal in the aqueduct as a result of increased inspiratory mouth pressure. A correlation between inspiratory mouth pressure and cope activity within the activated cluster in the lPAG across subjects was not significant (R = 0.20; p = 0.23; Figure E.4), providing confidence that this signal is a reflection of the lPAG involvement in the perception of intensity, and not noise from the aqueduct due to inspiratory pressure.

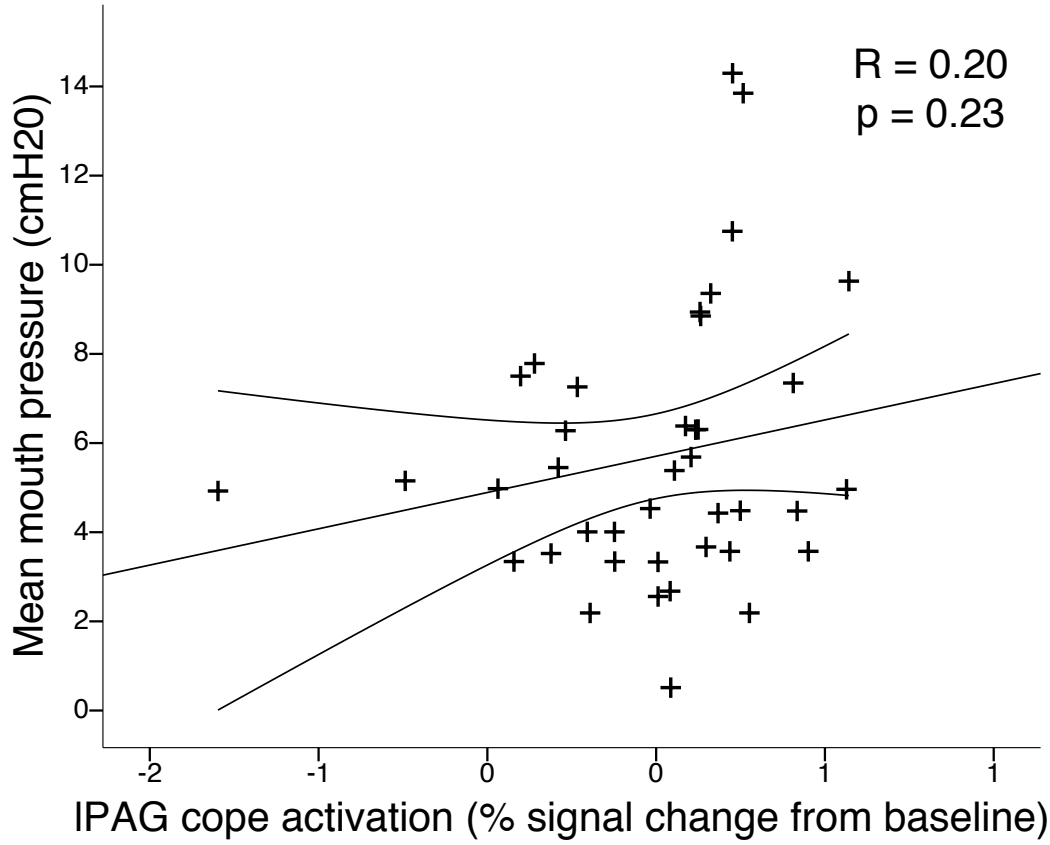

Figure E.4: No correlation was found between the cope activity in the activated region of the lPAG against the mean mouth pressure during inspiratory resistance.

References

Abraini, J., Bouquet, C., Joulia, F., Nicolas, M., and Kriem, B. (1998). Cognitive performance during a simulated climb of mount everest: implications for brain function and central adaptive processes under chronic hypoxic stress. *Pflügers Archiv*, 436(4):553–559.

Aldrich, T. K., Arora, N. S., and Rochester, D. F. (1982). The influence of airway obstruction and respiratory muscle strength on maximal voluntary ventilation in lung disease. *American Review of Respiratory Disease*, 126(2):195–199.

Alexander, G. E., DeLong, M. R., and Strick, P. L. (1986). Parallel organization of functionally segregated circuits linking basal ganglia and cortex. *Annual review of neuroscience*, 9(1):357–381.

Altose, M. D. (1985). Assessment and management of breathlessness. *CHEST Journal*, 88(2_Supplement):77S–83S.

Amunts, K., Schlaug, G., Jäncke, L., Steinmetz, H., Schleicher, A., Dabringhaus, A., and Zilles, K. (1997). Motor cortex and hand motor skills: structural compliance in the human brain. *Human Brain Mapping*, 5(3):206–215.

An, X., Bandler, R., Öngür, D., and Price, J. (1998). Prefrontal cortical projections to longitudinal columns in the midbrain periaqueductal gray in macaque monkeys. *Journal of Comparative Neurology*, 401(4):455–479.

Andersson, J. L., Jenkinson, M., and Smith, S. (2007). Non-linear registration, aka Spatial normalisation FMRIB technical report TR07JA2. *FMRIB Analysis Group of the University of Oxford*.

Arthurs, O. J. and Boniface, S. (2002). How well do we understand the neural origins of the fMRI BOLD signal? *TRENDS in Neurosciences*, 25(1):27–31.

Baev, K. V., Berezovskii, V. K., Kebkalo, T. G., and Savos' kina, L. A. (1985). Projection of forebrain structures of the cat to the hypothalamic locomotor area. *Neurophysiology*, 17(2):255–263.

Bailey, P. H. (2004). The Dyspnea-Anxiety-Dyspnea Cycle—COPD Patients' Stories of Breathlessness: "It's Scary /When you Can't Breathe". *Qualitative Health Research*, 14(6):760–778.

Baker, T. L., Fuller, D. D., Zabka, A. G., and Mitchell, G. S. (2001). Respiratory plasticity: differential actions of continuous and episodic hypoxia and hypercapnia. *Respiration physiology*, 129(1-2):25–35.

Ballantyne, D. and Scheid, P. (2001). Central chemosensitivity of respiration: a brief overview. *Respiration physiology*, 129(1-2):5–12.

Bandler, R., Keay, K. A., Floyd, N., and Price, J. (2000). Central circuits mediating patterned autonomic activity during active vs. passive emotional coping. *Brain research bulletin*, 53(1):95–104.

Bandler, R. and Shipley, M. T. (1994). Columnar organization in the midbrain periaqueductalgray: modules for emotional expression? *TRENDS in Neurosciences*, 17:379–389.

Banzett, R. B., Lansing, R. W., Evans, K. C., and Shea, S. A. (1996). Stimulus-response characteristics of co2-induced air hunger in normal subjects. *Respiration physiology*, 103(1):19–31.

Basnayake, S. D., Green, A. L., and Paterson, D. J. (2011). Mapping the central neurocircuitry that integrates the cardiovascular response to exercise in humans. *Experimental Physiology*, 97(1):no–no.

Bassett, D. and Howley, E. T. (2000). Limiting factors for maximum oxygen uptake and determinants of endurance performance. *Medicine and science in sports and exercise*, 32(1):70–84.

Bechara, A., Tranel, D., and Damasio, H. (2000). Characterization of the decision-making deficit of patients with ventromedial prefrontal cortex lesions. *Brain*, 123(11):2189–2202.

Behbehani, M. M. (1995). Functional characteristics of the midbrain periaqueductal gray. *Progress in neurobiology*, 46(6):575–605.

Beitz, A. J. (1982). The organization of afferent projections to the midbrain periaqueductal gray of the rat. *Neuroscience*, 7(1):133–159.

Belliveau, J., Kennedy, D., McKinstry, R., Buchbinder, B., Weisskoff, R., Cohen, M., Vevea, J., Brady, T., and Rosen, B. (1991). Functional mapping of the human visual cortex by magnetic resonance imaging. *Science*, 254(5032):716–719.

Benarroch, E. E. (2012). Periaqueductal gray An interface for behavioral control. *Neurology*, 78(3):210–217.

Bingel, U., Lorenz, J., Schoell, E., Weiller, C., and Büchel, C. (2006). Mechanisms of placebo analgesia: racc recruitment of a subcortical antinociceptive network. *Pain*, 120(1):8–15.

Boutellier, U. and Piwko, P. (1992). The respiratory system as an exercise limiting factor in normal sedentary subjects. *European journal of applied physiology and occupational physiology*, 64(2):145–152.

Brannan, S., Liotti, M., Egan, G., Shade, R., Madden, L., Robillard, R., Abplanalp, B., Stofer, K., Denton, D., and Fox, P. T. (2001). Neuroimaging of cerebral activations and deactivations associated with hypercapnia and hunger for air. *Proceedings of the National Academy of Sciences*, 98(4):2029–2034.

Brenes, G. A. (2003). Anxiety and chronic obstructive pulmonary disease: prevalence, impact, and treatment. *Psychosomatic medicine*, 65(6):963–970.

Brookes, J. C. W., Faull, O. K., Pattinson, K. T. S., and Jenkinson, M. (2013). Physiological Noise in Brainstem fMRI. *Frontiers in Human Neuroscience*, 7:1–13.

Brooks, J. C. W., Beckmann, C. F., Miller, K. L., Wise, R. G., Porro, C. A., Tracey, I., and Jenkinson, M. (2008). Physiological noise modelling for spinal functional magnetic resonance imaging studies. *Neuroimage*, 39(2):680–692.

Büchel, C., Bornhövd, K., Quante, M., Glauche, V., Bromm, B., and Weiller, C. (2002). Dissociable neural responses related to pain intensity, stimulus intensity, and stimulus awareness within the anterior cingulate cortex: a parametric single-trial laser functional magnetic resonance imaging study. *The Journal of Neuroscience*, 22(3):970–976.

Büchel, C., Morris, J., Dolan, R. J., and Friston, K. J. (1998). Brain systems mediating aversive conditioning: an event-related fmri study. *Neuron*, 20(5):947–957.

Byrne-Quinn, E., Weil, J. V., Sodal, I. E., Filley, G., and Grover, R. (1971). Ventilatory control in the athlete. *Journal of Applied Physiology*, 30(1):91–98.

Calford, M. (2002). Dynamic representational plasticity in sensory cortex. *Neuroscience*, 111(4):709–738.

Cameron, A. A., Khan, I. A., Westlund, K. N., Cliffer, K. D., and Willis, W. D. (1995). The efferent projections of the periaqueductal gray in the rat: A Phaseolus vulgarisleucoagglutinin study. I. Ascending projections. *The Journal of comparative neurology*, 351(4):568–584.

Canteras, N. S. and Goto, M. (1999). Fos-like immunoreactivity in the periaqueductal gray of rats exposed to a natural predator. *NeuroReport*, 10(413):6.

Carrieri-Kohlman, V., Gormley, J. M., Douglas, M. K., Paul, S. M., and Stulbarg, M. S. (1996). Exercise training decreases dyspnea and the distress and anxiety associated with it: monitoring alone may be as effective as coaching. *CHEST Journal*, 110(6):1526–1535.

Carrieri-Kohlman, V., Gormley, J. M., Eiser, S., Demir-Deviren, S., Nguyen, H., Paul, S. M., and Stulbarg, M. S. (2001). Dyspnea and the affective response during exercise training in obstructive pulmonary disease. *Nursing research*, 50(3):136–146.

Cavanna, A. E. and Trimble, M. R. (2006). The precuneus: a review of its functional anatomy and behavioural correlates. *Brain*, 129(3):564–583.

Celli, B. R., Cote, C. G., Marin, J. M., and Casanova, C. (2004). The Body-Mass Index, Airflow Obstruction, Dyspnea, and Exercise Capacity Index in Chronic Obstructive Pulmonary Disease. *New England Journal of Medicine*.

Cereda, C., Ghika, J., Maeder, P., and Bogousslavsky, J. (2002). Strokes restricted to the insular cortex. *Neurology*, 59(12):1950–1955.

Chou, T. C., Bjorkum, A. A., Gaus, S. E., Lu, J., Scammell, T. E., and Saper, C. B. (2002). Afferents to the Ventrolateral Preoptic Nucleus. *The Journal of neuroscience*.

Cohen, E. R., Ugurbil, K., and Kim, S.-G. (2002). Effect of Basal Conditions on the Magnitude and Dynamics of the Blood Oxygenation Level Dependent fMRI Response. *Journal of Cerebral Blood Flow & Metabolism*, 22(9):1042–1053.

Colebatch, J. G., Adams, L., Murphy, K., Martin, A. J., Lammertsma, A. A., Tochon-Danguy, H. J., Clark, J. C., Friston, K. J., and Guz, A. (1991). Regional cerebral blood flow during volitional breathing in man. *The Journal of physiology*, 443(1):91–103.

Corfield, D. R., Fink, G. R., Ramsay, S. C., Murphy, K., Harty, H. R., Watson, J. D., Adams, L., Frackowiak, R. S., and Guz, A. (2005). Evidence for limbic system activation during CO2-stimulated breathing in man. *The Journal of physiology*, 488(Pt 1):77–84.

Cowie, R. J. and Holstege, G. (1992). Dorsal mesencephalic projections to pons, medulla, and spinal cord in the cat: Limbic and non-limbic components. *The Journal of comparative neurology*, 319(4):536–559.

Craig, A. (2003). Interoception: the sense of the physiological condition of the body. *Current opinion in neurobiology*, 13(4):500–505.

Craig, A. D. (2002). How do you feel? interoception: the sense of the physiological condition of the body. *Nature reviews neuroscience*, 3(8):655–666.

Craig, A. D. (2009). How do you feel—now? the anterior insula and human awareness. *Nature Reviews Neuroscience*.

Craven, J. (2011). Major ascending and descending tracts in the spinal cord. *Anaesthesia & Intensive Care Medicine*, 12(1):26–27.

Critchley, H. D., Wiens, S., Rotshtein, P., Öhman, A., and Dolan, R. J. (2004). Neural systems supporting interoceptive awareness. *Nature neuroscience*, 7(2):189–195.

Dampney, R. A. L., Furlong, T. M., Horiuchi, J., and Iigaya, K. (2013). Role of dorsolateral periaqueductal grey in the coordinated regulation of cardiovascular and respiratory function. *Autonomic Neuroscience*, 175(1-2):17–25.

Dampney, R. A. L., Horiuchi, J., and McDowall, L. M. (2008). Hypothalamic mechanisms coordinating cardiorespiratory function during exercise and defensive behaviour. *Autonomic Neuroscience*, 142(1-2):3–10.

Davenport, P. W. and Vovk, A. (2009). Cortical and subcortical central neural pathways in respiratory sensations. *Respiratory physiology & neurobiology*, 167(1):72–86.

De Oca, B. M., DeCola, J. P., Maren, S., and Fanselow, M. S. (1998). Distinct regions of the periaqueductal gray are involved in the acquisition and expression of defensive responses. *The Journal of Neuroscience*, 18(9):3426–3432.

De Peuter, S., Van Diest, I., Lemaigre, V., Verleden, G., Demedts, M., and Van den Bergh, O. (2004). Dyspnea: The role of psychological processes. *Clinical psychology review*, 24(5):557–581.

Dempsey, J., Vidruk, E., and Mitchell, G. (1985). Pulmonary control systems in exercise: update. In *Federation proceedings*, volume 44, pages 2260–2270.

Devonshire, I. M., Papadakis, N. G., Port, M., Berwick, J., Kennerley, A. J., Mayhew, J. E. W., and Overton, P. G. (2012). Neurovascular coupling is brain region-dependent. *Neuroimage*, 59(3):1997–2006.

Duffin, J. and Hockman, C. H. (1972). Limbic forebrain and midbrain modulation and phase-switching of expiratory neurons. *Brain research*, 39(1):235.

Dutschmann, M., Mörschel, M., Kron, M., and Herbert, H. (2004). Development of adaptive behaviour of the respiratory network: implications for the pontine Kölliker-Fuse nucleus. *Respiratory physiology & neurobiology*, 143(2-3):155–165.

Duvernoy, H. M. (1995). *The Human Brain Stem and Cerebellum: Surface, Structure, Vascularization, and Three-dimensional Sectional Anatomy with MRI*. Spring-Verlag.

Eldridge, F., Millhorn, D., and Waldrop, T. (1981). Exercise hyperpnea and locomotion: parallel activation from the hypothalamus. *Science*, 211(4484):844–846.

Emery, C. F. (1994). Effects of Age on Physiological and Psychological Functioning among COPD Patients in an Exercise Program. *Journal of Aging and Health*, 6(1):3–16.

Engel, A. K., Fries, P., and Singer, W. (2001). Dynamic predictions: oscillations and synchrony in top-down processing. *Nature Reviews Neuroscience*, 2(10):704–716.

Erickson, K. I., Voss, M. W., Prakash, R. S., Basak, C., Szabo, A., Chaddock, L., Kim, J. S., Heo, S., Alves, H., White, S. M., Wojcicki, T. R., Mailey, E., Vieira, V. J., Martin, S. A., Pence, B. D., Woods, J. A., McAuley, E., and Kramer, A. F. (2011). Exercise training increases size of hippocampus and improves memory. *Proceedings of the National Academy of Sciences*, 108(7):3017–3022.

Ezra, M., Faull, O. K., Jbabdi, S., Pattinson, S., and Thomas, K. (2015). Connectivity-based segmentation of the periaqueductal gray matter in human with brainstem optimized diffusion mri. *Human brain mapping*.

Fairhurst, M., Wiech, K., Dunckley, P., and Tracey, I. (2007). Anticipatory brainstem activity predicts neural processing of pain in humans. *Pain*, 128(1-2):101–110.

Farmer, D. G., Bautista, T. G., Jones, S. E., Stanic, D., and Dutschmann, M. (2014). The midbrain periaqueductal grey has no role in the generation of the respiratory motor pattern, but provides command function for the modulation of respiratory activity. *Respiratory physiology & neurobiology*, 204:14–20.

Feinberg, D. A., Moeller, S., Smith, S. M., Auerbach, E., Ramanna, S., Glasser, M. F., Miller, K. L., Ugurbil, K., and Yacoub, E. (2010). Multiplexed Echo Planar Imaging for Sub-Second Whole Brain FMRI and Fast Diffusion Imaging. *PLOS ONE*, 5(12):e15710.

Feldman, J. L., Mitchell, G. S., and Nattie, E. E. (2003). BREATHING: Rhythmicity, Plasticity, Chemosensitivity. *Annual review of neuroscience*, 26(1):239–266.

Fields, H. (2004). State-dependent opioid control of pain. *Nature Reviews Neuroscience*, 5(7):565–575.

Fink, G. R., Corfield, D. R., Murphy, K., Kobayashi, I., Dettmers, C., Adams, L., Frackowiak, R. S., and Guz, A. (1996). Human cerebral activity with increasing inspiratory force: a study using positron emission tomography. *Journal of Applied Physiology*, 81(3):1295–1305.

Fransson, P. (2005). Spontaneous low-frequency bold signal fluctuations: An fmri investigation of the resting-state default mode of brain function hypothesis. *Human brain mapping*, 26(1):15–29.

Fried, I., Katz, A., McCarthy, G., Sass, K. J., Williamson, P., Spencer, S. S., and Spencer, D. D. (1991). Functional organization of human supplementary motor cortex studied by electrical stimulation. *The Journal of neuroscience*, 11(11):3656–3666.

Gabbott, P. L. A., Warner, T. A., Jays, P. R. L., Salway, P., and Busby, S. J. (2005). Prefrontal cortex in the rat: Projections to subcortical autonomic, motor, and limbic centers. *The Journal of comparative neurology*, 492(2):145–177.

Gallego, J., Nsegbe, E., and Durand, E. (2001). Learning in Respiratory Control. *Behavior modification*, 25(4):495–512.

Gerstein, G. L. and Perkel, D. H. (1969). Simultaneously recorded trains of action potentials: analysis and functional interpretation. *Science*, 164:828–830.

Glover, G. H., Li, T.-Q., and Ress, D. (2000). Image-Based Method for Retrospective Correction of Physiological Motion Effects in fMRI: RETROICOR. *Magnetic Resonance in Medicine*, 44:162–167.

Goble, D. J., Coxon, J. P., Van Impe, A., Geurts, M., Van Hecke, W., Sunaert, S., Wenderoth, N., and Swinnen, S. P. (2012). The neural basis of central proprioceptive processing in older versus younger adults: an important sensory role for right putamen. *Human brain mapping*, 33(4):895–908.

Godfrey, S., Edwards, R. H., Copland, G. M., and Gross, P. L. (1971). Chemosensitivity in normal subjects, athletes, and patients with chronic airways obstruction. *Journal of Applied Physiology*, 30(2):193–199.

Golder, F. J., Reier, P. J., and Bolser, D. C. (2001). Altered Respiratory Motor Drive after Spinal Cord Injury: Supraspinal and Bilateral Effects of a Unilateral Lesion. *The Journal of Neuroscience*, 21(21):8680–8689.

Gottfried, J. A. and Dolan, R. J. (2004). Human orbitofrontal cortex mediates extinction learning while accessing conditioned representations of value. *Nature neuroscience*, 7(10):1144–1152.

Gottfried, J. A., O'Doherty, J., and Dolan, R. J. (2002). Appetitive and aversive olfactory learning in humans studied using event-related functional magnetic resonance imaging. *The Journal of Neuroscience*, 22(24):10829–10837.

Gozal, D., Omidvar, O., Kirlew, K. A., Hathout, G. M., Hamilton, R., Lufkin, R. B., and Harper, R. M. (1995). Identification of human brain regions underlying responses to resistive inspiratory loading with functional magnetic resonance imaging. *Proceedings of the National Academy of Sciences*, 92(14):6607–6611.

Grafton, S., Fagg, A., and Arbib, M. (1998). Dorsal premotor cortex and conditional movement selection: a pet functional mapping study. *Journal of Neurophysiology*, 79(2):1092–1097.

Gray, M. A., Harrison, N. A., Wiens, S., and Critchley, H. D. (2007). Modulation of emotional appraisal by false physiological feedback during fmri. *PLoS One*, 2(6):e546.

Green, A. L. and Paterson, D. J. (2008). Identification of neurocircuitry controlling cardiovascular function in humans using functional neurosurgery: implications for exercise control. *Experimental Physiology*, 93(9):1022–1028.

Green, A. L., Wang, S., Purvis, S., and Owen, S. (2007). Identifying cardiorespiratory neurocircuitry involved in central command during exercise in humans. *The Journal of Physiology*.

Greicius, M. D. and Menon, V. (2004). Default-mode activity during a passive sensory task: uncoupled from deactivation but impacting activation. *Journal of cognitive neuroscience*, 16(9):1484–1492.

Greve, D. N. and Fischl, B. (2009). Accurate and robust brain image alignment using boundary-based registration. *Neuroimage*, 48(1):63–72.

Griffanti, L., Salimi-Khorshidi, G., Beckmann, C. F., Auerbach, E. J., Douaud, G., Sexton, C. E., Zsoldos, E., Ebmeier, K. P., Filippini, N., Mackay, C. E., et al. (2014). Ica-based artefact removal and accelerated fmri acquisition for improved resting state network imaging. *NeuroImage*, 95:232–247.

Groenewegen, H. J. (2003). The basal ganglia and motor control. *Neural plasticity*, 10(1-2):107–120.

Gwilym, S. E., Keltner, J. R., Warnaby, C. E., Carr, A. J., Chizh, B., Chessell, I., and Tracey, I. (2009). Psychophysical and functional imaging evidence supporting the presence of central sensitization in a cohort of osteoarthritis patients. *Arthritis & Rheumatism*, 61(9):1226–1234.

Handwerker, D. A., Ollinger, J. M., and D'Esposito, M. (2004). Variation of BOLD hemodynamic responses across subjects and brain regions and their effects on statistical analyses. *Neuroimage*, 21(4):1639–1651.

Harms, C. A., Wetter, T. J., Croix, C. M. S., Pegelow, D. F., and Dempsey, J. A. (2000). Effects of respiratory muscle work on exercise performance. *Journal of Applied Physiology*, 89(1):131–138.

Harper, R. M., Ni, H., and Zhang, J. (1991). *The Midbrain Periaqueductal Gray Matter: Functional, Anatomical, and Neurochemical Organization*. Springer US, Boston, MA.

Harvey, A. K., Pattinson, K. T. S., Brooks, J. C. W., Mayhew, S. D., Jenkinson, M., and Wise, R. G. (2008). Brainstem functional magnetic resonance imaging: Disentangling signal from physiological noise. *Journal of Magnetic Resonance Imaging*, 28(6):1337–1344.

Haxhiu, M. A., Yamamoto, B. K., Dreshaj, I. A., and Ferguson, D. G. (2002). Activation of the midbrain periaqueductal gray induces airway smooth muscle relaxation. *Journal of Applied Physiology*, 93(2):440–449.

Hayen, A., Herigstad, M., Kelly, M., Okell, T. W., Murphy, K., Wise, R. G., and Pattinson, K. T. S. (2013a). The effects of altered intrathoracic pressure on resting cerebral blood flow and its response to visual stimulation. *Neuroimage*, 66(C):479–488.

Hayen, A., Herigstad, M., and Pattinson, K. T. S. (2013b). Understanding dyspnea as a complex individual experience. *Clinical psychology review*, 24(5):557–581.

Hayen, A., Herigstad, M., Wiech, K., and Pattinson, K. T. (2015). Subjective evaluation of experimental dyspnoea: Effects of isocapnia and repeated exposure. *Respiratory physiology & neurobiology*, 208:21–28.

Hayward, L. F., Castellanos, M., and Davenport, P. W. (2004). Parabrachial neurons mediate dorsal periaqueductal gray evoked respiratory responses in the rat. *Journal of Applied Physiology*.

Hayward, L. F. and Von Reitzenstein, M. (2002). c-Fos expression in the midbrain periaqueductal gray after chemoreceptor and baroreceptor activation. *American Journal of Physiology-Heart and Circulatory Physiology*, 283(5):10.

Herigstad, M., Hayen, A., Evans, E., Hardinge, F. M., Davies, R. J., Wiech, K., and Pattinson, K. T. (2015). Dyspnea-related cues engage the prefrontal cortex: Evidence from functional brain imaging in copd. *CHEST Journal*.

Herigstad, M., Hayen, A., Wiech, K., and Pattinson, K. T. S. (2011). Dyspnoea and the brain. *Respiratory medicine*, 105(6):809–817.

Hill, K., Jenkins, S. C., Hillman, D. R., and Eastwood, P. R. (2004). Dyspnoea in COPD: Can inspiratory muscle training help? *Australian Journal of Physiotherapy*, 50(3):169–180.

Hoffman, J. (2014). *Physiological aspects of sport training and performance*. Human Kinetics.

Horiuchi, J., McDowall, L. M., and Dampney, R. A. L. (2009). Vasomotor and respiratory responses evoked from the dorsolateral periaqueductal grey are mediated by the dorsomedial hypothalamus. *The Journal of physiology*, 587(21):5149–5162.

Horn, E. M. and Waldrop, T. G. (1998). Suprapontine control of respiration. *Respiration physiology*, 114(3):201–211.

Huang, Z.-G., Subramanian, S. H., Balnave, R. J., Turman, A. B., and Moi Chow, C. (2000). Roles of periaqueductal gray and nucleus tractus solitarius in cardiorespiratory function in the rat brainstem. *Respiration physiology*, 120(3):185–195.

Hyam, J. A., Brittain, J.-S., Paterson, D. J., Davies, R. J. O., Aziz, T. Z., and Green, A. L. (2012). Controlling the Lungs Via the Brain. *Neurosurgery*, 70(2):469–478.

Ichiyama, R. M., Gilbert, A. B., Waldrop, T. G., and Iwamoto, G. A. (2002). Changes in the exercise activation of diencephalic and brainstem cardiorespiratory areas after training. *Brain research*, 947(2):225–233.

Jäncke, L., Shah, N., and Peters, M. (2000). Cortical activations in primary and secondary motor areas for complex bimanual movements in professional pianists. *Cognitive Brain Research*, 10(1):177–183.

Janssens, T., De Peuter, S., and Stans, L. (2011a). Dyspnea Perception in COPD. *CHEST Journal*, 140(3):618.

Janssens, T., De Peuter, S., Stans, L., Verleden, G., Troosters, T., Decramer, M., and Van den Bergh, O. (2011b). Dyspnea perception in copd: association between anxiety, dyspnea-related fear, and dyspnea in a pulmonary rehabilitation program. *CHEST Journal*, 140(3):618–625.

Jenkinson, M., Bannister, P., Brady, M., and Smith, S. (2002). Improved Optimization for the Robust and Accurate Linear Registration and Motion Correction of Brain Images. *Neuroimage*, 17(2):825–841.

Johnson, B. D., Aaron, E. A., Babcock, M. A., and Dempsey, J. A. (1996). Respiratory muscle fatigue during exercise: implications for performance. *Medicine and Science in Sports and Exercise*, 28(9):1129–1137.

Kabat, H. (1935). Electrical Stimulation of Points in the Forebrain and Midbrain: the Resultant Alterations in Blood Pressure. *Archives of Neurology and Psychiatry*, 34(5):931–955.

Kane, M. J. and Engle, R. W. (2002). The role of prefrontal cortex in working-memory capacity, executive attention, and general fluid intelligence: An individual-differences perspective. *Psychonomic bulletin & review*, 9(4):637–671.

Kaufman, M. P. and Forster, H. V. (1996). Reflexes controlling circulatory, ventilatory and airway responses to exercise. *Comprehensive Physiology*.

Keay, K. A. and Bandler, R. (2001). Parallel circuits mediating distinct emotional coping reactions to different types of stress. *Neuroscience & Biobehavioral Reviews*, 25(669):10.

Kjaer, T., Nowak, M., Kjær, K. W., Lou, A., and Lou, H. (2001). Precuneus–prefrontal activity during awareness of visual verbal stimuli. *Consciousness and cognition*, 10(3):356–365.

Kjaer, T. W., Nowak, M., and Lou, H. C. (2002). Reflective self-awareness and conscious states: Pet evidence for a common midline parietofrontal core. *Neuroimage*, 17(2):1080–1086.

Klein, D. F. (1993). False suffocation alarms, spontaneous panics, and related conditions: an integrative hypothesis. *Archives of general psychiatry*, 50(4):306–317.

Kolb, B. and Whishaw, I. Q. (1998). Brain plasticity and behaviour. *Annual review of psychology*, 49(1):43–64.

Kreuzer, F. (1982). Oxygen supply to tissues: The Krogh model and its assumptions. *Cellular and Molecular Life Sciences*, 38(12):1415–1426.

Kuwaki, T., Li, A., and Nattie, E. (2010). State-dependent central chemoreception: A role of orexin. *Respiratory physiology & neurobiology*, 173(3):7.

Kwong, K. K., Belliveau, J. W., Chesler, D. A., Goldberg, I. E., Weisskoff, R. M., Poncelet, B. P., Kennedy, D. N., Hoppel, B. E., Cohen, M. S., and Turner, R. (1992). Dynamic magnetic resonance imaging of human brain activity during primary sensory stimulation. *Proceedings of the National Academy of Sciences*, 89(12):5675–5679.

LaBar, K. S., Gatenby, J. C., Gore, J. C., LeDoux, J. E., and Phelps, E. A. (1998). Human amygdala activation during conditioned fear acquisition and extinction: a mixed-trial fmri study. *Neuron*, 20(5):937–945.

Lansing, R. W., Gracely, R. H., and Banzett, R. B. (2009). The multiple dimensions of dyspnea: Review and hypotheses. *Respiratory physiology & neurobiology*, 167(1):53–60.

Laroche, S., Davis, S., and Jay, T. M. (2000). Plasticity at hippocampal to prefrontal cortex synapses: dual roles in working memory and consolidation. *Hippocampus*, 10(4):438–446.

Lee, M. C., Zambreanu, L., Menon, D. K., and Tracey, I. (2008). Identifying Brain Activity Specifically Related to the Maintenance and Perceptual Consequence of Central Sensitization in Humans. *Journal of Neuroscience*, 28(45):11642–11649.

Ley, R. (1999). The modification of breathing behavior pavlovian and operant control in emotion and cognition. *Behavior Modification*, 23(3):441–479.

Linnman, C., Moulton, E. A., Barmettler, G., Becerra, L., and Borsook, D. (2012). Neuroimaging of the periaqueductal gray: State of the field. *Neuroimage*, 60(1):505–522.

Liotti, M., Brannan, S., Egan, G., Shade, R., Madden, L., Abplanalp, B., Robillard, R., Lancaster, J., Zamarripa, F. E., and Fox, P. T. (2001). Brain responses associated with consciousness of breathlessness (air hunger). *Proceedings of the National Academy of Sciences*, 98(4):2035–2040.

Lopes, L. T., Biancardi, V., Vieira, E. B., Leite-Panissi, C., Bícego, K. C., and Gargaglioni, L. H. (2014). Participation of the dorsal periaqueductal grey matter in the hypoxic ventilatory response in unanaesthetized rats. *Acta Physiologica*, 211(3):528–537.

Lopes, L. T., Patrone, L. G. A., Bícego, K. C., Coimbra, N. C., and Gargaglioni, L. H. (2012). Periaqueductal gray matter modulates the hypercapnic ventilatory response. *Pflügers Archiv European Journal of Physiology*, 464(2):155–166.

MacDonald, A. W., Cohen, J. D., Stenger, V. A., and Carter, C. S. (2000). Dissociating the role of the dorsolateral prefrontal and anterior cingulate cortex in cognitive control. *Science*, 288(5472):1835–1838.

Mahler, D. A., Moritz, E. D., and Loke, J. (1982). Ventilatory responses at rest and during exercise in marathon runners. *Journal of Applied Physiology*, 52(2):388–392.

Mandelbrot, B. B. and Van Ness, J. W. (1968). Fractional brownian motions, fractional noises and applications. *SIAM review*, 10(4):422–437.

Martin, B. J., Sparks, K. E., Zwillich, C. W., and Weil, J. V. (1978). Low exercise ventilation in endurance athletes. *Medicine and science in sports*, 11(2):181–185.

McArdle, W. D., Katch, F. I., and Katch, V. L. (2006). *Essentials of exercise physiology*. Lippincott Williams & Wilkins.

McKay, L. C., Adams, L., Frackowiak, R. S. J., and Corfield, D. R. (2008). A bilateral cortico-bulbar network associated with breath holding in humans, determined by functional magnetic resonance imaging. *Neuroimage*, 40(4):1824–1832.

Miller, E. K. and Cohen, J. D. (2001). An integrative theory of prefrontal cortex function. *Annual review of neuroscience*, 24(1):167–202.

Mink, J. W. (1996). The basal ganglia: focused selection and inhibition of competing motor programs. *Progress in neurobiology*, 50(4):381–425.

Mitchell, G. S., Baker, T. L., Nanda, S. A., Fuller, D. D., Zabka, A. G., Hodgeman, B. A., Bavis, R. W., Mack, K. J., and Olson, E. B. (2001). Invited Review: Intermittent hypoxia and respiratory plasticity. *Journal of Applied Physiology*, 90(6):2466–2475.

Mobbs, D., Petrovic, P., Marchant, J. L., Hassabis, D., Weiskopf, N., Seymour, B., Dolan, R. J., and Frith, C. D. (2007). When Fear Is Near: Threat Imminence Elicits Prefrontal-Periaqueductal Gray Shifts in Humans. *Science*, 317(5841):1079–1083.

Morrell, M. J., Finn, L., Kim, H., Peppard, P. E., Safwan Badr, M., and Young, T. (2000). Sleep fragmentation, awake blood pressure, and sleep-disordered breathing in a population-based study. *American journal of respiratory and critical care medicine*, 162(6):2091–2096.

Morschel, M. and Dutschmann, M. (2009). Pontine respiratory activity involved in inspiratory/expiratory phase transition. *Philosophical Transactions of the Royal Society B: Biological Sciences*, 364(1529):2517–2526.

Mucci, P., Prioux, J., Hayot, M., Ramonatxo, M., and Préfaut, C. (1998). Ventilation response to co2 and exercise-induced hypoxaemia in master athletes. *European journal of applied physiology and occupational physiology*, 77(4):343–351.

Nambu, A., Takada, M., Inase, M., and Tokuno, H. (1996). Dual somatotopical representations in the primate subthalamic nucleus: evidence for ordered but reversed body-map transformations from the primary motor cortex and the supplementary motor area. *The Journal of neuroscience*, 16(8):2671–2683.

Nelson, A. J. and Iwamoto, G. A. (2006). Reversibility of exercise-induced dendritic attenuation in brain cardiorespiratory and locomotor areas following exercise detraining. *Journal of Applied Physiology*, 101(4):1243–1251.

Nelson, A. J., Juraska, J. M., Musch, T. I., and Iwamoto, G. A. (2005). Neuroplastic adaptations to exercise: neuronal remodeling in cardiorespiratory and locomotor areas. *Journal of Applied Physiology*, 99(6):2312–2322.

Nishino, T. (2011). Dyspnoea: underlying mechanisms and treatment. *British journal of anaesthesia*, 106(4):463–474.

Ogawa, S., Tank, D. W., Menon, R., Ellermann, J. M., Kim, S. G., Merkle, H., and Ugurbil, K. (1992). Intrinsic signal changes accompanying sensory stimulation: functional brain mapping with magnetic resonance imaging. *Proceedings of the National Academy of Sciences*, 89(13):5951–5955.

Paterson, D. J. (2013). Defining the neuro-circuitry of exercise hyperpnoea. *The Journal of physiology*, pages 1–33.

Pattinson, K., Mitsis, G. D., Harvey, A. K., and Jbabdi, S. (2009a). Determination of the human brainstem respiratory control network and its cortical connections in vivo using functional and structural imaging. *Neuroimage*.

Pattinson, K. T. S., Governo, R. J., MacIntosh, B. J., Russell, E. C., Corfield, D. R., Tracey, I., and Wise, R. G. (2009b). Opioids Depress Cortical Centers Responsible for the Volitional Control of Respiration. *Journal of Neuroscience*, 29(25):8177–8186.

Pavlov, I. P. and Anrep, G. V. (2003). *Conditioned reflexes*, volume 614. Courier Corporation.

Pereira, E. A. C., Lu, G., Wang, S., Schweder, P. M., Hyam, J. A., Stein, J. F., Paterson, D. J., Aziz, T. Z., and Green, A. L. (2010). Ventral periaqueductal grey stimulation alters heart rate variability in humans with chronic pain. *Experimental Neurology*, 223(2):574–581.

Peters, J. H., McDougall, S. J., Mendelowitz, D., Koop, D. R., and Andresen, M. C. (2008). Isoflurane Differentially Modulates Inhibitory and Excitatory Synaptic Transmission to the Solitary Tract Nucleus. *Anesthesiology*, 108(4):675–683.

Ploghaus, A., Becerra, L., Borras, C., and Borsook, D. (2003). Neural circuitry underlying pain modulation: expectation, hypnosis, placebo. *Trends in cognitive sciences*, 7(5):197–200.

Poldrack, R. A. (2006). Can cognitive processes be inferred from neuroimaging data? *Trends in cognitive sciences*, 10(2):59–63.

Porro, C. A., Baraldi, P., Pagnoni, G., Serafini, M., Facchin, P., Maieron, M., and Nichelli, P. (2002). Does anticipation of pain affect cortical nociceptive systems? *the Journal of Neuroscience*, 22(8):3206–3214.

Price, D. D., Milling, L. S., Kirsch, I., Duff, A., Montgomery, G. H., and Nicholls, S. S. (1999). An analysis of factors that contribute to the magnitude of placebo analgesia in an experimental paradigm. *Pain*, 83(2):147–156.

Prisman, E., Slessarev, M., Han, J., Poublanc, J., Mardimae, A., Crawley, A., Fisher, J., and Mikulis, D. (2008). Comparison of the effects of independently-controlled end-tidal pco2 and po2 on blood oxygen level-dependent (bold) mri. *Journal of Magnetic Resonance Imaging*, 27(1):185–191.

Purves, D., Augustine, G. J., Fitzpatrick, D., Katz, L. C., LaMantia, A.-S., McNamara, J. O., Williams, S. M., et al. (2001). *The Association Cortices*. Sinauer Associates.

Radloff, L. S. (1977). The ces-d scale a self-report depression scale for research in the general population. *Applied psychological measurement*, 1(3):385–401.

Raichle, M. E., MacLeod, A. M., Snyder, A. Z., Powers, W. J., Gusnard, D. A., and Shulman, G. L. (2001). A default mode of brain function. *Proceedings of the National Academy of Sciences*, 98(2):676–682.

Raj, D., Anderson, A. W., and Gore, J. C. (2001). Respiratory effects in human functional magnetic resonance imaging due to bulk susceptibility changes. *Physics in medicine and biology*, 46(12):3331.

Reiss, S., Peterson, R. A., Gursky, D. M., and McNally, R. J. (1986). Anxiety sensitivity, anxiety frequency and the prediction of fearfulness. *Behaviour research and therapy*, 24(1):1–8.

Rhudy, J. L. and Meagher, M. W. (2000). Fear and anxiety: divergent effects on human pain thresholds. *Pain*, 84(1):65–75.

Ries, A. L., Kaplan, R. M., Limberg, T. M., and Prewitt, L. M. (1995). Effects of pulmonary rehabilitation on physiologic and psychosocial outcomes in patients with chronic obstructive pulmonary disease. *Annals of internal medicine*, 122(11):823–832.

Rikard-Bell, G. C., Bystrzycka, E. K., and Nail, B. S. (1985). Cells of origin of corticospinal projections to phrenic and thoracic respiratory motoneurones in the cat as shown by retrograde transport of HRP. *Brain research bulletin*, 14(1):39–47.

Rizvi, T. A., Ennis, M., Behbehani, M. M., and Shipley, M. T. (1991). Connections between the central nucleus of the amygdala and the midbrain periaqueductal gray: Topography and reciprocity. *The Journal of comparative neurology*, 303(1):121–131.

Rizzolatti, G., Fogassi, L., and Gallese, V. (2002). Motor and cognitive functions of the ventral premotor cortex. *Current opinion in neurobiology*, 12(2):149–154.

Roland, P. E., Larsen, B., Lassen, N., and Skinhoj, E. (1980). Supplementary motor area and other cortical areas in organization of voluntary movements in man. *Journal of neurophysiology*, 43(1):118–136.

Romer, L. M. and Polkey, M. I. (2008). Exercise-induced respiratory muscle fatigue: implications for performance. *Journal of Applied Physiology*, 104(3):879–888.

Roy, M., Shohamy, D., and Wager, T. D. (2012). Ventromedial prefrontal-subcortical systems and the generation of affective meaning. *Trends in cognitive sciences*, 16(3):147–156.

Ryan, J. W. and Waldrop, T. G. (1995). Hypoxia sensitive neurons in the caudal hypothalamus project to the periaqueductal gray. *Respiration physiology*, 100(3):185–194.

Rybak, I. A., Shevtsova, N. A., Paton, J., and Dick, T. E. (2004). Modeling the ponto-medullary respiratory network. *Respiratory physiology & neurobiology*.

Salimi-Khorshidi, G., Douaud, G., Beckmann, C. F., Glasser, M. F., Griffanti, L., and Smith, S. M. (2014). Automatic denoising of functional mri data: combining independent component analysis and hierarchical fusion of classifiers. *Neuroimage*, 90:449–468.

Salmon, P. (2001). Effects of physical exercise on anxiety, depression, and sensitivity to stress: a unifying theory. *Clinical psychology review*, 21(1):33–61.

Sanes, J. N. and Donoghue, J. P. (2000). Plasticity and primary motor cortex. *Annual review of neuroscience*, 23(1):393–415.

Satpute, A. B., Wager, T. D., Cohen-Adad, J., Bianciardi, M., Choi, J.-K., Buhle, J. T., Wald, L. L., and Barrett, L. F. (2013). Identification of discrete functional subregions of the human periaqueductal gray. *Proceedings of the National Academy of Sciences*, 110(42):17101–17106.

Schimitel, F. G., Machado de Almeida, G., Pitol, D. N., de Souza Armini, R., Tufik, S., and Schenberg, L. C. (2012). Evidence of a suffocation alarm system within the periaqueductal gray matter of the rat. *Neuroscience*.

Schoene, R., Lahiri, S., Hackett, P., Peters, R., Milledge, J., Pizzo, C., Sarnquist, F., Boyer, S., Graber, D., Maret, K., et al. (1984). Relationship of hypoxic ventilatory response

to exercise performance on mount everest. *Journal of Applied Physiology*, 56(6):1478–1483.

Schwartzstein, R. M., Simon, P. M., Weiss, J. W., Fencl, V., and Weinberger, S. E. (1989). Breathlessness Induced by Dissociation between Ventilation and Chemical Drive. *American Review of Respiratory Disease*, 139(5):1231–1237.

Scoggin, C., Doekel, R., Kryger, M., Zwillich, C., and Weil, J. (1978). Familial aspects of decreased hypoxic drive in endurance athletes. *Journal of Applied Physiology*, 44(3):464–468.

Sehlmeyer, C., Schöning, S., Zwitserlood, P., Pfleiderer, B., Kircher, T., Arolt, V., and Konrad, C. (2009). Human fear conditioning and extinction in neuroimaging: a systematic review. *PloS one*, 4(6):e5865.

Sessle, B. J., Ball, G. J., and Lucier, G. E. (1981). Suppressive influences from periaqueductal gray and nucleus raphe magnus on respiration and related reflex activities and on solitary tract neurons, and effect of naloxone. *Brain research*, 216(1):145–161.

Simmons, W. K., Avery, J. A., Barcalow, J. C., Bodurka, J., Drevets, W. C., and Bellgowan, P. (2013). Keeping the body in mind: insula functional organization and functional connectivity integrate interoceptive, exteroceptive, and emotional awareness. *Human brain mapping*, 34(11):2944–2958.

Smith, J. C., Abdala, A. P. L., Rybak, I. A., and Paton, J. F. R. (2009). Structural and functional architecture of respiratory networks in the mammalian brainstem. *Philosophical Transactions of the Royal Society B: Biological Sciences*, 364(1529):2577–2587.

Smith, S. M. (2002). Fast robust automated brain extraction. *Human brain mapping*, 17(3):143–155.

Smith, S. M. and Nichols, T. E. (2009). Threshold-free cluster enhancement: Addressing problems of smoothing, threshold dependence and localisation in cluster inference. *Neuroimage*, 44(1):83–98.

Smoller, J. W., Pollack, M. H., Otto, M. W., Rosenbaum, J. F., and Kradin, R. L. (1996). Panic anxiety, dyspnea, and respiratory disease: Theoretical and clinical considerations. *American Journal of Respiratory and Critical Care Medicine*, 154(1):6–17.

Sonetti, D. A., Wetter, T. J., Pegelow, D. F., and Dempsey, J. A. (2001). Effects of respiratory muscle training versus placebo on endurance exercise performance. *Respiration physiology*, 127(2):185–199.

Spielberger, C. D. (2010). *State-Trait Anxiety Inventory*. Wiley Online Library.

Stefan, K., Kunesch, E., Cohen, L. G., Benecke, R., and Classen, J. (2000). Induction of plasticity in the human motor cortex by paired associative stimulation. *Brain*, 123(3):572–584.

Stegmann, H., Kindermann, W., and Schnabel, A. (1981). Lactate kinetics and individual anaerobic threshold. *International journal of sports medicine*, 2(3):160–165.

Subramanian, H. H. (2012). Descending control of the respiratory neuronal network by the midbrain periaqueductal grey in the rat in vivo. *The Journal of physiology*, 591(1):109–122.

Subramanian, H. H., Balnave, R. J., and Holstege, G. (2008). The Midbrain Periaqueductal Gray Control of Respiration. *Journal of Neuroscience*, 28(47):12274–12283.

Swanney, M. P., Ruppel, G., Enright, P. L., Pedersen, O. F., Crapo, R. O., Miller, M. R., Jensen, R. L., Falaschetti, E., Schouten, J. P., Hankinson, J. L., et al. (2008). Using the lower limit of normal for the fev1/fvc ratio reduces the misclassification of airway obstruction. *Thorax*.

Thomason, M. E., Burrows, B. E., Gabrieli, J. D. E., and Glover, G. H. (2005). Breath holding reveals differences in fMRI BOLD signal in children and adults. *Neuroimage*, 25(3):824–837.

Topolovec, J. C., Gati, J. S., Menon, R. S., Shoemaker, J. K., and Cechetto, D. F. (2004). Human cardiovascular and gustatory brainstem sites observed by functional magnetic resonance imaging. *The Journal of comparative neurology*, 471(4):446–461.

Tracey, I., Ploghaus, A., Gati, J. S., Clare, S., Smith, S., Menon, R. S., and Matthews, P. M. (2002). Imaging Attentional Modulation of Pain in the Periaqueductal Gray in Humans. *The Journal of Neuroscience*, 22(7):5.

Trachtenberg, J. T., Chen, B. E., Knott, G. W., Feng, G., Sanes, J. R., Welker, E., and Svoboda, K. (2002). Long-term in vivo imaging of experience-dependent synaptic plasticity in adult cortex. *Nature*, 420(6917):788–794.

Tranel, D., Bechara, A., and Denburg, N. L. (2002). Asymmetric functional roles of right and left ventromedial prefrontal cortices in social conduct, decision-making, and emotional processing. *Cortex*, 38(4):589–612.

Trejo, J. L., Carro, E., and Torres-Alemán, I. (2001). Circulating Insulin-Like Growth Factor I Mediates Exercise-Induced Increases in the Number of New Neurons in the Adult Hippocampus. *The Journal of Neuroscience*, 21(5):1628–1634.

Turner, D. L., Bach, K. B., Martin, P. A., Olsen, E. B., Brownfield, M., Foley, K. T., and Mitchell, G. S. (1997). Modulation of ventilatory control during exercise. *Respiration physiology*, 110(2-3):277–285.

Uchida, R. R., Del-Ben, C. M., Busatto, G. F., Duran, F. L., Guimarães, F. S., Crippa, J. A., Araújo, D., Santos, A. C., and Graeff, F. G. (2008). Regional gray matter abnormalities in panic disorder: A voxel-based morphometry study. *Psychiatry research*, 163(1):21.

Urry, H. L., Van Reekum, C. M., Johnstone, T., Kalin, N. H., Thurow, M. E., Schaefer, H. S., Jackson, C. A., Frye, C. J., Greischar, L. L., Alexander, A. L., et al. (2006). Amygdala and ventromedial prefrontal cortex are inversely coupled during regulation of negative affect and predict the diurnal pattern of cortisol secretion among older adults. *The Journal of Neuroscience*, 26(16):4415–4425.

Van de Ven, M., Colier, W., Van der Sluijs, M., Kersten, B., Oeseburg, B., and Folgering, H. (2001). Ventilatory and cerebrovascular responses in normocapnic and hypercapnic copd patients. *European Respiratory Journal*, 18(1):61–68.

Van Den Heuvel, M. P. and Pol, H. E. H. (2010). Exploring the brain network: a review on resting-state fmri functional connectivity. *European Neuropsychopharmacology*, 20(8):519–534.

Vertes, R. P. and Crane, A. M. (1996). Descending projections of the posterior nucleus of the hypothalamus:Phaseolus vulgaris leucoagglutinin analysis in the rat. *The Journal of comparative neurology*, 374(4):607–631.

Vogt, B. A., Finch, D. M., and Olson, C. R. (1992). Functional heterogeneity in cingulate cortex: the anterior executive and posterior evaluative regions. *Cerebral cortex*, 2(6):435–443.

Volianitis, S., McConnell, A. K., Koutedakis, Y., McNaughton, L. R., Backx, K., and Jones, D. A. (2001). *Inspiratory muscle training improves rowing performance*. Lippincott Williams & Wilkins.

von Leupoldt, A., Sommer, T., Kegat, S., Eippert, F., Baumann, H. J., Klose, H., Dahme, B., and Büchel, C. (2009). Down-Regulation of Insular Cortex Responses to Dyspnea and

Pain in Asthma. *American journal of respiratory and critical care medicine*, 180(3):232–238.

Wager, T. D., Rilling, J. K., Smith, E. E., Sokolik, A., Casey, K. L., Davidson, R. J., Kosslyn, S. M., Rose, R. M., and Cohen, J. D. (2004). Placebo-induced changes in fmri in the anticipation and experience of pain. *Science*, 303(5661):1162–1167.

Waldrop, T. G., Eldridge, F. L., Iwamoto, G. A., and Mitchell, J. H. (1996). Central neural control of respiration and circulation during exercise. *Comprehensive Physiology*.

Wasserman, K., Whipp, B., Koyl, S., and Beaver, W. (1973). Anaerobic threshold and respiratory gas exchange during exercise. *Journal of applied physiology*, 35(2):236–243.

Wild, C. J., Davis, M. H., and Johnsrude, I. S. (2012). Human auditory cortex is sensitive to the perceived clarity of speech. *Neuroimage*, 60(2):1490–1502.

Woolrich, M. W., Behrens, T. E. J., Beckmann, C. F., Jenkinson, M., and Smith, S. M. (2004a). Multilevel linear modelling for FMRI group analysis using Bayesian inference. *Neuroimage*, 21(4):1732–1747.

Woolrich, M. W., Behrens, T. E. J., and Smith, S. M. (2004b). Constrained linear basis sets for HRF modelling using Variational Bayes. *Neuroimage*, 21(4):1748–1761.

Woolrich, M. W., Ripley, B. D., Brady, M., and Smith, S. M. (2001). Temporal Autocorrelation in Univariate Linear Modeling of FMRI Data. *Neuroimage*, 14(6):1370–1386.

Wymbs, N. F., Bassett, D. S., Mucha, P. J., Porter, M. A., and Grafton, S. T. (2012). Differential recruitment of the sensorimotor putamen and frontoparietal cortex during motor chunking in humans. *Neuron*, 74(5):936–946.

Zambreanu, L., Wise, R. G., Brooks, J. C. W., Iannetti, G. D., and Tracey, I. (2005). A role for the brainstem in central sensitisation in humans. Evidence from functional magnetic resonance imaging. *Pain*, 114(3):397–407.

Zhang, W., Hayward, L. F., and Davenport, P. W. (2007). Respiratory responses elicited by rostral versus caudal dorsal periaqueductal gray stimulation in rats. *Autonomic Neuroscience*, 134(1-2):45–54.

Zhang, Y., Brady, M., and Smith, S. (2001). Segmentation of brain mr images through a hidden markov random field model and the expectation-maximization algorithm. *Medical Imaging, IEEE Transactions on*, 20(1):45–57.